DIETARY INTERVENTIONS FOR IMPROVING FERTILITY

Macarena Bermudez Gonzalez

The Robinson Research Institute

School of Medicine

Discipline of Obstetrics and Gynaecology

University of Adelaide, Adelaide

Australia

Thesis submitted to the University of Adelaide in fulfillment of the requirements for admission to the degree of Doctor of Philosophy

March 2018

Abstract

Obesity has dramatically increased in the population in the last few decades, and data from the Australian Bureau of Statistics National Health Survey indicates that currently approximately half of the women in Australia are overweight or obese. The fact that many of these women are in their reproductive years is concerning. Obesity increases the risk of developing chronic diseases as well as having a negative effect on women's reproductive health, influencing the prevalence of subfertility, infertility and pregnancy complications. Polycystic Ovary Syndrome (PCOS) is the most common reproductive disorder in women and it is closely related to obesity. It is characterized by acyclicity, anovulation and increased levels of androgens in blood, as well as decreased rates of pregnancy.

Increased BMI has been associated with dysregulated menstrual cycles, anovulation or oligo-ovulation, and lower pregnancy rates. Recent evidence suggests that obesity causes the initiation of a pro-inflammatory state that extends to the adipose, liver, and muscle tissues. The increased release of proinflammatory cytokines from adipose tissue, such as interleukin 6 (IL-6) and tumor necrosis factor alpha (TNF-α), induces lipolysis, enhances cytokine release, and promotes insulin resistance. At the cellular level, it is characterized by mitochondrial dysfunction and the activation of stress pathways, namely Endoplasmic reticulum (ER)-stress and the Heat Shock Response (HSR). The different stress responses constitute a complex network that interacts not only with nascent polypeptides and stress-denatured proteins, but also with metabolic (insulin), hormonal (steroid hormones and their receptors) and immunological pathways (antigen presentation). That these pathways also affect ovarian function makes HSP a potential target for therapeutic interventions in obesity.

However, it is still not clear how obesity influences the ovarian environment, and how this affects stress pathways in ovarian cells, as well as its impact on oocyte homeostasis and the development of the preimplantation embryo.

Thus, I will explore how different factors impact the obesity phenotype in female mice, with special emphasis on ovarian function and the expression of stress responses in ovarian cells, and ultimately how they affect oocyte quality and developmental potential. For this, I will be using three different mouse models of obesity, namely a Dihydrotestosterone (DHT) -induced PCOS model, a High fat diet (HFD) -induced model and a High Sugar High Fat combination diet. Finally, I will determine if specific chaperone-inducing micronutrients can promote the induction of these cytoprotective HSP and/or normalize ER stress, in order to identify a natural fertility-protective diet.

Declaration

I certify that this work contains no material which has been accepted for the award of any other degree or diploma in my name in any university or other tertiary institution and, to the best of my knowledge and belief, contains no material previously published or written by another person, except where due reference has been made in the text. In addition, I certify that no part of this work will, in the future, be used in a submission in my name for any other degree or diploma in any university or other tertiary institution without the prior approval of the University of Adelaide and where applicable, any partner institution responsible for the joint award of this degree.

I give consent to this copy of my thesis, when deposited in the University Library, being made available for loan and photocopying, subject to the provisions of the Copyright Act 1968. I also give permission for the digital version of my thesis to be made available on the web, via the University's digital research repository, the Library Search and also through web search engines, unless permission has been granted by the University to restrict access for a period of time.

I acknowledge the support I have received for my research through the provision of an Australian Government Research Training Program Scholarship.

Macarena Bermudez Gonzalez

March 2018

Acknowledgements

I am thankful to the following people for making this work, and my success possible.

Thank you to my supervisory team, Becky and Linda, for the guidance and support during this project. Becky, thank you for your mentorship, your friendship, the early morning collections and the late night emails, and the 10 minute meetings that went on for hours.

Thank you to the team at the Ovarian Biology laboratory and the rest of the Robinson Research Institute for their friendship, and all the science stories shared over wine.

Hannah, thank you for being there for me through the tough times and for all the fun times together.

To my fellow #FutureLadyProfessors for sharing with me all the highs and lows during our postgraduate journey. Here's for us.

Thank you to all the staff in the Robinson Research Institute, Laboratory Animal Services and the Adelaide Medical School for their friendly smiles and endless patience.

My PhD was financially supported with grant funding from the National Health and Medical Research Council, and a scholarship from the University of Adelaide. I would also like to acknowledge the financial support of the Adelaide Medical School, the Faculty of Health and Medical Sciences, the University of Adelaide, the Healthy Development Adelaide research cluster, the Centre for Research Excellence in Polycystic Ovary Syndrome, the Lalor foundation, and the Marine Biological Laboratory for international and domestic travel opportunities and my postgraduate scholarship.

Lastly, thank you to my family for all the support during the last 5 years. To my mum, Maria, for always sending care packages when I was homesick. To my dearest Luci, Irene, Julie, Maria, Marina, Sara, Wen, Amanda, David, Pepe, Dani, Matthew and all my beloved friends back in Spain for always loving me, supporting me, and encouraging me to follow my dreams, even if they take me away from them. To my Australian family, especially Sarah, for keeping me sane, clean and fed during the writing of this thesis.

And finally, to Dave and Emlyn, thank you for just putting a smile on my face every day and giving the best hugs ever. Love you guys.

Abstracts arising from this thesis

- Gonzalez, M. Differences in ovarian follicle stress responses in dietary models of obesity. Invited speaker at the 2016 Annual Scientific Meeting of the Endocrine Society of Australia, the Society for Reproductive Biology and the Australian and New Zealand Bone and Mineral Society (ESA-SRB-ANZBMS), August 21st-24th, 2016 (QLD).
- Gonzalez, M. Differences in ovarian follicle stress responses in dietary models of obesity. Invited speaker at the RRI's Third Thursday scientific meeting, August 18th, 2016 (ADL).
- Gonzalez, M. Regulated Expression of Heat Shock Proteins during ovulation and oocyte maturation. Invited speaker at the Centre for Research Excellence Translating Nutritional Science to Good Health, September 23rd, 2015 (SA).
- Gonzalez, M. Regulated Expression of Heat Shock Proteins during ovulation and oocyte maturation. Invited speaker at the 2015 Annual Scientific Meeting of The Endocrine Society of Australia and The Society for Reproductive Biology (ESA-SRB), August 23rd-26thh, 2015 (SA).
- Gonzalez, M. Improving oocyte quality and embryo development by inducing Heat Shock Proteins in an overweight mouse model. XVIII Annual Frontiers in Reproduction (FIR) Symposium, June 11-13, 2015 (USA).
- Gonzalez, M. Regulated Expression of Heat Shock Proteins during ovulation and oocyte maturation. Poster presented at the 2014 Annual Scientific Meeting of The Endocrine Society of Australia and The Society for Reproductive Biology (ESA-SRB), August 24th-27th, 2014 (Vic).
- Gonzalez, M. Regulated Expression of Heat Shock Proteins during ovulation and oocyte maturation. Invited speaker at the 2014 SA Annual Scientific Meeting of The Australian Society for Medical Research, June 4th, 2014 (SA).

Table of contents

List of Figures

List of Tables

Abbreviations

aMEM	Minimum essential medium
ANOVA	Analysis of variance
BMI	Body mass index
C3C	Curcumin extract C3 Complex
CC	Cumulus cell/s
CD	Control diet
cDNA	complementary DNA
CI	Confidence interval
CL	Corpus luteum/corpora lutea
CO_2	Carbon dioxide
COC	Cumulus-oocyte complex/s
CTCF	Corrected total cell fluorescence
CTEF	Corrected total embryo fluorescence
DMSO	Dimethyl sulfoxide
DNA	Dexosirribonucleic acid
DO	Denuded oocyte/s
dpc	day post-coitus
DHT	Dihydrotestosterone
E	Embryonic day
ER stress	Endoplasmic reticulum stress
FCS	Foetal calf serum
FSH	Follicle Stimulating Hormone
g	Grams
GC	Granulosa cell/s

GCL	Granulosa luteal cell/s
GnRH	Gonadotropin-releasing Hormone
GV	Germinal vesicle
GVBD	Germinal vesicle break down
H	hour
hCG	Human Chorionic Gonadotropin
HEPES	4-(2-hydroxyethyl)-1-piperazineethanesulfonic acid
HFD	High fat diet
HSF	Heat shock factors
HSHFD	High sugar high fat diet
HSP	Heat shock protein/s
HSR	Heat shock response
ICM	Inner cell mass
IL	Interleukin
IP	Intra-peritoneal
IU	International units
IVF	In vitro fertilization
Kcal	Kilocalorie
Kg	Kilogram
KO	Knock out
LH	Luteinizing Hormone
MII	Metaphase II
mg	milligrams
Min	minute
mL	Millilitre
mM	Millimolar

nM	Nanomolar
mmol	Millimol
ul	Microlitre
um	Micron
mRNA	Messenger ribonucleic acid
NaCl	Sodium chloride
ng	Nanogram
O_2	Dioxygen, oxygen molecule
O/N	Overnight
°C	Degrees Celsius
P	Probability
P4	Progesterone
PBS	Phosphate buffer solution
PCOS	Polycystic ovary syndrome
PCR	Polymerase chain reaction
PFA	Paraformaldehyde
PMSG	Pregnant Mare Serum Gonadotropin
ROS	Reactive oxygen species
RNA	Ribonucleic acid
RpL19	Ribosomal protein L19
Rpm	Revolutions per minute
RT-PCR	Reverse transcription polymerase chain reaction
SEM	Standard error of the mean
TE	Trophectoderm
TNFa	Tumor Necrosis Factor Alpha
UPR	Unfolded protein response

Chapter 1: Introduction

The ovary is at the centre of female fertility, since it is where female gametes develop. This thesis focuses on processes in the ovary that influence oocyte development, release, fertilization and early embryo development. The current obesity epidemic affects many women in their reproductive years; therefore it investigates cellular processes that are disrupted in the ovary in response to obesity. One of these pathways is regulated by Heat Shock Proteins, a class of molecular chaperones which are cytoprotective and disrupted by obesity-induced cell stress in other tissues. I also then investigated whether dietary supplements could affect the expression of these chaperones and improve fertility in the context of obesity.

1.1 Ovarian function and female fertility

The female reproductive system is composed of different organs and structures in all animal species presenting sexual dimorphism. In mammals, the female reproductive tract encompasses the ovaries, fallopian tubes (or oviducts), uterus, vagina and external genitalia. The following text will focus in the ovary, where the female gametes or oocytes are produced and developed and provide a brief and updated review on what is known about the events that influence folliculogenesis and ovulation, and how they impact oocyte quality and developmental potential.

The mammalian ovary is unique in that it undergoes extensive cellular proliferation, differentiation and tissue remodelling during each reproductive cycle. It is typically composed of two main cell types: germ cells or oocytes; and specialised somatic cells, namely granulosa, theca and stromal cells [1, 2]. These associate in follicles, which are the functional structures of the ovary [3, 4], and which will grow and differentiate throughout the cycle and preimplantation embryo development (***Figure 1.1***). These supporting follicular cells have an essential role in achieving optimal oocyte maturation and quality [1]. The stromal cells constitute the base of the tissue, where the ovarian follicles and corpora lutea grow and develop. The theca cells form the outer layers of the ovarian follicles, whereas the granulosa cells (GC) from the inner cell layers. In the centre of every follicle is one single oocyte. Different types of structures can be found through the development of the ovary in mammals. Primordial germ cells (PGCs) migrate from the hindgut to the genital ridge, congregate in clusters in the early fetus (6 weeks gestation in humans or between embryonic day 9-10.5 in the mouse) [5-8]. It is following female-specific gene activation during fetal development that distinct structures develop in the early ovary [9, 10], and PGCs stop proliferating and enter meiosis at 10 weeks gestation in humans [6, 11] and on embryonic day 13.5 in the mouse [12-14], and shortly after that these oogonia are arrested in diplotene of Prophase I, forming the primordial follicles [10,

15]. Oocyte meiosis in mammals is very characteristic because the oocytes will remain dormant in this stage until sexual maturation or puberty occurs in the now adult female [16, 17]. It is believed that no primary oocytes form after birth, thus any given female is born with all the oocytes she will ever have [5].

Before the primordial follicles activate during puberty, they are surrounded by a layer of flattened follicular cells derived from stromal cells. With the maturation of the hypothalic-pituitary-gonadal (HPG) axis [18], primordial follicles are selected to enter the growing pool of follicles, with the majority being lost to atresia during the different stages [19] and the process culminating in the one follicle (or follicles, dependent on species) that will reach the final stages of maturation and ovulate [4]. Follicular growth during cyclic recruitment is initiated in a gonadotropin independent manner [20-23] when the granulosa cells surrounding the oocyte change their morphology from flat to cubic [17], and the follicles grow in size and form the zona pellucida. The zona pellucida forms as a layer of glycoprotein around the oocyte, which has been shown to be involved in sperm binding and fertilization, and even embryo viability [24-26]. For the next stage of follicular growth, the space between the oocyte and the GC starts expanding and fills with fluid. The theca and granulosa cells layers will start proliferation under hormonal control, increasing the number of their layers around the oocyte and constituting the pre-antral or secondary follicle. The layer of theca cells surrounding the follicle will differentiate into theca externa (outer layer) and the theca interna that starts steroid production [27].

The formation of the antral cavity or antrum determines that a section of GC directly surrounding the oocyte differentiates into cumulus cells (CC), acquiring round morphology and other molecular properties, forming the cumulus-oocyte complex or COC. These antral follicles are now receptive to follicular signalling [28, 29] as well as extraovarian regulation [30]. A surge in luteinizing hormone levels initiates a cascade of events in the preovulatory follicle that ultimately produces the breakdown of the follicle wall and the extrusion of the COC by ovulation [31, 32]. After ovulation, the remaining mural GC in the follicle start differentiating into luteal cells in a process called luteinisation and form the corpus luteum (CL). Luteal cells undergo a whole set of structural and molecular changes, the most notable of which is that they start progesterone (P4) production and release, which will be essential for the establishment and maintenance of early pregnancy[33]. If pregnancy does not occur, the luteal cells will decrease P4 production and begin apoptosis and deterioration, as the CL transforms into the corpus albicans [33].

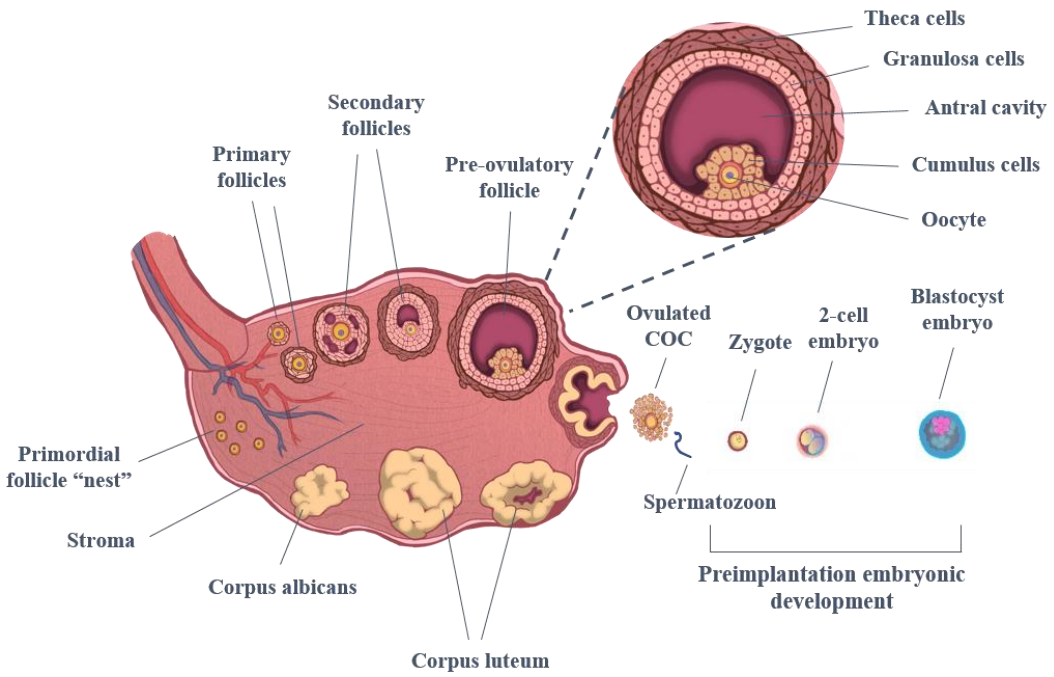

Figure 1.1 Ovarian morphology, follicular structure and preimplantation embryo development.

Overview of the morphology of the ovary, showing the different cell populations. The follicles are the functional structures in the ovary, and they change over time as they grow and mature during female reproductive life. After a mature, competent COC is released from the ovary during ovulation, it can be fertilized in the presence of spermatozoa in the female tract after coitus. If fertilization is successful, the now zygote will start several rounds of mitotic divisions during preimplantation development. When the embryo reaches the blastocyst stage, it will hatch out of the zona pellucida and begin the implantation process in the uterine wall.

1.1.1 Hormonal regulation of the ovarian cycle

Development and maturation of the ovarian follicles during each estrous cycle is controlled by the hypothalamic-pituitary-gonadal (HPG) axis through the action of gonadotrophin hormones (***Figure 1.2***). At the beginning of the cycle, pulses on gonadotropin-releasing hormone (GnRH) secreted by the hypothalamus stimulate the pituitary gland to release LH and follicle stimulating hormone (FSH), which will stimulate follicular growth and regulate the production of steroid and peptide hormones, mainly estrogen, progesterone and inhibins, [34, 35], as well as inhibit further increase in hormone production by the pituitary and hypothalamus via negative feedback. In humans, one dominant follicle is selected to finish development, while the rest stop growing and eventually enter atresia [36]. Estrogen production exert a preovulatory positive feedback that increases the frequency of GnRH pulses [37, 38], inducing a surge in LH levels. This will start the process of ovulation, characterized by the expansion of the COC as a result of the production and secretion of a hyaluronan-rich extra-cellular matrix by the CCs [39], as well as the resumption of meiosis. The latter is characterised by spindle formation, alignment of the chromosomes and extrusion of the first polar body, after which the oocyte is arrested in Metaphase II. Oocyte maturation and folliculogenesis are highly coordinated and mutually dependent processes [40]. In mice, approximately 11-12 hours after the LH surge, during ovulation, the COCs are released through the ovarian epithelium and into the oviduct. The remaining GC will differentiate into luteal cells to form a corpus luteum (CL) and start progesterone (P4) hormone production in a process known as luteinization, beginning the formation of the CL (reviewed in Stocco et al. 2007 [33]). After ovulation, the fully expanded COC adheres to and is transported by the ciliary epithelium of the oviduct, where fertilization can happen in the presence of sperm [41]. The fertilized oocyte or zygote then commences several rounds of mitosis or cleaves [42] and finally, cell differentiation into the blastocyst stage. During this process the embryo will travel down the fallopian tube and into the uterus, where it will initiate implantation in the vascularised, growing endometrium. Endometrial receptivity is the result of the coordinated action between E2 and P4 (reviewed by Carson et al, 2000 [43]). Briefly, uterine epithelial cell proliferation in mice is stimulated by an E2 surge on day 1 (post-coitus), followed by marked cell apoptosis after E2 levels decline on day 2. In the meantime, the CL will start production of P4 on day 3, initiating uterine stromal cell proliferation that is further induced by a surge on E2 levels on day 4. All these changes produce the necessary changes in the uterus to support blastocyst implantation and uterine decidualization in these first stages of pregnancy. In the absence of implantation, the CL will regress into the corpus albicans in a process characterized by the degeneration of the luteal cells

and subsequent decline in P4 production [33], which in turn induces the shedding of the endometrium at the start of a new menstrual cycle.

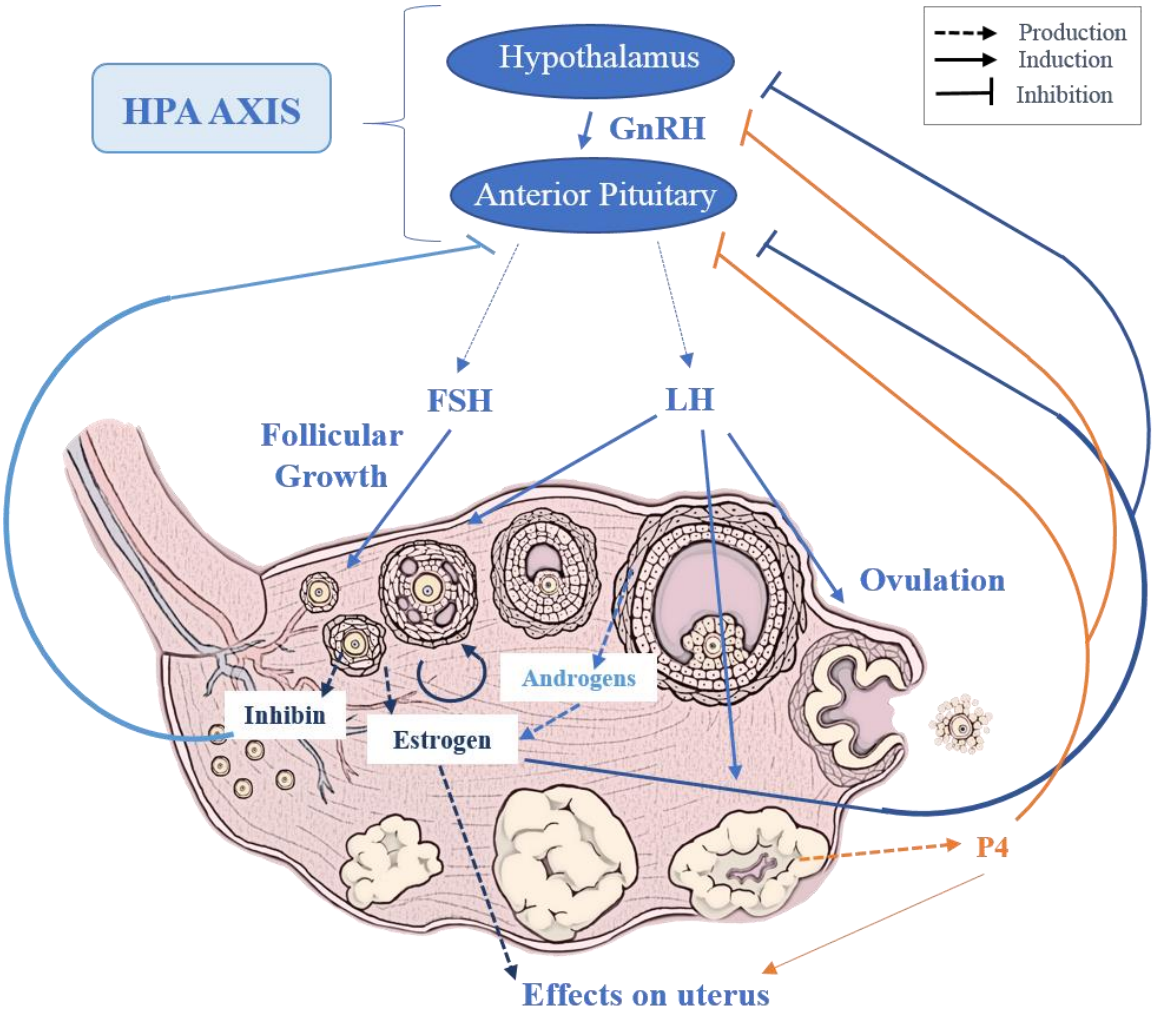

Figure 1.2 Hormonal regulation of ovarian function during the estrous cycle.

Growth and maturation of the ovarian follicles during each menstrual cycle is controlled by the hypothalamic-pituitary-gonadal (HPG) axis. Production of gonadotrophin releasing hormones (GnRH) by the pituitary stimulates the release of luteinizing hormone (LH) and follicle stimulating hormone (FSH) from the pituitary, which in turn stimulate granulosa cell production of estrogen (E2), inhibins and progesterone (P4) in antral follicles. These hormones will exert a local effect regulating follicle development as well as producing a negative feedback effect on GnRH release. The increase in GnRH pulse frequency produces an LH surge that will trigger the ovulation process, inducing the expansion of the cumulus-oocyte-complex (COC) and the resumption of meiosis in the oocyte. At this point, the COC is released through the ovarian epithelium and into the fallopian tube. The remaining follicular cells in the ruptured follicle will form the corpus luteum (CL) and increase P4 hormone production. Increasing levels of E2 and P4 initiate changes in the uterine epithelium, making it receptive for embryonic implantation. If fertilization happens, the embryo will travel down the oviduct and into the uterus, where it will initiate implantation and decidualization of the endometrium. In the absence of implantation, the CL will regress and P4 production will decline.

1.1.2 Ovulation

Ovulation is the process by which a mature, competent oocyte is released from the ovary, promoted by the LH surge [32]. Surprisingly, the exact mechanisms that allow the COC to get out of the ovary are not completely understood. In the mouse, the COC is released into the oviduct (mouse), where it will adhere to the ciliated epithelial cells in the infundibulum that will initiate oocyte transport down the reproductive tract while it awaits fertilization [44]. A fertilizable or competent oocyte has progressed to MII stage of meiosis and extruded the first polar body. However, this competency does not last long. In 4-6 hours after ovulation, the capacity of the oocyte to fertilize and produce a normal embryo is drastically diminished [45, 46], due to abnormal calcium oscillation patterns that lead to increased apoptosis and delayed embryonic development [47, 48], in a process known as post-ovulatory aging..

The CC constitute the first line of protection/nourishment for the oocyte, as well as having an essential role in regulating meiotic resumption and acquisition of developmental competence during follicular growth, directly supporting the oocyte through transzonal projections and gap junctions [49-53]. By the time the oocyte has reached MII and ovulation takes place, these unions have disappeared, but the CC still have an important role in oocyte fertilization. During their expansion prior to ovulation, the CC excrete a hyaluronidase-rich extra-cellular matrix and soluble factors that will act as chemo-attractants, leading the sperm to the COC and promoting capacitation and the initiation of the acrosome reaction [54-56]. In contrast, an abnormal CC expansion decreases fertilization chances in the oocytes [39]. Interestingly, there is some evidence suggesting that CC survival can influence the time-frame of oocyte fertilization and post-ovulatory aging. Giacomo et al showed that post-ovulatory changes resulting in hyaluronan release from the matrix and CC dispersion were temporally correlated to CC apoptosis and cell death; but the elevation of cyclic adenosine monophosphate (cAMP) levels prevented the disaggregation of ovulated COCs and prolonged CC survival, which resulted in an extended time for the oocyte fertilization in vitro [57].

1.1.3 Fertilization and preimplantation embryo development

Fertilization refers to the successful penetration of the genetic material from a spermatozoon which head has merged with the oocyte membrane.. In the mouse, the second polar body is extruded shortly (1-3 hours) after fertilization, then the DNA carried by the spermatozoon into the oocyte's cytoplasm after penetration condenses in a structure known as the male pronucleus. Afterwards, the female pronucleus is similarly formed [58]. When the two pronuclei meet in

the oocyte cytoplasm, they will merge together and form a diploid cell. The fertilized oocyte is now known as a 1-cell embryo or zygote, which will undergo several rounds of mitosis or cleavages for the next few days [42]. This period is known as preimplantation embryo development. While this process is taking place, the embryo descends through the oviduct into the uterus, where it will burrow into the receptive endometrial epithelium, initiating embryonic implantation and uterine decidualization [43].

Mammalian embryos go through similar cleavage stages during their preimplantation development following fertilization and although the duration is variable between species [59, 60], the succesful development of an embryo to the blastocyst stage is dependent on oocyte-related factors that affect its quality and developmental potential (reviewed in Nuttinck et al, 2018 [61])..

In humans, implantation normally take place approximately on embryonic day 7[62], while in the mouse implantation occurs around day 4.5 after mating [63]. Mouse embryogenesis is considered a classic model for human embryo development and the development of mouse pre-implantation embryos is very well characterized (***Figure 1.3***). Specifically, on day 1 after ovulation (day of fertilization) the zygote remains in the 1-cell stage. On day 1.5, about 20 hours after fertilization, the now 2-cell embryo has undergone first mitotic division or cleavage, resulting in two similarly sized cells or blastomeres. The embryo will then undergo second (3-cell), third (4-cell), and subsequent stages in 12 hour intervals until there are approximately 8 blastomeres. Approximately at this point, the mass of cells or morula undergoes a process known as compaction, where the cells change their properties and become highly packed, clear demarcation between cells disappears and the outlines of individual blastomeres cannot be distinguished, all while undergoing further rounds of divisions [64]. The embryo has been pluripotent up until the 8-cell stage, and shortly before compaction the blastomeres commence polarization and differentiation [65-67]. In subsequent cleavages, two types of blastomeres start to emerge: first, the external blastomeres positioned at the surface of the embryo and retain apical-basal polarity; and second, the internal blastomeres surrounded by neighbouring cells and devoid of polarity [68-72]. At this point, the blastocoel cavity starts forming and filling with fluid around day 3.5 [73], and will continue to expand and the embryos are now known as blastocysts. Between now and day 4.5, the expanding blastocysts will hatch out of the zona pellucida and are ready to burrow into the endometrium. The blastocyst embryo now possesses two characteristically different cell populations: the external cells or throphodermal epithelium (TE), and the internal cells or inner cell mass (ICM) [68]. Together, these 2 cell populations

will separately develop into the primary embryonic cell lineages (trophectoderm, epiblast and primitive endoderm)[74, 75]. The early embryo will slowly and progressively develop into the fetus during pregnancy.

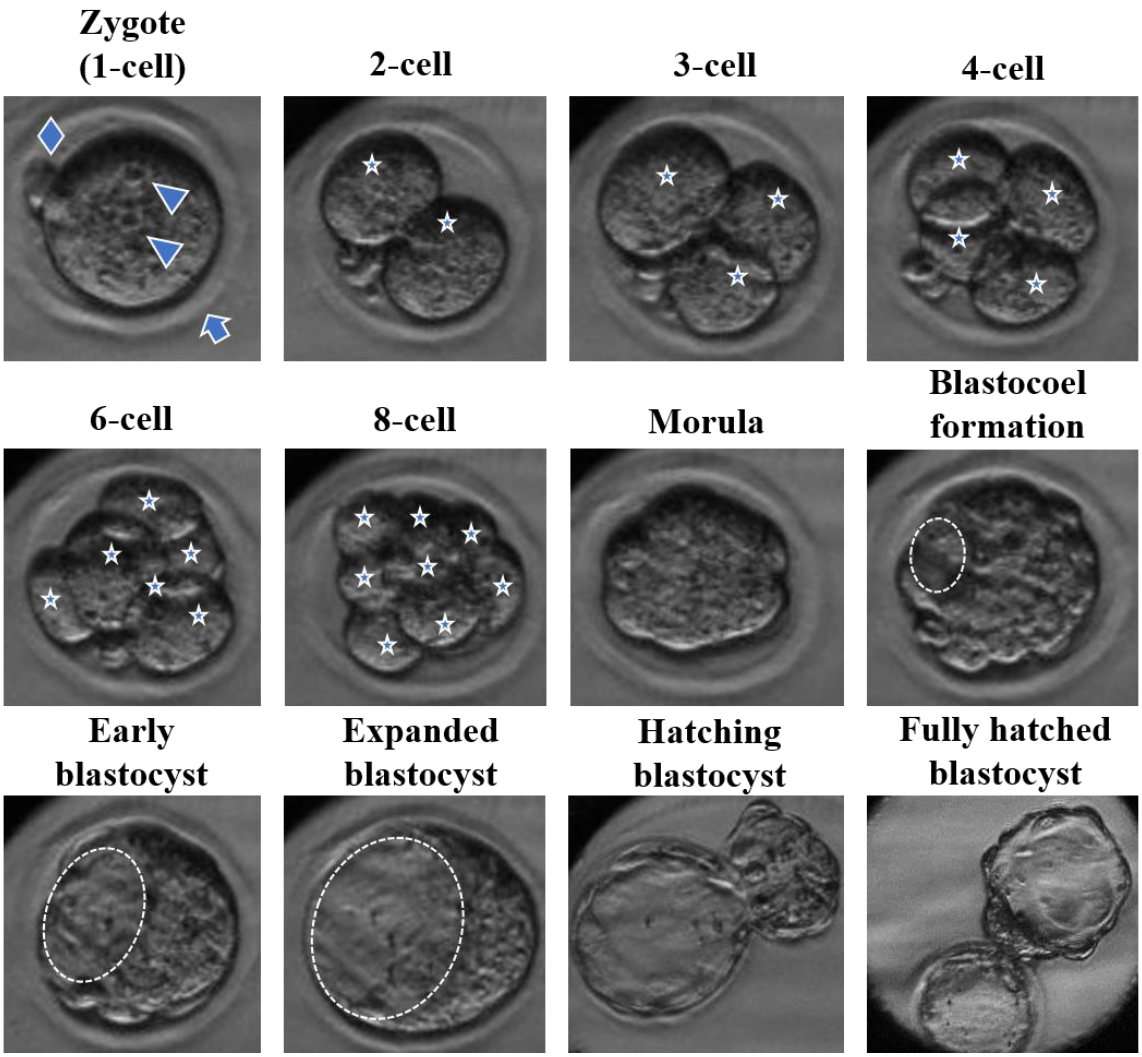

Figure 1.3 Developmental stages of the early mouse embryo.

Representative images of the different developmental stages of the preimplantation embryo, starting with the zygote or 1-cell embryo. The fertilized oocyte or zygote is characterized by the extrusion of the second polar body (◊), and presents 2 pronuclei, one from each parent (▲, arrowheads). The embryo will develop inside the zona pellucida (↑). The embryo subsequently goes through a series of mitotic divisions, resulting in an increasing number of blastomeres (*), this will continue until the embryo has ~16 blastomeres. During the morula stage, the blastomeres will undergo compaction, where the first cell-fate decisions occurs. Next, the blastocoel cavity (dotted line) starts to form and fill with fluid in the now blastocyst embryo. At this stage, the embryo has two types of blastomeres: the ICM and the trophoblasts. The blastocoel will expand until it occupies most of the volume. When the blastocyst hatches out of the zona pellucida, the embryo is ready to attach to the uterine wall and commence implantation.

1.1.4 Determinants of oocyte and embryo quality

The oocyte is a very specialized cell that despite its importance for the creation of new life, is still not well understood. New evidence keeps emerging reporting on factors that directly or indirectly influence oocyte quality.

Oocyte developmental competence is most definitely measured by its capacity to form an embryo; and more specifically the timely formation of an embryo. An embryo that has timely divisions and develops the trophectoderm and the ICM in sufficient numbers is more likely to reach a successful implantation [76, 77]. The two hallmarks of embryonic development are achievement of the 2-cell and blastocyst stages. The retrospective analysis of 100 human embryos using time-lapse imaging found that the first 48 hours of development reliably predicted which embryos would make it to the blastocyst stage [78]. A similar retrospective study including data from over 3,100 fresh cycles found that blastocyst morphology strongly determined clinical pregnancy and live birth rates [76]. On-time embryo development is an observational measure of embryo quality and consists in the identification and annotation of embryos that have reached a developmental stage at the appropriate time. Cultured mouse embryos are assessed on days 2 and 5 after in vitro fertilization (IVF) for 2-cell and blastocyst status, respectively. On day 2, embryos should have reached 2-cell status by approximately 46 hours post-hCG injection. A normal 2-cell embryo displays 2 symmetrical, uninucleate blastomeres. On day 5, embryos should have reached the blastocyst stage by 112 hours post-hCG injection. A normal blastocyst at this point presents clear trophectoderm and ICM cell populations, blastocoel cavity and may be hatching out of the zona pellucida.

There are many approaches to study molecular pathways that determine a good quality oocyte. In the human clinic, there are guidelines to identify morphological and other cues in order to judge a healthy and competent oocyte. Normal morphology, integrity of the oocyte membrane and the zona pellucida, presence of the meiotic spindle and first polar body are indicators of oocyte maturation and developmental potential. Animal studies are better able to dissect molecular markers of oocyte quality, as they allow the identification of intrinsic predictors of oocyte quality. Amongst these factors involved in cytoplasmic maturation of the oocyte, intracellular calcium levels, glucose-6-phosphate dehydrogenase (G6PDH) activity and mitochondrial profile are essential to produce a fully competent oocyte and thus ensure embryo quality (reviewed in Wang and Sun. 2006 [79], and Schatten et al. 2014 [80]). The oocyte's mitochondria is not only responsible for ATP production but also surround the meiotic apparatus during meiosis as they produce the necessary energy for spindle assembly,

chromosome alignment and polar body extrusion. It is believed that the mitochondria in the spermatozoon's midpiece are targeted and removed from the cytoplasm shortly after fertilization [81], therefore it is the mitochondria in the oocyte that will be passed to the embryo. Moreover, the early embryo will rely on the mother's mitochondria during the first days of development, until embryonic mitogenesis activates.

1.2 Obesity is a risk factor for infertility in women

Obesity is one of the most concerning non-communicable diseases and is increasing in incidence worldwide. Over-nutrition is a major non-genetic cause of increasing obesity levels, particularly in countries such as the USA and Australia [82]. Obesity is an important risk factor for the development of many chronic diseases, such as cardiovascular disease, obesity-related cancer, type 2 diabetes mellitus and metabolic syndrome [83]. The increase in body weight observed in obesity is accompanied by an increase in adipose tissue, which in turn is characterized by dysregulated adipokine release that impact macronutrient metabolism, reducing insulin sensitivity in target tissues. Also known as insulin resistance, it is defined by the impaired suppression of glucose output from the liver and the decrease of insulin-stimulated glucose uptake and metabolism in skeletal muscle and adipose tissue [84]. This in turn often leads to altered glucose homeostasis or hyperglycemia, resulting in high levels of circulating glucose that are a clinical marker for the diagnosis of type 2 diabetes. Other factors associated with obesity such as inflammation, mitochondrial dysfunction, hyperinsulinemia, lipotoxicity, oxidative stress and Endoplasmic reticulum stress (ER stress) are thought to contribute to the induction of insulin resistance, resulting in increased risk of type 2 diabetes in obese individuals.

Approximately half the women in Australia today are overweight or obese, with many young women in their reproductive years being affected. Although obesity has been widely studied, it is yet not fully understood what the mechanisms are underlying its effects on reproductive function and offspring development and health. The detrimental consequences of obesity on female fertility are well known, but the functional mechanisms and full extent by which diet, namely obesogenic high fat diets, alters gamete health and reproductive function remain elusive. In women, it is clear that being overweight or obese is associated with dysregulated menstrual cyclicity [85-87], longer time to conception [88, 89], increased risk of miscarriage [86, 89, 90], and increased risk of gestational diabetes [89, 91]. It is thought that the delay to conception and increased risk of miscarriage seen in obese women indicates that the gamete,

and or embryos, are of poorer quality, and that the tract may be a sub-optimal environment, unaccommodating to early embryo development.

Additionally, obesity is also associated with Polycystic Ovary syndrome, also known as PCOS. This syndrome is the most common endocrine disorder in women, affecting an estimated 5-10% of all female population, and considered a leading cause of infertility in women of reproductive age [92, 93]. PCOS is a constellation of pathologies but it is strictly diagnosed based on a set of definitions, also known as the Rotterdam criteria, establish in 2003 by the European Society for Human Reproduction (ESHRE) and the American Society of Reproductive Medicine (ASRM) [93]. Currently, a patient will receive diagnosis if she presents at least two of the three following traits: clinical and/or biochemical hyperandrogenism, polycystic ovaries on ultrasound, and oligo or anovulation [94]. Other physiological symptoms include irregular menstrual cycles, infertility, pelvic pain, excess body hair (hirsutism), weight gain, and acne. Women with PCOS are also at greater risk of suffering type 2 diabetes, metabolic syndrome, cardiovascular disease and high blood pressure.

1.2.1 Impairment of ovarian function in an obesity environment

Several studies have demonstrated that obesity-induced alterations to ovarian function are at least part of the mechanism by which obesity impacts female fertility. The relative risk of anovulatory infertility is 2.7 times higher (95% CI, 2.0-3.7) in women with BMI of 32 kg/m^2 or over at age 18 [95]. Previously, a review of retrospective clinical studies concluded that the weight of evidence indicates that obesity can cause anovulation [89]. This can happen through multiple parallel pathways. Obesity is associated with hyperandrogenism which may contribute to hormonal imbalance. In addition, anovulation appears to result directly from damage to the ovarian tissue, through lipotoxicity responses promoting cellular stress and apoptosis in follicle-supporting cells. This concept is supported by studies which report that mice with diet-induced obesity have diminished ovulation rates [96, 97] as well as compromised fertilization [97] and smaller litters [96], when compared to their control diet-fed counterparts. Several independent studies support that the oocytes themselves are also affected by obesity, and thus these observations of impaired fertilization and small litters are likely also a direct consequences of compromised oocyte quality. Oocytes from obese female mice exhibit impaired developmental competence [98-100] and altered preimplantation embryonic differentiation [99]. Further, oocytes from obese mice exhibit spindle defects at the MII stage [98, 100-102] , which is consistent with clinical reports, where a greater prevalence of spindle abnormalities and

misaligned chromosomes were observed in oocytes from obese women which failed to fertilize [103]. Jungheim et al [104] also found delayed germinal vesicle break down (GVBD) in oocytes from growing follicles in the ovaries of mice fed an obesogenic diet, suggesting that oocyte maturation and acquisition of competence were delayed.

1.2.2 Induction of cellular stress pathways by obesity

Evidence suggests that obesity causes the initiation of a proinflammatory state that is distinctive and outside the paradigm of classical inflammation. The inflammatory trigger in obesity is metabolic in nature, and thought to be caused by excess consumption of nutrients and evidence indicates that obesity causes the initiation of a proinflammatory state that extends to the adipose, liver, and muscle tissues [105, 106]. As a consequence of this, the levels of proinflammatory molecules are increased, and the inflammatory signalling pathways activate [105]. Obesity increases the release of proinflammatory cytokines such as interleukin 6 (IL-6) [107], and tumor necrosis factor alpha (TNF-α) from adipose tissue thereby inducing lipolysis, enhancing cytokine release, and promoting insulin resistance [108, 109], an additional complication of metabolic dysfunction. These results indicate that obesity induces a high lipid, systematic inflammatory environment that may be unfavourable to ovarian function.

Some of the physiological conditions that are strongly correlated to obesity are high levels of oxidative stress (ER stress and mitochondrial dysfunction), generalized low-grade inflammation, and impaired immune response. Evidence shows that obesity leads to increased levels of intracellular lipids, which are highly reactive oxidative species that cause damage to the ER, altering its state and function. This initiates a cascade of molecular events resulting in cell death, known as lipotoxicity [110]. Similarly, oxidative stress is one of the causes of the mitochondrial dysfunction associated to obesity in skeletal muscle [111].

The accumulation of adipose tissue and/or excessive perigonadal fat around the reproductive organs observed in obese individuals may increase inflammation and oxidative stress in the ovaries through the release of these substances, dysregulating the expression of cytoprotective Heat Shock proteins (HSP) and impacting ER and mitochondrial function, which can potentially affect reproductive function (***Figure 1.4***).

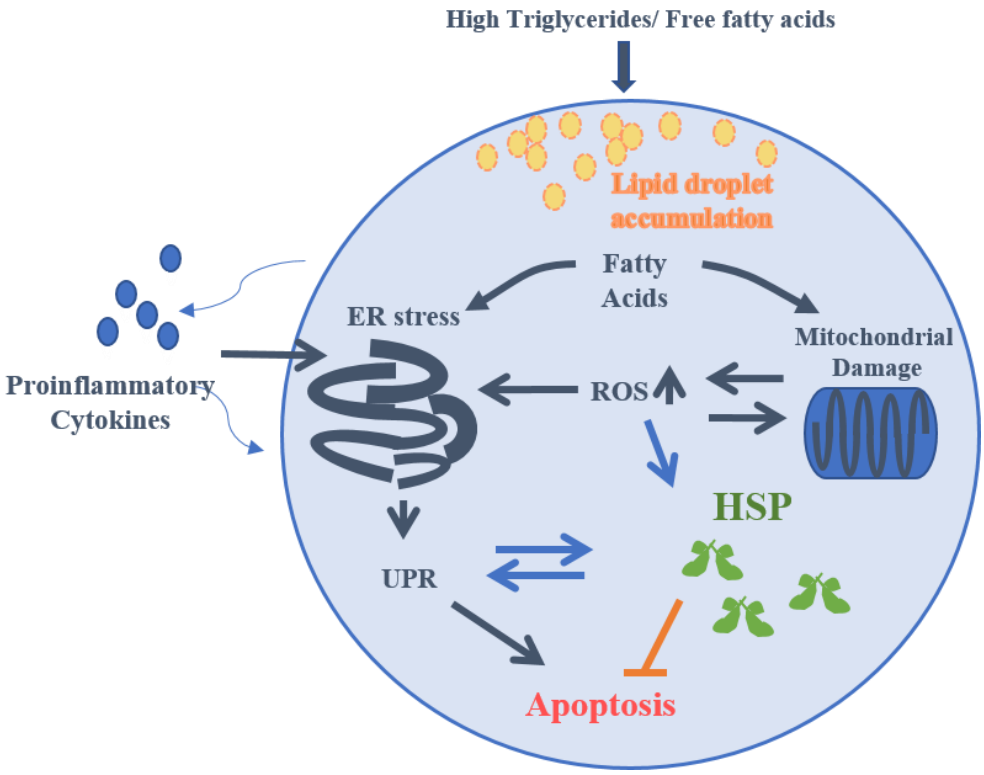

Figure 1.4 Cellular stress caused by obesity.

Proposed mechanism by which obesity may impact stress pathways in ovarian cells. Higher levels of triglycerides and free fatty acids in the ovarian environment leads to increased accumulation of cellular lipid, which in turn damages organelles like mitochondria and the ER and induces the release of proinflammatory cytokines. These events increase the amount of reactive oxygen species (ROS) produced by the mitochondria and initiate the unfolded protein response (UPR) by the ER. These in turn trigger the apoptotic pathways that will culminate in cellular death. Cytoprotective mechanisms such as HSP can restore cellular homeostasis and prevent apoptosis. HSP expression is increased in response to the accumulation of denatured or damaged proteins due to cellular stress, they will either re-fold proteins into their native configuration or tag them for elimination, this way reversing the UPR and stopping apoptosis.

1.3 Heat Shock Proteins

Heat Shock Proteins or HSP are some of the oldest proteins in living organisms. For many years they have been studied for their function as molecular chaperones, protecting the cell against the consequences of stress. However, evidence is emerging that they are also important to our reproductive health.

1.3.1 What are heat shock proteins?

The Heat Shock Response (HSR) was first discovered by Ritossa in 1962, in the chromosomes of salivary glands in *Drosophila* after exposure to elevated temperatures [112]. The HSR is the consequence of the expression of HSP [113]. These proteins exist in every living organism, not only in animals but also in the plant, fungi, protist, eubacteria and archaebacterial kingdoms. They are highly conserved proteins, not only in their amino acid and nucleotide sequence, but also in their function and (partly) their antigen structure [114, 115]. The major function of HSP is that of molecular chaperones [116]. They actively participate in the folding, transport and assembly of intracellular proteins; as well as intervening in the regulation of apoptotic pathways, where they play a key role in the fate of denatured proteins which cannot be re-folded or repaired [117]. However, they can perform a much wider range of functions due to the action of modulators or co-chaperones [118]. These proteins constitute a very important cell survival mechanism under unfavourable conditions.

We can differentiate two main types of HSP: on one hand there are gene products that are mostly induced by specific stimuli (stress-inducible or HSP), and on the other hand there are those protein products that are mostly expressed constitutively (constitutive, cognate or HSC) [119]. They are ubiquitous in all tissues, although some present isoforms that are only expressed in a specific tissue [120] (i.e. HSPA1L, the testis-specific isoform of HSPA1A [121]). HSP were traditionally thought to have an intracellular location. But it is now known that this is not always the case, as they can have intra- or extracellular localisation (reviewed in De Maio et al, 2013 [122]). Some of them can be found on the surface of normal [123] and tumor cells [124], or they can be excreted into the extracellular space by necrotic and non-necrotic cells alike and can be found in the serum under both physiological conditions [125] and disorders [126].

Heat stress is not the only stimulus that produces expression of HSP, but they are also involved in several processes essential for cellular function under both physiological and pathological conditions [127]. As an example, the sex steroid receptors are found in heterocomplexes that

contain HSP, including association with HSPA1B, which functions as a chaperone for the correct folding of the hormone binding domain of receptors into their high affinity steroid binding configuration [128]. HSPA1B has a role in both steroidogenesis and trafficking of steroid receptors, so much that expression of estrogen receptor alpha has been shown to protect female mice against the adverse effect of a high fat diet, which appears to be mediated by increased levels of this HSP, together with increased circulating adiponectin and adipogenic capacity [129]. On the other hand, HSP90AA1 has been shown to be an inhibitor of ovarian aromatase and estrogen production in bovine oocytes [130].

HSP70 is the most conserved family within the HSP (see Appendix 1 for gene information on members of the HSP70 family). The "HSP70 machine" is an ATP-dependent chaperone complex. The core protein is an HSP70 family protein, and associates with two co-chaperones: a DNAJ (involved in client binding), and a HSPH (or Nucleotide Exchange Factor, NEF). It has been proposed that the DNAJ co-chaperone is the key to the functional diversity of the chaperone machine [131]. The HSP70 chaperone machine, especially HSPA1A/B and their co-chaperone DNAJB1, are the strongest stress-inducible proteins [119]. The HSP70 family contains the two most studied of the HSP: HSPA1A and HSPA1B. These two proteins are the product of two genes, HSPA1A and HSPA1B, whose products only differ by two amino acids and which are believed to be fully interchangeable proteins [127]. This is the reason why in many cases they are referred to as HSPA1A/B or HSP70i. They are involved in a wide variety of processes, but they have been the focus of extensive research for their involvement in cancerous processes, especially for their high expression in cancer cells that are resistant to some drugs, which makes them a highly studied chemotherapeutic target. It has been observed that they can be used as a marker of cellular damage in reproductive organs [132]. The research group led by Chowdhuri has published a few studies showing that HSPA1A/B expression can be used as a marker for cellular damage in the female reproductive organs of *Drosophila*, after exposure of the flies to chemicals [132-134]. A similar observation was made in mammals, where high levels of serum HSPA1A were found to denote ovarian damage due to ROS in rats [135]. In this study, researchers reported that injection with Prostaglandin F2alpha ($PGF_{2\alpha}$), an initiator of luteal regression, caused an increase in HSPA1A/B in the CL of immature rats 9 days after superovulation induction [135]. $PGF_{2\alpha}$ had been previously shown to produce superoxide radicals, lipid peroxidation and membrane breakdown [136]. Oxidative agents can cause site-specific damage in the cells, which would explain the expression of HSPA1A/B.

The HSP90 family is the second highest conserved and expressed after the HSP70 family (see Appendix 2 for gene information on members of the HSP90). Similarly to HSP70, HSP90 proteins constitute the core of a chaperone machine, and require the collaboration of co-chaperones [137]. In mammals, the most studied are HSP90AA1 and HSP90AB1, which are two cytosolic isoforms of the same gene [138]. Although they share an 86% homology, they are not interchangeable [139], therefore must have different functions and regulation processes.

1.3.2 Regulation of Heat Shock Proteins

Due to the importance of the HSR as a cell survival mechanism, it is not surprising to find that it has several levels of regulation. The first level of regulation is the induction of the HSR. There are several conditions that can initiate it, but it is the damage to cellular proteins that seems to be the general trigger.

The first step is the activation of the Heat Shock Factors (HSF), which are transcription factors that regulate the gene expression of downstream HSP. There are four HSF, from which three have been found in mammals (HSF 1, 2 and 4) [140, 141]. Of these, HSF1 and HSF2 seem to be of critical importance in reproduction [142-144]. The development of double knockout models has shown that the different HSF interact together to regulate complex processes such as cellular differentiation, by way of regulating the expression of not only HSP but also other non-HSP such as the fibroblast growth factor [145, 146]. HSF1 has been showed to be a major maternal factor, while HSF2 is barely detectable in the mouse oocyte cytoplasm [143], although it seems to play an important role in organogenesis in the mouse embryo [147]. Maternal factors found in the oocyte's cytoplasm are essential for oocyte competence, especially during fertilization, as they are thought to remodel the paternal genes and trigger their expression [148].

HSF1 is generally localized in the cytoplasm as monomers, which become activated upon the presence of denatured proteins as a consequence of stress (***Figure 1.5***). They form homo-trimers and undergo phosphorylation, after which they translocate into the nucleus and now have the capacity to bind DNA. Once inside the nucleus, these trimers form distinctive large granules [149]. HSF bind to inverted –NGAAN sequences in the promoter region [150], called Heat Shock Elements (HSE), up regulating transcription of mRNA that will result in the expression of HSP. These HSP will induce their chaperone function and bind to the denatured proteins to try and fold them back into their native configuration and recover functionality. If this is not achieved, then the denatured protein is tagged for elimination by the proteasome machine or through autophagy processes. Once the molecular chaperones have finished their task, i.e. there are not anymore denatured proteins to bind to, they bind to other free HSF1

monomers in the cytoplasm, preventing their activation and stalling the transcription and production of more HSP, therefore ending the HSR [149].

While HSF1 had already been reported to be very abundant in mouse oocytes [143], previous studies indicated that inducible HSPA (HSPA1A/B) were expressed at very low levels [151]. Using a HSPA1B-Luc transgene in a knock-out mouse model for HSF1, Le Masson and Christians reported that in both HSF1 depleted oocytes and embryos, the levels of activity of the transgene were significantly reduced [142]. This study showed that HSF1 is the regulator of HSPA1B in oocytes and early embryos [142].

From knockout mouse models we know that Hsf1 $^{-/-}$ female mice are infertile, and it is at best difficult to collect properly fertilized oocytes from them [142]. The first HSF1 knockout phenotype was described by Xiao et al in 1999 [152], with both its endotoxemia-induced survival and female infertility being further characterized by Christians [153]. Hsf1$^{-/-}$ oocytes show several deviations from the normal development process, as shown by a delay of the GVBD and disappearance of the nucleus, a partial block in Metaphase I (MI), and the display of abnormal asymmetric division. These are the result of the low HSP90AA1 expression, that is directly regulated by HSF1, since the same effects are observed in wild type oocytes (Hsf1 $^{-/+}$ and Hsf1 $^{+/+}$) treated with an HSP90AA1 inhibitor, 17AAG [151]. These defects originate in oogenesis, as demonstrated by the fact that preovulatory Hsf1$^{-/-}$ oocytes display ultrastructural abnormalities (Golgi apparatus, cortical actin-cytoskeleton, cytoplasmic aggregates), as well as mitochondrial dysfunction, in conjunction with markedly increased production of reactive oxygen species (ROS) [144].

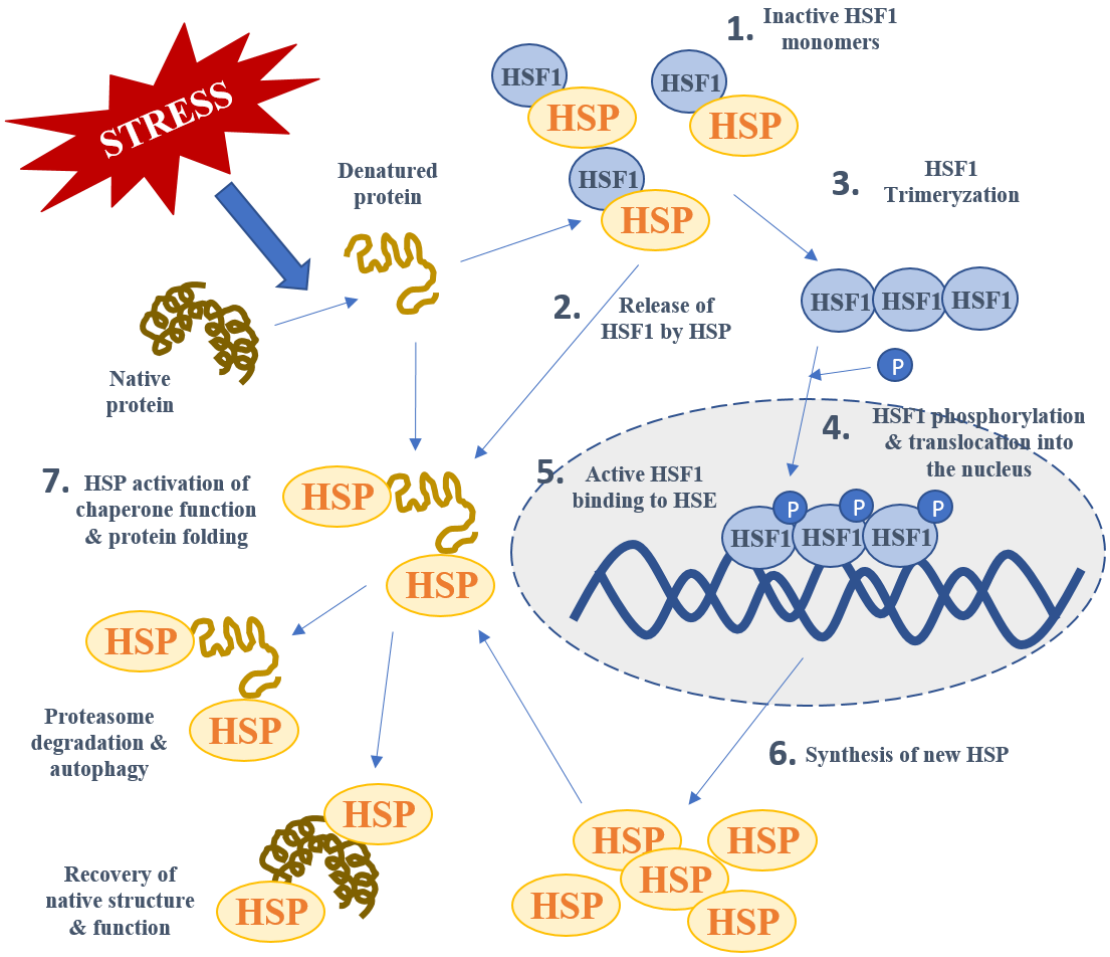

Figure 1.5 Induction of the HSR by HSF1 in mammalian cells.

Diagram showing the basic molecular mechanisms of the HSR. Inactive HSF1 monomers are bound to HSP in the absence of stress (1). Damaged or denatured proteins cause HSP to release HSF1 (2), which then aggregates into trimers (3) and is phosphorylated upon activation, translocating to the nucleus (4). Here, active HSF1 binds to the DNA via the HSEs (5) and up-regulates the expression of new HSP (6), which will either refold proteins to their functional state or tag them for degradation (7). In the absence of denatured proteins, HSP are free to bind to HSF1 again, inactivating the transcription factor and stopping HSP synthesis.

1.3.3 Heat Shock Proteins in fertility

The presence and role of HSP in human reproduction has been documented from gametogenesis to embryo development [154], to birth [155]. The involvements of HSP in the processes of spermatogenesis and male fertility have been the focus of extensive research whereas relatively little is known of their roles in females (see Tables 1-A and 1-B). Recently, the focus on the role of these proteins on female reproduction seems to be increasing, as proteomic research gives new insights on their connection to fertility [156-168]. Expression of members of the HSP superfamily has been observed in different tissues of the human female reproductive system such as the endometrium, cervix and oviduct [169-176]. Although most of these studies already hinted at the existence of profiles of expression of heat shock proteins that correlate with the menstrual cycle long ago, again it is often unclear which specific gene product they are referring to. HSPA1A and HSPA8 were observed in tissue samples from human ectocervix and endometrium, where they were preferentially expressed in non-proliferating, differentiated epithelial cells [170]. The expression of both proteins in the ectocervix has been shown to be greater in the stratum cornea than in the stroma [170].

Analysis of endometrial tissue has showed a similar gradient, with the expression of HSPA1A and HSPA8 in the glandular epithelia [170], increasing during the proliferative phase [169, 170, 173] with a peak after ovulation [171]; although observations on HSPA1A expression have not always been consistent [173]. Evidence exists that expression of these two proteins is higher in the endometrium of infertile women when compared to a fertile control group [169].

In the mouse, proteomic analysis of the ovary in an ovarian cycle model has shown that there is differential expression of HSPA5 and HSPA8 throughout the cycle, with a peak during ovulation [158]. Other stress proteins that showed a change in expression levels (but not statistically significant) were HSPA4, HSPA9, SERPINH1, HSP90AB1, HSP90B1, and HSP60 [158].

From these examples, the expression of HSP does not remain static through time, but it is rather dynamic, with levels of protein expression fluctuating along time and structures. Variable levels of expression are observed for the different proteins in correspondence with each phase throughout the menstrual cycle as well as during normal and abnormal pregnancies [155]. They can also vary due to disease and/or immune responses.

Therefore, it is not surprising that expression of HSP occur during both female and male gametogenesis (detailed in Tables 1-A and 1-B for members of the HSP70, HSP90 and

chaperonin families). The specific stage of maturation of mammalian oocytes determines their ability to induce a heat shock response [177]. In porcine oocytes, there is constitutive expression of the whole HSP70 machinery, throughout the process of follicle development in both somatic cells and oocytes, with HSPA1A/B at the core of this system, guiding the conformation of newly synthesized proteins [178]. In porcine oocytes, the HSP70 machine is fully active in the absence of environmental stress, where it maintains protein homeostasis, facilitating protein folding and suppressing protein aggregation [178]. This is due to fully-grown oocytes storing a larger amount of matured proteins, in contrast to their lower synthesis of nascent polypeptides [179-181].

It was previously thought that there was no expression of HSPA1A/B in oocytes, and that HSPA8, HSPA5 and HSPA9 were the only ones constitutively expressed throughout oogenesis [182]. Earlier research on the heat shock response in oogenesis showed that pre- and post-ovulatory mouse oocytes could not induce the expression of HSPA1A/B at elevated temperatures [183, 184]. Similar results were reported for other mammalian species [180, 185]. HSP70 family members were not detected in synaptonemal complexes of pachytene oocytes from fetal mouse ovaries, in contrast to their detection in spermatocytes [186]. It was therefore concluded that oocytes were unable to express inducible HSP70, but just showed expression of cognate members of the family [182]. Pennarossa et al, just in 2012 argued that these in-vitro studies had not recapitulated the physiological architecture of the ovary, by using isolated COCs or denuded oocytes [178]. In addition to this, it was not until 2006 that a differential method for the immunohistochemical detection of the inducible HSPA1A and HSPA1B in paraffin-embedded human tissue was published; reporting that thermal antigen retrieval in citric buffer was critical [187]. There was a similar view on HSP90 being constitutively expressed, as acute heat stress did not alter the levels of HSP90AB1 in bovine ovarian follicular fluid [188].

Gene Name (Adapted from [127])	Tissue expression (Cellular localization) (adapted from [189])	General function and roles in the gonads and/or embryo (where known)	Specific function and/or localization to the Ovary/Follicle/COC (where known)
HSPA1A	Ubiquitous (cytosol)	Stress inducible chaperone, core of the HSP 70 chaperone machine	Localized to the oolemma of ovulated mouse oocytes [167]
HSPA1B	Ubiquitous (cytosol)	Stress inducible chaperone, core of the HSP 70 chaperone machine, thought to be completely interchangeable with HSPA1A	Localized to the oolemma of ovulated mouse oocytes [167]
HSPA1L	Testis (cytosol)	HSPA1A testis-specific isoform, stress inducible, post-meiotic spermatogenesis	Not found in female reproductive organs.
HSPA2	Testis /Ubiquitous (cytosol/nucleus)	Stress inducible, CDC2 kinase chaperone, spermatogenesis	Absence of HSPA2 expression during oogenesis might indicate essential differences between male and female meiotic apparatus [189].
HSPA5	Ubiquitous (Endoplasmic Reticulum)	Glucose regulated, highly expressed in preimplantation embryos [190], High expression in embryonic heart and inducible by hypoglycemia [191].	Localized to the oolemma of ovulated mouse oocytes [167]
HSPA6	Brain, Liver, Ovary, Saliva (cytosol/nucleus)	Completely stress Inducible	Unknown
HSPA7	Unknown (unknown)	Stress inducible, considered a pseudogene, may be homologous to HSPA6.	Unknown

Table 1-A. Summary of data on members of the HSP70 family and their reproductive role.

Gene Name (Adapted from [127])	Tissue expression (Cellular localization) (adapted from [189])	General function and roles in the gonads and/or embryo (where known)	Specific function and/or localization to the Ovary/Follicle/COC (where known)
HSPA8	Ubiquitous (cytosol/nucleus)	House-keeping protein	Constitutive expression in the ovary
HSPA9	B cell, brain, liver, ovary, platelet, saliva (Mitochondria)	House-keeping protein. Primary in mitochondria but also found in ER, plasma membrane and cytoplasmic vesicles.	Unknown
HSPA12A	Endothelia, brain, heart, kidney, muscle, testis (unknown)	Unknown	Unknown
HSPA12B	Endothelia, ubiquitous (unknown)	Unknown	Unknown
HSPA13	Ubiquitous/unknown (microsomes)	House-keeping protein	Unknown
HSPA14	Ubiquitous (ribosome associated complex)	Unknown	Unknown

Table 1-B (cont.). Summary of data on members of the HSP70 family and their reproductive role.

HSP Superfamily	Gene Name (Adapted from [127])	Tissue expression (Cellular localization) (adapted from [189])	General function and roles in the gonads and/or embryo (where known)	Specific function and/or localization to the Ovary/Follicle/COC (where known)
HSP90	HSP90AA1	Testis, Ovary	Spermatogenesis. 86% homologous to HSPCB (Hsp90β) but not interchangeable, highly expressed in preimplantation embryos [139].	Major HSP expressed by mature follicles and is down-regulated by the absence of HSF1 [151]. Key for oocyte maturation [151].
	HSP90AA2	Ubiquitous (cytosol)	Unknown. Considered a pseudogene.	Unknown
	HSP90AB1	Ovary (cytoplasm)	High expression in the mouse pre-implantation embryo [192]. Essential for trophoblast differentiation and placental labyrinth development [193].	Localized to the ovary, and highly expressed in granulosa cells [151]
	HSP90B1	Ubiquitous (ER)	Absence causes peri-implantation embryonic lethality [194, 195].	Localized to the oolemma of ovulated mouse oocytes [167, 196].
	TRAP1	Skeletal muscle, liver, heart, brain, kidney, pancreas, lung, placenta and bladder [197] (mitochondria)	Absence causes embryonic death, either before blastula or during gastrulation [198].	Unknown
Chaperonins	HSPD1	Ubiquitous (Mitochondria), ovary	Forms a 2 step-folding mechanism with HSPE1 in normal eukaryotic cells, known as the HSP60/10 protein folding machine [199]	Expression in oocyte only in pre-antral follicles, whereas positive expression in all the cell types of antral follicles, in both human and mouse [200].
	HSPE1	Ubiquitous (Mitochondria), ovary	Downregulated expression in PCOS ovaries, except in theca cells [163]	

Table 1-C. Summary of data on members of the HSP70 family and their reproductive role.

1.3.4 Ovarian cellular stress in response to obesity

Obesity is associated with increased circulating lipids and the intracellular accumulation of particular lipids, such as the saturated fatty acid palmitic acid. In non-adipose tissues such as liver and muscle, this triggers lipotoxicity, a process involving ER stress, mitochondrial dysfunction and ultimately apoptosis [201]. Recently this increase in lipid content has been observed in the ovary in response to obesity, and more specifically in the cells of ovarian follicles. Some studies have reported that both GV [97, 102] and ovulated COC [97] collected from female mice fed obesogenic diets, often high in saturated fats, had a significantly higher neutral lipid content when stained using the fluorescent lipid dye BODIPY 493/503. It has also been previously shown [97, 100, 202] that these increases in lipid levels are associated with lipotoxicity responses, such as ER stress gene expression and altered mitochondrial function, in COCs and oocytes respectively. Interestingly, these changes in oocytes were also associated with a reduction in mitochondrial DNA (mtDNA) copy number in blastocysts and fetal tissue [100].

The regulation of immune pathways in normal ovarian function is yet not clearly understood, even though some processes in the ovary, especially ovulation, have been extensively characterised as controlled inflammation (reviewed in Richards et al. 2002 [203]). Even less is known about how these pathways are influenced by obesity, or conversely, how obesity-induced inflammation affects ovarian function. Nteeba et al [204] had also found elevated expression levels of Tnfa, and members of the TNFa pathway, such as REL-associated protein (RELA) and the Inhibitor of nuclear factor kappa-B kinase beta (IKK-β), in the ovaries from obese mice. This was accompanied by increased levels of Il-6 and Nitric oxide synthase 2 (Nos2). Abnormal expression of Il-6 has been implicated in reproductive disorders [205] and ovarian hyperstimulation syndrome [206], especially in conjunction with other proinflammatory cytokines [204]. The influence of obesity on the ovarian follicular environment is also apparent through the changes in follicular fluid composition; with increases in lipid, insulin and glucose being positively correlated with BMI [207].

Not much is known whether obesity dysregulates the HSR or influences HSP function. It has been previously shown that ER stress marker HSPA5, a HSP that specifically localizes to the ER, is up-regulated in GC and COC of mice fed a high fat diet (HFD) [97]. Similarly, higher levels of Hspa1a and Hspa1b were found in granulosa-luteal cells (GLC) and COC from heavier females in a hyperphagia-induced obesity mouse model [100]. These results suggest that obesity induces an imbalance between inflammatory, ER stress and HSR and other intrinsic

pathways in the ovarian cells, and that this could be the driver behind the detrimental effect of obesity on ovarian function. It was demonstrated that heat treatment increased mitochondrial enzyme activity in the skeletal muscle of mice fed a HFD [208]. Young et al proved that HSPA1A/B and HSP90AB1 facilitate import of nuclear encoded proteins into the mitochondria and are thus crucial in maintaining the structural and functional integrity of the mitochondria [209]. In animal models, BALB/c mice kept on a diet high in saturated fat for 4 months, showed higher levels of HSPA1A/B and less resistance to apoptosis in splenic lymphocytes, as opposed to those fed a diet rich in unsaturated fatty acids [210].

Not much is yet known on how inflammation and lipotoxicity caused by maternal diet affect preimplantation embryo development. In the over-fed obese rat model [211], single-embryo microarray analysis showed that genes involved in cell cycle and adhesion, embryonic development, and chromatin and epigenetic regulation were altered in blastocysts from obese females. Further GSEA analysis of gene enrichment based on cellular localization showed reduced levels for 69 transcripts localizing to the mitochondria in embryos from obese females [211]. Real-time qPCR validation confirmed decreased mRNA levels for Mitochondrial Transcription Factor A (TFAM) and Nuclear Respiratory Factor (NRF1). The findings collectively suggest that exposure to maternal obesity produces global disruptions in mitochondrial gene expression in the peri-implantation embryo.

1.4 Inducers of Heat Shock Proteins

There is great interest in finding natural alternatives, or nutraceuticals, for use instead of synthetic drugs. There are some desirable characteristics that should be considered when choosing a potential therapeutic: an easily accessible and abundant source, historic use in aboriginal/native/folk medicine, low toxicity, few or no secondary effects, several beneficial health outcomes (can be used to treat several conditions). This section will focus on two phytochemical compounds that unite all of these traits: Curcumin (natural phenol derived from the Turmeric root, *Curcuma longa*), and Tex-OE (patented extract from the Prickly Pear Cactus, *Opuntia ficus indica* [212]. Another important common feature is that they are chaperone inducers, meaning that administration of these compounds stimulates HSP activity.

The beneficial effects of chaperone inducer treatment for type II diabetes had already been observed in 1999 by Hooper et al [213]; although evidence in a rodent model was not demonstrated until almost a decade later by Chung et al [214]. Hooper et al had shown that a 3

week hot-tub therapy treatment slightly lowered blood glucose levels in diabetic patients [213]. The latter study by Chung et al using an in vivo insulin resistance model showed that the effects of a HFD could be diminished by a weekly heat treatment, despite the decreased HSPA1A levels observed in the HFD group to begin with [214]. These results were confirmed in another in vivo model using rats fed a HFD, where heat treatment prevented the development of glucose intolerance and peripheral insulin resistance [208]. Both studies showed there was an increase of HSPA1 and HSPB1 in skeletal muscle that correlated with a decrease in c-Jun N-terminal kinase (JNK) and IKK-β activation, suggesting an association between increased expression of stress-inducible HSP and the decrease in the inflammation due to insulin resistance after heat shock treatment.

1.4.1 Curcumin

Curcumin is extracted from the rhizome of the turmeric plant (*Curcuma longa*), which belongs to the Ginger family. It is added to food as a spice and natural colorant in many regions, especially in Asia. Curcumin (diferuloylmethane) is a low molecular weight polyphenol that is present in 2-8% in most turmeric preparations, and it is regarded as the most pharmaceutically active of its components [105]. In contrast to Opuntia, there has been extensive research on the medicinal properties of curcumin. This research has reinforced the knowledge on this substance provided by traditional medicine, such as its antioxidant, hypolipidemic and anti-inflammatory properties, which highlight its potential as an anti-diabetic and anti-cancer nutraceutical [215].

Curcumin can be commonly found as a standardized 95% pure curcuminoid preparation. This formula normally contains curcumin (~80%), desmethoxycurcumin (~10-20%), and bisdesmethoxycurcumin (<5%) [105]. Curcumin has no dose-limiting toxicities and has been consumed by humans in dosages up to 12g/d without significant side effects [216].

Curcumin has also been shown to reduce inflammation by inhibiting the activation of JNK and Nuclear factor kB (NF-κB), promoters of inflammation pathways [217, 218]. It has been proven to induce HSPA1 expression [105, 219]. HSPA1 and HSPB1 are known inhibitors of JNK and other pro-inflammatory kinases [220, 221]. This hints to the possibility that an increased expression of these HSP by curcumin treatment can reduce the inflammatory processes caused by obesity. Curcumin has also been reported to reduce macrophage infiltration in the perigonadal adipose tissue [105], which could have indirect beneficial effects on the ovary by lowering the release of proinflammatory cytokines.

Curcumin is shown to improve glucose metabolism [105]. Diet supplementation with curcumin extract has already been reported to reduce adiposity and weight-gain in both genetic obesity [105], and HFD-induced obesity [105, 222] mouse models. However, a recent study from Wang et al (2013) found that the addition of curcumin to a calorie restriction dietary treatment did not have any accumulative effect on the benefits provided by the reduction in caloric intake in a group of diet-induced obese mice [223], suggesting that diet may modulate the efficacy of curcumin treatment.

Obesity, oxidative stress and inflammation are all inter-related. In terms of oxidative stress, obesity and increased levels of ER stress in the adipose tissue are strongly associated [105]. Now, inflammation can contribute to increase this oxidative stress in the adipose tissue of obese individuals [224]. Substances able to reduce this oxidative stress have been found to improve insulin resistance and glycemic status in obesity mouse models [105]. Curcumin caused a reduction in ER stress with increased gene expression of heat shock proteins, among others [105]. Curcumin has also inhibited lipid peroxidation in high-fat-fed hamsters [225]. Curcumin can also increase antioxidant vitamin levels, which are depleted due to high-fat-diet induced oxidative stress [226, 227]. This antioxidant property could be beneficial for protecting against the development of diabetes in obese individuals [228]. A study of diabetic rats showed that curcumin increased the activity of the antioxidant enzyme glutathione peroxidase and decreased oxidative stress [215, 229].

Due to its hydrophobic and highly lipophilic chemical structure, curcumin is poorly absorbed from the gastrointestinal tract into circulation [230]. Some studies have shown that co-supplementation with other substances like piperine or lipids can increase the effectiveness of the absorption of curcumin by the intestine. A very recent study, however, did not find any difference in the co-administration of curcumin and piperine to curcumin alone [223]. Several studies have found that the administration of curcumin in a lipidic environment helped increase its bioavailability, and therefore allow for higher levels of curcumin in blood [231, 232].

Very few studies have explored the effects of curcumin on fertility, and these have mainly been carried out in males. Surprisingly, the treatment of mouse sperm in vitro using purified curcumin extracts reduced motility, capacitation and fertilization rates [233], while male mice injected with a curcumin solution presented a block in spermatogenesis [234]. These results suggest a contraceptive effect of curcumin on male fertility, however the effect of dietary treatment with curcumin on female fertility has not been investigated yet.

1.4.2 Opuntia

Opuntia sp. is a genus of xerophytes that belongs to the *Cactaceae* family. These plants thrive in dry and hot climate, being found in abundance in arid and semi-arid areas around the world where they are traditionally used for several purposes. However, it is their use in natural medicine that has attracted the interest of some researchers. Both the fruit and cladodes of the *Opuntia* species contain high levels of phytochemicals with therapeutic activities, and a very low toxicity [235, 236]. These phytochemicals include amino acids, antioxidants, organic acids, phenols, polysaccharides, and thiols; which have been proven to have a positive effect on health [237]. Of special interest in regards to their potential use in reproductive medicine are the effects against oxidative stress [236, 238, 239], inflammation [239, 240], and hyperglycemia [238], among others described below.

Although the healing properties of the *Opuntia* genus are well known in traditional medicine, there has not yet been much definitive research using the compounds extracted from this cactus. From the *Opuntia* species that have been used in different studies (Table 1-C), only those using *Opuntia ficus indica* measured the effect on the expression of HSP. The extract obtained from this species has been shown to stimulate the expression of heat shock proteins when administered before, during or after the stress [236, 241, 242]. One of them is already patented and commercialised by ICP Ltd. for both animal and human consumption, under the name Tex-OE (or derivatives) [212]. It seems to be a photochemical with high potential to aid in the treatment of affections derived from stress.

Administration of diverse extracts derived from this plant does not cause significant increases in body weight [235, 236, 238, 243], and at the same time reduces plasma lipid levels [235]. This also adds to its potential in the treatment of PCOS and other obesity-related syndromes.

Very little is known about the effect of *Opuntia* extracts on fertility, and the results are contradictory. A study by Bajaj and Gupta, 2012 [243] found lower testosterone levels in male rats treated with a methanol extract from phyllocladodes obtained from another *Opuntia* species, *O. dillenii*, as well as reduced sperm count, motility and suppression of fertility. Similarly, another study showed similar results after oral administration of an *O. elatior* extract [244]. This among other observations led the researchers to conclude that administration of this extract significantly reduced fertility during the treatment. Surprisingly, the addition of an *O. ficus indica* extract to the cryopreservation media has been shown to prevent human sperm DNA fragmentation [245]. However, it hints to the possibility that it can positively affect

hyperandrogenism, characteristic of women with PCOS. Thus, this thesis will be the first to examine the effects of an *Opuntia ficus indica* extract in female fertility.

Opuntia Species	Plant Part	Experimental model	Dosage and administration	Purpose/Object of study	HSP expression profile	Results	Reference
O. ficus indica	Extract powder/ Cladodes	Male BALB/c mice (Mus musculus)	IP injection of extract at 50 mg/Kg Body Weight before or after either 15 or 30 days treatment by Aflatoxin B1 (AFB1)	Evaluation of the hepatoprotective effect of cactus cladode extract on AFB1-induced liver damage as a Hepatocellular carcinoma model in mice	Administration of the extract before or after exposure to the mycotoxin reduced the expression of both Hsp70 and Hsp27 down to the basal levels observed in the control group.	Supplementation of the cladode extract prevented the effects of genotoxicity on liver function, causing a significant reduction on levels of biomarkers for early and late stages of oxidative damage, as well as decreased expression of apoptosis markers.	Nutrition & Metabolism, 2011 [241]
O. ficus indica	Extract powder in 1:1 ethanol: water mixture/ Cladodes	6 wk. old BALB/c mice (Mus musculus)	IP injection of extract at doses of 25, 50 and 100 mg/Kg Body Weight 24h prior to a single IP injection of mycotoxin zearalenone (ZEN) at 40 mg/Kg Body Weight	Evaluation of the safety and efficacy of the cactus cladodes to prevent the oxidative damage produced by the ZEN in kidney and liver	Dose-dependent progressive Inhibition of the induction in the synthesis of Hsp70 and Hsp25 caused by the toxin	Administration of the extract caused a significant reduction on levels of all biomarkers evaluated, representing both early (catalase activity and expression of Hsp70/27) and late (lipid peroxidation and protein carbonyls generation) stages of oxidative damage	Food and Chemical Toxicology, 2008 [236]
O. ficus indica	Tex-OE/ Fruit	Common Carp (Cyprinus carpio L.) fingerlings (5 cm length)	2ul Pro-Tex in 50L of H_2O Exp.Grp. was immersed in solution for 2h before ammonia challenge	Survival after exposure to lethal ammonia toxicity in carps treated with a Tex-OE solution.	Induction of Hsp 40, 70 and 110 in muscle, Hsp 70 in gill	1h-LD50 increased from 50% to 95% 1h-LD100 increased from 0 to 20%	Journal of Fish Diseases, 2012 [242]

Table 1-D. Summary of data on rodent studies using Opuntia

Opuntia Species	Plant Part	Experimental model	Dosage and administration	Purpose/Object of study	HSP expression profile	Results	Reference
O. ficus indica	Tex-OE/ Fruit	Broiler chickens (species not specified)	Dosage of 1 mL/10 kg Biomass in drinking water for 4h on both day 1 and 4 after arrival on farm	To demonstrate the effect of Tex-OE on the growth performance and conversion of broilers	Tex-OE boosts chaperone levels (data not shown)	A positive trend in the use of Tex-OE was observed in the individual trials; however, it was not significantly different due to the variation in the SE between trials. When the data was pooled together, the Feed Conversion Ratio (FCR) was significantly higher in treated groups. Increased live weight (g) and decreased mortality (%) were also observed in the treated groups, although they were not statistically significant.	British Poultry Science, 2014 [246]
O. joconostle	Methanolic extract/ Seeds	Male 8 wk old CD-1 mice (Mus musculus)	Doses of 0.5,1,2&5g/Kg Body Weight once a day for 6 days, plus hypercholesterolemic diet or not	Evaluation of the hypolipidemic effect of the methanolic extract in mice fed a hypercholesterolemic diet	Not determined	Diet supplementation succeeded in reducing cholesterol and LDL-C in hypercholesterolemic mice	Plant Foods Hum Nutr, 2012 [235]
O. humifusa	Lyophilized powder/ Fruits	Female 6 wk old SPF BALB/c mice (Mus musculus)	Standard pellet containing either 1% or 3% (wet weight) of the powder, fed for 3 weeks before induction of carcinogenesis with DMBA in experimental groups	Effects of dietary supplementation with cactus pear fruit on a two-stage model of skin carcinogenesis in mice	Not determined	Diet supplementation reduced papilloma formation and epidermal hyperplasia, suggesting chemoprevention effects	Asian Pacific journal of Cancer prevention, 2012 [239]

Table 1-E (cont.). Summary of data on rodent studies using Opuntia

Opuntia Species	Plant Part	Experimental model	Dosage and administration	Purpose/Object of study	HSP expression profile	Results	Reference
O. dillenii	ODP-Ia/ Cladodes	Male 5 wk old Chinese Kunming mice (Mus musculus)	Intragastric administration of 50, 100 and 200 mg/ Kg Body Weight once a day for 3 weeks after diabetes induction with Streptozotocin (STZ) (IP injection)	Study of the anti-diabetic effects of ODP-Ia in STZ-induced diabetic mice	Not determined	ODP-Ia administration had hypoglycaemic effect, protected against peroxidation damage, aided in the recovery of tissue function, improved the sensitivity of target cells to insulin, and regulated carbohydrate, fat, protein, calcium and phosphate metabolism thus controlling the blood glucose and serum lipid levels	Phytomedicine, 2011 [238]
O. dillenii	100% Methanolic extract/ Cladodes	Male Wistar albino rats (150-180 g) (Rattus norvegicus)	Animals in the experimental groups were treated orally with 50 mg/ Kg body weight per day for 30 days, using distilled water as vehicle. Not specified if administration was through the drinking water or else.	Study of the reversible antifertility and antispermatogenic activity of the methanolic extract in the reproduction of male rats	Not determined	Sperm density and motility, as well as conception and birth rates, were significantly decreased on treated groups. Histological alterations were observed, showing degradation of spermatogenesis. Testosterone levels were significantly reduced on treated animals. In the biochemical analysis of the reproductive organs: protein, glycogen, SOD and GSH levels were reduced. In contrast, lipid peroxidation and cholesterol levels in these organs were significantly increased. In both body and organ weight, and haematological analysis, no significant changes were observed between the treated and control groups	Andrologia, 2012 [243]
O. dillenii	Lyophilized preparation from a crude aqueous extract/ Fruits	Male Sprague-Dawley rats (120-150 g) (Rattus norvegicus) and male 8 wk Swiss albino mice (Mus musculus)	IP injection of solution at 50, 100, 200 and 400 mg/Kg, followed by either writhing test, hot-plate test or carrageenan-induced paw edema	Evaluation of the antinociceptive activity of the extract using the writhing test and the hot-plate test, plus investigation of its anti-inflammatory effect using the carrageenan-induced edema test.	Not determined	Administration of the aqueous extract exhibited central analgesic properties, associated with anti-inflammatory effects on acute inflammatory processes	Journal of Ethnopharmacology, 1999 [240]

Table 1-C (cont.). Summary of data on rodent studies using Opuntia

1.5 SUMMARY

The prevalence of obesity is a worrying trend that currently affects half of the women in Australia. Obesity is associated with infertility and pregnancy complications, as it has a negative effect on ovulation and pregnancy rates. Increased BMI is associated with a pro-inflammatory response which is characterized by mitochondrial dysfunction and activation of stress pathways, such as ER stress and HSR, at the cellular level.

To elucidate the mechanisms by which obesity influences the ovarian environment, I investigated the expression of HSP proteins during follicle maturation and ovulation. Then, I explored how factors such as increased BMI, hyperandrogenism and diet affects stress pathways in ovarian cells, as well as oocyte competence. Finally, I used chaperone-inducing micronutrients to determine if the therapeutic activation of HSP can reverse the impact of obesity on female fertility (***Figure 1.6***).

1.6 HYPOTHESIS AND AIMS

1.6.1 SPECIFIC HYPOTHESIS AND AIMS

Hypothesis 1: Heat Shock Protein cytoprotective chaperones have distinct expression and localization in the mouse ovary across follicle growth and oocyte maturation.

To address this hypothesis the following aims were completed:

- Characterise the expression and localization of HSF1 and selected HSP in the mouse ovary during ovarian stimulation, with special attention to expression in ovarian preovulatory follicular cells, cumulus cells and oocytes.
- Measure gene expression of HSF1 and selected HSP in granulosa, luteal and cumulus cells at different time points during ovarian stimulation.

Hypothesis 2: Obesogenic hormones and diets distinctly disrupt female metabolism and impact ovarian function. This occurs in association with ovarian cell dysregulation of stress pathways, especially the Heat Shock Response in somatic cells. Obesity affects oocyte developmental competence, irrespectively of type of obesogenic insult.

To address this hypothesis the following aims were completed:

- Develop and characterize the metabolic and reproductive phenotypes of three different mouse models of obesity: 1) Dihydrotestosterone-induced obesity model of Polycystic Ovary Syndrome; 2) High fat diet-induced obesity model; and 3) High fat High sugar-induced obesity model.
- Determine whether obesity dysregulates stress pathways in ovarian cells, by measuring gene expression of HSP and ER stress markers.
- Determine whether obesity decreases oocyte quality, by assessing ovulation and mitochondrial profile of ovulated oocytes.
- Determine whether obesity negatively impacts oocyte developmental potential, by assessing preimplantation embryo development and embryonic mitochondrial activity.

Hypothesis 3: Ovarian function and oocyte developmental potential can be restored by dietary intervention with chaperone-inducing compounds.

To address this hypothesis the following aims were completed:

- Develop dietary treatments containing Curcumin and Opuntia to administer to obese mice and characterise the effect of the intervention on the obesity phenotype.
- Determine whether treatment with Curcumin will improve ovarian function, by analysing ovulation and oocyte quality via assessment of early embryonic development and mitochondrial activity of mature oocytes and blastocyst embryos.
- Determine whether treatment with Opuntia will improve ovarian function, by analysing ovulation, ovarian somatic cell gene expression and oocyte quality via assessment of early embryonic development and mitochondrial activity of mature oocytes and blastocyst embryos.

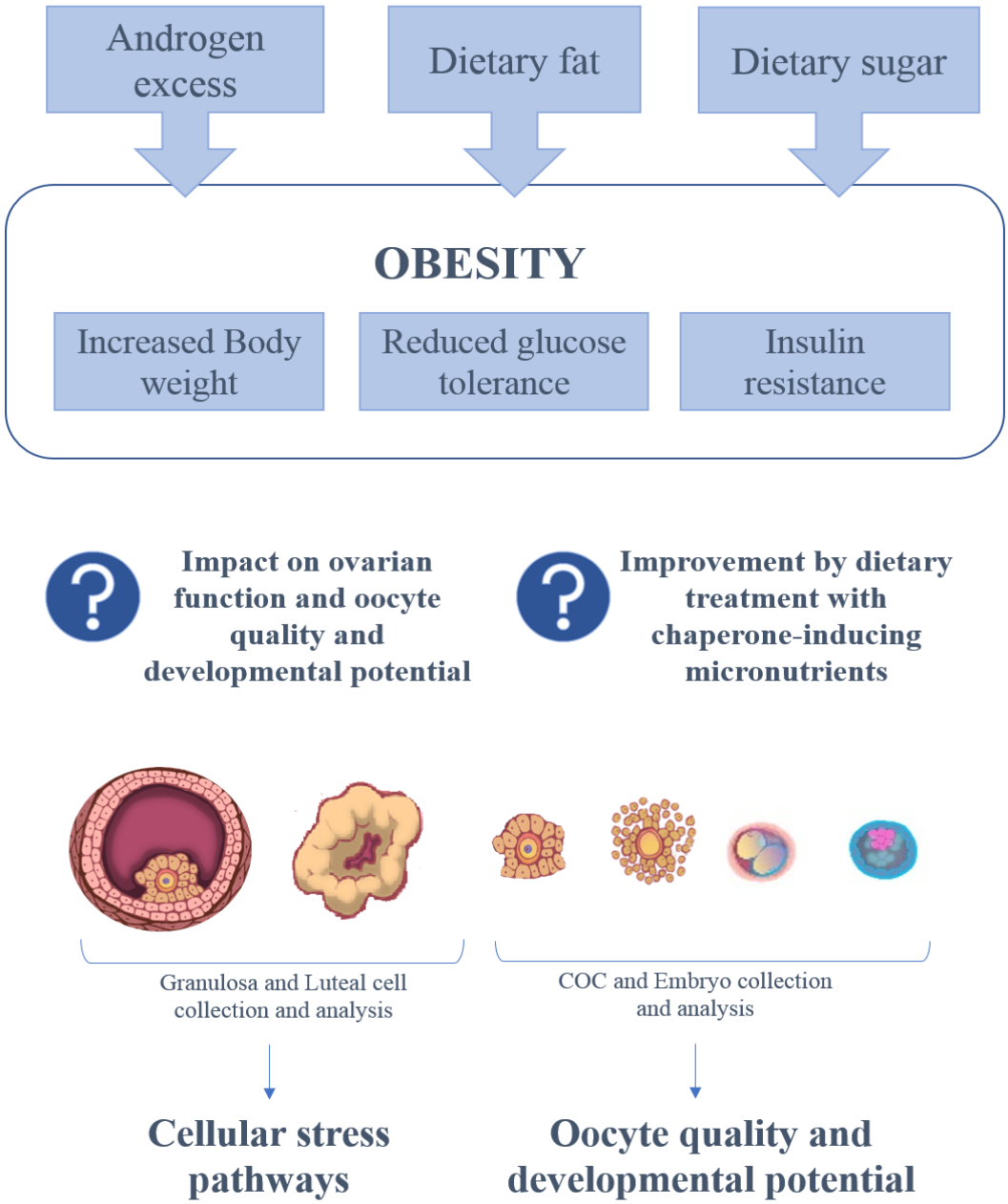

Figure 1.6 Investigating the impact of obesity and chaperone-inducing micronutrients on ovarian cells.

Factors such as increased body weight, hormonal imbalance and the type of diet shape the obesity phenotype, and this could have consequences on female reproduction. However, how these factors affect ovarian function is not clearly understood. To explore this topic, this thesis shows how key ovarian cells and structures, such as granulosa and luteal cells, respond to cellular stress caused by obesity. Moreover, it presents an investigation on oocyte quality markers during growth and maturation in both MI and MII oocytes, and their developmental potential after fertilization by analysing embryonic development at the 2-cell and blastocyst stages. Finally, it demonstrates that dietary intervention with specific chaperone-inducing micronutrients can mitigate the effects of obesity in female fertility.

1.7 References

1. Berkholtz CB, Shea LD, Woodruff TK. Extracellular matrix functions in follicle maturation. In: Seminars in reproductive medicine, vol. 24: NIH Public Access; 2006: 262.
2. Peters H, Byskov AG, Himelstein-braw R, Faber M. Follicular growth: the basic event in the mouse and human ovary. Journal of Reproduction and Fertility 1975; 45:559-566.
3. Adhikari D, Liu K. Molecular mechanisms underlying the activation of mammalian primordial follicles. Endocrine reviews 2009; 30:438-464.
4. McGee EA, Hsueh AJ. Initial and cyclic recruitment of ovarian follicles. Endocrine reviews 2000; 21:200-214.
5. Grive KJ, Freiman RN. The developmental origins of the mammalian ovarian reserve. Development 2015; 142:2554.
6. Hartshorne G, Lyrakou S, Hamoda H, Oloto E, Ghafari F. Oogenesis and cell death in human prenatal ovaries: what are the criteria for oocyte selection? Molecular Human Reproduction 2009; 15:805-819.
7. Molyneaux KA, Stallock J, Schaible K, Wylie C. Time-lapse analysis of living mouse germ cell migration. Developmental biology 2001; 240:488-498.
8. Anderson R, Copeland TK, Schöler H, Heasman J, Wylie C. The onset of germ cell migration in the mouse embryo. Mechanisms of development 2000; 91:61-68.
9. Konishi I, Fujii S, Okamura H, Parmley T, Mori T. Development of interstitial cells and ovigerous cords in the human fetal ovary: an ultrastructural study. Journal of anatomy 1986; 148:121.
10. Pepling ME, Spradling AC. Female mouse germ cells form synchronously dividing cysts. Development 1998; 125:3323-3328.
11. Wilhelm D, Yang JX, Thomas P. Mammalian sex determination and gonad development. In: Current topics in developmental biology, vol. 106: Elsevier; 2013: 89-121.
12. Bowles J, Knight D, Smith C, Wilhelm D, Richman J, Mamiya S, Yashiro K, Chawengsaksophak K, Wilson MJ, Rossant J. Retinoid signaling determines germ cell fate in mice. Science 2006; 312:596-600.
13. Bullejos M, Koopman P. Germ cells enter meiosis in a rostro-caudal wave during development of the mouse ovary. Molecular Reproduction and Development: Incorporating Gamete Research 2004; 68:422-428.
14. Menke DB, Koubova J, Page DC. Sexual differentiation of germ cells in XX mouse gonads occurs in an anterior-to-posterior wave. Developmental biology 2003; 262:303-312.
15. Hirshfield AN. Heterogeneity of cell populations that contribute to the formation of primordial follicles in rats. Biology of reproduction 1992; 47:466-472.
16. Gougeon A. Regulation of ovarian follicular development in primates: facts and hypotheses. Endocrine reviews 1996; 17:121-155.
17. Hirshfield AN. Development of Follicles in the Mammalian Ovary. In: Jeon KW, Friedlander M (eds.), International Review of Cytology, vol. 124: Academic Press; 1991: 43-101.
18. Norris DO, Lopez KH. Chapter 4 - The Endocrinology of the Mammalian Ovary. In: Norris DO, Lopez KH (eds.), Hormones and Reproduction of Vertebrates. London: Academic Press; 2011: 59-72.
19. Hsueh AJ, Billig H, Tsafriri A. Ovarian follicle atresia: a hormonally controlled apoptotic process. Endocrine reviews 1994; 15:707-724.

20. Cattanach B, IDDON CA, Charlton H, CHIAPPA SA, Fink G. Gonadotrophin-releasing hormone deficiency in a mutant mouse with hypogonadism. Nature 1977; 269:338.
21. Dierich A, Sairam MR, Monaco L, Fimia GM, Gansmuller A, LeMeur M, Sassone-Corsi P. Impairing follicle-stimulating hormone (FSH) signaling in vivo: targeted disruption of the FSH receptor leads to aberrant gametogenesis and hormonal imbalance. Proceedings of the National Academy of Sciences 1998; 95:13612-13617.
22. Abel MH, Wootton AN, Wilkins V, Huhtaniemi I, Knight PG, Charlton HM. The effect of a null mutation in the follicle-stimulating hormone receptor gene on mouse reproduction. Endocrinology 2000; 141:1795-1803.
23. Kumar TR, Wang Y, Lu N, Matzuk MM. Follicle stimulating hormone is required for ovarian follicle maturation but not male fertility. Nature genetics 1997; 15:201.
24. Rankin T, Familari M, Lee E, Ginsberg A, Dwyer N, Blanchette-Mackie J, Drago J, Westphal H, Dean J. Mice homozygous for an insertional mutation in the Zp3 gene lack a zona pellucida and are infertile. Development 1996; 122:2903-2910.
25. Rankin T, Talbot P, Lee E, Dean J. Abnormal zonae pellucidae in mice lacking ZP1 result in early embryonic loss. Development 1999; 126:3847-3855.
26. Rankin TL, O'Brien M, Lee E, Wigglesworth K, Eppig J, Dean J. Defective zonae pellucidae in Zp2-null mice disrupt folliculogenesis, fertility and development. Development 2001; 128:1119-1126.
27. Magoffin DA. Ovarian theca cell. The international journal of biochemistry & cell biology 2005; 37:1344-1349.
28. Woodruff TK, D'Agostino J, Schwartz NB, Mayo KE. Dynamic changes in inhibin messenger RNAs in rat ovarian follicles during the reproductive cycle. Science 1988; 239:1296-1299.
29. Edson MA, Nagaraja AK, Matzuk MM. The mammalian ovary from genesis to revelation. Endocrine reviews 2009; 30:624-712.
30. Rao MC, Midgley Jr AR, Richards JS. Hormonal regulation of ovarian cellular proliferation. 1978.
31. Elvin JA, Matzuk MM. Mouse models of ovarian failure. Reviews of reproduction 1998; 3:183-195.
32. Richards JS, Russell DL, Ochsner S, Hsieh M, Doyle KH, Falender AE, Lo YK, Sharma SC. Novel signaling pathways that control ovarian follicular development, ovulation, and luteinization. Recent Prog Horm Res 2002; 57:195-220.
33. Stocco C, Telleria C, Gibori G. The Molecular Control of Corpus Luteum Formation, Function, and Regression. Endocrine Reviews 2007; 28:117-149.
34. Mason HD, Martikainen H, Beard RW, Anyaoku V, Franks S. Direct gonadotrophic effect of growth hormone on oestradiol production by human granulosa cells in vitro. J Endocrinol 1990; 126:R1-4.
35. Vanderhyden BC, Tonary AM. Differential Regulation of Progesterone and Estradiol Production by Mouse Cumulus and Mural Granulosa Cells by a Factor(s) Secreted by the Oocyte. Biology of Reproduction 1995; 53:1243-1250.
36. Fauser B, van Heusden AM. Manipulation of human ovarian function: physiological concepts and clinical consequences. Endocrine reviews 1997.
37. Moenter SM, Caraty A, Karsch FJ. The estradiol-induced surge of gonadotropin-releasing hormone in the ewe. Endocrinology 1990; 127:1375-1384.
38. Moenter SM, Caraty A, Locatelli A, Karsch FJ. Pattern of gonadotropin-releasing hormone (GnRH) secretion leading up to ovulation in the ewe: existence of a preovulatory GnRH surge. Endocrinology 1991; 129:1175-1182.
39. Russell DL, Salustri A. Extracellular matrix of the cumulus-oocyte complex. Semin Reprod Med 2006; 24:217-227.

40. Eppig JJ. Oocyte control of ovarian follicular development and function in mammals. Reproduction 2001; 122:829-838.
41. Coy P, García-Vázquez FA, Visconti PE, Avilés M. Roles of the oviduct in mammalian fertilization. Reproduction (Cambridge, England) 2012; 144:649-660.
42. Hafez EaH, B. Fertilization and Cleavage. In: Hafez BHaE (ed.) Reproduction in Farm Animals; 2016.
43. Carson DD, Bagchi I, Dey SK, Enders AC, Fazleabas AT, Lessey BA, Yoshinaga K. Embryo implantation. Dev Biol 2000; 223:217-237.
44. Chang MC. Transport of eggs from the fallopian tube to the uterus as a function of oestrogen. Nature 1966; 212:1048-1049.
45. Marston JH, Chang MC. THE FERTILIZABLE LIFE OF OVA AND THEIR MORPHOLOGY FOLLOWING DELAYED INSEMINATION IN MATURE AND IMMATURE MICE. J Exp Zool 1964; 155:237-251.
46. Tarin JJ, Perez-Albala S, Aguilar A, Minarro J, Hermenegildo C, Cano A. Long-term effects of postovulatory aging of mouse oocytes on offspring: a two-generational study. Biol Reprod 1999; 61:1347-1355.
47. Igarashi H, Takahashi T, Takahashi E, Tezuka N, Nakahara K, Takahashi K, Kurachi H. Aged mouse oocytes fail to readjust intracellular adenosine triphosphates at fertilization. Biol Reprod 2005; 72:1256-1261.
48. Igarashi H, Takahashi E, Hiroi M, Doi K. Aging-related changes in calcium oscillations in fertilized mouse oocytes. Mol Reprod Dev 1997; 48:383-390.
49. Luciano AM, Lodde V, Beretta MS, Colleoni S, Lauria A, Modina S. Developmental capability of denuded bovine oocyte in a co-culture system with intact cumulus-oocyte complexes: role of cumulus cells, cyclic adenosine 3',5'-monophosphate, and glutathione. Mol Reprod Dev 2005; 71:389-397.
50. Chian RC, Lim JH, Tan SL. State of the art in in-vitro oocyte maturation. Curr Opin Obstet Gynecol 2004; 16:211-219.
51. Chen J, Torcia S, Xie F, Lin CJ, Cakmak H, Franciosi F, Horner K, Onodera C, Song JS, Cedars MI, Ramalho-Santos M, Conti M. Somatic cells regulate maternal mRNA translation and developmental competence of mouse oocytes. Nat Cell Biol 2013; 15:1415-1423.
52. Chang HC, Liu H, Zhang J, Grifo J, Krey LC. Developmental incompetency of denuded mouse oocytes undergoing maturation in vitro is ooplasmic in nature and is associated with aberrant Oct-4 expression. Hum Reprod 2005; 20:1958-1968.
53. Conti M, Hsieh M, Zamah AM, Oh JS. Novel signaling mechanisms in the ovary during oocyte maturation and ovulation. Mol Cell Endocrinol 2012; 356:65-73.
54. Kim E, Yamashita M, Kimura M, Honda A, Kashiwabara S, Baba T. Sperm penetration through cumulus mass and zona pellucida. Int J Dev Biol 2008; 52:677-682.
55. Jin M, Fujiwara E, Kakiuchi Y, Okabe M, Satouh Y, Baba SA, Chiba K, Hirohashi N. Most fertilizing mouse spermatozoa begin their acrosome reaction before contact with the zona pellucida during in vitro fertilization. Proc Natl Acad Sci U S A 2011; 108:4892-4896.
56. Eisenbach M, Giojalas LC. Sperm guidance in mammals - an unpaved road to the egg. Nat Rev Mol Cell Biol 2006; 7:276-285.
57. Di Giacomo M, Camaioni A, Klinger FG, Bonfiglio R, Salustri A. Cyclic AMP-elevating Agents Promote Cumulus Cell Survival and Hyaluronan Matrix Stability, Thereby Prolonging the Time of Mouse Oocyte Fertilizability. The Journal of Biological Chemistry 2016; 291:3821-3836.

58. Howlett SK, Bolton VN. Sequence and regulation of morphological and molecular events during the first cell cycle of mouse embryogenesis. Journal of Embryology and Experimental Morphology 1985; 87:175.
59. Nagy ZP, Liu J, Joris H, Devroey P, Van Steirteghem A. Fertilization and early embryology: Time-course of oocyte activation, pronucleus formation and cleavage in human oocytes fertilized by intracytoplasmic sperm injection. Human Reproduction 1994; 9:1743-1748.
60. SF. G. Early mammalian development. In: Developmental Biology. 6th edition. Sunderland (MA): Sinauer Associates.; 2000.
61. Nuttinck F. Oocyte related factors impacting on embryo quality: relevance for in vitro embryo production. Anim. Reprod 2018; 15:271-277.
62. Bergh PA, Navot D. The impact of embryonic development and endometrial maturity on the timing of implantation**Presented at the 46th Annual Meeting of the American Fertility Society, Washington, DC, October 15 to 18, 1990. Fertility and Sterility 1992; 58:537-542.
63. Paria BC, Huet-Hudson YM, Dey SK. Blastocyst's state of activity determines the "window" of implantation in the receptive mouse uterus. Proceedings of the National Academy of Sciences 1993; 90:10159.
64. Whitten WK. Nutrient Requirements for the Culture of Preimplantation Embryos in Vitro. In: Raspé G (ed.) Schering Symposium on Intrinsic and Extrinsic Factors in Early Mammalian Development, Venice, April 20 to 23, 1970: Pergamon; 1971: 129-141.
65. Johnson MH, Ziomek CA. Induction of polarity in mouse 8-cell blastomeres: specificity, geometry, and stability. J Cell Biol 1981; 91:303-308.
66. Reeve WJ. Cytoplasmic polarity develops at compaction in rat and mouse embryos. J Embryol Exp Morphol 1981; 62:351-367.
67. Reeve WJ, Ziomek CA. Distribution of microvilli on dissociated blastomeres from mouse embryos: evidence for surface polarization at compaction. J Embryol Exp Morphol 1981; 62:339-350.
68. Fleming TP. A quantitative analysis of cell allocation to trophectoderm and inner cell mass in the mouse blastocyst. Dev Biol 1987; 119:520-531.
69. Handyside AH. Time of commitment of inside cells isolated from preimplantation mouse embryos. J Embryol Exp Morphol 1978; 45:37-53.
70. Handyside AH. Immunofluorescence techniques for determining the numbers of inner and outer blastomeres in mouse morulae. J Reprod Immunol 1981; 2:339-350.
71. Johnson MH, Ziomek CA. The foundation of two distinct cell lineages within the mouse morula. Cell 1981; 24:71-80.
72. Suwinska A, Czolowska R, Ozdzenski W, Tarkowski AK. Blastomeres of the mouse embryo lose totipotency after the fifth cleavage division: expression of Cdx2 and Oct4 and developmental potential of inner and outer blastomeres of 16- and 32-cell embryos. Dev Biol 2008; 322:133-144.
73. Aziz M, Alexandre H. The origin of the nascent blastocoele in preimplantation mouse embryos ultrastructural cytochemistry and effect of chloroquine. Roux Arch Dev Biol 1991; 200:77-85.
74. Gardner RL. Origin and differentiation of extraembryonic tissues in the mouse. Int Rev Exp Pathol 1983; 24:63-133.
75. Nichols J, Zevnik B, Anastassiadis K, Niwa H, Klewe-Nebenius D, Chambers I, Scholer H, Smith A. Formation of pluripotent stem cells in the mammalian embryo depends on the POU transcription factor Oct4. Cell 1998; 95:379-391.
76. Thompson SM, Onwubalili N, Brown K, Jindal SK, McGovern PG. Blastocyst expansion score and trophectoderm morphology strongly predict successful clinical

pregnancy and live birth following elective single embryo blastocyst transfer (eSET): a national study. Journal of Assisted Reproduction and Genetics 2013; 30:1577-1581.
77. Shapiro BS, Harris DC, Richter KS. Predictive value of 72-hour blastomere cell number on blastocyst development and success of subsequent transfer based on the degree of blastocyst development. Fertil Steril 2000; 73:582-586.
78. Wong CC, Loewke KE, Bossert NL, Behr B, De Jonge CJ, Baer TM, Reijo Pera RA. Non-invasive imaging of human embryos before embryonic genome activation predicts development to the blastocyst stage. Nat Biotechnol 2010; 28:1115-1121.
79. Wang Q, Sun Q-Y. Evaluation of oocyte quality: morphological, cellular and molecular predictors. Reproduction, Fertility and Development 2006; 19:1-12.
80. Schatten H, Sun Q-Y, Prather R. The impact of mitochondrial function/dysfunction on IVF and new treatment possibilities for infertility. Reproductive Biology and Endocrinology : RB&E 2014; 12:111.
81. Rojansky R, Cha M-Y, Chan DC. Elimination of paternal mitochondria in mouse embryos occurs through autophagic degradation dependent on PARKIN and MUL1. eLife 2016; 5:e17896.
82. Swinburn B, Sacks G, Ravussin E. Increased food energy supply is more than sufficient to explain the US epidemic of obesity. Am J Clin Nutr 2009; 90:1453-1456.
83. Mokdad AH, Ford ES, Bowman BA, Dietz WH, Vinicor F, Bales VS, Marks JS. Prevalence of obesity, diabetes, and obesity-related health risk factors, 2001. JAMA 2003; 289:76-79.
84. Maeda N, Shimomura I, Kishida K, Nishizawa H, Matsuda M, Nagaretani H, Furuyama N, Kondo H, Takahashi M, Arita Y, Komuro R, Ouchi N, et al. Diet-induced insulin resistance in mice lacking adiponectin/ACRP30. Nat Med 2002; 8:731-737.
85. Douchi T, Kuwahata R, Yamamoto S, Oki T, Yamasaki H, Nagata Y. Relationship of upper body obesity to menstrual disorders. Acta Obstet Gynecol Scand 2002; 81:147-150.
86. Lash MM, Armstrong A. Impact of obesity on women's health. Fertil Steril 2009; 91:1712-1716.
87. Wei S, Schmidt MD, Dwyer T, Norman RJ, Venn AJ. Obesity and menstrual irregularity: associations with SHBG, testosterone, and insulin. Obesity (Silver Spring) 2009; 17:1070-1076.
88. Brewer CJ, Balen AH. The adverse effects of obesity on conception and implantation. Reproduction 2010; 140:347-364.
89. Metwally M, Li TC, Ledger WL. The impact of obesity on female reproductive function. Obesity Reviews 2007; 8:515-523.
90. Boots C, Stephenson MD. Does obesity increase the risk of miscarriage in spontaneous conception: a systematic review. Semin Reprod Med 2011; 29:507-513.
91. Jungheim ES, Moley KH. Current knowledge of obesity's effects in the pre- and periconceptional periods and avenues for future research. Am J Obstet Gynecol 2010; 203:525-530.
92. Hirschberg AL. Polycystic ovary syndrome, obesity and reproductive implications. Womens Health (Lond Engl) 2009; 5:529-540; quiz 541-522.
93. Fauser BC, Tarlatzis BC, Rebar RW, Legro RS, Balen AH, Lobo R, Carmina E, Chang J, Yildiz BO, Laven JS, Boivin J, Petraglia F, et al. Consensus on women's health aspects of polycystic ovary syndrome (PCOS): the Amsterdam ESHRE/ASRM-Sponsored 3rd PCOS Consensus Workshop Group. Fertil Steril 2012; 97:28-38.e25.
94. Rotterdam EA-SPCWG. Revised 2003 consensus on diagnostic criteria and long-term health risks related to polycystic ovary syndrome. Fertil Steril 2004; 81:19-25.

95. Pandey S, Pandey S, Maheshwari A, Bhattacharya S. The impact of female obesity on the outcome of fertility treatment. J Hum Reprod Sci 2010; 3:62-67.
96. Ma X, Hayes E, Prizant H, Srivastava RK, Hammes SR, Sen A. Leptin-Induced CART (Cocaine- and Amphetamine-Regulated Transcript) Is a Novel Intraovarian Mediator of Obesity-Related Infertility in Females. Endocrinology 2016; 157:1248-1257.
97. Wu LL, Dunning KR, Yang X, Russell DL, Lane M, Norman RJ, Robker RL. High-fat diet causes lipotoxicity responses in cumulus-oocyte complexes and decreased fertilization rates. Endocrinology 2010; 151:5438-5445.
98. Luzzo KM, Wang Q, Purcell SH, Chi M, Jimenez PT, Grindler N, Schedl T, Moley KH. High Fat Diet Induced Developmental Defects in the Mouse: Oocyte Meiotic Aneuploidy and Fetal Growth Retardation/Brain Defects. PLoS One 2012; 7:e49217.
99. Minge CE, Bennett BD, Norman RJ, Robker RL. Peroxisome proliferator-activated receptor-gamma agonist rosiglitazone reverses the adverse effects of diet-induced obesity on oocyte quality. Endocrinology 2008; 149:2646-2656.
100. Wu LL, Russell DL, Wong SL, Chen M, Tsai TS, St John JC, Norman RJ, Febbraio MA, Carroll J, Robker RL. Mitochondrial dysfunction in oocytes of obese mothers: transmission to offspring and reversal by pharmacological endoplasmic reticulum stress inhibitors. Development 2015; 142:681-691.
101. Boots CE, Boudoures A, Zhang W, Drury A, Moley KH. Obesity-induced oocyte mitochondrial defects are partially prevented and rescued by supplementation with co-enzyme Q10 in a mouse model. Hum Reprod 2016; 31:2090-2097.
102. Boudoures AL, Chi M, Thompson A, Zhang W, Moley KH. The Effects of Voluntary Exercise on Oocyte Quality in a Diet-Induced Obese Murine Model. Reproduction 2016; 151:261-270.
103. Machtinger R, Combelles CMH, Missmer SA, Correia KF, Fox JH, Racowsky C. The association between severe obesity and characteristics of failed fertilized oocytes. Human Reproduction 2012; 27:3198-3207.
104. Jungheim ES, Schoeller EL, Marquard KL, Louden ED, Schaffer JE, Moley KH. Diet-Induced Obesity Model: Abnormal Oocytes and Persistent Growth Abnormalities in the Offspring. Endocrinology 2010; 151:4039-4046.
105. Weisberg SP, Leibel R, Tortoriello DV. Dietary curcumin significantly improves obesity-associated inflammation and diabetes in mouse models of diabesity. Endocrinology 2008; 149:3549-3558.
106. Weisberg SP, McCann D, Desai M, Rosenbaum M, Leibel RL, Ferrante AW, Jr. Obesity is associated with macrophage accumulation in adipose tissue. J Clin Invest 2003; 112:1796-1808.
107. Yudkin JS, Kumari M, Humphries SE, Mohamed-Ali V. Inflammation, obesity, stress and coronary heart disease: is interleukin-6 the link? Atherosclerosis 2000; 148:209-214.
108. Souza SC, Palmer HJ, Kang YH, Yamamoto MT, Muliro KV, Paulson KE, Greenberg AS. TNF-alpha induction of lipolysis is mediated through activation of the extracellular signal related kinase pathway in 3T3-L1 adipocytes. J Cell Biochem 2003; 89:1077-1086.
109. Berg AH, Scherer PE. Adipose tissue, inflammation, and cardiovascular disease. Circ Res 2005; 96:939-949.
110. Borradaile NM, Han X, Harp JD, Gale SE, Ory DS, Schaffer JE. Disruption of endoplasmic reticulum structure and integrity in lipotoxic cell death. J Lipid Res 2006; 47:2726-2737.
111. Geiger PC, Gupte AA. Heat shock proteins are important mediators of skeletal muscle insulin sensitivity. Exerc Sport Sci Rev 2011; 39:34-42.

112. Ritossa F. Discovery of the heat shock response. Cell Stress Chaperones 1996; 1:97-98.
113. Tissiéres A, Mitchell HK, Tracy UM. Protein synthesis in salivary glands of Drosophila melanogaster: relation to chromosome puffs. Journal of molecular biology 1974; 84:389-398.
114. Robert J, Ménoret A, Basu S, Cohen N, Srivastava PK. Phylogenetic conservation of the molecular and immunological properties of the chaperones gp96 and hsp70. European journal of immunology 2001; 31:186-195.
115. Gupta RS. Phylogenetic analysis of the 90 kD heat shock family of protein sequences and an examination of the relationship among animals, plants, and fungi species. Molecular biology and evolution 1995; 12:1063-1073.
116. Pelham HR. Speculations on the functions of the major heat shock and glucose-regulated proteins. Cell 1986; 46:959-961.
117. Parsell D, Lindquist S. The function of heat-shock proteins in stress tolerance: degradation and reactivation of damaged proteins. Annual review of genetics 1993; 27:437-496.
118. Feder ME, Hofmann GE. Heat-shock proteins, molecular chaperones, and the stress response: evolutionary and ecological physiology. Annual review of physiology 1999; 61:243-282.
119. Vos MJ, Hageman J, Carra S, Kampinga HH. Structural and functional diversities between members of the human HSPB, HSPH, HSPA, and DNAJ chaperone families. Biochemistry 2008; 47:7001-7011.
120. Tanguay RM, Wu Y, Khandjian EW. Tissue-specific expression of heat shock proteins of the mouse in the absence of stress. Dev Genet 1993; 14:112-118.
121. Ito Y, Ando A, Ando H, Ando J, Saijoh Y, Inoko H, Fujimoto H. Genomic structure of the spermatid-specific hsp70 homolog gene located in the class III region of the major histocompatibility complex of mouse and man. J Biochem 1998; 124:347-353.
122. De Maio A, Vazquez D. Extracellular heat shock proteins: a new location, a new function. Shock 2013; 40:239-246.
123. Liao DF, Jin ZG, Baas AS, Daum G, Gygi SP, Aebersold R, Berk BC. Purification and identification of secreted oxidative stress-induced factors from vascular smooth muscle cells. J Biol Chem 2000; 275:189-196.
124. Kuroita T, Tachibana H, Ohashi H, Shirahata S, Murakami H. Growth stimulating activity of heat shock protein 90 alpha to lymphoid cell lines in serum-free medium. Cytotechnology 1992; 8:109-117.
125. Tytell M, Greenberg SG, Lasek RJ. Heat shock-like protein is transferred from glia to axon. Brain Res 1986; 363:161-164.
126. Basu S, Binder RJ, Suto R, Anderson KM, Srivastava PK. Necrotic but not apoptotic cell death releases heat shock proteins, which deliver a partial maturation signal to dendritic cells and activate the NF-kappa B pathway. Int Immunol 2000; 12:1539-1546.
127. Kampinga HH, Hageman J, Vos MJ, Kubota H, Tanguay RM, Bruford EA, Cheetham ME, Chen B, Hightower LE. Guidelines for the nomenclature of the human heat shock proteins. Cell Stress Chaperones 2009; 14:105-111.
128. Salvetti NR, Baravalle C, Mira GA, Gimeno EJ, Dallard BE, Rey F, Ortega HH. Heat shock protein 70 and sex steroid receptors in the follicular structures of induced ovarian cysts. Reprod Domest Anim 2009; 44:805-814.
129. Ribas V, Nguyen MT, Henstridge DC, Nguyen AK, Beaven SW, Watt MJ, Hevener AL. Impaired oxidative metabolism and inflammation are associated with insulin resistance in ERalpha-deficient mice. Am J Physiol Endocrinol Metab 2010; 298:E304-319.

130. Driancourt MA, Guet P, Reynaud K, Chadli A, Catelli MG. Presence of an aromatase inhibitor, possibly heat shock protein 90, in dominant follicles of cattle. J Reprod Fertil 1999; 115:45-58.
131. Kampinga HH, Craig EA. The HSP70 chaperone machinery: J proteins as drivers of functional specificity. Nat Rev Mol Cell Biol 2010; 11:579-592.
132. Siddique HR, Mitra K, Bajpai VK, Ravi Ram K, Saxena DK, Chowdhuri DK. Hazardous effect of tannery solid waste leachates on development and reproduction in Drosophila melanogaster: 70kDa heat shock protein as a marker of cellular damage. Ecotoxicol Environ Saf 2009; 72:1652-1662.
133. Mukhopadhyay I, Siddique HR, Bajpai VK, Saxena DK, Chowdhuri DK. Synthetic pyrethroid cypermethrin induced cellular damage in reproductive tissues of Drosophila melanogaster: Hsp70 as a marker of cellular damage. Arch Environ Contam Toxicol 2006; 51:673-680.
134. Gupta SC, Siddique HR, Mathur N, Mishra RK, Mitra K, Saxena DK, Chowdhuri DK. Adverse effect of organophosphate compounds, dichlorvos and chlorpyrifos in the reproductive tissues of transgenic Drosophila melanogaster: 70kDa heat shock protein as a marker of cellular damage. Toxicology 2007; 238:1-14.
135. Narayansingh RM, Senchyna M, Vijayan MM, Carlson JC. Expression of prostaglandin G/H synthase (PGHS) and heat shock protein-70 (HSP-70) in the corpus luteum (CL) of prostaglandin F2 alpha-treated immature superovulated rats. Can J Physiol Pharmacol 2004; 82:363-371.
136. Sawada M, Carlson JC. Association of lipid peroxidation during luteal regression in the rat and natural aging in the rotifer. Exp Gerontol 1985; 20:179-186.
137. Wandinger SK, Richter K, Buchner J. The Hsp90 chaperone machinery. J Biol Chem 2008; 283:18473-18477.
138. Hahn JS. The Hsp90 chaperone machinery: from structure to drug development. BMB Rep 2009; 42:623-630.
139. Barnier JV, Bensaude O, Morange M, Babinet C. Mouse 89 kD heat shock protein. Two polypeptides with distinct developmental regulation. Exp Cell Res 1987; 170:186-194.
140. Nakai A, Tanabe M, Kawazoe Y, Inazawa J, Morimoto RI, Nagata K. HSF4, a new member of the human heat shock factor family which lacks properties of a transcriptional activator. Mol Cell Biol 1997; 17:469-481.
141. Sarge KD, Zimarino V, Holm K, Wu C, Morimoto RI. Cloning and characterization of two mouse heat shock factors with distinct inducible and constitutive DNA-binding ability. Genes Dev 1991; 5:1902-1911.
142. Le Masson F, Christians E. HSFs and regulation of Hsp70.1 (Hspa1b) in oocytes and preimplantation embryos: new insights brought by transgenic and knockout mouse models. Cell Stress Chaperones 2011; 16:275-285.
143. Christians E, Michel E, Adenot P, Mezger V, Rallu M, Morange M, Renard JP. Evidence for the involvement of mouse heat shock factor 1 in the atypical expression of the HSP70.1 heat shock gene during mouse zygotic genome activation. Mol Cell Biol 1997; 17:778-788.
144. Bierkamp C, Luxey M, Metchat A, Audouard C, Dumollard R, Christians E. Lack of maternal Heat Shock Factor 1 results in multiple cellular and developmental defects, including mitochondrial damage and altered redox homeostasis, and leads to reduced survival of mammalian oocytes and embryos. Dev Biol 2010; 339:338-353.
145. Fujimoto M, Izu H, Seki K, Fukuda K, Nishida T, Yamada S, Kato K, Yonemura S, Inouye S, Nakai A. HSF4 is required for normal cell growth and differentiation during mouse lens development. EMBO J 2004; 23:4297-4306.

146. Min JN, Zhang Y, Moskophidis D, Mivechi NF. Unique contribution of heat shock transcription factor 4 in ocular lens development and fiber cell differentiation. Genesis 2004; 40:205-217.
147. Min JN, Han MY, Lee SS, Kim KJ, Park YM. Regulation of rat heat shock factor 2 expression during the early organogenic phase of embryogenesis. Biochim Biophys Acta 2000; 1494:256-262.
148. Chastant S, Christians E, Campion E, Renard JP. Quantitative control of gene expression by nucleocytoplasmic interactions in early mouse embryos: consequence for reprogrammation by nuclear transfer. Mol Reprod Dev 1996; 44:423-432.
149. Morimoto RI. Regulation of the heat shock transcriptional response: cross talk between a family of heat shock factors, molecular chaperones, and negative regulators. Genes Dev 1998; 12:3788-3796.
150. Fernandes MTOBaJTL. Structure and regulation of heat shock gene promoters. In: R.I. Morimoto AT, and C. Georgopolis (ed.) The biology of heat shock proteins and molecular chaperones. Cold Spring Harbor, NY: Cold Spring Harbor Laboratory Press; 1994: 375-393.
151. Metchat A, Akerfelt M, Bierkamp C, Delsinne V, Sistonen L, Alexandre H, Christians ES. Mammalian heat shock factor 1 is essential for oocyte meiosis and directly regulates Hsp90alpha expression. J Biol Chem 2009; 284:9521-9528.
152. Xiao X, Zuo X, Davis AA, McMillan DR, Curry BB, Richardson JA, Benjamin IJ. HSF1 is required for extra-embryonic development, postnatal growth and protection during inflammatory responses in mice. EMBO J 1999; 18:5943-5952.
153. Christians E, Davis AA, Thomas SD, Benjamin IJ. Maternal effect of Hsf1 on reproductive success. Nature 2000; 407:693-694.
154. Hartl FU, Hayer-Hartl M. Converging concepts of protein folding in vitro and in vivo. Nature structural & molecular biology 2009; 16:574-581.
155. Molvarec A, Tamasi L, Losonczy G, Madach K, Prohaszka Z, Rigo J, Jr. Circulating heat shock protein 70 (HSPA1A) in normal and pathological pregnancies. Cell Stress Chaperones 2010; 15:237-247.
156. Wilhelm D, Huang E, Svingen T, Stanfield S, Dinnis D, Koopman P. Comparative proteomic analysis to study molecular events during gonad development in mice. Genesis 2006; 44:168-176.
157. Twigt J, Steegers-Theunissen RP, Bezstarosti K, Demmers JA. Proteomic analysis of the microenvironment of developing oocytes. Proteomics 2012; 12:1463-1471.
158. Satoh M, Tokoro M, Ikegami H, Nagai K, Sono Y, Shin SW, Nishikawa S, Saeki K, Hosoi Y, Iritani A, Fukuda A, Morimoto Y, et al. Proteomic analysis of the mouse ovary in response to two gonadotropins, follicle-stimulating hormone and luteinizing hormone. J Reprod Dev 2009; 55:316-326.
159. Peng Q, Yang H, Xue S, Shi L, Yu Q, Kuang Y. Secretome profile of mouse oocytes after activation using mass spectrum. J Assist Reprod Genet 2012; 29:765-771.
160. Misiti S, Stigliano A, Borro M, Gentile G, Michienzi S, Cerquetti L, Bucci B, Argese N, Brunetti E, Simmaco M, Toscano V. Proteomic profiles in hyperandrogenic syndromes. J Endocrinol Invest 2010; 33:156-164.
161. Maniwa J, Izumi S, Isobe N, Terada T. Studies on substantially increased proteins in follicular fluid of bovine ovarian follicular cysts using 2-D PAGE and MALDI-TOF MS. Reprod Biol Endocrinol 2005; 3:23.
162. Maloney A, Clarke PA, Naaby-Hansen S, Stein R, Koopman JO, Akpan A, Yang A, Zvelebil M, Cramer R, Stimson L, Aherne W, Banerji U, et al. Gene and protein expression profiling of human ovarian cancer cells treated with the heat shock protein 90 inhibitor 17-allylamino-17-demethoxygeldanamycin. Cancer Res 2007; 67:3239-3253.

163. Ma X, Fan L, Meng Y, Hou Z, Mao YD, Wang W, Ding W, Liu JY. Proteomic analysis of human ovaries from normal and polycystic ovarian syndrome. Mol Hum Reprod 2007; 13:527-535.
164. Insenser M, Martinez-Garcia MA, Montes R, San-Millan JL, Escobar-Morreale HF. Proteomic analysis of plasma in the polycystic ovary syndrome identifies novel markers involved in iron metabolism, acute-phase response, and inflammation. J Clin Endocrinol Metab 2010; 95:3863-3870.
165. Insenser M, Escobar-Morreale HF. Application of proteomics to the study of polycystic ovary syndrome. J Endocrinol Invest 2011; 34:869-875.
166. Corton M, Botella-Carretero JI, Lopez JA, Camafeita E, San Millan JL, Escobar-Morreale HF, Peral B. Proteomic analysis of human omental adipose tissue in the polycystic ovary syndrome using two-dimensional difference gel electrophoresis and mass spectrometry. Hum Reprod 2008; 23:651-661.
167. Calvert ME, Digilio LC, Herr JC, Coonrod SA. Oolemmal proteomics--identification of highly abundant heat shock proteins and molecular chaperones in the mature mouse egg and their localization on the plasma membrane. Reprod Biol Endocrinol 2003; 1:27.
168. Ambekar AS, Nirujogi RS, Srikanth SM, Chavan S, Kelkar DS, Hinduja I, Zaveri K, Prasad TS, Harsha HC, Pandey A, Mukherjee S. Proteomic analysis of human follicular fluid: A new perspective towards understanding folliculogenesis. J Proteomics 2013; 87:68-77.
169. Nip MM, Miller D, Taylor PV, Gannon MJ, Hancock KW. Expression of heat shock protein 70 kDa in human endometrium of normal and infertile women. Hum Reprod 1994; 9:1253-1256.
170. Mangurten AB, Brader KR, Loos BM, Lee E, Quiroga AI, Bathori J, Lurain JR, Laszlo A, Phillips B. Hsp70 and Hsc70 are preferentially expressed in differentiated epithelial cells in normal human endometrium and ectocervix. Cell Stress Chaperones 1997; 2:168-174.
171. Tabibzadeh S, Broome J. Heat shock proteins in human endometrium throughout the menstrual cycle. Infectious diseases in obstetrics and gynecology 1999; 7:5-9.
172. Mariani ML, Souto M, Fanelli MA, Ciocca DR. Constitutive expression of heat shock proteins hsp25 and hsp70 in the rat oviduct during neonatal development, the oestrous cycle and early pregnancy. J Reprod Fertil 2000; 120:217-223.
173. Tabibzadeh S, Kong QF, Satyaswaroop PG, Babaknia A. Heat shock proteins in human endometrium throughout the menstrual cycle. Hum Reprod 1996; 11:633-640.
174. Pires ES, Khole VV. A block in the road to fertility: autoantibodies to heat-shock protein 90-beta in human ovarian autoimmunity. Fertil Steril 2009; 92:1395-1409.
175. Koshiyama M, Konishi I, Nanbu K, Nanbu Y, Mandai M, Komatsu T, Yamamoto S, Mori T, Fujii S. Immunohistochemical localization of heat shock proteins HSP70 and HSP90 in the human endometrium: correlation with sex steroid receptors and Ki-67 antigen expression. J Clin Endocrinol Metab 1995; 80:1106-1112.
176. Gruidl M, Buyuksal A, Babaknia A, Fazleabas AT, Sivarajah S, Satyaswaroop PG, Tabibzadeh S. The progressive rise in the expression of alpha crystallin B chain in human endometrium is initiated during the implantation window: modulation of gene expression by steroid hormones. Mol Hum Reprod 1997; 3:333-342.
177. Neuer A, Spandorfer SD, Giraldo P, Dieterle S, Rosenwaks Z, Witkin SS. The role of heat shock proteins in reproduction. Human reproduction update 2000; 6:149-159.
178. Pennarossa G, Maffei S, Rahman MM, Berruti G, Brevini TA, Gandolfi F. Characterization of the constitutive pig ovary heat shock chaperone machinery and its response to acute thermal stress or to seasonal variations. Biol Reprod 2012; 87:119.

179. Wassarman P. The mammalian ovum. In: Knobil EN, J. (ed.) The physiology of reproduction. New York: Raven Press; 1988: 69-102.
180. Lanska V, Chmelikova E, Sedmikova M, Petr J, Rajmon R, Jeseta M, Rozinek J. Expression of heat shock protein70 in pig oocytes: heat shock response during oocyte growth. Anim Reprod Sci 2006; 96:154-164.
181. Liu CH, Yang CC, Lin DP, Wu MH, Tsai KJ. Stored of Hsp72/Hsp73 in germinal vesicle-stage mouse oocytes. Reprod Domest Anim 2004; 39:19-24.
182. Dix DJ. Hsp70 expression and function during gametogenesis. Cell Stress Chaperones 1997; 2:73-77.
183. Curci A, Bevilacqua A, Mangia F. Lack of heat-shock response in preovulatory mouse oocytes. Dev Biol 1987; 123:154-160.
184. Hendrey J, Kola I. Thermolability of mouse oocytes is due to the lack of expression and/or inducibility of Hsp70. Mol Reprod Dev 1991; 28:1-8.
185. Edwards JL, Hansen PJ. Differential responses of bovine oocytes and preimplantation embryos to heat shock. Mol Reprod Dev 1997; 46:138-145.
186. Allen JW, Dix DJ, Collins BW, Merrick BA, He C, Selkirk JK, Poorman-Allen P, Dresser ME, Eddy EM. HSP70-2 is part of the synaptonemal complex in mouse and hamster spermatocytes. Chromosoma 1996; 104:414-421.
187. Malusecka E, Zborek A, Krzyzowska-Gruca S, Krawczyk Z. Immunohistochemical detection of the inducible heat shock protein hsp70: a methodological study. J Histochem Cytochem 2006; 54:183-190.
188. Guzeloglu A, Ambrose JD, Kassa T, Diaz T, Thatcher MJ, Thatcher WW. Long-term follicular dynamics and biochemical characteristics of dominant follicles in dairy cows subjected to acute heat stress. Anim Reprod Sci 2001; 66:15-34.
189. Christians ES, Zhou Q, Renard J, Benjamin IJ. Heat shock proteins in mammalian development. Semin Cell Dev Biol 2003; 14:283-290.
190. Kim SK, Kim YK, Lee AS. Expression of the glucose-regulated proteins (GRP94 and GRP78) in differentiated and undifferentiated mouse embryonic cells and the use of the GRP78 promoter as an expression system in embryonic cells. Differentiation 1990; 42:153-159.
191. Barnes JA, Smoak IW. Glucose-regulated protein 78 (GRP78) is elevated in embryonic mouse heart and induced following hypoglycemic stress. Anat Embryol (Berl) 2000; 202:67-74.
192. Loones MT, Rallu M, Mezger V, Morange M. HSP gene expression and HSF2 in mouse development. Cell Mol Life Sci 1997; 53:179-190.
193. Voss AK, Thomas T, Gruss P. Mice lacking HSP90beta fail to develop a placental labyrinth. Development 2000; 127:1-11.
194. Mao C, Wang M, Luo B, Wey S, Dong D, Wesselschmidt R, Rawlings S, Lee AS. Targeted Mutation of the Mouse Grp94 Gene Disrupts Development and Perturbs Endoplasmic Reticulum Stress Signaling. PLOS ONE 2010; 5:e10852.
195. Wanderling S, Simen BB, Ostrovsky O, Ahmed NT, Vogen SM, Gidalevitz T, Argon Y. GRP94 is essential for mesoderm induction and muscle development because it regulates insulin-like growth factor secretion. Mol Biol Cell 2007; 18:3764-3775.
196. Zhang P, Ni X, Guo Y, Guo X, Wang Y, Zhou Z, Huo R, Sha J. Proteomic-based identification of maternal proteins in mature mouse oocytes. BMC Genomics 2009; 10:348.
197. Yoshida S, Tsutsumi S, Muhlebach G, Sourbier C, Lee MJ, Lee S, Vartholomaiou E, Tatokoro M, Beebe K, Miyajima N, Mohney RP, Chen Y, et al. Molecular chaperone TRAP1 regulates a metabolic switch between mitochondrial respiration and aerobic glycolysis. Proc Natl Acad Sci U S A 2013; 110:E1604-1612.

198. Messler S, Kropp S, Episkopou V, Felici A, Wurthner J, Lemke R, Jerabek-Willemsen M, Willecke R, Scheu S, Pfeffer K, Wurthner JU. The TGF-beta signaling modulators TRAP1/TGFBRAP1 and VPS39/Vam6/TLP are essential for early embryonic development. Immunobiology 2011; 216:343-350.
199. Weissman JS, Hohl CM, Kovalenko O, Kashi Y, Chen S, Braig K, Saibil HR, Fenton WA, Horwich AL. Mechanism of GroEL action: productive release of polypeptide from a sequestered position under GroES. Cell 1995; 83:577-587.
200. Fan L, Fan L, Ling J, Ma X, Cui YG, Liu JY. Involvement of HSP10 during the ovarian follicular development of polycystic ovary syndrome: Study in both human ovaries and cultured mouse follicles. Gynecol Endocrinol 2009; 25:392-397.
201. Kusminski CM, Shetty S, Orci L, Unger RH, Scherer PE. Diabetes and apoptosis: lipotoxicity. Apoptosis 2009; 14:1484-1495.
202. Wu LL, Russell DL, Norman RJ, Robker RL. Endoplasmic reticulum (ER) stress in cumulus-oocyte complexes impairs pentraxin-3 secretion, mitochondrial membrane potential (DeltaPsi m), and embryo development. Mol Endocrinol 2012; 26:562-573.
203. Richards JS, Russell DL, Ochsner S, Espey LL. Ovulation: new dimensions and new regulators of the inflammatory-like response. Annu Rev Physiol 2002; 64:69-92.
204. Nteeba J, Ortinau LC, Perfield JW, Keating AF. Diet-induced obesity alters immune cell infiltration and expression of inflammatory cytokine genes in mouse ovarian and peri-ovarian adipose depot tissues. Mol Reprod Dev 2013; 80:948-958.
205. Prins JR, Gomez-Lopez N, Robertson SA. Interleukin-6 in pregnancy and gestational disorders. J Reprod Immunol 2012; 95:1-14.
206. Loret de Mola JR, Flores JP, Baumgardner GP, Goldfarb JM, Gindlesperger V, Friedlander MA. Elevated interleukin-6 levels in the ovarian hyperstimulation syndrome: ovarian immunohistochemical localization of interleukin-6 signal. Obstet Gynecol 1996; 87:581-587.
207. Pantasri T, Wu LL, Hull ML, Sullivan TR, Barry M, Norman RJ, Robker RL. Distinct localisation of lipids in the ovarian follicular environment. Reprod Fertil Dev 2015; 27:593-601.
208. Gupte AA, Bomhoff GL, Swerdlow RH, Geiger PC. Heat treatment improves glucose tolerance and prevents skeletal muscle insulin resistance in rats fed a high-fat diet. Diabetes 2009; 58:567-578.
209. Young JC, Hoogenraad NJ, Hartl FU. Molecular chaperones Hsp90 and Hsp70 deliver preproteins to the mitochondrial import receptor Tom70. Cell 2003; 112:41-50.
210. Romano Carratelli C, Nuzzo I, Vitiello T, Galdiero E, Galdiero F. The effect of dietary lipid manipulation on murine splenic lymphocytes apoptosis and heat shock protein over expression. FEMS Immunol Med Microbiol 1999; 24:19-25.
211. Shankar K, Zhong Y, Kang P, Lau F, Blackburn ML, Chen JR, Borengasser SJ, Ronis MJ, Badger TM. Maternal obesity promotes a proinflammatory signature in rat uterus and blastocyst. Endocrinology 2011; 152:4158-4170.
212. Pharmacology ILIoC. Our extracts. In.
213. Hooper PL. Hot-tub therapy for type 2 diabetes mellitus. N Engl J Med 1999; 341:924-925.
214. Chung J, Nguyen AK, Henstridge DC, Holmes AG, Chan MH, Mesa JL, Lancaster GI, Southgate RJ, Bruce CR, Duffy SJ, Horvath I, Mestril R, et al. HSP72 protects against obesity-induced insulin resistance. Proc Natl Acad Sci U S A 2008; 105:1739-1744.
215. Aggarwal BB, Sundaram C, Malani N, Ichikawa H. Curcumin: the Indian solid gold. Adv Exp Med Biol 2007; 595:1-75.
216. !!! INVALID CITATION !!! [185, 186].

217. Weber WM, Hunsaker LA, Roybal CN, Bobrovnikova-Marjon EV, Abcouwer SF, Royer RE, Deck LM, Vander Jagt DL. Activation of NFkappaB is inhibited by curcumin and related enones. Bioorg Med Chem 2006; 14:2450-2461.
218. Pendurthi UR, Williams JT, Rao LVM. Inhibition of tissue factor gene activation in cultured endothelial cells by curcumin - Suppression of activation of transcription factors Egr-1, AP-1, and NF-kappa B. Arteriosclerosis Thrombosis and Vascular Biology 1997; 17:3406-3413.
219. Kanitkar M, Bhonde RR. Curcumin treatment enhances islet recovery by induction of heat shock response proteins, Hsp70 and heme oxygenase-1, during cryopreservation. Life Sci 2008; 82:182-189.
220. Park KJ, Gaynor RB, Kwak YT. Heat shock protein 27 association with the I kappa B kinase complex regulates tumor necrosis factor alpha-induced NF-kappa B activation. J Biol Chem 2003; 278:35272-35278.
221. Gehrig SM, van der Poel C, Sayer TA, Schertzer JD, Henstridge DC, Church JE, Lamon S, Russell AP, Davies KE, Febbraio MA, Lynch GS. Hsp72 preserves muscle function and slows progression of severe muscular dystrophy. Nature 2012; 484:394-398.
222. Ejaz A, Wu D, Kwan P, Meydani M. Curcumin inhibits adipogenesis in 3T3-L1 adipocytes and angiogenesis and obesity in C57/BL mice. J Nutr 2009; 139:919-925.
223. Wang J, Vanegas SM, Du X, Noble T, Zingg JM, Meydani M, Meydani SN, Wu D. Caloric restriction favorably impacts metabolic and immune/inflammatory profiles in obese mice but curcumin/piperine consumption adds no further benefit. Nutr Metab (Lond) 2013; 10:29.
224. Higdon JV, Frei B. Obesity and oxidative stress: a direct link to CVD? Arterioscler Thromb Vasc Biol 2003; 23:365-367.
225. Jang EM, Choi MS, Jung UJ, Kim MJ, Kim HJ, Jeon SM, Shin SK, Seong CN, Lee MK. Beneficial effects of curcumin on hyperlipidemia and insulin resistance in high-fat-fed hamsters. Metabolism 2008; 57:1576-1583.
226. Manjunatha H, Srinivasan K. Protective effect of dietary curcumin and capsaicin on induced oxidation of low-density lipoprotein, iron-induced hepatotoxicity and carrageenan-induced inflammation in experimental rats. FEBS J 2006; 273:4528-4537.
227. Kalpana C, Menon VP. Modulatory effects of curcumin on lipid peroxidation and antioxidant status during nicotine-induced toxicity. Pol J Pharmacol 2004; 56:581-586.
228. Alappat L, Awad AB. Curcumin and obesity: evidence and mechanisms. Nutr Rev 2010; 68:729-738.
229. Arun N, Nalini N. Efficacy of turmeric on blood sugar and polyol pathway in diabetic albino rats. Plant Foods Hum Nutr 2002; 57:41-52.
230. Ireson CR, Jones DJ, Orr S, Coughtrie MW, Boocock DJ, Williams ML, Farmer PB, Steward WP, Gescher AJ. Metabolism of the cancer chemopreventive agent curcumin in human and rat intestine. Cancer Epidemiol Biomarkers Prev 2002; 11:105-111.
231. Baum L, Lam CW, Cheung SK, Kwok T, Lui V, Tsoh J, Lam L, Leung V, Hui E, Ng C, Woo J, Chiu HF, et al. Six-month randomized, placebo-controlled, double-blind, pilot clinical trial of curcumin in patients with Alzheimer disease. J Clin Psychopharmacol 2008; 28:110-113.
232. Lim GP, Chu T, Yang F, Beech W, Frautschy SA, Cole GM. The curry spice curcumin reduces oxidative damage and amyloid pathology in an Alzheimer transgenic mouse. Journal of Neuroscience 2001; 21:8370-8377.
233. Naz RK. Can curcumin provide an ideal contraceptive? Mol Reprod Dev 2011; 78:116-123.

234. Xia X, Cai H, Qin S, Xu C. Histone acetylase inhibitor curcumin impairs mouse spermiogenesis-an in vitro study. PLoS One 2012; 7:e48673.
235. Osorio-Esquivel O, Ortiz-Moreno A, Garduno-Siciliano L, Alvarez VB, Hernandez-Navarro MD. Antihyperlipidemic effect of methanolic extract from Opuntia joconostle seeds in mice fed a hypercholesterolemic diet. Plant Foods Hum Nutr 2012; 67:365-370.
236. Zourgui L, Golli EE, Bouaziz C, Bacha H, Hassen W. Cactus (Opuntia ficus-indica) cladodes prevent oxidative damage induced by the mycotoxin zearalenone in Balb/C mice. Food Chem Toxicol 2008; 46:1817-1824.
237. Manach C, Hubert J, Llorach R, Scalbert A. The complex links between dietary phytochemicals and human health deciphered by metabolomics. Mol Nutr Food Res 2009; 53:1303-1315.
238. Zhao LY, Lan QJ, Huang ZC, Ouyang LJ, Zeng FH. Antidiabetic effect of a newly identified component of Opuntia dillenii polysaccharides. Phytomedicine : international journal of phytotherapy and phytopharmacology 2011; 18:661-668.
239. Lee JA, Jung BG, Lee BJ. Inhibitory effects of Opuntia humifusa on 7, 12-dimethyl-benz[a]anthracene and 12-O-tetradecanoylphorbol-13- acetate induced two-stage skin carcinogenesis. Asian Pac J Cancer Prev 2012; 13:4655-4660.
240. Loro JF, del Rio I, Perez-Santana L. Preliminary studies of analgesic and anti-inflammatory properties of Opuntia dillenii aqueous extract. J Ethnopharmacol 1999; 67:213-218.
241. Brahmi D, Bouaziz C, Ayed Y, Ben Mansour H, Zourgui L, Bacha H. Chemopreventive effect of cactus Opuntia ficus indica on oxidative stress and genotoxicity of aflatoxin B1. Nutr Metab (Lond) 2011; 8:73.
242. Sung YY, Roberts RJ, Bossier P. Enhancement of Hsp70 synthesis protects common carp, Cyprinus carpio L., against lethal ammonia toxicity. J Fish Dis 2012; 35:563-568.
243. Bajaj VK, Gupta RS. Fertility suppression in male albino rats by administration of methanolic extract of Opuntia dillenii. Andrologia 2012; 44 Suppl 1:530-537.
244. MC R, . S, T S. Reversible antifertility effect of Opuntia elatior Mill. fruit extract. 2017 2017; 4:6.
245. Meamar M, Zribi N, Cambi M, Tamburrino L, Marchiani S, Filimberti E, Fino MG, Biggeri A, Menezo Y, Forti G, Baldi E, Muratori M. Sperm DNA fragmentation induced by cryopreservation: new insights and effect of a natural extract from Opuntia ficus-indica. Fertility and Sterility; 98:326-333.
246. Parker CD, Prins C, Saliba C, Gutierrez G, Serrar M. Effect of TEX-OE((R)) treatment on the development of heat shock proteins in commercial broiler chicks and the impact on performance indicators in the grow-out period. Br Poult Sci 2014; 55:592-597.

Chapter 2: Expression and localization of Heat Shock Proteins during ovulation and oocyte maturation in the mouse ovary

2.1 Introduction

HSP are a diverse group of proteins with myriad cellular functions, particularly well characterised for their roles in stress responses. Their major activity is that of molecular chaperones, regulating the folding or recycling of denatured proteins in the cytoplasm. Not only this, but many studies have shown that HSP participate in numerous physiological processes, including female reproduction, as well as in pathological conditions as detailed below.

HSF1 is the main transcription factor that regulates the expression of inducible HSP characteristic of the HSF-dependent heat response [247]. HSF1 monomers upon activation join to form homotrimers, which also undergo phosphorylation. This is followed by their translocation from the cytoplasm to the nucleus, where the complex binds to promoter sequences for HSP genes. Female mice lacking the Hsf1 gene are infertile, presenting both gamete and embryonic defects. Hsf1 gene knock-out breeding in different mouse strains show prenatal lethality of the F1, the point at which this occurs having varying penetrance in different genetic backgrounds [153, 248]. Surviving, adult $Hsf1^{-/-}$ females can ovulate morphologically healthy oocytes; however these present partial meiotic arrest and symmetric division during the first polar body extrusion. This poor oocyte quality is due to a failure to induce several downstream HSP, the most affected being Hsp90aa1 [151]. Moreover, Hsf1 has long been known as a maternal effect factor [153]. Embryos derived from $Hsf1^{-/-}$ females present early developmental arrest at the 1-2 cell stage after natural mating [144, 153].

HSPA1A and HSPA1B (Hsp70) are the most studied of the HSP. They are highly conserved homologue proteins, which are thought to be completely interchangeable. They generally present cytoplasmic localization where they function as molecular chaperones, typically after insult-induced cellular stresses. In contrast to other HSP chaperones, HSP70 bind indiscriminately to exposed hydrophobic residues on denatured proteins, without substrate specificity regarding the client protein itself. Mouse KO models for either Hspa1a [249-252], Hspa1b [249], or both of these genes [253, 254] do not appear to present any reproductive deficiencies or phenotypic abnormalities during embryonic development and adulthood under specific pathogen free conditions, except for 12% body weight reduction in newborn double KO pups [254]. Yet there are no details as to if and how female fertility and reproductive function was assessed, other than in vivo mating, followed by analysis of the Mendelian distribution of the offspring genotypes. These two proteins are induced in high levels by stress, however, and are known to elicit important cell survival mechanism under these conditions, thus it is possible that they may not have an essential role in reproduction under normal

physiological circumstances but may be induced by cellular stress. Moreover, the regulation of the expression of these genes is highly tissue and germ-line specific [177], in addition to their complex intra-cellular regulatory mechanisms and have been routinely analysed in other reproductive tissues such as the testes and uteri [255, 256], yet their patterns of expression in ovarian cells have not been well characterised.

HSPA5 (Grp78, Bip) is normally localised to the ER in cells and it is involved in the UPR, as a molecular chaperone. No null pups for Hspa5 are born when heterozygous Hspa5$^{+/-}$ mice are interbred indicating that loss of Hspa5 is embryonic lethal (ref here as well). These mice produce zygotes that will develop into morphologically normal blastocysts, both in-vivo and in-vitro. However shortly after E3.5, the majority of Hspa5$^{-/-}$ embryos are unable to hatch out of the zona pellucida, and when they do they undergo degeneration, likely due to increased apoptosis levels of the ICM and a proliferation defect [257]. Hspa5 localisation in ovarian cells is not well described and any specific role in oocyte maturation has not been investigated.

HSP90AA1 (HSP90 alpha) is a mainly cytosolic protein, co-chaperoning with HSPA1A/B during heat stress episodes. HSP90AA1 is highly homologous with HSP90AB1, but the two genes are independently regulated. They are both highly expressed in most somatic cells, even in the absence of stress [258] but they acquire specialised functions in specific cell types such as the ovary. Analysis of mRNA levels for major HSR members Hspb1, Hspd1, Hspa1a/b, Hsp90aa1, Hsp90ab1 and Hsph1 by real-time PCR has shown that the expression of HSP90AA1 was highly increased in mature oocytes while HSP90AB1 was highly increased in the surrounding cumulus cells in ovulated COC complexes [151, 193]. Although only Hsp90aa1$^{-/-}$ male mice are infertile [259, 260], accumulation of this protein within the growing oocyte is required to achieve a normal meiosis. Metchat et al found that, in female Hsf1$^{-/-}$ knockout mice, oocytes in the ovary were depleted of HSP90AA1 resulting in a defective phenotype that is characterised by a higher proportion of oocytes presenting blocked meiosis, spindle defects and/or uneven cytokinesis during the extrusion of the first polar body. Similar observations were made in oocytes grown in vitro in the presence of 17AAG, a HSP90AA1 inhibitor, indicating that the abnormal meiotic phenotype was due to the absence of functional HSP90AA1 in the oocyte [151]. The fact that female mice lacking the Hsp90aa1 gene are fertile under controlled laboratory conditions suggests that there could be functional redundancy with another chaperone, likely an isoform that will take over meiosis regulation in the absence of Hsp90aa1.

HSP90B1 (Grp94) is a UPR marker and resident molecular chaperone in the ER compartment together with HSPA5. Null mutation of HSP90B1 is lethal by day 7 post-fertilisation, when embryos fail to develop mesoderm, primitive streak or the proamniotic cavity [194, 195]. Interestingly, proteomic analysis of isolated MII mouse oocytes using gel electrophoresis and mass spectrometry, identified HSP90B1 as one of the more abundant maternal proteins involved in oogenesis [196]. However, the early embryonic death of Hsp90b1$^{-/-}$ mice has made it difficult to study the influence of this protein in female fertility and reproductive potential. Audouard et al developed an oocyte-specific deletion of Hsp90b1 using a Zp3-cre transgenic mouse line [261-263]. Phenotypic analysis showed normal meiosis and fertilisation in mature oocytes until the first mitotic division, which was impaired in mutant Hsp90b1$^{-/-}$ zygotes [264].

HSPD1 (Hsp60) is primarily involved in the folding and transport of proteins through the inner mitochondrial matrix, where it is essential for adequate mitochondrial function and homeostasis regulation [265, 266]. Whereas a 50% reduction on the amount of HSPD1 seems compatible with overall embryonic development and prenatal viability, Hspd1$^{-/-}$ embryos die shortly after implantation, appearing smaller around day 6 after fertilisation, and progressively retarding their growth and finally degenerating by day 8.5. The findings from this KO model suggest that the lethal phenotype arises just after the mitochondrial biogenesis resumes in the embryo, once its maternal HSPD1 reserves have been exhausted [267].

In the ovary, the induction of HSP70 proteins, namely HSPA1A/B and HSPA8 (HSC70), have been shown to be necessary for luteal regression and inhibition of hormone dependent steroidogenesis in the rat ovary [268]. However the study does not distinguish between the three different proteins forms, which can be functionally different [256], therefore their individual contribution to luteal regression remains unknown. Thus, these changes in HSP expression might somehow affect GLC function and follicular development by their interaction with steroid hormone processes.

Therefore Knock-Out (KO) mouse models demonstrate that many HSPs are essential for female reproduction and, in the case of HSF1, act as maternal factors, and/or are essential for embryo viability. However, the mechanisms by which HSPs influence oocyte maturation and ovulation are still largely unknown. As described above, several studies have characterised the detrimental effects the absence of these proteins have on female fertility and reproduction in general. However, a lot is still unknown about their function in normal physiological conditions prior and around the time of ovulation, as there has been no systematic characterisation of the expression of HSP in the normal mammalian ovary across oocyte maturation and ovulation.

Thus, for this study, we used these HSP-KO studies as a guide to choose key proteins across different HSP families that are essential for oocyte and/or embryo development, namely HSF1, HSPA1A, HSPA1B, HSPA5, HSP90AA1, HSP90B1, and HSPD1. Expression of mRNA and protein of each of these genes was analysed in the peri-ovulatory period in the mouse ovary. This information is essential in order to understand their potential roles in stress responses within the ovary, and how it might respond to stressors such as heat stress, metabolic stress or obesity, and even aging.

2.2 Aim of the study

This study characterized the expression and localization across oocyte maturation and ovulation of HSF1 and several HSP that are both stress-inducible and important for female fertility in the mouse.

2.3 Materials and Methods

2.3.1 Animals and tissue collection

Pre-pubertal CBAF1 female mice at 21 days old and 11-13 g of body weight were purchased from Laboratory Animal Services (University of Adelaide). All experiments were approved by the University of Adelaide Animal Ethics Committee (approval M-2012-230) and conducted according to the Australian Code of Practice for the Care and Use of Animals for Scientific Purposes.

To stimulate follicular growth, all mice received an intraperitoneal (IP) injection of Pregnant Mare Serum Gonadotropin (PMSG; National Hormone and Peptide Program, Torrence, USA) in sterile 0.9% saline at a dose of 5 IU/12 g of body weight. At 48 hours post-PMSG, some mice received a second IP injection of human chorionic Gonadotropin (hCG; Pregnyl, Merck Sharp & Dohme Pty Ltd, Australia) in sterile 0.9% saline at a dose of 5 IU/10 g of body weight; to trigger ovulation. Groups of 12-20 mice were humanely killed by cervical dislocation in the following time sequence: at 44 hours post-PMSG injection (0h of hCG), 8h post-hCG, 11.5h post-hCG and 13h post-hCG injection. Ovaries (and oviducts at the 11.5 and 13 h time points) were dissected and either fixed immediately in 4% paraformaldehyde (PFA; Sigma-Aldrich, Missouri, USA) for immunohistochemistry or placed in HEPES-buffered GIBCO minimal essential medium (aMEM, Life Technologies Australia Pty Ltd) for the collection of

granulosa/luteal cells (GLCs) and cumulus cells (CCs) for RNA or confocal microscopy of whole cumulus-oocyte complexes (COCs) or denuded oocytes (DOs).

Briefly both ovaries were collected by post-mortem ventral dissection and placed in HEPES-aMEM at 37°C. GCs, GLCs and whole COCs were collected by puncturing the ovary using a 30G needle. Half of the COCs in each group were fixed in 4% PFA at RT for 15-20 minutes, then transferred to a phosphate buffer saline (PBS; 80 nM Na_2HPO_4, 20 mM NaH_2PO_4, 100 mM NaCl) solution containing 1mg/ml of polyvinylpyrrolidone (PVP; Sigma-Aldrich), and stored at 4°C. After COC removal, the granulosa cells were processed for mRNA extraction.

The remaining COCs were treated with hyaluronidase at 0.05% v/v to isolate the oocytes. These were fixed in 4% PFA containing 2% Triton X-100 (Sigma Aldrich) at RT for 10 min, then transferred to PBS-PVP for storage at 4°C. The remaining cumulus cells isolated at time points 11.5 and 13 h post-hCG were collected and processed for mRNA extraction.

2.3.2 Immunohistochemistry

Ovaries were collected at the different time points during the time sequence experiment, then transferred directly into 4% paraformaldehyde-PBS solution for fixation overnight at 4°C, after which tissues were washed 3x in PBS, and samples were then placed in cassettes and immersed in 75% Ethanol prior to paraffin embedding.

Five-micron tissue sections were de-waxed in xylene followed by rehydration in decreasing concentrations of ethanol and then PBS. Antigen retrieval was done by boiling the slides in citrate buffer solution (10 mM sodium citrate; Sigma Aldrich), for 20 min at 90°C, followed by rinsing in PBS containing 0.025% Tween-20 (PBST; Sigma Aldrich). Sections were then incubated with 3% H_2O_2 solution (Sigma Aldrich) in PBST, then blocked in 10% serum (from the host species of the secondary antibody) in PBST for 1 hour at RT. Ovary sections were then permeabilized in 0.2% Triton X-100 in PBST solution, followed by incubation in the primary antibody solution (diluted at the appropriate concentrations in 1% secondary-host serum in PBST; see complete list of antibodies on Appendix 3), in a humid chamber overnight at 4°C. Following washing in PBST, sections were incubated for 1 hour in a 1:1000 biotinylated secondary antibody solution in 10% secondary-host serum in PBST (Biotinylated goat-anti-rabbit, biotinylated rabbit-anti-goat; Millipore Corporation, Billerica, MA). Ovary sections were then incubated with streptavidin-conjugated horseradish peroxidase (HRP) solution (Vectastain ABC Kit, Vector Laboratories, Burlingame, CA) for 1h at RT and then detection

was done using diaminobenzidine (DAB kit, Vector Laboratories) as per manufacturer's instructions. Sections were then counter-stained using Haematoxylin solution at 4 g/L for 5 s (solution Gill No. 2, Sigma-Aldrich), and then dehydrated in increasing concentrations of ethanol followed by air drying overnight prior to mounting. Negative controls were incubated with either no primary antibody or with species and irrelevant isotype matched primary antibodies. For a complete list of antibodies and specific dilutions used for each of them, see Table 3.1.

2.3.3 Granulosa-luteal and cumulus cell isolation and RT-PCR

HEPES-buffered α-MEM containing either GC (or GCL, at 13h post-hCG) or CCs was collected and centrifuged at 1200G for 2 min to gently pellet the cells. The supernatant was discarded and the cell pellet snap-frozen in liquid nitrogen and stored at -80°C for later gene expression analysis.

Total RNA was extracted from frozen cell pellets using Trizol (Thermo Fisher Scientific, Massachusetts, USA) following the manufacturer's instructions. RNA samples were treated with DNAFREE DNAse (Life Technologies) to remove any residual DNA. After this, 1 ul was taken from each sample to quantify RNA and DNA content by measuring the ratio of absorbance between 260 and 280 nm using a spectrophotometer (Thermo Fisher Nanodrop spectrophotometer, Thermo Fisher Scientific). The manufacturer's instructions indicate that a ratio of ~1.8 is considered pure for DNA whereas a ratio of ~2.0 is considered pure for RNA. A given sample was considered free of DNA contamination when they had a 260/280 value of 1.98 or more. Afterwards, 5 ng/mL of mRNA were used to make cDNA by RT-PCR in 10 uL reactions using Supertranscript III reverse transcriptase (Life Technologies) in MicroAmp Fast Optical 96-Well Reaction Plate (Life Technologies). Quantitative real-time PCR was performed in triplicate with Quantstudio 12k Flex Real-time PCR system (Thermo Fisher Scientific), using Taqman Fast Universal Master Mix and hydrolysis probes (Life Technologies). The efficiency and specificity of the Taqman probes used in this assay is batch tested by the manufacturer and shown to be of almost 100%. Gene products measured were HSF1, HSPA5, HSPA1A, HSPA1B, HSP90AA1, HSP90B1, HSPD1, ATF4 and XBP1s (see Appendix 4 for primer details). These genes are key markers for the activation of cellular stress pathways, namely the Heat Shock Response (HSR) and Endoplasmic Reticulum Stress (ER stress). Real time PCR data was analysed using the $2^{-(\Delta\Delta CT)}$ method. Expression of target genes was normalised against the expression of ribosomal protein L19 (rpl19), which was used as a validated internal control

for every sample. The use of this reference gene has previously been validated for analysing mRNA levels in ovarian cells from mice [99, 100, 202]. Fold changes in gene expression were relative to expression levels in GCs collected at 44h post-PMSG injection. The calibrator sample in this case represents the amount of transcript that is expressed in the whole tissue, from which to obtain the relative number of mRNA copies of the target genes in the cell population of interest.

2.3.4 Confocal Immunocytochemistry

For immunocytochemistry, whole COCs and oocytes were blocked in 10% goat or rabbit serum in PBS-PVP for 1 hour at RT; then incubated in primary antibody plus 1% serum (from the host species of the secondary antibody) PBS-PVP solution overnight at 4°C (see for antibody details). Samples were incubated in 1:1000 Alexa Fluor 594 (Abcam, Cambridge, UK) in PBS-PVP at RT for 1 hour. Samples were mounted in 5-7 uL of DAKO Fluorescent Mounting Medium (Agilent Technologies, California, USA) on microscope glass slides (Lomb Menzel-Gläser Superfrost Plus; Thermo Scientific, Massachusetts, USA) and under 15x15 mm coverslips. Secure-seal spacers were used in the mounting of oocytes (one well, 13 mm diameter, 0.12 mm deep; Molecular Probes, Oregon, USA). Imaging was done using Leica SP5 Spectral Scanning Confocal Microscope (Adelaide Microscopy Services, University of Adelaide). All images were captured on identical microscope settings and using the cell nucleus as reference for focal plane.

Two negative controls were included to test the specificity of every antibody. These were primary antibody and isotype controls. The primary antibody control was used to test the specificity of the secondary antibodies in binding their targeted primary antibodies. In the 'no primary antibody' negative control the specific antibodies against the targeted protein are omitted, and only 1% secondary host-serum solution was used for overnight incubation. A negative result (i.e. no DAB staining) indicates that there is no non-specific binding by the secondary antibody. For the 'isotype' negative controls, the primary antibody solution was substituted with a non-specific Ig of the same primary class (i.e.: IgG or IgM) as the primary antibody, in order to test their specificity binding to the target protein. Negative staining indicates there is no non-specific binding of the secondary antibody. Positive or partially positive staining shows where non-specific binding occurs, i.e. that the detection method binds to epitopes other than the target protein it has been raised against.

2.3.5 Statistics

All measures are reported as mean ± the standard error of the mean (SEM), unless indicated otherwise. Data were analysed using the statistics software GraphPad Prism 6 v008 for Windows (GraphPad software Inc., La Jolla, CA). Statistical significance was determined by either unpaired One-way ANOVA or t-test as indicated. Gene expression in granulosa cells was analysed by One-Way ANOVA and post-hoc Tukey's multiple comparisons test; while comparison between cumulus cells at 2 time-points was done by unpaired Student's t-test. P values of <0.05 were considered statistically significant.

2.4 Results and Discussion

Expression of HSF1, HSPA1A/B, HSPA5, HSP90AA1, HSP90B1, HSPD1 were detected using immunohistochemistry of whole ovary sections to localize each protein's expression to different cell subpopulations within the ovarian follicle as well as intracellularly. Measures of protein levels of each gene were complemented with mRNA analysis of gene expression in granulosa and cumulus cells at each of the different time points. A more detailed examination of protein expression and intracellular localization in the COC and oocyte was conducted using immunofluorescent labelling and confocal visualisation.

Ovarian sections stained for HSF1 showed strong protein expression throughout the follicle. (Figure 2.1.A). Prior to hCG treatment (44 hours post-PMSG injection), HSF1 expression was detected in theca, granulosa and cumulus cells. In the oocyte, expression of HSF1 was primarily localized to the germinal vesicle. At 8 hours post-hCG injection, expression of HSF1 was similar, continuing to be highly localized around the nucleolus in the oocyte and remaining high in the granulosa cells. At 11.5 hours post-hCG, expression was visibly lower in the cytoplasm of cumulus cells. In the rest of the follicle, decreased levels of expression were also observed, except for the most antral layer of granulosa cells, which showed a slightly higher intensity of HSF1 positive staining in their cytoplasm compared to mural or cumulus cells. At 13 hours post-hCG, HSF1 was highly expressed in luteal cells.

Hsf1 mRNA expression in GLC generally mirrored that of the protein observed by immunohistochemistry. In GLC, Hsf1 mRNA levels were highest at 13 hours post-hCG, and lowest at 11.5 hours post-hCG (Figure 2.1.B) a similar pattern to that of protein levels detected by immunohistochemistry. Hsf1 gene expression in CC at 11.5 and 13 hours post-hCG was

increased when compared to GLC at the same time point, although the differences between cell types were not significant.

Detection of HSF1 in COC using confocal immunofluorescence confirmed the characteristic localisation to the GV during oocyte maturation (Figure 2.1.C and D). In both COC and isolated oocytes, HSF1 shows strong localization to the GV but exclusion from the nucleolus, at 0 and 8 hours post-hCG. At 11.5 hours post-hCG, coincident with GVBD, HSF1 staining in the nucleus was no longer observed.

Thus, in the gonadotropin-stimulated mouse ovary, Hsf1 protein levels are high in the oocyte during PMSG-induced folliculogenesis, where the protein strongly localized to the GV. The protein is also abundantly expressed in GC and CC during this time. Interestingly, expression levels for both mRNA and protein decreased around the time of ovulation most dramatically in GLC before returning to high levels during the formation of the corpus luteum at 13 hours post-hCG injection.

The localisation of HSF1 to the GV was expected because of its transcription factor activity. However, at 11.5 hours post-hCG injection, GVBD has happened and transcription has ceased in the oocyte. HSF1 is no longer localized around the DNA, likely due to the decrease in transcriptional activity and the dissolution of the GV envelope, prompting the dissociation and the de-phosphorylation of HSF1 protein homo-trimers. It is also around this time when ovulation happens, with expression levels for Hsf1 decreasing overall in the ovarian follicle. Interestingly, gene expression levels did not decrease in the CC around the time of ovulation, and furthermore both gene and protein expression were increased in GLC post-ovulation. This expression pattern might suggest that HSF1 has a role in ovulation and/or corpus luteum formation, however $Hsf1^{-/-}$ females have not been reported to have abnormal ovaries or ovulation defects [269] and thus the role of HSF1 in cumulus and granulosa cell function is unknown. We speculate that it may regulate some aspect of steroidogenesis or terminal differentiation/ luteinisation in these cells. HSF1 is known to directly regulate expression of Hsp90aa1 not only in oocytes [151], but in all eukaryotic cells [270], where it forms multi-protein complexes with other cofactors, binding to steroid receptors (reviewed in Schopf et al. 2017 [271] and in Pratt et al. 1997 [272]). Gonadotropin-stimulated primary GC produce high levels of P4, as well as increased expression of Hsp90aa1, which then forms complexes with cytoplasmic steroid receptors, suggesting that this chaperone is involved in the regulation of steroid hormone action [273]; and thus HSF1 in granulosa cells may indirectly influence steroid receptor activity or localisation. Furthermore, HSF1 has been shown to also regulate post-

translational mRNA modification of downstream HSP [274] and it may be via this function that it impacts oocyte developmental competence and/or potentially ovarian somatic cell functions.

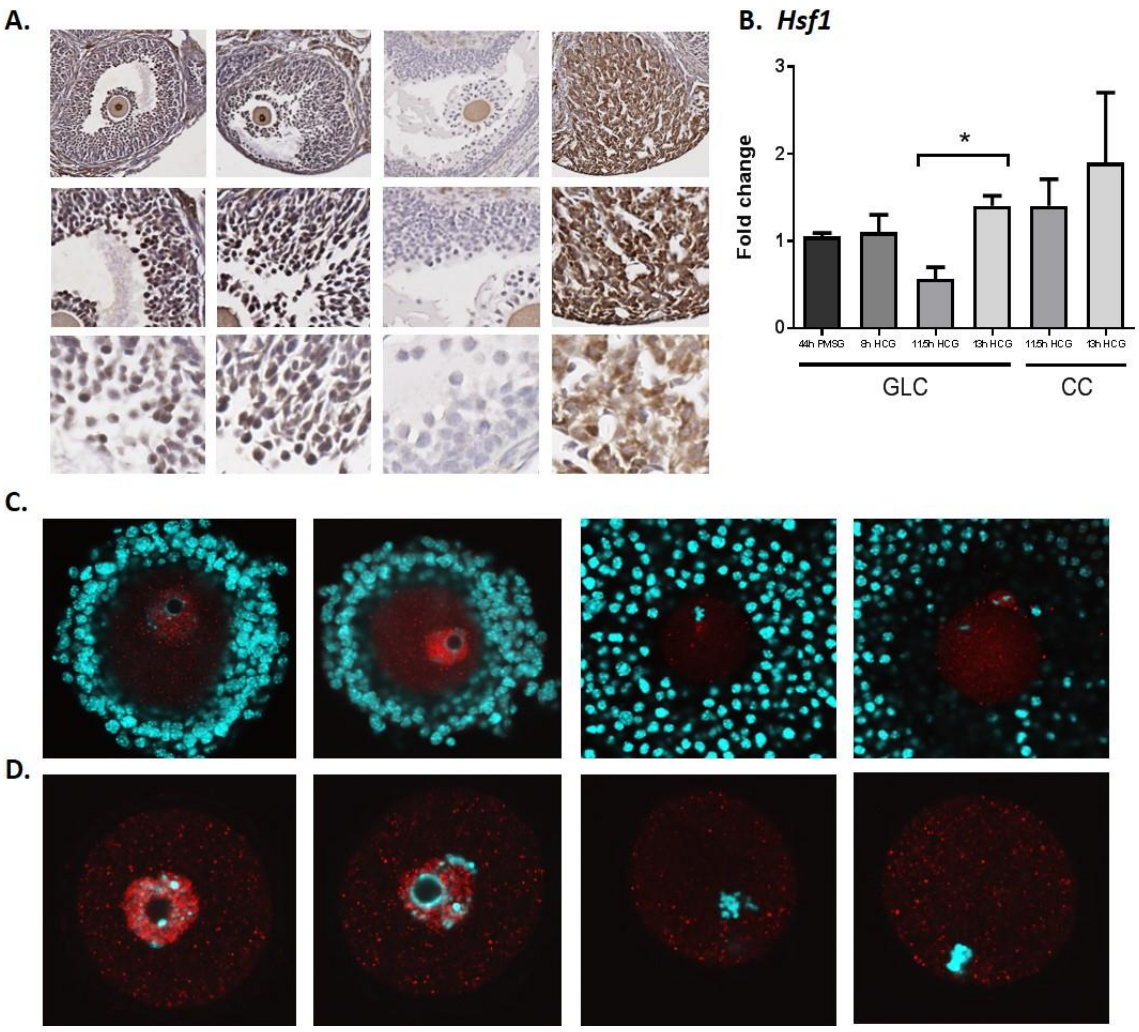

Figure 2.1 Expression and localisation of HSF1 in the mouse ovarian follicle in response to LH surge.

A. Immunohistochemistry for HSF1. One representative image is shown per time point. First row shows images of whole ovarian follicles and CL (far right) at 20X magnification; second row is the granulosa and luteal cells at 40X magnification; and third row are detailed images of granulosa and cumulus cells (or luteal cells) at 63X magnification. **B.** mRNA levels analyzed by qRT-PCR. N= 3 samples of GLC/CC pooled from 4-6 animals per timepoint. Statistical analysis was One-way ANOVA (GLC) or Student's t-test (CC) * P=0.0153. **C/D.** Representative confocal images of whole cumulus-oocyte complexes (C) and denuded oocytes (D). A, C, D are representative images of tissues analyzed from at least 4 mice per timepoint (from left to right: 44h post-PMSG; 8h post-hCG, 11.5h post-hCG and 13h post-hCG).

HSPA1A/B expression in granulosa cells during luteinisation was clearly detected by immunohistochemistry (Figure 2.2.A). The a-HSP70 antibody detects both HSPA1A and HSPA1B because they differ by only two amino acids (E110D, N499S), being more than 99% identical in gene sequence, Hsp70-1a (NM_005345) and Hsp70-1b (NM_005346). Prior to hCG, HSPA1A/B showed strong expression throughout the follicle, including in the oocyte, with localization primarily cytoplasmic in all cells. At 8 hours post-hCG injection, expression levels and localization remained relatively constant. At 11.5 hours post-hCG, expression had diminished in the follicle, primarily in the mural GC, with the inner antral GC layer and the CC exhibiting maintained expression intensity. At 13 hours post-hCG, HSPA1A/B was localized to the CL, although expression levels had decreased compared to earlier time points.

Analysis of Hspa1a and Hspa1b mRNA levels by qRT-PCR in GLC showed similar kinetics across the time points (Figure 2.2.B). Both genes showed mostly constant expression with Hspa1a exhibiting more variability at 8 and 13 hours post-hCG in GLC, although no significant differences were found. mRNA levels in GC generally reflected those of the protein. Interestingly, expression of both genes in CC significantly decreased between 11.5 and 13 hours post-hCG, concurrent with ovulation.

Immunofluorescence of isolated COC showed HSPA1A/B exhibited relatively consistent expression in the cytoplasm of cumulus cells during expansion and ovulation (Figure 2.2.C), similar to immunohistochemistry of ovarian sections (Figure 2.2.A), even though mRNA levels dramatically decreased between 11.5 and 13h post-hCG (Figure 2.2.B). In oocytes HSPA1A/B was excluded from the GV and interestingly, showed some increased localization to the meiotic spindle at 11.5 hours post-hCG. This pattern of localization and expression was identical between COC and denuded oocytes (DO) (Figure 2.2.C and .D).

We observed that the expression levels of both Hspa1a and Hspa1b were high in ovarian follicular cells during ovarian stimulation, where the protein showed cytoplasmic location. Interestingly, in oocytes both proteins showed partial localisation to the spindle during the resumption of meiosis. We also observed that, in CC, Hspa1a and Hspa1b are dramatically downregulated concurrent with ovulation. However, after ovulation has occurred, expression levels decrease markedly in CC while slightly increasing in luteal cells. In oocytes, protein levels appeared constant across maturation and post-ovulation. Although it had previously been reported that Hspa1a/b were expressed at very low levels in fully grown oocytes [151, 275], our data suggest this protein is highly localised to the oocyte's cytoplasm, which we speculate is due to cytoplasmic protein accumulation. This is consistent with findings from Christians et

al [276], where they used a Hsp70.1(Hspa1a)Luc transgene and showed that it was unexpectedly highly expressed in fully grown oocytes.

Mice that are KO for Hspa1a/Hspa1b do not present an infertility phenotype [249]. However, we were interested in studying these proteins because of their inducibility by stress. Our observations suggest that the expression of these proteins around the time of ovulation would allow for these chaperones to protect the cells from cellular stress if it were to occur. In the past, several studies have characterised the lack of inducibility of Hspa1a/b by heat stress in mouse oocytes and early embryos [143, 183, 277, 278], unlike what happens in adult somatic cells. Despite the presence of Hsf1 [143], Hspa1a/b in murine oocytes lose the ability to be induced by heat stress in the oocyte as they acquire full size and antrum formation within the follicle, and finally is shut down in fully mature oocytes [278]. However, the opposite has been shown for the accompanying follicular cells [278]. Our observations suggest that constitutive levels of Hspa1a/b in cumulus cells follow those of the oocyte, as mRNA levels decline in CC from ovulated COC in less than 2 hours after ovulation. Taken together, these findings validate previous reports on the presence of Hspa1a/b in the oocyte across maturation and ovulation, suggesting that the time from ovulation until blastocyst embryonic stage is a window of vulnerability against stress for the ovulated COC, likely as a result of their lack of inducibility by HSF1. Although Hspa1a and Hspa1b are thought to have homologous functions, their basal expression differ slightly in the majority of the tissues, where usually Hspa1a has the highest mRNA levels of the two [256]

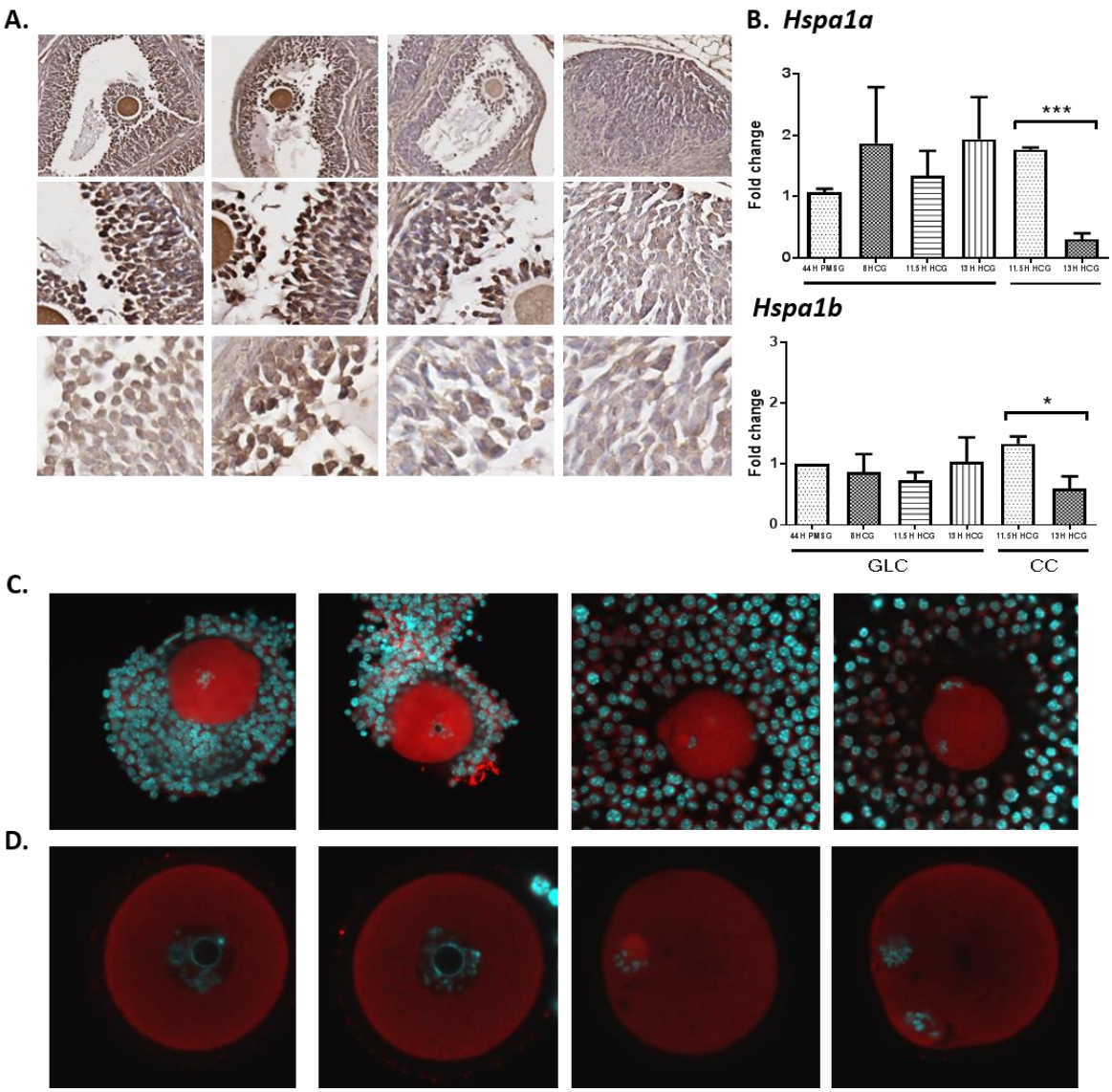

Figure 2.2 Expression and localisation of HSPA1A/B in the mouse ovarian follicle in response to LH surge

A. Immunohistochemistry for HSPA1A/B. One representative image is shown per time point. First row shows images of whole ovarian follicles and CL (far right) at a 20X magnification; second row is the granulosa and luteal cells at a 40X magnification; and the third row are detailed images of granulosa and cumulus cells (or luteal cells) at 63X magnification. **B.** mRNA levels analysis by qRT-PCR. N= 3 samples of GLC/CC pooled from 4-6 animals per time point. Statistical analysis was by One-Way ANOVA (GLC) or Student's t-test (CC) *** P= 0.0004, * P= 0.0422. **C/D.** Representative confocal images of whole cumulus-oocyte complexes (C) and denuded oocytes (D). A, C, D are representative images of tissues analysed from at least 4 mice per time point (from left to right: 44h post-PMSG, 8h post-hCG, 11.5h post-hCG and 13h post-hCG).

Immunohistochemical analysis of HSPA5 showed that it was expressed throughout the follicle and the CL during follicular maturation (***Figure 2.3.A***). Prior to hCG, HSPA5 showed high levels of expression throughout the GC and theca cells layers. Localization was cytoplasmic in theca, GC and CC. Interestingly intracellular localisation in GC transitioned from a smooth homogeneous pattern prior to hCG to a more punctate granular texture at 8 hours post-hCG. At 11.5 hours post-hCG, the strongest expression was observed in the thin layer of apical epithelial cells. At 13 hours post-hCG, high levels of expression were observed in the CL and again the protein was cytoplasmic consistent with ER localisation.

Hspa5 mRNA levels in GLC were at their highest at 44 hours post-PMSG, significantly decreasing by 11.5 hours post-hCG and remaining low at 13h (***Figure 2.3.B***). mRNA levels in CC also did not change between 11.5 and 13 hours post-hCG. Hspa5 mRNA levels appeared higher in CC than in GLC but this was not statistically significant. In general, the changes in mRNA levels in GLC mirrored those of the protein.

HSPA5 was only very faintly detected in cumulus cells and whole COCs and DOs by immunofluorescence (***Figure 2.3.C*** and ***.D***). In CCs, there were no marked changes in this very low level of protein expression levels. However, in both COCs and DOs, there was localization of HSPA5 to the GV. In contrast to HSF1 which was localised throughout the GV, HSPA5 showed a more specifically localised distribution within the GV, with fluorescence detected as puncta around the DNA. This was also observed at 8 hours post-hCG, although the intensity of the fluorescence was weaker. At 11.5 hours post-hCG, there was partial localization of HSPA5 to the area surrounding the spindle. This restricted localisation in oocytes observed by confocal is different to the homogeneous staining that was detected in oocytes by immunohistochemistry of ovarian sections. The most likely explanation is that a thinner section will allow better permeabilization, resulting in better antibody penetration and richer staining. The paraffin-embedded ovarian tissue sections used were 5 nm thick, whereas the whole mouse oocytes used for the whole-mount immunodetection experiments were typically around 72 um.

Overall, expression levels for Hspa5 were high in the follicular cells after ovarian stimulation, namely GC and CC. As ovulation approached, protein and mRNA levels for Hspa5 decreased in GC; and protein localisation was concentrated in the inner layers of GC and the CC. Hspa5 mRNA abundance reached its lowest level around the time of ovulation, with mRNA levels higher in CC than in GLC during this time. At the cellular level, HSPA5 protein presented a cytoplasmic localisation but interestingly appeared concentrated to the apical region in some GC, particularly in antral GC following the LH surge. It is possible this staining pattern

represents some specialised region of the granulosa cell ER. HSPA5 is considered to be an endemic protein to the ER and a well-known marker for the activation of the UPR in this organelle. The high level of expression across follicular maturation and ovulation indicates that the UPR is important for follicular maturation. It is also a marker of the high ER activity in normal ovarian cells. Harada et al had shown that upregulation of the UPR in the cumulus cells correlates with fertilization success of the oocyte in humans [279].

Surprisingly, HSPA5 localisation in the oocyte was not cytoplasmic. While HSPA5 is normally located to the ER, it has also been shown to localize to other cellular structures such as the surface of tumor cells, where it forms a complex with epidermal growth factor-CFC CRIPTO to enhance tumor growth via the inhibition of Transforming growth factor beta (TGF-β) signalling [280]. It has also been shown to relocate from the ER lumen to the cytosol and as an ER transmembrane protein during induction of ER stress, where it prevents the release of caspases from the ER to inhibit the cytoplasmic component of the ER stress-induced apoptotic cascade [281]. Prior to hCG, HSPA5 localised to the GV; later localising to the outer region of the meiotic spindle and the first polar body during ovulation. Even though no gene transcription, gene repression or DNA-binding activity has been yet demonstrated for this protein from in vitro nor in vivo studies, one proteomics study detected the presence of HSPA5 in nuclear protein samples purified from human spermatozoa by gel electrophoresis and mass spectrophotometry [282]. To the best of our knowledge, this is the first evidence of its GV localisation in mammalian oocytes, and these results suggest that HSPA5 could have a specialised function as regulating gene expression or repression or participate in DNA stabilisation in preparation for the resumption of meiosis.

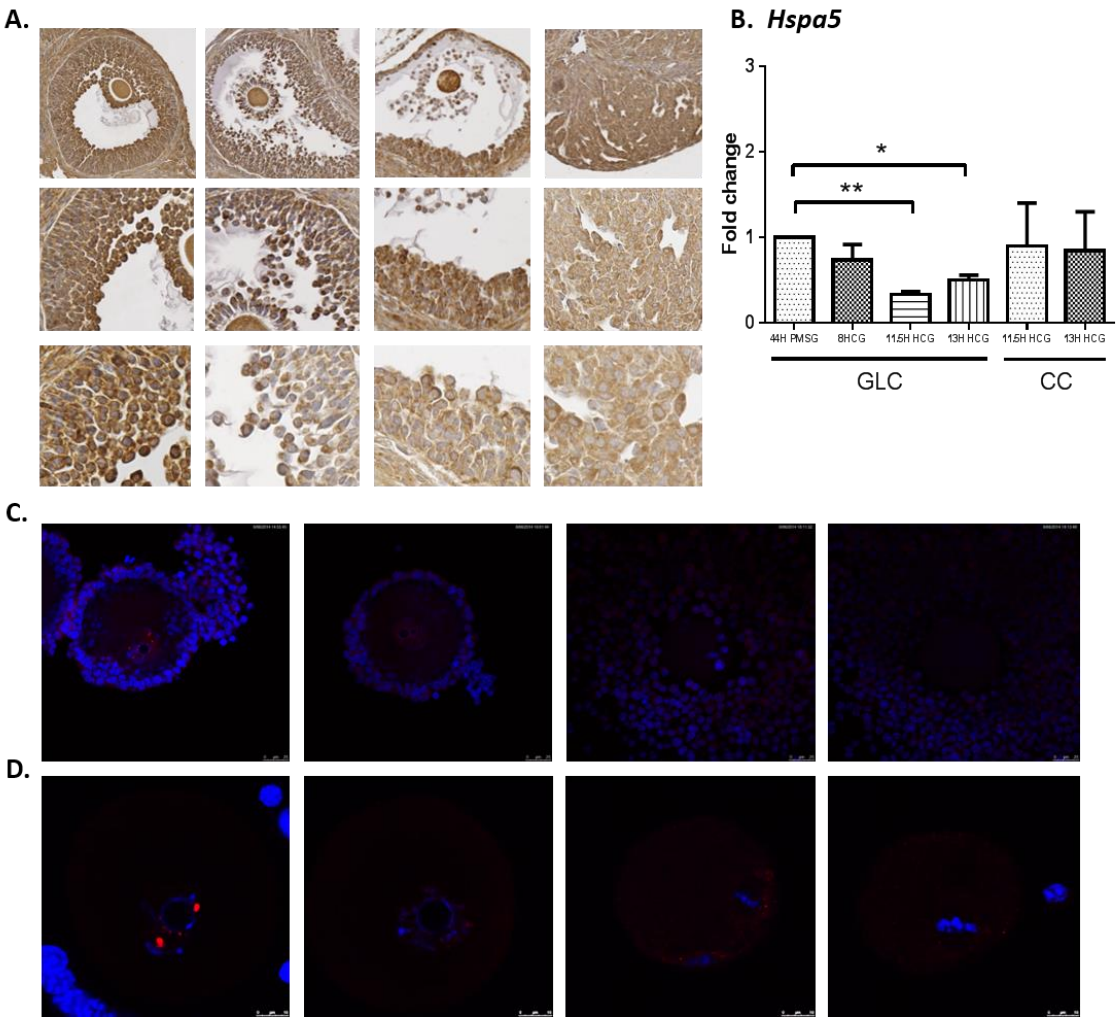

Figure 2.3 Expression and localisation of HSPA5 in the mouse ovarian follicle in response to LH surge.

A. Immunohistochemistry for HSPA5. One representative image is shown per time point. First row shows images of whole ovarian follicles and CL (far right) at a 20X magnification; second is the granulosa and luteal cells at 40X magnification; and third row are detailed images of granulosa and cumulus cells (or luteal cells) at 63X magnification. **B.** mRNA levels were analyzed by qRT-PCR. N = 3 samples of GLC/CC pooled from 4-6 animals per time point. Statistical analysis was One-Way ANOVA (GLC) or Student's t-test (CC) */** P=0.0067. **C/D.** Representative confocal images of whole cumulus-oocyte complexes (C) and denuded oocytes (D). A, C, D are representative images of tissues analyzed from at least 4 mice per time point (from left to right: 44h post-PMSG, 8h post-hCG, 11.5h post-hCG and 13h post-hCG).

HSP90AA1 (HSP90-alpha) is another well-characterised cytoplasmic chaperone like HSPA1A/B; and it has been shown to be necessary for successful meiosis in the oocyte [151]. HSP90AA1 was detected in ovarian somatic cells, namely the granulosa cell layer and the corpora lutea (***Figure 2.4.A***). Prior to hCG, HSP90AA1 was expressed in the cytoplasm of the GC, with highest expression in the antral cell layer and CC. At 8h and 11.5h post-hCG, expression was maintained in the antral GC layer and CC. In the oocyte, the HSP90AA1 protein can be seen localized to the spindle at 11.5h post-hCG. At 13 hours post-hCG, expression was prevalent in the CL, where the protein localized to the cytoplasm of luteal cells.

Hsp90aa1 gene expression in GC decreased across the time points analysed, reaching the lowest expression at 11.5h post-hCG, then sharply increasing again in GLC to the point of highest expression at 13h post-hCG. This was consistent with the visual assessment of protein levels. In CCs, mRNA levels at 11.5h post-hCG were higher than those in GC and were unchanged at 13h post-hCG. (***Figure 2.4***)

Expression of HSP90AA1 in CC was not clearly visible, although weak fluorescence was detected in COC at 44 hours post-PMSG (***Figure 2.4.C***). Dynamic changes in HSP90AA1 localization in the oocyte during maturation and ovulation could be visualised by confocal immunofluorescence (***Figure 2.4.D***). At 44 hours post-PMSG and 8h post-hCG, HSP90AA1 showed a diffuse cytoplasmic distribution, but greater localisation to the cortical areas of the oocyte cytoplasm particularly at 8 hours post-hCG. At 11.5 hours post-hCG, the protein exhibited strong localization to the meiotic spindle as well as cortical cytoplasm. At 13 hours post-hCG, HSP90AA1 was still localized to the spindle and the cytoplasm, but the intensity of fluorescence had diminished.

Overall, expression of Hsp90aa1 in the ovarian follicle was mainly localised to the antral GC and CC, and to the CL after ovulation. Hsp90aa1 has been shown to bind to steroid hormone receptors to form the functional receptor complexes in response to progesterone production in GC [273]. The decrease in Hsp90aa1 expression in GC around ovulation and the following increase are likely due to the increase in progesterone production and progesterone receptors in these cells as they transition from granulosa to luteal cells. Additionally, Hsp90aa1 was expressed in the peri- and post-ovulation CC. Our observations of HSP90aa1 localisation to the spindle in the oocyte around the time of ovulation is consistent with its established role in the normal progression of meiosis and the acquisition of metaphase II [151].

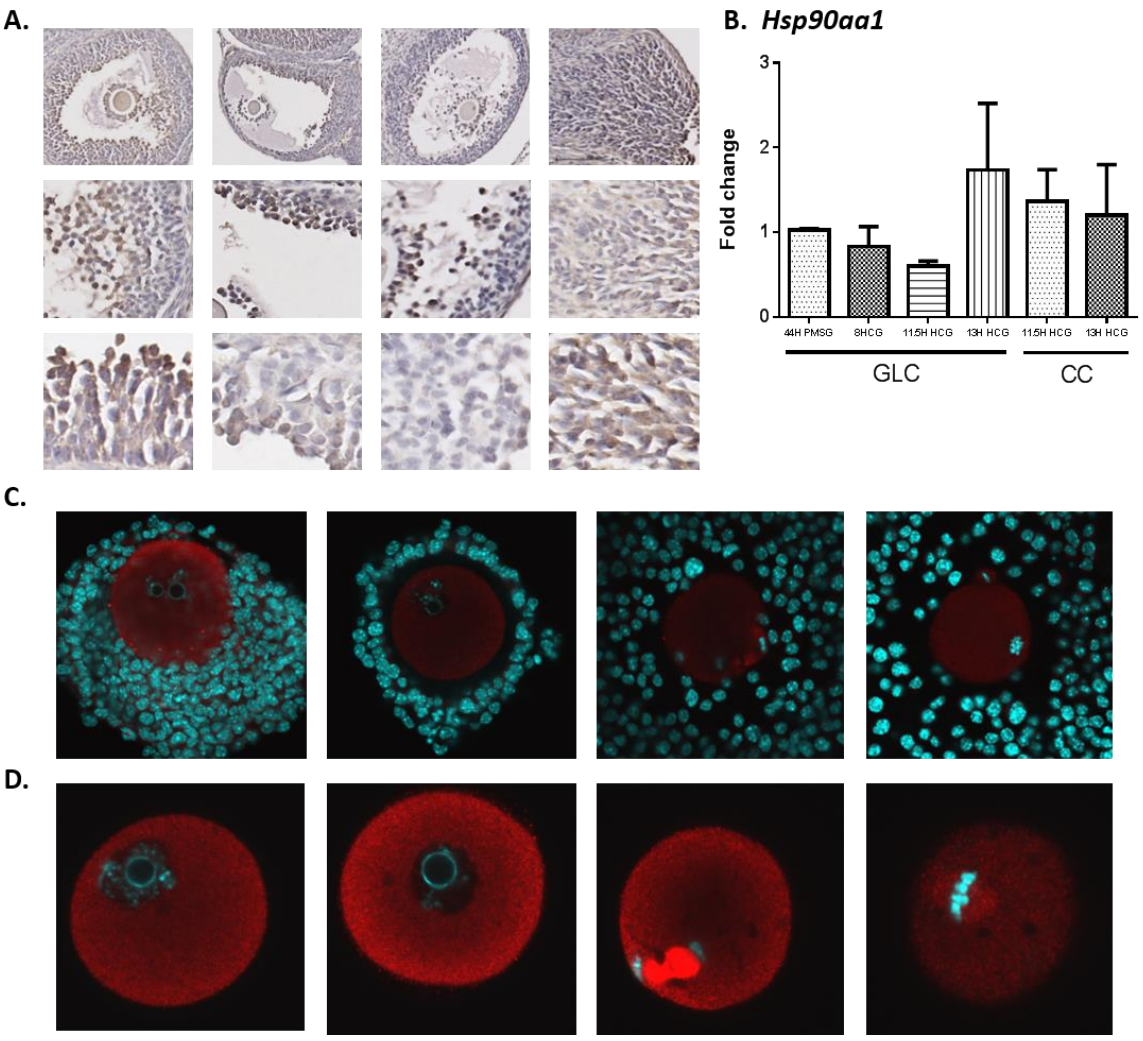

Figure 2.4 Expression and localisation of Hsp90AA1 in the mouse ovarian follicle in response to LH surge.

A. Immunohistochemistry for HSP90AA1. One representative image is shown per time point. First row shows images of whole ovarian follicles and CL (far right) at 20X magnification; second row is the granulosa and luteal cells at 40X magnification; and third row are detailed images of granulosa and cumulus cells (or luteal cells) at 63X magnification. **B.** mRNA levels analyzed by qRT-PCR. N = 3 samples of GLC/CC pooled from 4-6 animals per time point. Statistical analysis was One-way ANOVA (GLC) or Student's t-test (CC). **C/D.** Representative confocal images of whole cumulus-oocyte complexes (C) and denuded oocytes (D). A, C, D are representative images of tissues analyzed from at least 4 mice per time point (from left to right: 44h post-PMSG, 8h post-hCG, 11.5h post-hCG and 13h post-hCG).

HSP90B1 (GRP94, TRA1) is another ER-resident chaperone, but its role in ovarian function and ovulation is largely unknown. HSP90B1 was strongly expressed in the cytoplasm of granulosa cells and acquired a granular distribution following the hCG surge (***Figure 2.5.A***). HSP90B1 staining intensity in ovarian follicles was highest at 44 hours post-PMSG and was detected in multiple cell types in the follicle. In the GC, it showed a smooth cytoplasmic distribution, with highest intensity in the antral cell layer. The CC and the oocyte also showed high expression of HSP90B1 with cytoplasmic localisation. By 8 hours post-hCG, HSP90B1 protein expression decreased in the cytoplasm of GC and acquired a granular texture. This was also observed in the cytoplasm of CC. In the oocyte, protein became localized to the outer areas of the cytoplasm and the plasma membrane. At 11.5 hours post-hCG, expression appeared decreased further, and in both GC and CC its distribution was more irregular and punctate. In the oocyte, localization was maintained to the outer cytoplasm and the plasma membrane. Expression of the protein was also detected in the cytoplasm of luteal cells at 13 hours post-hCG.

Hsp90b1 gene expression analysis of GLC showed levels were relatively static during follicular growth, then sharply decreasing at 11.5h post-hCG, followed by an increase again at 13h. In CCs, expression of Hsp90b1 was higher than in GLC at the same time points, but mirrored what was observed in the GLC, with mRNA levels rising at 13h post-hCG (***Figure 2.5.B***). These changes in gene expression levels were not significantly different when analysed statistically.

Immunofluorescence detection of HSP90B1 in COC and DO showed that HSP90B1 was highly localized to the plasma membrane in the oocyte (***Figure 2.5.D***). HSP90B1 also showed dynamic expression in the CC (***Figure 2.5.C***), localizing to the outer CC layer at 44 hours post-PMSG, and then showing strong expression and cytoplasmic localization in all CC by 8h post-hCG. At 11.5 hours post-hCG, intensity of fluorescence diminished in almost all cells of the expanded CC. Interestingly, then at 13 hours post-hCG, expression increased and was detectable in the cytoplasm of the majority of the cells. In oocytes, the protein remains consistently localized to the plasma membrane and the cortical cytoplasm.

In summary, protein levels for HSP90B1 were consistent across follicular maturation, ovulation and formation of the CL, presenting a non-uniform texture in GLC and CC. The texture changes of HSP90B1 in the cytoplasm of granulosa cells fits the conformational changes occurring in the ER during differentiation and luteinisation [283]. Protein levels were reflective of mRNA levels, appearing the highest in the early follicle and the luteal cells, with the lowest expression in GC and CCs around ovulation. Interestingly, although HSP90B1 was uniformly expressed

in CCs during follicular growth, it did not localise to all the CCs in the ovulated COC. This variation in protein expression is likely due to cellular changes in the cumulus cells during ovulation [284]. The increase in Hsp90b1 mRNA levels in CC after ovulation is an indication of acquisition of competence in bovine oocytes. In vitro matured bovine COC treated with a low dose of the protein kinase C (PKC)-activator phorbol myristate acetate (PMA) showed higher expression of Hsp90b1 in CC [285] that was associated with improved oocyte competence and developmental potential [286]. Even though HSP90B1 is one of the chaperones native to the ER in most cells, it is highly localized to the plasma membrane of the oocyte across maturation and ovulation, hinting that HSP90B1 could be acting as a signalling molecule. This signalling function has been observed in primary breast cancer cell cultures, where membrane-bound HSP90B1 was shown to stimulate cell proliferation by facilitating human epidermal growth factor receptor 2 (HER2) dimerization [287]. Additionally, HSP90B1 has also been shown to play an important role in the completion of cytokinesis during the first mitosis in mouse zygotes [264], a role that is likely to require its accumulation in the outer cytoplasm and the membrane.

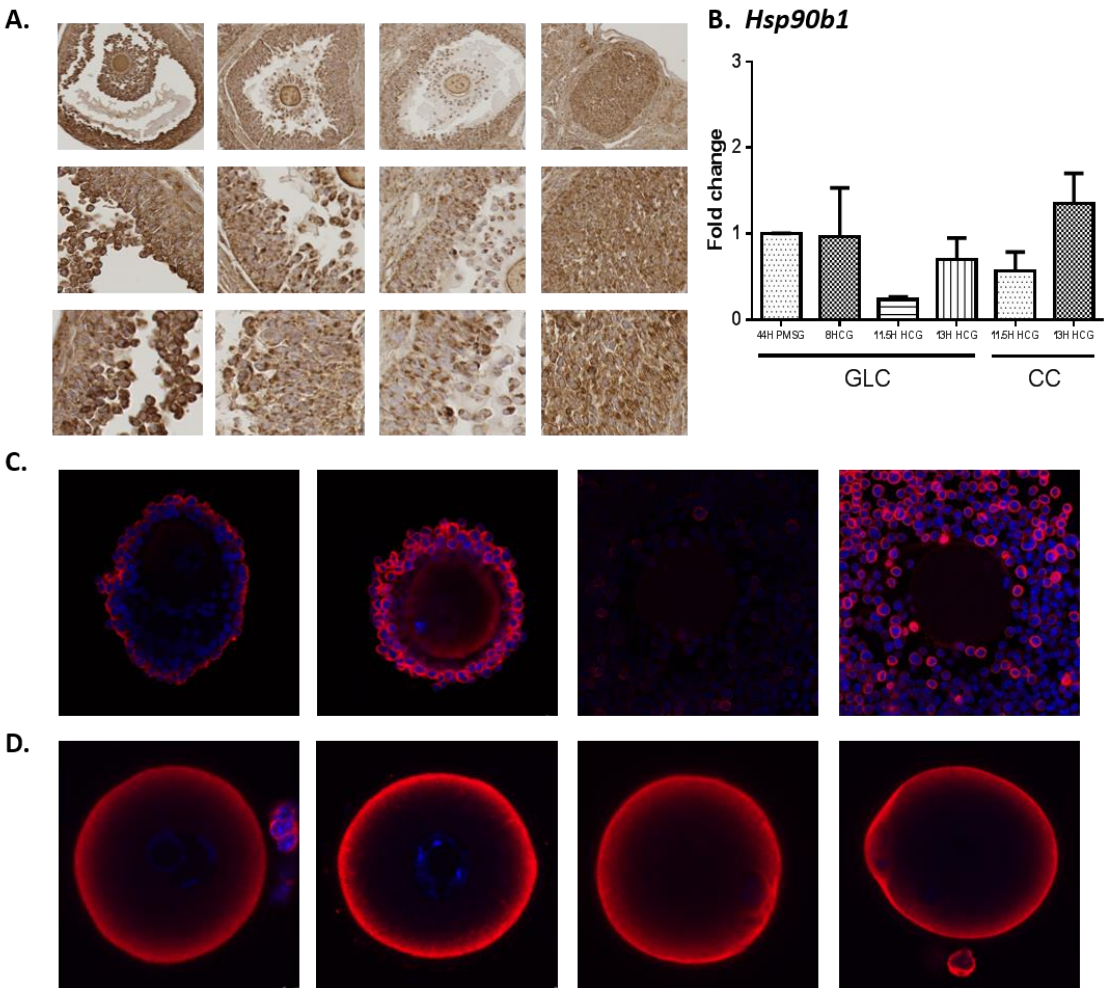

Figure 2.5 Expression and localisation of HSP90B1 in the mouse ovarian follicle in response to LH surge.

A. Immunohistochemistry for HSP90B1. One representative image is shown per time point. First row shows images of whole ovarian follicles and CL (far right) at 20X magnification; second row is the granulosa and luteal cells at 40X magnification; and third row are detailed images of granulosa and cumulus cells (or luteal cells) at 63X magnification. **B.** mRNA levels analyzed by qRT-PCR. N = 3 samples of GLC/CC pooled from 4-6 animals per time point. Statistical analysis was One-way ANOVA (GLC) or Student's t-test (CC). **C/D.** Representative confocal images of whole cumulus-oocyte complexes (C) and denuded oocytes (D). A, C, D are representative images of tissues analyzed from at least 4 mice per time point (from left to right: 44h post-PMSG, 8h post-hCG, 11.5h post-hCG and 13h post-hCG).

HSPD1 (HSP60, GROEL) is known to be localized to the mitochondria but little is known about its expression in the ovary. HSPD1 immunohistochemistry showed HSPD1 expression in GC which interestingly appeared to be expressed at different levels within GC of the same follicle (***Figure 2.6.A***). Prior to hCG, HSPD1 protein was most prominently expressed in the theca cells. In the GC and CC, HSPD1 was not uniformly distributed and localized primarily to cells in the cumulus oophorus. This pattern was maintained at 8 hours post-hCG, although expression had decreased. At 11.5 hours post-hCG, only a few isolated cells showed protein expression. Interestingly in the GC layer HSPD1 was cytoplasmic in some cells but exhibited distinct nuclear staining in others. At 13 hours post-hCG, HSPD1 protein was highly expressed in the luteal cells of mature CL while expression was not detected in recently formed CL. HSPD1 expression was heterogeneously expressed in mature degenerating CL of the previous cycle (images not shown).

Hspd1 gene expression in GLC and CC did not change significantly across the ovulatory timeframe although levels were variable between animals particularly at 8h post-hCG and 13h post-hCG before and after the time of ovulation (around 11.5h post-hCG). Expression was the lowest at 11.5h post-hCG in both GLCs and CCs (***Figure 2.6.B***).

Immunofluorescence detection of HSPD1 did not show detectable protein in cumulus cells and only weak punctate fluorescent signal in oocytes at most time points (***Figure 2.6.C*** and ***.D***). However, specifically at 11.5h post-hCG HSPD1 was clearly localised surrounding the meiotic spindle. Fluorescence intensity then decreased again throughout the oocyte at 13 hours post-hCG.

In summary, HSPD1 localised strongly to the theca cell layer during folliculogenesis. Within the ovarian follicle, the protein concentrated to cells in the cumulus oophorus area, with expression levels decreasing until the time of ovulation, although this was not observed in the whole-mounted stained COC. The discrepancy between protein levels detected between the ovarian sections and the whole COC are likely due to different penetration levels of the antibody in the fixed tissues. HSPD1 localisation in GLC and CC was mainly cytoplasmic, although in some cells it also localised to the nucleus. HSPD1 is normally localized to inner mitochondrial matrix however, our observations suggest it may also localise to the nucleus, in proximity to the DNA. This mitochondrial chaperone has been shown to localise to other parts of the mammalian cell under certain conditions of stress, such as the plasma membrane, ER, peroxisomes and other vesicle-like structures [288, 289]. Taken together, these findings suggest that HSPD1 could perform other roles outside of the mitochondria, but likely in the membranes of different organelles. In the oocyte, HSPD1 concentrated around the meiotic spindle at 11.5h

post-hCG, following the distribution of the mitochondria during chromosome segregation and polar body extrusion [290].

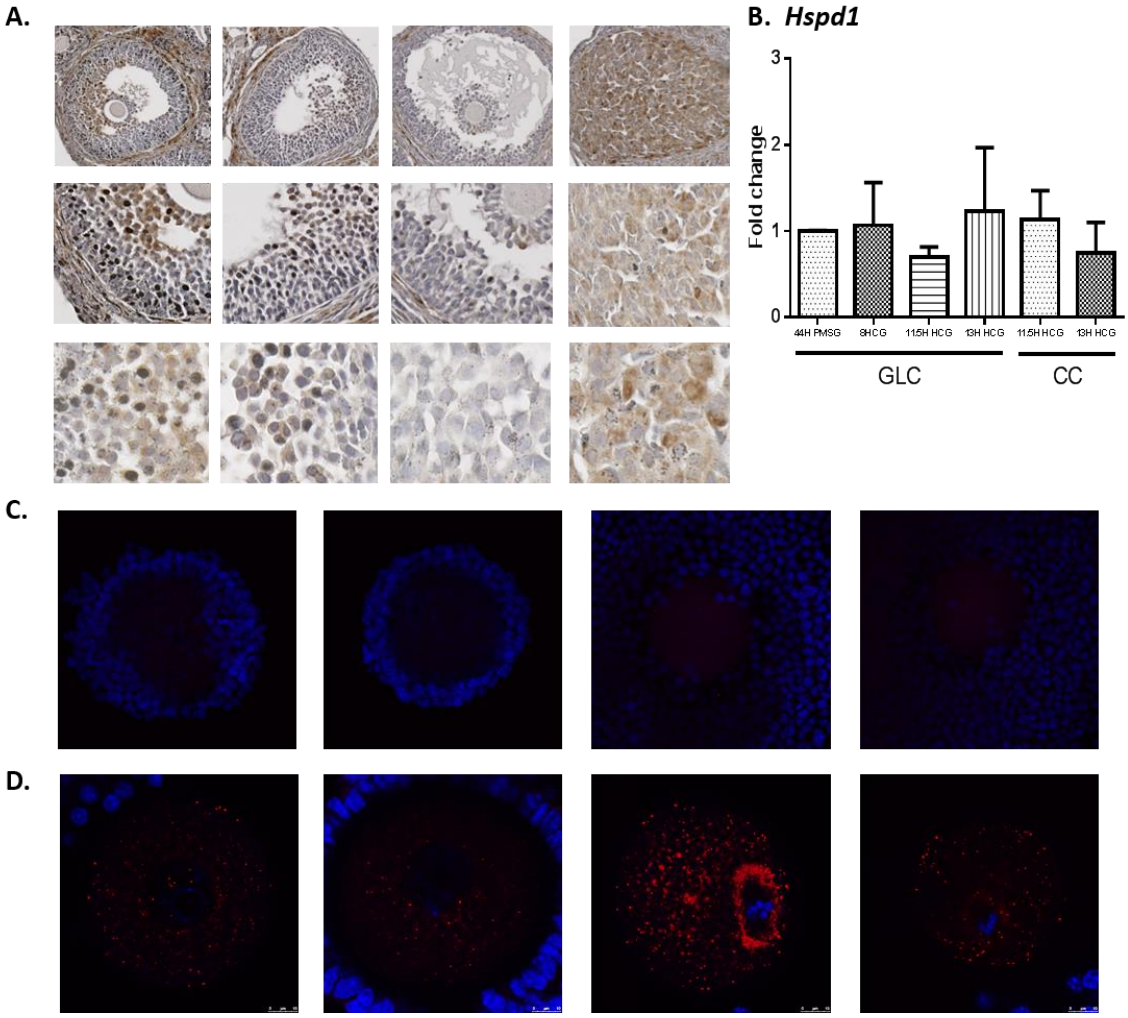

Figure 2.6 Expression and localisation of HSPD1 in the mouse ovarian follicle in response to LH surge.

A. Immunohistochemistry for HSPD1. One representative image is shown per time point. First row shows images of whole ovarian follicles and CL (far right) at 20X magnification; second row is the granulosa and luteal cells at 40X magnification; and third row are detailed images of granulosa and cumulus cells (or luteal cells) at 63X magnification. **B.** mRNA levels analysed by qRT-PCR. N = 3 samples of GLC/CC pooled from 4-6 animals per time point. Statistical analysis was One-way ANOVA (GLC) or Student's t-test (CC). **C/D.** Representative confocal images of whole cumulus-oocyte complexes (C) and denuded oocytes (D). A, C, D are representative images of tissues analysed from at least 4 mice per time point (from left to right: 44h post-PMSG, 8h post-hCG, 11.5h post-hCG and 13h post-hCG).

2.5 Conclusions

These results show that the ovulatory LH surge triggers a change in the expression of the proteins of the Heat Shock network in both the oocyte and the granulosa cells. A number of the analysed HSP as well as HSF1 exhibit dynamic expression and localisation in the ovarian follicle during ovulation and oocyte maturation. This is likely reflective of their important roles in cytoprotective mechanisms and the role they play in assuring the competence of the matured oocytes.

Supporting follicular cells have an essential role in achieving optimal oocyte maturation and quality. The GC help nurture the oocyte since the very early stages of follicular development. They are responsible for the production of oestradiol in response to increasing levels of FSH that will trigger follicular growth [34, 35]. In GC, each of the genes studied exhibited regulated expression with consistently lowest expression at 11.5h post-hCG, the time point immediately prior to ovulation. After ovulation, as they luteinise, GC reduce estradiol and increase P4 production; and form the CL (reviewed in Stocco et al, 2007 [33]). Both HSP protein and gene expression analysis show that expression levels of each gene increase again in luteal cells. We hypothesize that this occurs in concert with the change in the type of steroid receptors expressed in these cells as they differentiate from granulosa to luteal cells during luteinisation, where the HSP must be induced in order to bind and regulate the function of steroid receptors. It has already been shown that some heat shock proteins such as HSPA1B and HSP90AA1 bind hormone receptors in other cell types (reviewed in [291]). Specifically, HSPA1B ensures the correct folding of the hormone binding domain of receptors into their high affinity steroid binding configuration [128]; while surges in progesterone production in luteal cells induce intra-cellular HSP90AA1 to form the functional progesterone receptor complexes [273].

The CC have an essential role in regulating meiotic resumption and acquisition of developmental competence during follicular growth, directly supporting the oocyte through cytoplasmic projections and gap junctions [49-53]. By the time the oocyte has reached MII and ovulation takes place, these unions have disappeared, but the CC still have an important role in oocyte fertilisation. During their expansion prior to ovulation, the CC excrete a hyaluronidase-rich extra-cellular matrix and soluble factors that will act as sperm chemo-attractants, and promote capacitation and the initiation of the acrosome reaction [54-56]; while abnormal CC expansion decreases the fertilisation chances in the oocytes [39]. Moreover, there is some evidence suggesting that CC survival can influence the time-frame of oocyte fertilisation and post-ovulatory aging. Giacomo et al showed that post-ovulatory changes resulting in

hyaluronan release from the matrix and CC dispersion were temporally correlated to CC apoptosis and cell death; but elevation of cAMP levels prevented the disaggregation of ovulated COC and prolonged CC survival, which resulted in an extended time for the oocyte to be fertilized in vitro [57]. HSP expression in CC during and after ovulation was not uniform. mRNA levels increased for Hsf1 and Hsp90b1, mirroring the expression pattern in GLC. Protein levels for HSP90B1 strongly increased in the CC of ovulated COC, although this was not a uniform distribution. It is likely that HSP90B1 plays a role in the very high level of protein production and secretion that rapidly occurs in CC in response to the LH surge. We speculate that the increase in Hsf1 expression is likely supporting HSP90B1 expression at this time point and suggest that it may have an unknown function in CC during the fertilisation window. In contrast, HSPA1A/B expression decreases in CC after ovulation. Gene expression levels for Hspa5, Hsp90aa1 and Hspd1 remain mostly unchanged in these cells during this time, accompanied by low protein levels.

Overall, these results also indicate that the HSP studied are indeed expressed and specifically localized in the oocyte during and after ovulation. This could mean that these proteins are maternal factors that accumulate in the oocyte for later use by the embryo. HSF1 is a known maternal factor [144], meaning this particular protein's half-life in the mouse spans from prior to ovulation to its activation prior to the zygotic genome activation, which in the mouse occurs during the first mitotic division (from 1-cell to 2-cells). However, unlike $HSF1^{-/-}$ embryos which are arrested at the 1-cell stage [292], the lack of other HSP proteins present embryonic lethality at later stages, when the embryo can transcribe and synthesise its own proteins. Whether these HSP are accumulated and remain not functional until their activation in later embryonic stages or they have yet unknown functions in the oocyte and/or during fertilisation is still unclear.

Overall, these data suggest that HSP could have unknown specialised functions in supporting ovarian cells and COC, which warrant further exploration.

2.6 References

33. Stocco C, Telleria C, Gibori G. The Molecular Control of Corpus Luteum Formation, Function, and Regression. Endocrine Reviews 2007; 28:117-149.
34. Mason HD, Martikainen H, Beard RW, Anyaoku V, Franks S. Direct gonadotrophic effect of growth hormone on oestradiol production by human granulosa cells in vitro. J Endocrinol 1990; 126:R1-4.
35. Vanderhyden BC, Tonary AM. Differential Regulation of Progesterone and Estradiol Production by Mouse Cumulus and Mural Granulosa Cells by a Factor(s) Secreted by the Oocyte. Biology of Reproduction 1995; 53:1243-1250.
39. Russell DL, Salustri A. Extracellular matrix of the cumulus-oocyte complex. Semin Reprod Med 2006; 24:217-227.
49. Luciano AM, Lodde V, Beretta MS, Colleoni S, Lauria A, Modina S. Developmental capability of denuded bovine oocyte in a co-culture system with intact cumulus-oocyte complexes: role of cumulus cells, cyclic adenosine 3',5'-monophosphate, and glutathione. Mol Reprod Dev 2005; 71:389-397.
50. Chian RC, Lim JH, Tan SL. State of the art in in-vitro oocyte maturation. Curr Opin Obstet Gynecol 2004; 16:211-219.
51. Chen J, Torcia S, Xie F, Lin CJ, Cakmak H, Franciosi F, Horner K, Onodera C, Song JS, Cedars MI, Ramalho-Santos M, Conti M. Somatic cells regulate maternal mRNA translation and developmental competence of mouse oocytes. Nat Cell Biol 2013; 15:1415-1423.
52. Chang HC, Liu H, Zhang J, Grifo J, Krey LC. Developmental incompetency of denuded mouse oocytes undergoing maturation in vitro is ooplasmic in nature and is associated with aberrant Oct-4 expression. Hum Reprod 2005; 20:1958-1968.
53. Conti M, Hsieh M, Zamah AM, Oh JS. Novel signaling mechanisms in the ovary during oocyte maturation and ovulation. Mol Cell Endocrinol 2012; 356:65-73.
54. Kim E, Yamashita M, Kimura M, Honda A, Kashiwabara S, Baba T. Sperm penetration through cumulus mass and zona pellucida. Int J Dev Biol 2008; 52:677-682.
55. Jin M, Fujiwara E, Kakiuchi Y, Okabe M, Satouh Y, Baba SA, Chiba K, Hirohashi N. Most fertilizing mouse spermatozoa begin their acrosome reaction before contact with the zona pellucida during in vitro fertilization. Proc Natl Acad Sci U S A 2011; 108:4892-4896.
56. Eisenbach M, Giojalas LC. Sperm guidance in mammals - an unpaved road to the egg. Nat Rev Mol Cell Biol 2006; 7:276-285.
57. Di Giacomo M, Camaioni A, Klinger FG, Bonfiglio R, Salustri A. Cyclic AMP-elevating Agents Promote Cumulus Cell Survival and Hyaluronan Matrix Stability, Thereby Prolonging the Time of Mouse Oocyte Fertilizability. The Journal of Biological Chemistry 2016; 291:3821-3836.
99. Minge CE, Bennett BD, Norman RJ, Robker RL. Peroxisome proliferator-activated receptor-gamma agonist rosiglitazone reverses the adverse effects of diet-induced obesity on oocyte quality. Endocrinology 2008; 149:2646-2656.
100. Wu LL, Russell DL, Wong SL, Chen M, Tsai TS, St John JC, Norman RJ, Febbraio MA, Carroll J, Robker RL. Mitochondrial dysfunction in oocytes of obese mothers: transmission to offspring and reversal by pharmacological endoplasmic reticulum stress inhibitors. Development 2015; 142:681-691.
128. Salvetti NR, Baravalle C, Mira GA, Gimeno EJ, Dallard BE, Rey F, Ortega HH. Heat shock protein 70 and sex steroid receptors in the follicular structures of induced ovarian cysts. Reprod Domest Anim 2009; 44:805-814.

143. Christians E, Michel E, Adenot P, Mezger V, Rallu M, Morange M, Renard JP. Evidence for the involvement of mouse heat shock factor 1 in the atypical expression of the HSP70.1 heat shock gene during mouse zygotic genome activation. Mol Cell Biol 1997; 17:778-788.
144. Bierkamp C, Luxey M, Metchat A, Audouard C, Dumollard R, Christians E. Lack of maternal Heat Shock Factor 1 results in multiple cellular and developmental defects, including mitochondrial damage and altered redox homeostasis, and leads to reduced survival of mammalian oocytes and embryos. Dev Biol 2010; 339:338-353.
151. Metchat A, Akerfelt M, Bierkamp C, Delsinne V, Sistonen L, Alexandre H, Christians ES. Mammalian heat shock factor 1 is essential for oocyte meiosis and directly regulates Hsp90alpha expression. J Biol Chem 2009; 284:9521-9528.
153. Christians E, Davis AA, Thomas SD, Benjamin IJ. Maternal effect of Hsf1 on reproductive success. Nature 2000; 407:693-694.
177. Neuer A, Spandorfer SD, Giraldo P, Dieterle S, Rosenwaks Z, Witkin SS. The role of heat shock proteins in reproduction. Human reproduction update 2000; 6:149-159.
183. Curci A, Bevilacqua A, Mangia F. Lack of heat-shock response in preovulatory mouse oocytes. Dev Biol 1987; 123:154-160.
193. Voss AK, Thomas T, Gruss P. Mice lacking HSP90beta fail to develop a placental labyrinth. Development 2000; 127:1-11.
194. Mao C, Wang M, Luo B, Wey S, Dong D, Wesselschmidt R, Rawlings S, Lee AS. Targeted Mutation of the Mouse Grp94 Gene Disrupts Development and Perturbs Endoplasmic Reticulum Stress Signaling. PLOS ONE 2010; 5:e10852.
195. Wanderling S, Simen BB, Ostrovsky O, Ahmed NT, Vogen SM, Gidalevitz T, Argon Y. GRP94 is essential for mesoderm induction and muscle development because it regulates insulin-like growth factor secretion. Mol Biol Cell 2007; 18:3764-3775.
196. Zhang P, Ni X, Guo Y, Guo X, Wang Y, Zhou Z, Huo R, Sha J. Proteomic-based identification of maternal proteins in mature mouse oocytes. BMC Genomics 2009; 10:348.
202. Wu LL, Russell DL, Norman RJ, Robker RL. Endoplasmic reticulum (ER) stress in cumulus-oocyte complexes impairs pentraxin-3 secretion, mitochondrial membrane potential (DeltaPsi m), and embryo development. Mol Endocrinol 2012; 26:562-573.
247. Christians ES, Benjamin IJ. The stress or heat shock (HS) response: insights from transgenic mouse models. Methods 2005; 35:170-175.
248. Xiao X, Zuo X, Davis AA, McMillan DR, Curry BB, Richardson JA, Benjamin IJ. HSF1 is required for extra-embryonic development, postnatal growth and protection during inflammatory responses in mice. The EMBO Journal 1999; 18:5943-5952.
249. Huang L, Mivechi NF, Moskophidis D. Insights into regulation and function of the major stress-induced hsp70 molecular chaperone in vivo: analysis of mice with targeted gene disruption of the hsp70.1 or hsp70.3 gene. Mol Cell Biol 2001; 21:8575-8591.
250. Lee S-H, Kim M, Yoon B-W, Kim Y-J, Ma S-J, Roh J-K, Lee J-S, Seo J-S. Targeted hsp70.1 Disruption Increases Infarction Volume After Focal Cerebral Ischemia in Mice. Stroke 2001; 32:2905-2912.
251. Van Molle W, Wielockx B, Mahieu T, Takada M, Taniguchi T, Sekikawa K, Libert C. HSP70 protects against TNF-induced lethal inflammatory shock. Immunity 2002; 16:685-695.
252. Shim E-H, Kim J-I, Bang E-S, Heo J-S, Lee J-S, Kim E-Y, Lee J-E, Park W-Y, Kim S-H, Kim H-S, Smithies O, Jang J-J, et al. Targeted disruption of hsp70.1 sensitizes to osmotic stress. EMBO Reports 2002; 3:857-861.
253. Hampton CR, Shimamoto A, Rothnie CL, Griscavage-Ennis J, Chong A, Dix DJ, Verrier ED, Pohlman TH. HSP70.1 and -70.3 are required for late-phase protection

induced by ischemic preconditioning of mouse hearts. Am J Physiol Heart Circ Physiol 2003; 285:H866-874.
254. Hunt CR, Dix DJ, Sharma GG, Pandita RK, Gupta A, Funk M, Pandita TK. Genomic instability and enhanced radiosensitivity in Hsp70.1- and Hsp70.3-deficient mice. Mol Cell Biol 2004; 24:899-911.
255. Hunt C, Calderwood S. Characterization and sequence of a mouse hsp70 gene and its expression in mouse cell lines. Gene 1990; 87:199-204.
256. Daugaard M, Rohde M, Jäättelä M. The heat shock protein 70 family: Highly homologous proteins with overlapping and distinct functions. FEBS Lett 2007; 581:3702-3710.
257. Luo S, Mao C, Lee B, Lee AS. GRP78/BiP is required for cell proliferation and protecting the inner cell mass from apoptosis during early mouse embryonic development. Mol Cell Biol 2006; 26:5688-5697.
258. Sreedhar AS, Kalmar E, Csermely P, Shen YF. Hsp90 isoforms: functions, expression and clinical importance. FEBS Lett 2004; 562:11-15.
259. Grad I, Cederroth CR, Walicki J, Grey C, Barluenga S, Winssinger N, De Massy B, Nef S, Picard D. The Molecular Chaperone Hsp90α Is Required for Meiotic Progression of Spermatocytes beyond Pachytene in the Mouse. PLOS ONE 2011; 5:e15770.
260. Kajiwara C, Kondo S, Uda S, Dai L, Ichiyanagi T, Chiba T, Ishido S, Koji T, Udono H. Spermatogenesis arrest caused by conditional deletion of Hsp90α in adult mice. Biology Open 2012; 1:977-982.
261. Yang Y, Liu B, Dai J, Srivastava PK, Zammit DJ, Lefrançois L, Li Z. Heat Shock Protein gp96 Is a Master Chaperone for Toll-like Receptors and Is Important in the Innate Function of Macrophages. Immunity 2007; 26:215-226.
262. Lan ZJ, Xu X, Cooney AJ. Differential oocyte-specific expression of Cre recombinase activity in GDF-9-iCre, Zp3cre, and Msx2Cre transgenic mice. Biol Reprod 2004; 71:1469-1474.
263. de Vries WN, Binns LT, Fancher KS, Dean J, Moore R, Kemler R, Knowles BB. Expression of Cre recombinase in mouse oocytes: a means to study maternal effect genes. Genesis 2000; 26:110-112.
264. Audouard C, Le Masson F, Charry C, Li Z, Christians ES. Oocyte-targeted deletion reveals that hsp90b1 is needed for the completion of first mitosis in mouse zygotes. PLoS One 2011; 6:e17109.
265. Lin KM, Lin B, Lian IY, Mestril R, Scheffler IE, Dillmann WH. Combined and individual mitochondrial HSP60 and HSP10 expression in cardiac myocytes protects mitochondrial function and prevents apoptotic cell deaths induced by simulated ischemia-reoxygenation. Circulation 2001; 103:1787-1792.
266. Cheng MY, Hartl FU, Martin J, Pollock RA, Kalousek F, Neuper W, Hallberg EM, Hallberg RL, Horwich AL. Mitochondrial heat-shock protein hsp60 is essential for assembly of proteins imported into yeast mitochondria. Nature 1989; 337:620.
267. Christensen JH, Nielsen MN, Hansen J, Füchtbauer A, Füchtbauer E-M, West M, Corydon TJ, Gregersen N, Bross P. Inactivation of the hereditary spastic paraplegia-associated Hspd1 gene encoding the Hsp60 chaperone results in early embryonic lethality in mice. Cell Stress and Chaperones 2010; 15:851-863.
268. Khanna A, Aten RF, Behrman HR. Heat shock protein-70 induction mediates luteal regression in the rat. Mol Endocrinol 1995; 9:1431-1440.
269. Abane R, Mezger V. Roles of heat shock factors in gametogenesis and development. FEBS Journal 2010; 277:4150-4172.

270. Trinklein ND, Murray JI, Hartman SJ, Botstein D, Myers RM. The role of heat shock transcription factor 1 in the genome-wide regulation of the mammalian heat shock response. Mol Biol Cell 2004; 15:1254-1261.
271. Schopf FH, Biebl MM, Buchner J. The HSP90 chaperone machinery. Nature Reviews Molecular Cell Biology 2017; 18:345.
272. Pratt WB, Toft DO. Steroid receptor interactions with heat shock protein and immunophilin chaperones. Endocr Rev 1997; 18:306-360.
273. Ben-Ze'ev A, Amsterdam A. Regulation of heat shock protein synthesis by gonadotropins in cultured granulosa cells. Endocrinology 1989; 124:2584-2594.
274. Gómez AV, Córdova G, Munita R, Parada GE, Barrios ÁP, Cancino GI, Álvarez AR, Andrés ME. Characterizing HSF1 Binding and Post-Translational Modifications of hsp70 Promoter in Cultured Cortical Neurons: Implications in the Heat-Shock Response. PLOS ONE 2015; 10:e0129329.
275. Bensaude O, Babinet C, Morange M, Jacob F. Heat shock proteins, first major products of zygotic gene activity in mouse embryo. Nature 1983; 305:331-333.
276. Christians E, Boiani M, Garagna S, Dessy C, Redi CA, Renard JP, Zuccotti M. Gene expression and chromatin organization during mouse oocyte growth. Dev Biol 1999; 207:76-85.
277. Hahnel AC, Gifford DJ, Heikkila JJ, Schultz GA. Expression of the major heat shock protein (hsp 70) family during early mouse embryo development. Teratog Carcinog Mutagen 1986; 6:493-510.
278. Curci A, Bevilacqua A, Fiorenza MT, Mangia F. Developmental regulation of heat-shock response in mouse oogenesis: identification of differentially responsive oocyte classes during Graafian follicle development. Dev Biol 1991; 144:362-368.
279. Harada M, Nose E, Takahashi N, Hirota Y, Hirata T, Yoshino O, Koga K, Fujii T, Osuga Y. Evidence of the activation of unfolded protein response in granulosa and cumulus cells during follicular growth and maturation. Gynecol Endocrinol 2015; 31:783-787.
280. Shani G, Fischer WH, Justice NJ, Kelber JA, Vale W, Gray PC. GRP78 and Cripto form a complex at the cell surface and collaborate to inhibit transforming growth factor beta signaling and enhance cell growth. Mol Cell Biol 2008; 28:666-677.
281. Rao RV, Peel A, Logvinova A, del Rio G, Hermel E, Yokota T, Goldsmith PC, Ellerby LM, Ellerby HM, Bredesen DE. Coupling endoplasmic reticulum stress to the cell death program: role of the ER chaperone GRP78. FEBS Lett 2002; 514:122-128.
282. de Mateo S, Castillo J, Estanyol JM, Ballesca JL, Oliva R. Proteomic characterization of the human sperm nucleus. Proteomics 2011; 11:2714-2726.
283. Ben-Ze'ev A, Kohen F, Amsterdam A. Gonadotropin-induced differentiation of granulosa cells is associated with the co-ordinated regulation of cytoskeletal proteins involved in cell-contact formation. Differentiation 1987; 34:222-235.
284. Tamba S, Yodoi R, Morimoto K, Inazumi T, Sukeno M, Segi-Nishida E, Okuno Y, Tsujimoto G, Narumiya S, Sugimoto Y. Expression profiling of cumulus cells reveals functional changes during ovulation and central roles of prostaglandin EP2 receptor in cAMP signaling. Biochimie 2010; 92:665-675.
285. Assidi M, Dufort I, Ali A, Hamel M, Algriany O, Dielemann S, Sirard M-A. Identification of Potential Markers of Oocyte Competence Expressed in Bovine Cumulus Cells Matured with Follicle-Stimulating Hormone and/or Phorbol Myristate Acetate In Vitro. Biology of Reproduction 2008; 79:209-222.
286. Ali A, Sirard MA. Protein kinases influence bovine oocyte competence during short-term treatment with recombinant human follicle stimulating hormone. Reproduction 2005; 130:303-310.

287. Li X, Sun L, Hou J, Gui M, Ying J, Zhao H, Lv N, Meng S. Cell membrane gp96 facilitates HER2 dimerization and serves as a novel target in breast cancer. International Journal of Cancer 2015; 137:512-524.
288. Soltys BJ, Falah M, Gupta RS. Identification of endoplasmic reticulum in the primitive eukaryote Giardia lamblia using cryoelectron microscopy and antibody to Bip. J Cell Sci 1996; 109 (Pt 7):1909-1917.
289. Chandra D, Choy G, Tang DG. Cytosolic accumulation of HSP60 during apoptosis with or without apparent mitochondrial release: evidence that its pro-apoptotic or pro-survival functions involve differential interactions with caspase-3. J Biol Chem 2007; 282:31289-31301.
290. Calarco PG. Polarization of mitochondria in the unfertilized mouse oocyte. Developmental Genetics 1995; 16:36-43.
291. Pratt WB, Toft DO. Steroid Receptor Interactions with Heat Shock Protein and Immunophilin Chaperones*. Endocrine Reviews 1997; 18:306-360.
292. Christians E, Davis AA, Thomas SD, Benjamin IJ. Embryonic development: Maternal effect of Hsf1 on reproductive success. Nature 2000; 407:693-694.

Chapter 3: Heat shock protein expression in granulosa cells of female mice with mild obesity induced by Dihydrotestosterone

3.1 Introduction

Polycystic ovary syndrome, otherwise known as PCOS, is the most common infertility disorder in women, affecting 5-10% of reproductive age women [93]. In Australia, the prevalence of PCOS is estimated at 10-12% in the general population [293]. PCOS is even more prevalent in Aboriginal populations, where it is estimated to affect 15-18% of women [294, 295].

PCOS is a complex syndrome encompassing a variety of symptoms, with affected women experiencing one or more symptoms as well as different combinations of symptoms. PCOS is strictly diagnosed, by a set of definitions known as the Rotterdam criteria [93]. The original previous criteria for the diagnosis of PCOS were established at the 1990 National Institutes of Health (NIH)-sponsored conference on PCOS which set the diagnosis criteria as 1) evidence of hyperandrogenism and 2) irregular menstrual cycles. In 2003, the Rotterdam European Society for Human Reproduction/American Society of Reproductive Medicine (ESHRE/ASRM)-sponsored PCOS consensus workshop group broadened the diagnosis criteria. Thus currently, the clinical expression of PCOS includes at least two of the following three symptoms: 1) oligo and/or anovulation, 2) clinical and/or biochemical hyperandrogenism, and/or 3) polycystic ovaries on ultrasound [94]. The ovarian hallmark of PCOS is the presence of fluid-filled ovarian cysts, however physiological symptoms include irregular menstrual cycles, infertility, pelvic pain, hirsutism (excess body hair), weight gain, and acne. Women with PCOS are also at greater risk of suffering type 2 diabetes, metabolic syndrome, cardiovascular disease and high blood pressure. Additionally, PCOS is more common in obese women and women with an affected first degree female relative (mother or a sister). Despite its frequency, there is still much unknown about what is the underlying cause of PCOS that may give rise to the many and diverse symptoms.

Hyperandrogenism has been identified as one of the most consistently expressed PCOS traits, and the most likely to be caused by an inheritable phenotype. Legro et al [296] reported that high circulating androgen levels were persistent within women in a same family with history of PCOS. They found that sisters of diagnosed patients had an almost 50% chance of presenting hyperandrogenism (accompanied by anovulation or not) compared to sisters of unaffected women. Moreover, their androgen blood serum concentration was similar to those of their affected sisters.

This increase in circulating androgens is thought to be behind the abnormal ovarian [297] and liver function [298, 299] in PCOS patients, the latter of which has in turn been shown to be

associated with insulin resistance and metabolic syndrome [299]. In support of this concept, metabolic phenotypes have also been reported in androgen-exposed animal models [300, 301] but the link between hyperandrogenism and insulin resistance or hyperinsulinemia has yet to be clarified.

There is some evidence that suggests that components of stress responses are dysregulated in ovarian cells of PCOS patients, but this has not been extensively characterized. Differential proteomic analysis has shown some members from the Heat Shock Protein (HSP) family are dysregulated in ovarian tissues collected from a small sample of diagnosed women (n=3) presenting irregular menstrual cycles and infertility during wedge resection surgery. While HSP47 (SERPINH1) and HSPE1 (HSP10) presented decreased expression in oocytes and granulosa cells, respectively; HSPB1 (HSP27) protein levels were upregulated in the PCOS ovaries, and it was extensively expressed in ovarian cells, particularly in stromal cells [163]. Similarly, a larger study (n=10) found downregulation of HSPA5 (GRP78) but higher levels of HSP90B1 (GRP94) were identified in protein samples from ovarian biopsies collected from acyclic, unstimulated patients [302]. In these studies, HSR expression was not compared to hyperandrogenemia so it is not known if androgens are responsible for the observed alterations. However, a study in cultured mouse granulosa cells observed lower expression of mitochondria-specific HSPE1 in granulosa cells treated with testosterone [303].

On the other hand, the weight gain associated with PCOS is likely to contribute to the dysregulation of cellular homeostasis and stress response pathways in the ovarian environment. It has been shown that culture of mouse cumulus oocyte complexes in follicular fluid collected from obese women caused the overexpression of marker genes for ER stress and the unfolded protein response (UPR), namely HSPA5, ATF4, ATF6 and spliced XBP1 (XBP1s) [304]. Moreover, increased gene expression of ATF4 and XBP1s, and cellular stress markers HSPA1A and HSPA1B, was observed in granulosa cells and cumulus-oocyte complexes of obese mice; whether obesity was genetic [100]or in response to a high-fat diet [97]The induction of ER stress gene expression in these obese models occurred in conjunction with increased levels of intracytoplasmic lipid in the oocytes and impaired oocyte mitochondrial activity [97, 100], neither of which has been examined in hyperandrogenic models. These stress responses are a complex network that is not only cytoprotective under insults but also play an important role in normal ovarian function, thus it is likely that disruptions could contribute to abnormal ovarian dynamics, disrupted follicle growth and ovulation and CL development.

There is some evidence that oocyte quality and competence are also negatively affected by PCOS. Abnormal expression of genes associated with chromosome alignment and segregation is thought to contribute to impaired embryo development in PCOS patients undergoing IVF [305], but more factors could be involved. Morphologically normal oocytes retrieved for in vitro fertilization from gonadotropin-stimulated patients have a markedly different gene expression profile to those from stimulated, normal ovulatory women; with significant differences in abundance in approximately 5% of transcripts identified [305]. Interestingly, promoter analysis found that 68 of these differentially expressed genes also contained putative binding sites for androgen receptor and/or peroxisome proliferating receptor ɣ. Later annotation of the data showed that a subset of these genes is involved in chromosome dynamics during cell division. These findings suggest that the decreased pregnancy rates observed in women with PCOS can be explained by suboptimal oocyte quality due to abnormal ovarian folliculogenesis as a result of both excess androgens and other molecular defects associated with the syndrome [305]. A study by Rajani et al in 2012 analyzed follicular samples from PCOS women undergoing oocyte retrieval for IVF. They reported a significantly higher proportion of immature (MI) oocytes isolated from the follicular aspirations after spindle examination under inverted microscope, while showing increased estimated ROS levels in the accompanying follicular fluid by chemiluminescence assay [306]. These data suggest that molecular mechanisms underlying oocyte quality are affected in PCOS and thus need further investigation.

Thus, this study sought to directly examine whether DHT-induced obesity contributes to poor oocyte quality that is associated with altered levels of HSP. It utilized an established mouse model, developed by Walters et al [300]. These researchers comprehensively compared four different androgen-exposed mouse models and demonstrated that the regimen in which young, adult female mice were given a subcutaneous implant releasing 10 mg of DHT to a serum concentration of 1.64 ± 0.32 ng/mL over 90 days caused several of the metabolic symptoms seen in human PCOS patients. These included increased body weight, elevated circulating DHT levels and hepatic steatosis. Importantly, the DHT mice also exhibited disrupted estrus cycles and abnormal ovarian follicle development. However, due to the novelty of this model, many metabolic and reproductive aspects have yet to be characterized, including the extent if any of insulin resistance and glucose insensitivity and whether oocyte quality and developmental potential are affected by the high circulating androgen levels.

In this study, we used this DHT-implant PCOS mouse model to investigate the influence of hyperandrogenism in glucose metabolism and the stress response of ovarian granulosa cells. Additionally, we characterized ovulatory function and oocyte quality and developmental potential in DHT-exposed female mice. Lastly a panel of stress response genes including HSPs were examined in ovarian granulosa cells of DHT-exposed mice.

3.2 Materials and Methods

3.2.1 Animals

A first cohort of mice, kindly supplied by Dr Kirsty Walters (ANZAC Research Institute, University of Sydney) from her laboratory breeding colony [300], had already been implanted as previously reported [300] prior to arrival. A second cohort consisted of C57BL6J female mice at 3 weeks old that were purchased from the Animal Resources Centre (Canning Vale, Australia). Mice were implanted with 1-cm SILASTIC brand implant (id, 1.47 mm; od, 1.95 mm, Dow Corning Corp, catalogue no. 508–006) containing 10mg DHT or blank, provided by Dr Kirsty Walters [300]. The implants were inserted subcutaneously by surgery under tribromoethanol anaesthesia and remained for 90 days. During this time, animals were fed 10% fat rodent chow (i.e. breeder chow; Specialty Feeds, WA, Australia), and the body weights measured fortnightly. All experiments were approved by the University of Adelaide Animal Ethics Committee (approval M-2015-113) and followed the Australian Code for the Care and Use of Animals for Scientific Purposes.

3.2.2 Metabolic tests.

Glucose and Insulin Tolerance Tests were carried out, as previously described [307] over a 2 week period. At approximately 3 months of age, animals (N=11-15) were challenged with either IP injection of 2 g/Kg glucose or 0.75 IU/Kg insulin (Actrapid; Novo Nordisk Australia, NSW, Australia) in 0.9% saline solution, for glucose or insulin tolerance tests respectively. Prior to the glucose injection only, the animals had been fasted for 6 hours (from 8 am to 2 pm). Blood samples were obtained from a tail tip prick, and the blood glucose levels measured on glucose strips via glucometer (AccuChek Performa Monitor, Roche Diagnostics, Indianapolis, USA). Blood glucose levels were measured at 0, 15, 30, 60, 90 and 120 min post-injection.

3.2.3 Ovarian stimulation and tissue collection.

To examine ovulation and collect ovarian cells at precise times in the ovarian cycle, mice underwent hormonally-induced ovarian hyperstimulation. To stimulate follicular growth, female mice received an intraperitoneal (IP) injection of Pregnant Mare Serum Gonadotropin (PMSG; National Hormone and Peptide Program, Torrence, USA) in sterile 0.9% saline at a dose of 5 IU/12 g of body weight. At 48 hours post-PMSG, the mice received a second IP injection of human chorionic Gonadotropin (hCG; Pregnyl, Merck Sharp & Dohme Pty Ltd, Australia) in sterile 0.9% saline at a dose of 5 IU/10 g of body weight; to induce ovulation. The mice then were humanely killed by cervical dislocation at 14 hours post-hCG injection and the reproductive tracts were dissected and placed in HEPES-buffered GIBCO minimal essential medium (aMEM, Life Technologies Australia Pty Ltd) at 37°C. Ovulated cumulus-oocyte complexes (COC) were collected by tearing open the oviduct, while unovulated Graafian follicles visible in the ovary were punctured using 30G needles to collect the COC.

3.2.4 Granulosa-luteal cell collection and gene expression analysis by RT-qPCR

Granulosa-luteal (GLC) were collected by puncturing the ovary using a 30G needle. GLC were collected in 1500 uL of HEPES-buffered aMEM and pelleted by centrifuging the media at 1200 rpm for 3 min at 4°C. The supernatant was discarded, and the cell pellet was snap-frozen in liquid nitrogen and stored at -80°C until use. GLC and COC were acquired individually for every mouse.

Total RNA was extracted from frozen cell pellets using Trizol (Thermo Fisher Scientific, Massachusetts, USA) following the manufacturer's instructions. RNA samples were treated with DNAFREE DNAse (Life Technologies, California, USA) to remove any residual DNA. After this, 1 ul was taken from each sample to quantify RNA and DNA content by measuring the ratio of absorbance between 260 and 280 nm using a spectrophotometer (Thermo Fisher Nanodrop spectrophotometer, Thermo Fisher Scientific). The manufacturer's instructions indicate that a ratio of ~1.8 is considered pure for DNA whereas a ratio of ~2.0 is considered pure for RNA. A given sample was considered free of DNA contamination when they had a 260/280 value of 1.98 or more. RNA concentration and purity were determined by Nanodrop (Thermo Fisher Scientific). 200 ng of mRNA were used to make cDNA at 5 ng/mL by RT-PCR in 10 uL reactions using Supertranscript III reverse transcriptase (Life Technologies, USA) in MicroAmp Fast Optical 96-Well Reaction Plate (Life Technologies). Quantitative real-time

PCR was performed in triplicate with Quantstudio 12k Flex Real-time PCR system (Thermo Fisher Scientific), using Taqman Fast Universal Master Mix and hydrolysis probes (Taqman, Life Technologies). The efficiency and specificity of the Taqman probes used in this assay is batch tested by the manufacturer and shown to be of almost 100%. Gene products measured were HSF1, HSPA5, HSPA1A, HSPA1B, HSP90AA1, HSP90AB1, HSP90B1, HSPD1, ATF4 and XBP1s (see Appendix 4 for primer details). These genes are key markers for the activation of cellular stress pathways, namely the Heat Shock Response (HSR) and Endoplasmic reticulum stress (ER stress). Real time PCR data was analysed using the $2^{-(\Delta\Delta CT)}$ method. Expression of target genes was normalised against the expression of ribosomal protein L19 (rpl19), which was used as a validated internal control for every sample. The use of this reference gene has previously been validated for analysing mRNA levels in ovarian cells from mice [99, 100, 202]. Fold changes in gene expression were relative to a whole ovary (collected at 44h post-PMSG injection) cDNA sample, which was included as an internal standard in each run.

3.2.5 Quantification of ovulation and analysis of oocyte quality

Ovulated COC collected by tearing open the oviduct and unovulated COC punctured from Graafian follicles were counted separately. Oocytes were then isolated from the COC using hyaluronidase (1000 I.U./mL; Invitrogen, California, USA) in HEPES aMEM media with 1mg/ml polyvinylpyrrolidone (PVP, Sigma-Aldrich, Missouri, USA) at 37°C, to observe their morphology. Oocytes presenting a spherical shape, and uniformity and integrity of the cytoplasm were considered as morphologically normal and healthy. Presence of the first polar body indicates the oocyte is in metaphase II (MII) and is a marker of the state of maturation of the oocyte. In contrast, oocytes presenting an unshapely, damaged or fragmented cytoplasm were considered morphologically unhealthy.

Neutral lipid content was measured by staining the oocytes with BODIPY 493/503 neutral lipid dye (D-3922, Invitrogen) at 1 ug/mL for 30 min at 37°C, followed by counter-stain with Hoechst 33342 DNA dye (Sigma-Aldrich, Missouri, USA) at 0.5 ug/mL for 10 min at 37°C, followed by thorough washing in aMEM with PVP. Imaging was done by Leica TCS SP5 spectral scanning confocal microscope system (Heerbrugg, Switzerland). Mitochondrial activity was measured by staining the oocytes with Mitotracker Orange (MTO) CM-H2TMRos mitochondrial dye (Life Technologies) at 500 nM for 30 min in the dark, followed by washing

in aMEM supplemented in 1% fetal calf serum. Cell toxicity, background fluorescence and autofluorescence were controlled for by replacing the respective dyes with vehicle (DMSO, Sigma-Aldrich) and Hoechst 33342 DNA stain only as control. Fluorescence intensity was determined using ImageJ Fiji software (National Institutes of Health, Maryland, USA), then quantified by corrected total cell fluorescence (CTCF), which determines the levels of fluorescence in a given region of a confocal section, using the formula: CTCF = Integrated Density – [(Area of selected cell) x (Mean fluorescence of background readings)]. Integrated density is the product of the total Area and Mean Gray Value. This quantification is based on the published method from Burgess et al [308].

3.2.6 In vitro fertilisation and analysis of pre-implantation embryo development

Female C57BL6 mice were humanely killed by cervical dislocation at 16 hours after injection with hCG; and the ovulated COC were collected and fertilised in vitro (IVF) using sperm collected from a 6 week old, non-virgin C57BL6 male (the protocol for IVF and the culture of pre-implantation embryos is detailed in Appendix 5). Briefly, COC were placed in Research Vitro Fertilisation Medium (COOK Medical, QLD, Australia) with sperm at 1:10 (10ul:100uL) concentration. (Sperm sample had been previously collected from the epididymis and vas deferens and left to capacitate for 1 hour in Research Vitro Fertilisation Medium at 37°C in 6% CO_2, 21% O_2). After 4 hours, the presumptive zygotes were collected, washed and placed in Research Vitro Cleave medium (10 zygotes/20 uL drop; COOK Medical) for in-vitro embryo culture to blastocyst stage at 37°C in 6% CO_2, 21% O_2. Developmental embryonic stage of the pre-implantation embryos was assessed and recorded daily for 5 days. On-time development of the embryos was analysed by assessing their developmental stage every 24 hours. Embryos from each individual female were kept separate throughout the analysis.

3.2.7 Statistical analysis

All measures are reported as mean ± the standard error of the mean (SEM), unless indicated otherwise. Data were analysed using the statistics software GraphPad Prism 6 v008 for Windows (GraphPad software Inc., California, USA). The analysis of body weight over time was done by a repeated measures ANOVA. Area under the curve (AUC) values for glucose and insulin were calculated using the trapezoid rule [309]. Statistical significance was determined

by Two-way ANOVA, Student's t-test or Fisher's exact test as indicated. P values of <0.05 were considered statistically significant.

3.3 Results

3.3.1 Metabolic changes induced by DHT-exposure in female mice

In order to model PCOS in mice, female C57BL6J mice were implanted with DHT (or vehicle) pellets, as previously described by Caldwell et al [300]. The animals were weighed fortnightly to monitor body weight changes over the course of the 90 day treatment. DHT treatment increased body weight in female C57BL6J mice compared to control mice treated with blank implants. Body weights were significantly increased in DHT-treated females compared to controls from week 10 (approximately 75 days after receiving the implant) (Figure 3.1.A). At the conclusion of the 90-day treatment period, female mice with DHT implants had a significantly increased average body weight of 25.23 ± 0.32 g (Figure 3.1.B), while those with blank implants presented an average body weight of 23.64 ± 0.36 g; (N=22, P=0.002). This 6.3% increase in body weight was statistically significant and similar to the 9% increase in body weight reported in the original publication characterizing this hyperandrogenic model [300].

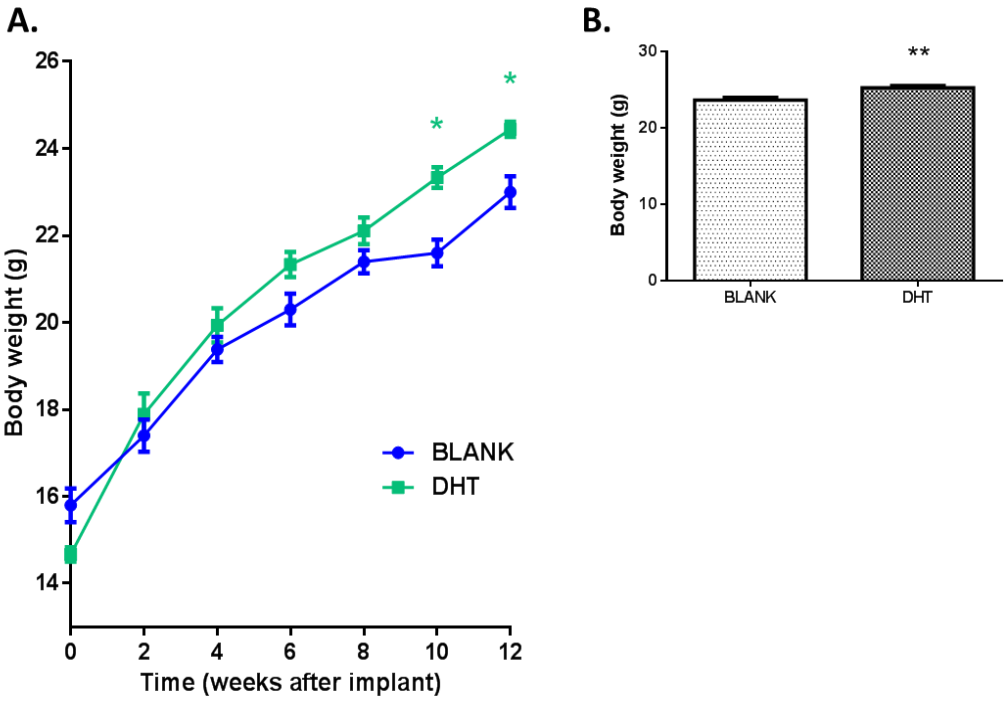

Figure 3.1 Effect of DHT exposure on body weight.

A. Body weights in female mice with either Blank or Dihydrotestosterone (DHT) implant * P=0.001. N=9-10 female mice per treatment group. **B.** Body weights at 12 weeks after implant surgery at the time of tissue collection. ** P=0.002. N=22 female mice per treatment group. Results are shown as mean ± SEM. Statistical analysis was Two-way ANOVA (A) or Student's t-Test (B).

In order to determine whether DHT exposure impacted glucose metabolism, the ability of the mice to maintain blood glucose levels in response to a glucose challenge was measured. At 10 weeks into the treatment circulating glucose levels in blood after glucose challenge were not different in DHT-exposed mice compared to the controls (Figure 3.2.A). This was confirmed by comparing the average AUC between the two treatment groups; which were not significantly different (Figure 3.2.B); with DHT-treated females having an average value of 1523 ± 74.18 AU (arbitrary units), and blank-treatment females 1441.5 ± 65.41 AU. However, glucose levels at baseline (6 hours after fasting) were significantly higher in the DHT group (N=9-10; P=0.04), with DHT-treated females showing an average of 8.19 ± 0.25 mmol/mL compared to blank controls with an average of 7.3 ± 0.32 mmol/mL (Figure 3.2.C).

Whether DHT exposure affected ability to maintain blood glucose levels in response to an insulin challenge was analysed at 11 weeks into the treatment. DHT-treated females showed significantly increased circulating glucose levels at 60 min after insulin injection (N=7-9; P=0.02), with significantly higher blood glucose readings (average of 6.96 ± 1.21 mmol/mL) compared to blank-treated females (3.78 ± 0.41 mmol/mL) (Figure 3.2.D). The difference in insulin tolerance was confirmed by significantly higher AUC values (N=7-9; P=0.04) in DHT-treated females (921.61 ± 109.3 AU) when compared to the control group (672.43 ± 50.94 AU) (Figure 3.2.E). These findings indicate that chronic DHT exposure not only increases baseline fasting blood glucose levels but also decreases insulin sensitivity in female mice.

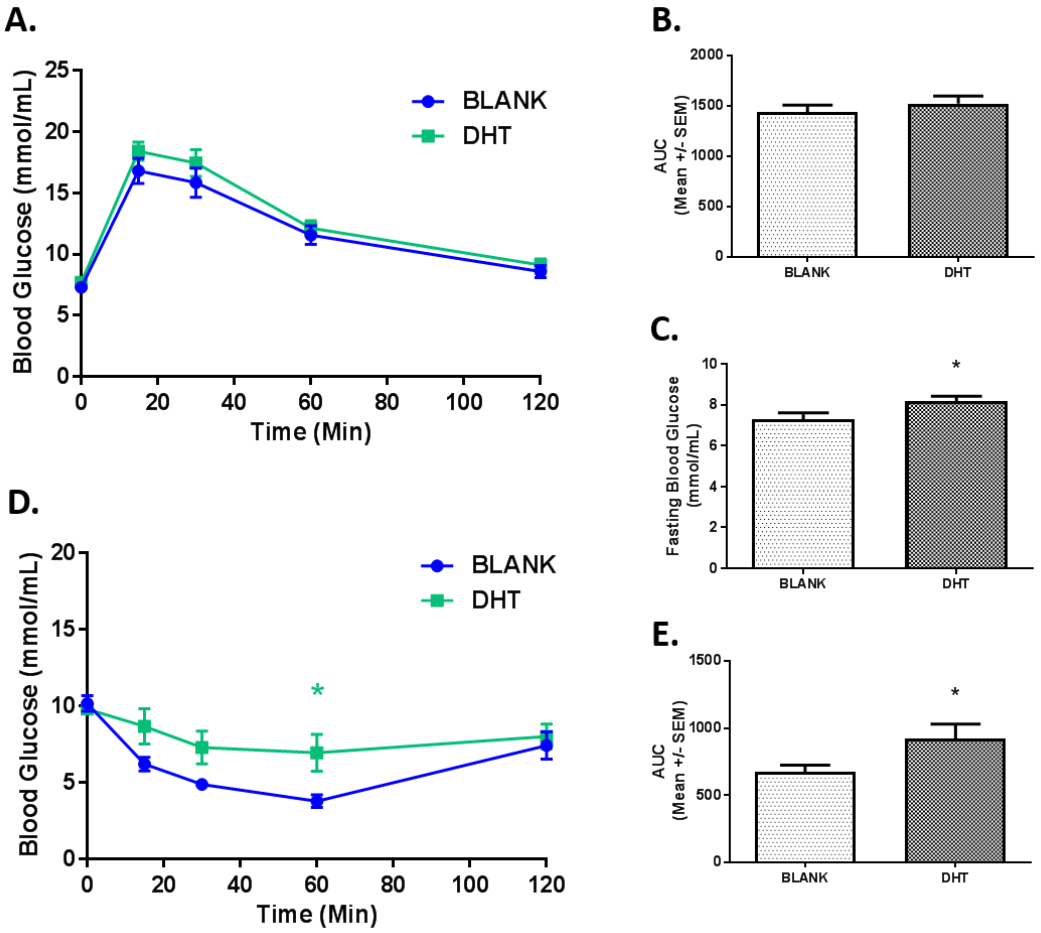

Figure 3.2 Effect of DHT treatment in female mice on responsiveness to either glucose or insulin challenges.

A. Glucose tolerance test (GTT) at 10 weeks after treatment with DHT or blank implant. **B.** AUC values for GTT. **C.** Fasting blood glucose levels after 10 weeks of treatment. * P=0.04. **D.** Insulin Tolerance Test (ITT) at 11 weeks after treatment with DHT or blank implant. * P=0.0007. **E.** AUC values for ITT * P=0.04. N=9-10 female mice per treatment group. Results are shown as mean ± SEM. Statistical analysis was either Two-Way ANOVA (A, D) or Student's T-test (B, C, E).

3.3.2 Expression of cellular stress genes in granulosa cells in mice exposed to DHT

To characterise the impact of DHT on ovarian function, mice exposed to either DHT or blank implants were treated with PMSG and hCG to synchronise ovulation, and the granulosa-luteal cells collected at 14 hours post-hCG injection for analysis of HSR and ER stress gene expression markers.

HSR genes examined included the transcription factor Hsf1, and seven other genes belonging to three different HSP families: the HSPA family (HSPA5, HSPA1A, HSPA1B), HSP90 family (HSP90AA1, HSP90AB1, HSP90B1), and HSP60 (HSPD1); all of which are downstream targets of HSF1. Comparison of the relative expression of each gene between the DHT and blank groups showed that mRNA levels were unchanged for most genes. Specifically, genes that were not altered by DHT were: HSF1, HSPA5, HSPA1A (*Figure 3.3*.A, B, C.), HSP90AA1, HSP90AB1, and HSP90B1 (Figure 3.4.A, B, C.). Ovarian cells from DHT-exposed females had different albeit not significantly, expression of two genes. HSPA1B mRNA was lower, with a 31.5% decrease in cells from DHT-treated females compared to controls (Figure 3.3.D). In contrast, HSPD1 mRNA was 27.1% decreased, albeit not significantly, in the GLC from DHT females (Figure 3.4.D).

Markers for the activation of the ER-stress response, were also examined. Notably HSPA5 is considered an ER stress response gene (Figure 3.3.B). In addition, gene expression levels for mRNA of both ATF4 and XBP1s (Figure 3.5.A and .B, respectively) were not different in GLC from DHT treated females compared to controls. These results suggest that chronic androgen exposure (or hyperandrogenemia) does not profoundly impact on the normal stress response pathways of GLC at the time of ovulation.

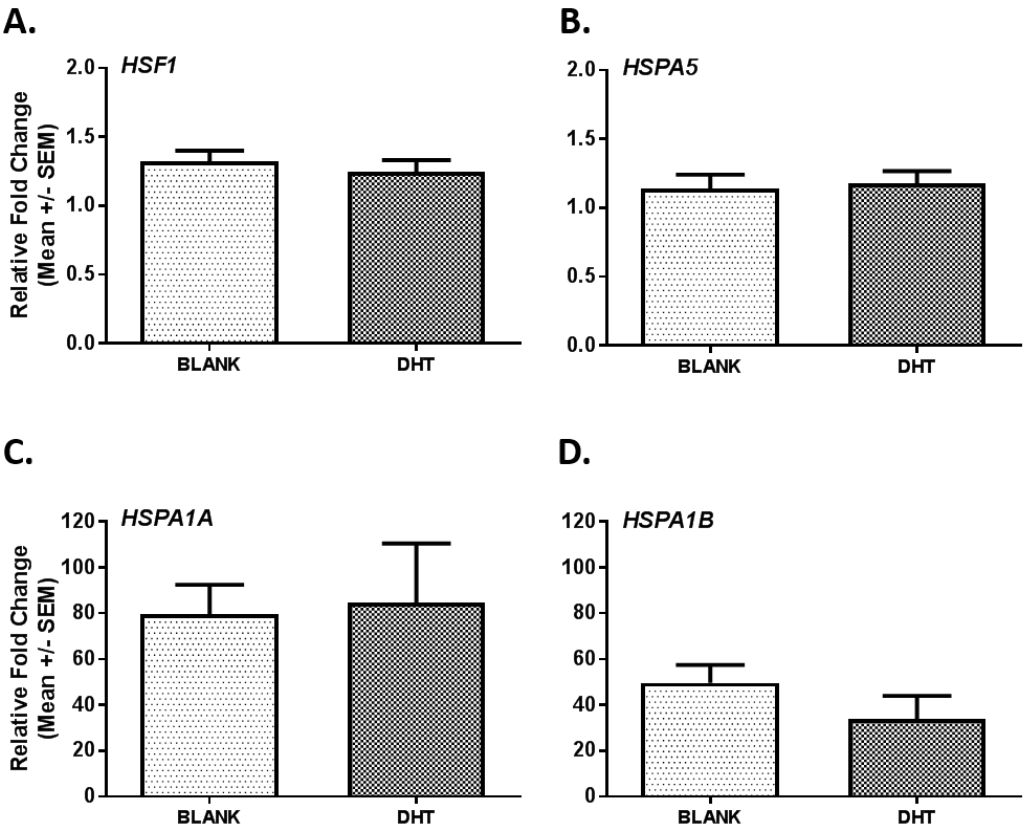

Figure 3.3 Effect of DHT treatment on the expression of Heat Shock Response genes in granulosa cells.

Expression of mRNA for HSF1 (**A**), HSPA5 (**B**), HSPA1A (**C**) and HSPA1B (**D**) were analyzed in GLC of mice that had been treated with either DHT or blank implants for 90 days followed by ovarian stimulation with PMSG and hCG for 14h. N=9-10 GLC samples from individual mice. Results are mean ± SEM. Relative gene expression is normalized to Rpl19 reference gene expression and relative to a whole ovary calibrator. Statistical analysis was Student's T-test.

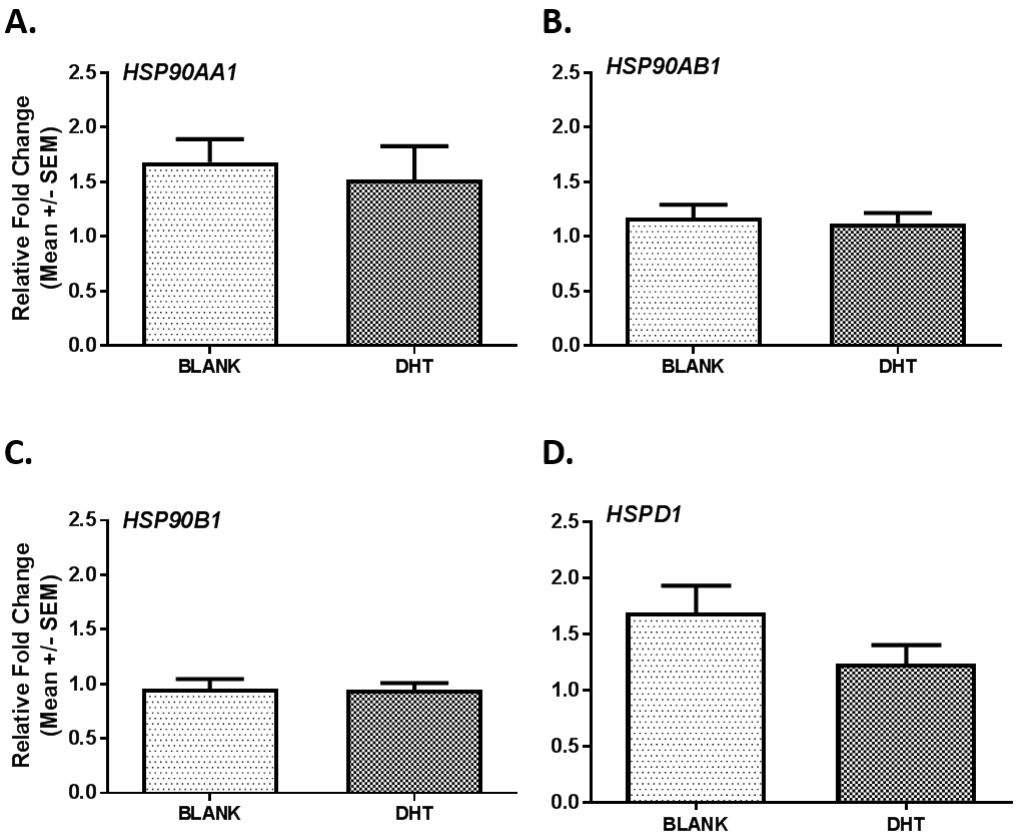

Figure 3.4 Effect of DHT treatment on the expression of Heat Shock Response genes in granulosa cells.

Expression of mRNA for HSP90AA1 (**A**), HSP90AB1 (**B**), HSP90B1 (**C**) and HSPD1 (**D**) were analyzed in GLC of mice that had been treated with either DHT or blank implants for 90 days followed by ovarian stimulation with PMSG and hCG for 14h. N=9-10 GLC samples from individual mice. Results are mean ± SEM. Relative gene expression is normalized to Rpl19 reference gene expression and relative to a whole ovary calibrator. Statistical analysis was Student's T-test.

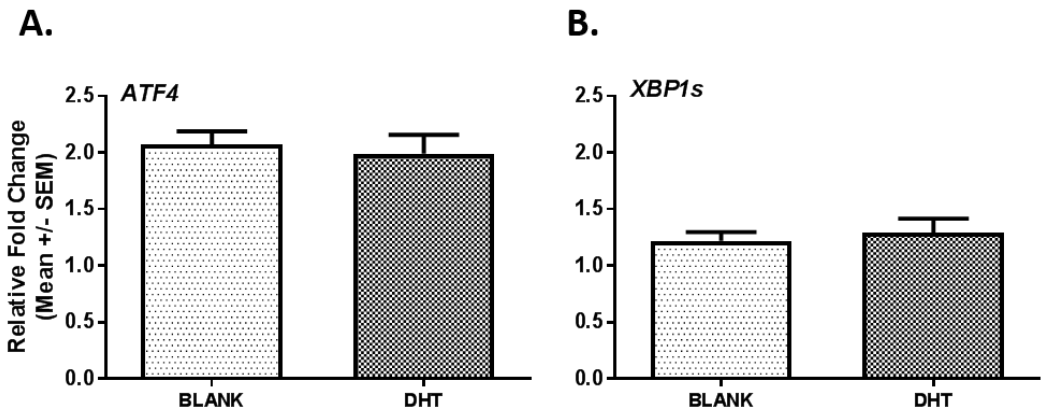

Figure 3.5 Effect of DHT treatment on the expression of ER stress genes in granulosa cells.

Expression of mRNA for ATF4 (**A**), and XBP1s (**B**) were analyzed in GLC of mice that had been treated with either DHT or blank implants for 90 days followed by ovarian stimulation with PMSG and hCG for 14h. N=9-10 GLC samples from individual mice. Results are mean ± SEM. Relative gene expression is normalized to Rpl19 reference gene expression and relative to a whole ovary calibrator. Statistical analysis was Student's T-test.

3.3.3 Ovulation and oocyte quality are affected after DHT-exposure

In parallel the effect of increased androgen levels on ovulation, and oocyte quality and developmental potential was investigated. COC were collected from both the oviduct and unruptured Graafian follicles at 14h post-hCG treatment and counted. DHT-treated females had significantly fewer ovulated COC in the oviduct than blank-treated females (12 ± 1.57 vs 19.92 ± 2.25 oocytes, respectively; N=12-13; P=0.008) (Figure 3.6.A). Further, the number of unovulated COC remaining in unruptured pre-ovulatory follicles in the ovary (Figure 3.6.B), was significantly greater in DHT-treated females than in blank-treated (2.85 ± 0.67 vs 1.17 ± 0.32 follicles, respectively; N=13-12; P=0.04). Additionally, the total sum of COCs was significantly lower in ovaries from DHT-treated females, which yielded on average 8 COCs fewer than those from blank-treated mice (14.9 ± 1.8 vs 21.9 ± 2.5, respectively; N=12-13; P = 0.03). This shows that androgen exposure partially impairs follicle growth and ovulation, even after ovarian hyperstimulation.

Oocyte quality and maturation was assessed in ovulated oocytes by analysing their morphology. Oocytes presenting a spherical shape, and uniformity and integrity of the cytoplasm were deemed morphologically healthy. The percentage of morphologically healthy oocytes (Figure 3.6.C) was slightly lower (69.87 ± 6.58 %) in COC collected from the DHT group than in the blank group (78.88 ± 3.98 %) but this reduction was not statistically significant. The percentage of oocytes that had successfully matured, i.e. reached MII at 14h post-hCG, (Figure 3.6.D) was higher, but not significantly, in DHT (54.17 ± 7.77 %) than in blank-treated females (44.16 ± 5.16 %). Thus, DHT treatment does not have a significant impact on the morphology and maturation of ovulated oocytes.

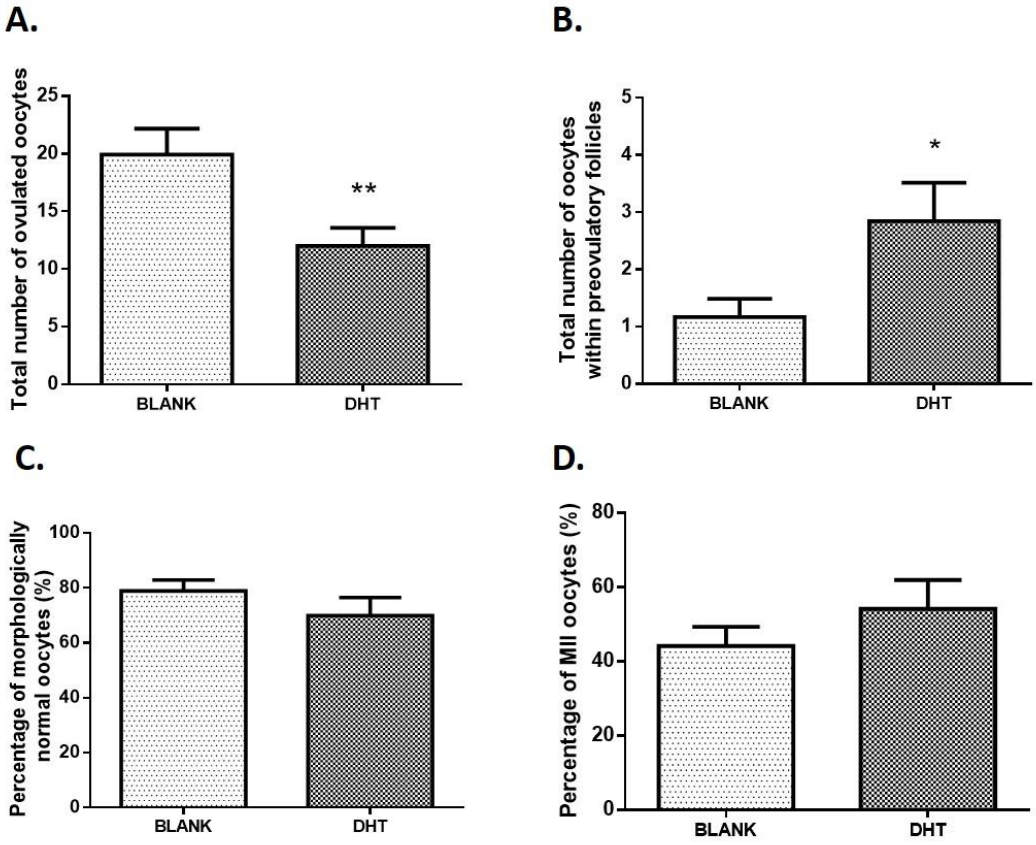

Figure 3.6 Effect of in vivo DHT treatment on oocyte number and morphology.

A. Total number of ovulated oocytes collected from the oviduct at 14 h post-hCG **P=0.008. **B.** Total number of oocytes punctured from non-ovulated preovulatory ovarian follicles at the same time point * P=0.04. **C.** Percentage of morphologically normal oocytes from total ovulated oocytes. **D.** Percentage of oocytes at metaphase II (MII) from total ovulated oocytes. N=13 (BLANK), 12 (DHT) female mice. Results are shown as mean ± SEM. Statistical analysis was Student's T-test.

Intracellular markers of oocyte quality, lipid content and relative mitochondrial activity, were also analysed in the ovulated MII oocytes. Those from DHT-treated females had decreased lipid content (Figure 3.7.A); with CTCF quantification showing (Figure 3.7.B) a reduction (76.42 ± 3.76 AU) in oocytes from DHT-treated females compared to those from blank-treated females (114.29 ± 22.4 AU). MTO activity dye showed similar levels in oocytes from the DHT-treated and control groups (Figure 3.7.C). Quantification (Figure 3.7.D) verified this result with CTCF values for MTO assay (Figure 3.7.D) similar in oocytes from both the DHT-treated (518.6 ± 72.76 AU) and blank-treated (502.77 ± 36.38 AU) females. These findings suggest that oocytes from DHT-treated females do not have overtly altered cytoplasmic lipid content or mitochondrial activity when compared to oocytes from control females.

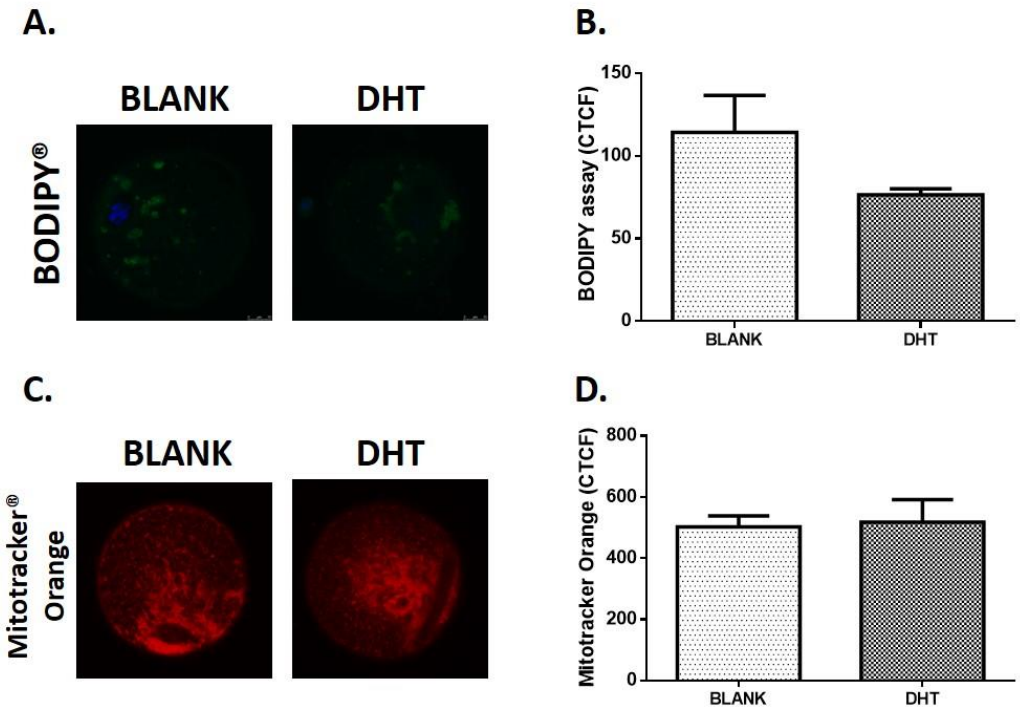

Figure 3.7 Effects of in vivo DHT treatment on lipid content and mitochondrial activity of ovulated oocytes.

A. Representative images of ovulated oocytes stained with BODIPY lipid dye. **B.** Corrected Total Cell Fluorescence (CTCF) analysis of BODIPY stained oocytes. **C.** Representative images of ovulated oocytes stained with MTO mitochondrial activity dye. **D.** CTCF analysis of MTO stained oocytes. N=10 (BLANK), 15 (DHT) oocytes per treatment group. Results are shown as mean ± SEM. Statistical analysis was Student's T-test.

Oocyte developmental competence was tested by performing in vitro fertilisation (IVF) and embryo culture for 5 days. On day 2, at 46 hours post-hCG injection, embryos were checked for first cleave (Figure 3.8.A). A higher percentage of 2-cell (or greater) embryos was observed in the DHT-treated (72 %) than in blank-treated group (66.0 %). On day 5, at 113 hours post-hCG injection, blastocysts were counted (Figure 3.8.B). Remarkably, none of the 2 cell embryos from the DHT-treated group developed to blastocysts, while 87% of the 2 cell embryos from the blank-treated females developed to blastocysts as expected. Morphological assessment showed (Figure 3.8.C, D and E) that embryos from DHT-treated females did not develop beyond the 4-cell/8-cell stage while blank-treated embryos developed to early blastocysts (10.83 %) and fully expanded blastocysts (51.53 %) as expected. In some instances, multiple spermatozoa were observed inside the zona pellucida of embryos derived from DHT-exposed oocytes (Figure 3.8.E). These results suggest that oocyte quality and developmental potential are significantly compromised in females exposed to high levels of androgens.

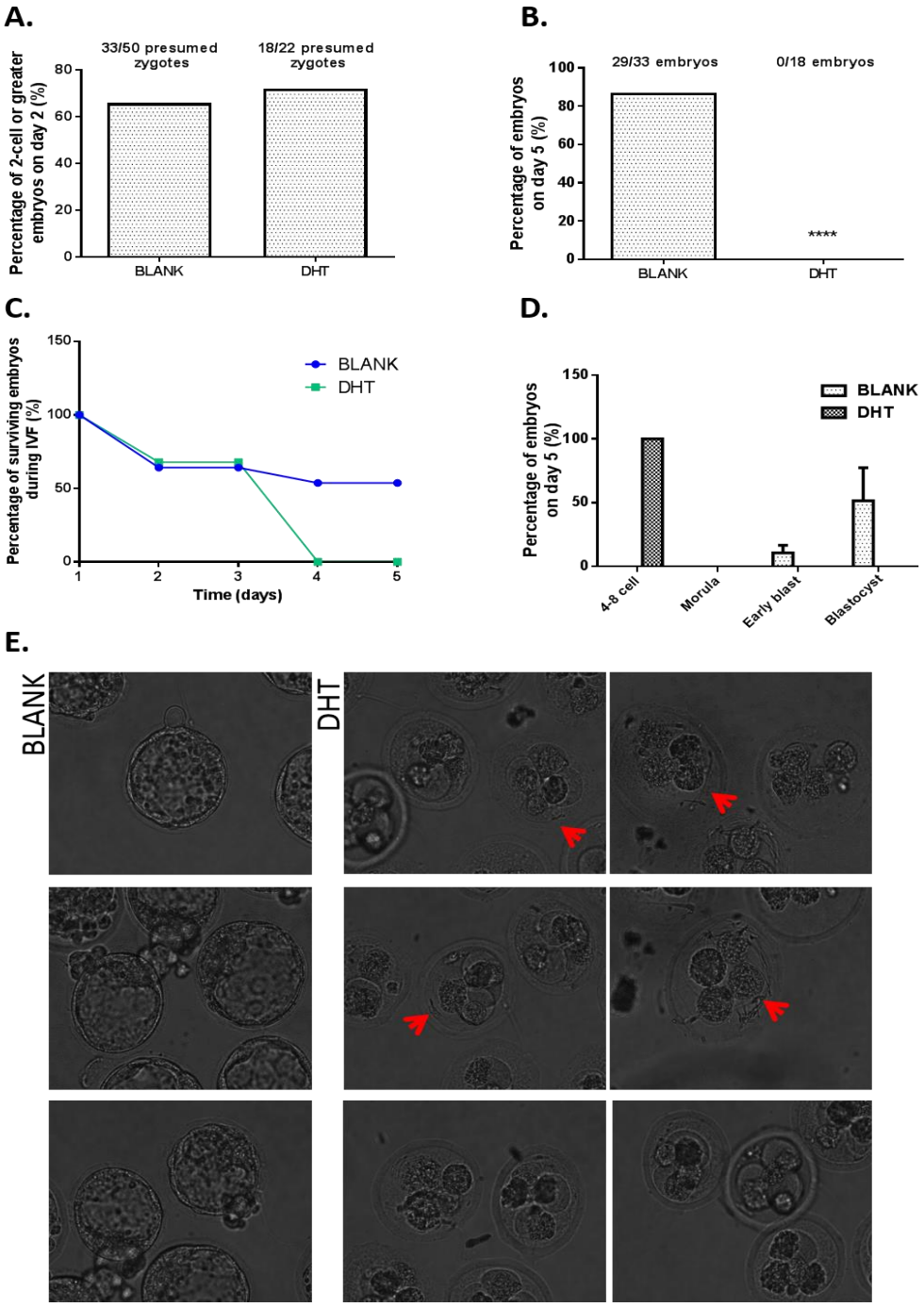

Figure 3.8 Effects of in vivo DHT treatment on oocyte developmental competence.

A. Percentage of embryos with 2 cells or greater from starting number of oocytes (SO) on IVF day 2. **B.** Percentage of blastocysts from 2-cell embryos at 113 hours on IVF day 5 **** P<0.0001. **C.** Percentage of embryos that continued development across the culture period from each treatment group. **D.** Percentage of embryos at each developmental stage on IVF day 5. **E.** Representative images of embryos on IVF day 5. Red arrows indicate spermatozoa inside the zona pellucida. N=3 mice per treatment group. Results are mean ± SEM. Statistical analysis was Fisher's exact Test (A, B).

3.4 Discussion

Overall, these findings indicate that hyperandrogenemia in females affects systemic metabolism and reproductive potential. Specifically, the results show that chronic exposure to high androgens in mice caused mild fasting hyperglycemia and impaired insulin tolerance. This was associated with reduced ovulation, even in response to gonadotropin stimulation, and poor oocyte quality that was manifested as arrested embryo development. Given that PCOS is diagnosed in 75% of anovulatory women [310], further studies using this model to find therapeutic targets to improve fertility treatment could benefit a large proportion of the PCOS population.

PCOS is clearly associated with a metabolic phenotype. Approximately 50% of women with PCOS are insulin resistant and hyperinsulinemic, and have 5 to 10 times higher risk of developing type 2 diabetes; while in turn, women already suffering from type 2 diabetes are more likely to develop PCOS [311]. These dysregulations in metabolism are also related to overweight and adiposity in PCOS women, especially the increased accumulation of abdominal fat. Girls predisposed to insulin-resistance and overweight are at greater risk of developing PCOS during their adolescence [312], which suggests that it is the presence of metabolic syndrome features, in particular obesity and hyperinsulinemia, that induce the hyperandrogenism characteristic of women with PCOS [313, 314]. Further evidence of this relationship is that PCOS patients treated with the insulin sensitizer Metformin show reduced androgen levels after treatment [315]. There is a strong correlation between high circulating androgen levels and hyperinsulinemia in obese women with PCOS, when compared to weight-matched non-PCOS controls [316]. Moreover, in vitro studies have shown that hyperinsulinemia directly stimulates ovarian steroidogenesis by increasing thecal cell proliferation and androgen secretion, and it has been speculated that hyperinsulinemia could stimulate adrenal steroidogenesis in a similar manner [315, 317]. Thus, body weight, glucose metabolism and high circulating androgen levels are fundamental traits affecting the severity of the PCOS phenotype; yet whether hyperandrogenemia alone triggers insulin resistance or whether hyperinsulinemia stimulates excess androgen production is not entirely understood and is likely to vary in different forms and etiologies of the syndrome.

The clinical relevance of mouse models of PCOS is sometimes questioned because ovarian development and the nature of the ovulatory cycles in this species is quite different from humans. However, there is accumulating evidence that the more recently developed rodent hyperandrogenic PCOS models share many of the key symptoms and phenotypical variability

that characterize this syndrome, particularly the metabolic features (reviewed in [318]). These models are created by exposing rats and mice to different androgens either pre- or postnatally. Prenatal exposure to DHT dysregulates the estrous cycle and produces polycystic ovaries where follicles present a thicker granulosa cell layer [300, 319, 320]; but prenatal treatment using Testosterone (T) and Testosterone Propionate (TP) does not always affect cyclicity or ovarian function and follicle morphology [321-326]. In contrast, postnatal treatment with the androgens DHT, T, TP or Dehydroepiandrosterone (DHEA), or the aromatase inhibitor Letrozole, induces hyperandrogenism, acyclicity, anovulation and polycystic ovaries in varying degrees [300, 322, 324, 326-334]. Importantly, what makes the postnatal androgen treatment of rodents a particularly valid model for the disease is that the treated females also express metabolic phenotypes, similar to the features of PCOS. Particularly, postnatal DHT treatment dysregulates body composition and metabolism, producing increased body weight and adipose tissue, especially in the abdomen, plus enlarged adipocytes, high leptin and cholesterol levels, insulin resistance and abnormal liver function [300, 335-338]. PCOS patients often exhibit similar characteristics [93, 339-342].

Caldwell et al [300] developed a mouse model that offers insight into the biology behind the effects of long term exposure to elevated circulating levels of androgens, one of the most common symptoms of PCOS, in female physiology. Previous studies using post-natal treatment with DHT in rats to produce PCOS symptoms mimicked some of the metabolic and ovarian features of the syndrome in humans [336, 337], however the treatment did not produce the hyperandrogenism or hormonal imbalance characteristic of the syndrome [336]. This hyperandrogenic mouse model has now been further characterized herein by showing that the DHT-exposure leads to dysregulated glucose metabolism and has a negative effect on oocyte quality. Postnatal DHT exposure was previously shown to increase body weight and abdominal adiposity in rodents [300, 336-338], and the above data verifies this. Notably, Caldwell et al had previously observed very little impact of high androgen levels on glucose metabolism in this postnatal DHT-treated mouse model [300]. For their analysis of insulin tolerance, mice were fasted for 6 hours prior to the baseline glucose reading and insulin injection [300, 343]. Herein a slightly different method was used to analyse glucose and insulin tolerance where mice are fasted before the glucose tolerance test only. These tests revealed that fasting blood glucose levels were significantly higher in the androgen exposed group, and that these females also presented reduced insulin tolerance; further evidence that excess androgens lead to metabolic dysfunction.

The reported dysregulation of HSPA5 in mouse ovarian cells in response to obesity [97] prompted the current investigation into whether HSP chaperones are globally affected by hyperandrogenemia and/or mild obesity. PCOS ovaries often feature abnormal follicle development but how ovarian HSP are functionally affected remains unclear. Park et al previously reported dysregulated HSP90AA1 levels in whole ovaries and in the GC from cystic follicles from rats exposed to a high dose of adrenocorticotropic hormone (ACTH), mimicking the upregulated ACTH and cortisol stress responses seen in PCOS women [344], and suggested that this chaperone may have a role in the abnormal development of cystic follicles in this model [345]. However, in this current study, DHT exposure didn't significantly impact gene expression for eight different HSR genes analysed in post-ovulatory GLC. Expression levels were slightly lower for HSPA1B and HSPD1 in GLC from the DHT group, but not significantly different. This was somewhat surprising since the HSR transcriptome of GC has been suggested to be relatively sensitive compared to other somatic cells, at least in response to heat stress [346, 347]. Thus, the reported differences in regulation of ovarian HSP in PCOS models are likely due to the different phenotypes, especially the hormonal profiles, as HSP expression and function is likely to be differentially modulated by obesity, hormones and type of cellular stress.

An additional stress response pathway, the ER stress response was also analysed. The ER stress response, is characterised by the activation of the Unfolded Protein Response (UPR) concurrent with an increase in ROS, triggered by accumulation of denatured proteins within the ER. GC collected from PCOS patients and DHEA-treated PCOS mice were observed to have upregulated ER stress marker genes (HSPA5, ATF4 and XBP1s), which was proposed to promote ovarian fibrosis by inducing pro-fibrotic factors TGFβ-1 and CTGF [348]. This upregulation of the ER stress pathway in ovarian samples was in the absence of obesity in both human and mouse. Our group has previously shown that ER stress genes are upregulated in GLC from obese mice [97, 100]. Surprisingly, ER stress markers, including HSPA5, were not upregulated in the GLC from the androgen-exposed mice in this study, even though they were overweight. That the ER stress markers are not dramatically upregulated indicates the lack of obesity-induced cellular stress as observed in the more profoundly affected obesity models. The reason for the discrepancy in ER stress gene induction in the DHEA-induced PCOS model [348] and our DHT-induced PCOS model may be caused by the type of androgen administered, which could have different effects on GC. Additionally, our model used C57BL6 or C57BL6-background mice while the Takahashi model used Balb/C mice, which present different stress-related phenotypes to C57BL6 mice and have been reported to be more susceptible to

physiological stresses [349-351]. Cumulatively, the analyses of ER stress and HSR stress gene expression suggest that either these pathways are not directly dysregulated by androgens or that the mild degree of obesity induced by DHT treatment is not sufficient to trigger these stress responses. These androgen-exposed mice only had about 6.3% increase in body weight when compared to the untreated females, while we have previously found ovarian stress pathways were dysregulated in both HFD-induced and hyperphagia-induced obesity models, where the obese females presented 11% and 53% increased body weight compared to controls, respectively [97, 100].

One of the diagnostic criteria for PCOS is ovarian dysfunction, with most patients presenting either anovulation or oligo-ovulation, with the latter defined as a single serum progesterone (P4) level of 10 nmol/L or higher indicative of recent spontaneous ovulation [352-354]. Oligo-ovulatory women present a milder phenotype of ovarian dysfunction and can regain regular menstrual cycles and become pregnant after ovulation induction treatment using clomiphene citrate. However, anovulatory women present more severe ovarian dysfunction and rarely regain cyclicity, although they have a higher chance of pregnancy after treatment with recombinant FSH (rFSH) [355, 356]. Androgen-exposure produces an equivalent oligo-ovulatory phenotype in mice, with serum P4 concentration at 1.1 nmol/L, approximately a 92% reduction compared to controls [300]. In the current study, there was an approximately 33% reduction in the total number of COCs (both ovulated and non-ovulated), which may be due to the higher levels of follicular atresia reported in this mice }.[300]. Further, even though ovarian hyperstimulation induced ovulation in DHT-treated mice, albeit there was an almost 40% reduction in the number of oocytes collected compared to the blank-treated controls. Consequently, the majority of the oocytes remained inside their unruptured follicles. These findings validate and build on previous reports on the abnormal follicular morphology and development in this PCOS model [300], as well as mimicking the clinical ovarian response to gonadotropin stimulation seen in anovulatory PCOS patients. Interestingly, the ovulated oocytes appeared morphologically normal and similar proportions had progressed to MII in both groups. There was a trend towards lower lipid content, but this was not significant and would have been unexpected in light of multiple reports of increased oocyte lipid content with obesity [97, 202, 357]. Similarly, oocyte mitochondrial activity appeared normal. Thus, there were no overt markers of oocyte maturation or morphology to suggest dysregulation of meiosis or altered cytoplasmic maturation. Despite this, embryo development was profoundly blocked at the 4-8 cell stage. These effects on oocyte quality and embryonic development are likely

caused by the hyperandrogenemia, as opposed to the metabolic defects, since they are more severe than the obesity-induced embryo defects reported by others ([97, 100]. Embryo glucose uptake is one important developmental process which commences at the 4-8 cell stage [358, 359], and thus it is possible that the hyperandrogenic follicular environment in the DHT-treated mice affects this facet of differentiation or other essential aspects of embryogenesis.

In conclusion, these results further characterise the human PCOS-like phenotype of this hyperandrogenic mouse model, by showing that exposure to elevated DHT causes abnormal glucose metabolism and oligo-ovulation. The analyses of ER stress and HSR stress markers in ovarian follicular cells showed that these mechanisms are not disrupted, at least not at the mRNA level, by hyperandrogenism in this model. However, high circulating androgen levels had negative effects on oocyte developmental competence which should be examined further in future studies in order to better understand the effects of hyperandrogenemia on oocyte quality.

3.5 References

93. Fauser BC, Tarlatzis BC, Rebar RW, Legro RS, Balen AH, Lobo R, Carmina E, Chang J, Yildiz BO, Laven JS, Boivin J, Petraglia F, et al. Consensus on women's health aspects of polycystic ovary syndrome (PCOS): the Amsterdam ESHRE/ASRM-Sponsored 3rd PCOS Consensus Workshop Group. Fertil Steril 2012; 97:28-38.e25.
94. Rotterdam EA-SPCWG. Revised 2003 consensus on diagnostic criteria and long-term health risks related to polycystic ovary syndrome. Fertil Steril 2004; 81:19-25.
97. Wu LL, Dunning KR, Yang X, Russell DL, Lane M, Norman RJ, Robker RL. High-fat diet causes lipotoxicity responses in cumulus-oocyte complexes and decreased fertilization rates. Endocrinology 2010; 151:5438-5445.
99. Minge CE, Bennett BD, Norman RJ, Robker RL. Peroxisome proliferator-activated receptor-gamma agonist rosiglitazone reverses the adverse effects of diet-induced obesity on oocyte quality. Endocrinology 2008; 149:2646-2656.
100. Wu LL, Russell DL, Wong SL, Chen M, Tsai TS, St John JC, Norman RJ, Febbraio MA, Carroll J, Robker RL. Mitochondrial dysfunction in oocytes of obese mothers: transmission to offspring and reversal by pharmacological endoplasmic reticulum stress inhibitors. Development 2015; 142:681-691.
163. Ma X, Fan L, Meng Y, Hou Z, Mao YD, Wang W, Ding W, Liu JY. Proteomic analysis of human ovaries from normal and polycystic ovarian syndrome. Mol Hum Reprod 2007; 13:527-535.
202. Wu LL, Russell DL, Norman RJ, Robker RL. Endoplasmic reticulum (ER) stress in cumulus-oocyte complexes impairs pentraxin-3 secretion, mitochondrial membrane potential (DeltaPsi m), and embryo development. Mol Endocrinol 2012; 26:562-573.
293. March WA, Moore VM, Willson KJ, Phillips DI, Norman RJ, Davies MJ. The prevalence of polycystic ovary syndrome in a community sample assessed under contrasting diagnostic criteria. Hum Reprod 2010; 25:544-551.
294. Davis SR, Knight S, White V, Claridge C, Davis BJ, Bell R. Preliminary indication of a high prevalence of polycystic ovary syndrome in indigenous Australian women. Gynecol Endocrinol 2002; 16:443-446.
295. Boyle JA, Cunningham J, O'Dea K, Dunbar T, Norman RJ. Prevalence of polycystic ovary syndrome in a sample of Indigenous women in Darwin, Australia. Med J Aust 2012; 196:62-66.
296. Legro RS, Driscoll D, Strauss JF, Fox J, Dunaif A. Evidence for a genetic basis for hyperandrogenemia in polycystic ovary syndrome. Proceedings of the National Academy of Sciences 1998; 95:14956-14960.
297. González F, Rote NS, Minium J, Kirwan JP. Reactive Oxygen Species-Induced Oxidative Stress in the Development of Insulin Resistance and Hyperandrogenism in Polycystic Ovary Syndrome. The Journal of Clinical Endocrinology & Metabolism 2006; 91:336-340.
298. Kim JJ, Kim D, Yim JY, Kang JH, Han KH, Kim SM, Hwang KR, Ku SY, Suh CS, Kim SH, Choi YM. Polycystic ovary syndrome with hyperandrogenism as a risk factor for non-obese non-alcoholic fatty liver disease. Alimentary Pharmacology & Therapeutics 2017; 45:1403-1412.
299. Karoli R, Fatima J, Chandra A, Gupta U, Islam FU, Singh G. Prevalence of hepatic steatosis in women with polycystic ovary syndrome. J Hum Reprod Sci 2013; 6:9-14.
300. Caldwell AS, Middleton LJ, Jimenez M, Desai R, McMahon AC, Allan CM, Handelsman DJ, Walters KA. Characterization of reproductive, metabolic, and endocrine features of polycystic ovary syndrome in female hyperandrogenic mouse models. Endocrinology 2014; 155:3146-3159.

301. Hogg K, Wood C, McNeilly AS, Duncan WC. The in utero programming effect of increased maternal androgens and a direct fetal intervention on liver and metabolic function in adult sheep. PLoS One 2011; 6:e24877.
302. Li L, Zhang J, Deng Q, Li J, Li Z, Xiao Y, Hu S, Li T, Tan Q, Li X, Luo B, Mo H. Proteomic Profiling for Identification of Novel Biomarkers Differentially Expressed in Human Ovaries from Polycystic Ovary Syndrome Patients. PLoS One 2016; 11:e0164538.
303. Zhao KK, Cui YG, Jiang YQ, Wang J, Li M, Zhang Y, Ma X, Diao FY, Liu JY. Effect of HSP10 on apoptosis induced by testosterone in cultured mouse ovarian granulosa cells. Eur J Obstet Gynecol Reprod Biol 2013; 171:301-306.
304. Yang X, Wu LL, Chura LR, Liang X, Lane M, Norman RJ, Robker RL. Exposure to lipid-rich follicular fluid is associated with endoplasmic reticulum stress and impaired oocyte maturation in cumulus-oocyte complexes. Fertil Steril 2012; 97:1438-1443.
305. Wood JR, Dumesic DA, Abbott DH, Strauss JF, 3rd. Molecular abnormalities in oocytes from women with polycystic ovary syndrome revealed by microarray analysis. J Clin Endocrinol Metab 2007; 92:705-713.
306. Rajani S, Chattopadhyay R, Goswami SK, Ghosh S, Sharma S, Chakravarty B. Assessment of oocyte quality in polycystic ovarian syndrome and endometriosis by spindle imaging and reactive oxygen species levels in follicular fluid and its relationship with IVF-ET outcome. Journal of Human Reproductive Sciences 2012; 5:187-193.
307. Chen M, Wu L, Wu F, Wittert GA, Norman RJ, Robker RL, Heilbronn LK. Impaired Glucose Metabolism in Response to High Fat Diet in Female Mice Conceived by In Vitro Fertilization (IVF) or Ovarian Stimulation Alone. PLOS ONE 2014; 9:e113155.
308. Burgess A, Vigneron S, Brioudes E, Labbe JC, Lorca T, Castro A. Loss of human Greatwall results in G2 arrest and multiple mitotic defects due to deregulation of the cyclin B-Cdc2/PP2A balance. Proc Natl Acad Sci U S A 2010; 107:12564-12569.
309. Matthews JN, Altman DG, Campbell MJ, Royston P. Analysis of serial measurements in medical research. BMJ 1990; 300:230-235.
310. Kousta E, White DM, Franks S. Modern use of clomiphene citrate in induction of ovulation. Human reproduction update 1997; 3:359-365.
311. Ovalle F, Azziz R. Insulin resistance, polycystic ovary syndrome, and type 2 diabetes mellitus. Fertil Steril 2002; 77:1095-1105.
312. Lewy VD, Danadian K, Witchel SF, Arslanian S. Early metabolic abnormalities in adolescent girls with polycystic ovarian syndrome. J Pediatr 2001; 138:38-44.
313. Rosenfield RL. Polycystic ovary syndrome and insulin-resistant hyperinsulinemia. J Am Acad Dermatol 2001; 45:S95-104.
314. Maliqueo M, Sir-Petermann T, Perez V, Echiburu B, de Guevara AL, Galvez C, Crisosto N, Azziz R. Adrenal function during childhood and puberty in daughters of women with polycystic ovary syndrome. J Clin Endocrinol Metab 2009; 94:3282-3288.
315. De Leo V, la Marca A, Petraglia F. Insulin-lowering agents in the management of polycystic ovary syndrome. Endocr Rev 2003; 24:633-667.
316. Burghen GA, Givens JR, Kitabchi AE. Correlation of Hyperandrogenism with Hyperinsulinism in Polycystic Ovarian Disease*. The Journal of Clinical Endocrinology & Metabolism 1980; 50:113-116.
317. Bremer AA, Miller WL. The serine phosphorylation hypothesis of polycystic ovary syndrome: a unifying mechanism for hyperandrogenemia and insulin resistance. Fertil Steril 2008; 89:1039-1048.
318. Walters KA, Allan CM, Handelsman DJ. Rodent models for human polycystic ovary syndrome. Biol Reprod 2012; 86:149, 141-112.

319. Wu XY, Li ZL, Wu CY, Liu YM, Lin H, Wang SH, Xiao WF. Endocrine traits of polycystic ovary syndrome in prenatally androgenized female Sprague-Dawley rats. Endocr J 2010; 57:201-209.
320. Sullivan SD, Moenter SM. Prenatal androgens alter GABAergic drive to gonadotropin-releasing hormone neurons: implications for a common fertility disorder. Proc Natl Acad Sci U S A 2004; 101:7129-7134.
321. Fels E, Bosch LR. Effect of prenatal administration of testosterone on ovarian function in rats. Am J Obstet Gynecol 1971; 111:964-969.
322. Huffman L, Hendricks SE. Prenatally injected testosterone propionate and sexual behavior of female rats. Physiol Behav 1981; 26:773-778.
323. Slob AK, den Hamer R, Woutersen PJ, van der Werff ten Bosch JJ. Prenatal testosterone propionate and postnatal ovarian activity in the rat. Acta Endocrinol (Copenh) 1983; 103:420-427.
324. Swanson HE, Werfftenbosch JJ. The "Early-Androgen" Syndrome; Differences in Response to Pre-Natal and Post-Natal Administration of Various Doses of Testosterone Propionate in Female and Male Rats. Acta Endocrinol (Copenh) 1964; 47:37-50.
325. Swanson HE, Werff ten Bosch JJ. The "early-androgen" syndrome; effects of pre-natal testosterone propionate. Acta Endocrinol (Copenh) 1965; 50:379-390.
326. Tyndall V, Broyde M, Sharpe R, Welsh M, Drake AJ, McNeilly AS. Effect of androgen treatment during foetal and/or neonatal life on ovarian function in prepubertal and adult rats. Reproduction 2012; 143:21-33.
327. Edwards DA. Neonatal administration of androstenedione, testosterone or testosterone propionate: effects on ovulation, sexual receptivity and aggressive behavior in female mice. Physiol Behav 1971; 6:223-228.
328. Beloosesky R, Gold R, Almog B, Sasson R, Dantes A, Land-Bracha A, Hirsh L, Itskovitz-Eldor J, Lessing JB, Homburg R, Amsterdam A. Induction of polycystic ovary by testosterone in immature female rats: Modulation of apoptosis and attenuation of glucose/insulin ratio. Int J Mol Med 2004; 14:207-215.
329. Weisz J, Lloyd CW. Estrogen and androgen production in vitro from 7-3-H-progesterone by normal and polycystic rat ovaries. Endocrinology 1965; 77:735-744.
330. Arai Y, Yamanouchi K, Mizukami S, Yanai R, Shibata K, Nagasawa H. Induction of anovulatory sterility by neonatal treatment with 5 beta-dihydrotestosterone in female rats. Acta Endocrinol (Copenh) 1981; 96:439-443.
331. Ota H, Fukushima M, Maki M. Endocrinological and histological aspects of the process of polycystic ovary formation in the rat treated with testosterone propionate. Tohoku J Exp Med 1983; 140:121-131.
332. Kamijo T, Mizunuma H, Yamada K, Ibuki Y. In vitro fertilization of androgen sterilized mice. Life Sci 1994; 55:527-531.
333. McDonald PG, Doughty C. Comparison of the effect of neonatal administration of testosterone and dihydrotestosterone in the female rat. J Reprod Fertil 1972; 30:55-62.
334. Pinilla L, Trimino E, Garnelo P, Bellido C, Aguilar R, Gaytan F, Aguilar E. Changes in pituitary secretion during the early postnatal period and anovulatory syndrome induced by neonatal oestrogen or androgen in rats. J Reprod Fertil 1993; 97:13-20.
335. Roland AV, Nunemaker CS, Keller SR, Moenter SM. Prenatal androgen exposure programs metabolic dysfunction in female mice. J Endocrinol 2010; 207:213-223.
336. Manneras L, Cajander S, Holmang A, Seleskovic Z, Lystig T, Lonn M, Stener-Victorin E. A new rat model exhibiting both ovarian and metabolic characteristics of polycystic ovary syndrome. Endocrinology 2007; 148:3781-3791.
337. Johansson J, Feng Y, Shao R, Lonn M, Billig H, Stener-Victorin E. Intense electroacupuncture normalizes insulin sensitivity, increases muscle GLUT4 content,

and improves lipid profile in a rat model of polycystic ovary syndrome. Am J Physiol Endocrinol Metab 2010; 299:E551-559.
338. Yanes LL, Romero DG, Moulana M, Lima R, Davis DD, Zhang H, Lockhart R, Racusen LC, Reckelhoff JF. Cardiovascular-renal and metabolic characterization of a rat model of polycystic ovary syndrome. Gend Med 2011; 8:103-115.
339. Barber TM, Franks S. Adipocyte biology in polycystic ovary syndrome. Mol Cell Endocrinol 2013; 373:68-76.
340. Abbott DH, Barnett DK, Bruns CM, Dumesic DA. Androgen excess fetal programming of female reproduction: a developmental aetiology for polycystic ovary syndrome? Hum Reprod Update 2005; 11:357-374.
341. Azziz R, Carmina E, Dewailly D, Diamanti-Kandarakis E, Escobar-Morreale HF, Futterweit W, Janssen OE, Legro RS, Norman RJ, Taylor AE, Witchel SF. The Androgen Excess and PCOS Society criteria for the polycystic ovary syndrome: the complete task force report. Fertil Steril 2009; 91:456-488.
342. Goodarzi MO, Dumesic DA, Chazenbalk G, Azziz R. Polycystic ovary syndrome: etiology, pathogenesis and diagnosis. Nat Rev Endocrinol 2011; 7:219-231.
343. Brennan-Speranza TC, Henneicke H, Gasparini SJ, Blankenstein KI, Heinevetter U, Cogger VC, Svistounov D, Zhang Y, Cooney GJ, Buttgereit F, Dunstan CR, Gundberg C, et al. Osteoblasts mediate the adverse effects of glucocorticoids on fuel metabolism. J Clin Invest 2012; 122:4172-4189.
344. Benson S, Arck PC, Tan S, Hahn S, Mann K, Rifaie N, Janssen OE, Schedlowski M, Elsenbruch S. Disturbed stress responses in women with polycystic ovary syndrome. Psychoneuroendocrinology 2009; 34:727-735.
345. Park E, Cockrem JF, Han KH, Kim DH, Jung MH, Chu JP. Stress-induced activation of ovarian heat shock protein 90 in a rat model of polycystic ovary syndrome. J Obstet Gynaecol Res 2012; 38:396-407.
346. Li L, Wu J, Luo M, Sun Y, Wang G. The effect of heat stress on gene expression, synthesis of steroids, and apoptosis in bovine granulosa cells. Cell Stress and Chaperones 2016; 21:467-475.
347. Collier RJ, Collier JL, Rhoads RP, Baumgard LH. Invited Review: Genes Involved in the Bovine Heat Stress Response1. J Dairy Sci 2008; 91:445-454.
348. Takahashi N, Harada M, Hirota Y, Nose E, Azhary JM, Koike H, Kunitomi C, Yoshino O, Izumi G, Hirata T, Koga K, Wada-Hiraike O, et al. Activation of Endoplasmic Reticulum Stress in Granulosa Cells from Patients with Polycystic Ovary Syndrome Contributes to Ovarian Fibrosis. Sci Rep 2017; 7:10824.
349. Olfe J, Domanska G, Schuett C, Kiank C. Different stress-related phenotypes of BALB/c mice from in-house or vendor: alterations of the sympathetic and HPA axis responsiveness. BMC Physiol 2010; 10:2.
350. Serrano J, Casanova-Martí À, Blay M, Terra X, Ardévol A, Pinent M. Defining Conditions for Optimal Inhibition of Food Intake in Rats by a Grape-Seed Derived Proanthocyanidin Extract. Nutrients 2016; 8:652.
351. Cramer NP, Xu X, Christensen C, Bierman A, Tankersley CG, Galdzicki Z. Strain variation in the adaptation of C57Bl6 and BALBc mice to chronic hypobaric hypoxia. Physiol Behav 2015; 143:158-165.
352. Wathen NC, Perry L, Lilford RJ, Chard T. Interpretation of single progesterone measurement in diagnosis of anovulation and defective luteal phase: observations on analysis of the normal range. Br Med J (Clin Res Ed) 1984; 288:7-9.
353. Israel R, Mishell DR, Jr., Stone SC, Thorneycroft IH, Moyer DL. Single luteal phase serum progesterone assay as an indicator of ovulation. Am J Obstet Gynecol 1972; 112:1043-1046.

354. Carmina E, Chu MC, Longo RA, Rini GB, Lobo RA. Phenotypic variation in hyperandrogenic women influences the findings of abnormal metabolic and cardiovascular risk parameters. J Clin Endocrinol Metab 2005; 90:2545-2549.
355. Burgers JA, Fong SL, Louwers YV, Valkenburg O, de Jong FH, Fauser BC, Laven JS. Oligoovulatory and anovulatory cycles in women with polycystic ovary syndrome (PCOS): what's the difference? J Clin Endocrinol Metab 2010; 95:E485-489.
356. Homburg R, Hendriks ML, Konig TE, Anderson RA, Balen AH, Brincat M, Child T, Davies M, D'Hooghe T, Martinez A, Rajkhowa M, Rueda-Saenz R, et al. Clomifene citrate or low-dose FSH for the first-line treatment of infertile women with anovulation associated with polycystic ovary syndrome: a prospective randomized multinational study. Hum Reprod 2012; 27:468-473.
357. Jungheim ES, Macones GA, Odem RR, Patterson BW, Lanzendorf SE, Ratts VS, Moley KH. Associations between free fatty acids, cumulus oocyte complex morphology and ovarian function during in vitro fertilization. Fertility and sterility 2011; 95:1970-1974.
358. Leese HJ, Barton AM. Pyruvate and glucose uptake by mouse ova and preimplantation embryos. J Reprod Fertil 1984; 72:9-13.
359. Lane M, Gardner DK. Lactate regulates pyruvate uptake and metabolism in the preimplantation mouse embryo. Biol Reprod 2000; 62:16-22.

Chapter 4: Effects of distinct obesogenic diets on female metabolism and ovarian stress responses

4.1 Introduction

The rise in obesity has been deemed one of the biggest health challenges of this century, with accumulating evidence from transgenerational studies suggesting that it not only affects the obese individual, but their offspring for generations to follow. The Australian Institute of Health and Welfare (AIHW) has reported that almost 2 in 3 adults are overweight or obese, constituting a 9% increase since 1995 [360, 361]. As much as 5% of the burden of disease was attributable to obesity in 2011 [361], but this is likely to increase in the future, since currently 1 in 4 Australian children between 2 and 17 years old are overweight or obese [362].

Over-nutrition, particularly of Western-style diets high in fat and sugar, are a major underlying cause of increasing obesity levels, at least in industrialized countries such as the USA [363, 364]. However, there is little understanding of whether different types of obesogenic diets differentially impact human physiology. This information is needed to develop strategies to mitigate the detrimental effects of obesity.

Increased consumption of sugar has recently gained increasing attention, and especially the consumption of fructose-sweetened food products and beverages has been linked to the rise in obesity and metabolic syndrome in the last few decades [364, 365]. Recent studies looking at the effect of fructose consumption on reproductive function found a 30% decrease in pregnancy rates in female mice fed a 60% fructose diet for 6 weeks [366, 367]. Females that did get pregnant presented impaired decidualization [366], which was accompanied by lipid accumulation and increased levels of oxidative stress in the placenta, foetal loss and pregnancy complications, resulting in smaller litters [367]. Since these infertility phenotypes were not associated with increased body weight, these studies show that dietary fructose can negatively affect female reproductive function. Another study showed that female rats on a high fructose diet for 28 days had longer estrous cycles, and bigger ovaries possessing more corpora lutea than control diet-fed animals [368]. There are currently no studies that have investigated the effects of fructose on ovarian function. Thus, how fructose directly impacts folliculogenesis, ovulation and oocyte quality are still unknown.

Obesity is known for inducing a systemic low-grade inflammatory state that affects target tissues such as adipose tissue, liver, and muscle [106, 369]. As part of this, levels of pro-inflammatory molecules are increased, and inflammatory signalling pathways are activated [369]. Obesity increases the release of proinflammatory cytokines such as IL-6 [107], and TNF-α from adipose tissue thereby inducing lipolysis, enhancing cytokine release, and promoting insulin resistance [108, 109]. It has been shown that ovaries from HFD-fed female mice had

upregulated inflammatory markers [370], but the analysis of whole homogenised ovary did not permit identification of which cell populations were impacted. Thus, a part of this study was to investigate whether fructose consumption exacerbates this obesity-induced ovarian inflammatory response.

There is a relationship between obesity, stress pathways and insulin metabolism dysfunction. In target tissues such as skeletal muscle, obesity is associated with cytokine dysregulation, increased levels of ROS and ER stress at the cellular level, as well as higher HSPA1A expression (reviewed in Henstridge et al. 2014 [371]). Other HSP are also dysregulated by metabolic syndrome. Insulin-resistance reduced the expression of HSPB1 (HSP25) in skeletal muscle of aged rats [372]. Obese non-diabetic patients have increased levels of HSPA5 (Grp94), HSPD1 (HSP60), HSP90AA1 (HSP90) in adipose tissue [373] while DNAJB3 (HSP40) is decreased [374]. Downregulation of HSPD1 in the hypothalamus in a mouse model of type 2 diabetes caused hypothalamic insulin resistance and mitochondrial dysfunction [375]. However, it is not known if and how obesity affects the regulation of these key stress pathways in ovarian follicles.

This chapter describes experiments to determine if the addition of high fructose sugar to high fat diet increases the detrimental effects on metabolic health, oocyte quality and inflammation. Additionally, the work aimed to investigate whether two distinct chronic long-term obesogenic diets affect the HSR pathway in the somatic cells of the pre-ovulatory follicle in line with exacerbated effects on metabolic health.

4.2 Materials and Methods

4.2.1 Animals

To study the effect of obesogenic diets on ovarian function, C57BL6J female mice were purchased at 6 weeks of age from the Animal Resources Centre (Canning Vale, Australia). Mice were randomly assigned one of three dietary treatments upon arrival: control (CD; N = 11), high fat (HFD; N = 11), or high-sugar high-fat diet (HSHFD; N = 15) and kept on their assigned diets for 40 weeks. The diets were made in-house and the composition of each one is shown in Appendix 6 (CD) and 7 (HFD). Briefly, the CD contained 10% Kcal from fat, while both HFD and HSHFD had 60% Kcal derived from fat. In addition, the HSHFD animals had ad libitum access to 13% w/v of high-fructose corn syrup (1247 KJ/100 g; Daesang Corporation, South Korea) in the drinking water. This is similar to the concentration found in commercial

sweetened beverages and that has been shown to alter estrous cycle in rats [376]. All dietary treatments were given ad libitum. Body weights were recorded periodically: fortnightly from 6 to 22 weeks of age, then once every 3 weeks from 22 to 33 weeks of age, then once every 4 weeks until the end of the experiment.

All experiments were approved by the University of Adelaide Animal Ethics Committee (approval M-2013-086) and followed the Australian Code for the Care and Use of Animals for Scientific Purposes.

4.2.2 Metabolic tests

Glucose and Insulin Tolerance Tests were carried out, as previously described [307] over a 2 week period. At 3 and 7 months of age, animals were challenged with either IP injection of 2 g/Kg glucose or 0.75 IU/Kg insulin (Actrapid; Novo Nordisk Australia, NSW, Australia), in 0.9% saline solution for glucose or insulin tolerance tests respectively. Prior to the glucose injection only, the animals had been fasted for 6 hours (from 8 am to 2 pm). Blood samples were obtained from a tail tip prick, and the blood glucose levels measured on glucose strips and a glucometer (AccuChek Performa Monitor, Roche Diagnostics, Indianapolis, USA). Blood glucose levels were measured at 0, 15, 30, 60, 90 and 120 min post-injection.

4.2.3 Assessment of estrous cycle

Following 36 weeks into the diet, cyclicity was monitored daily across groups for 15 days (N=8-9). The stage of the estrus cycle was determined through microscopical observation of vaginal epithelial cell morphology from vaginal smears, as described by Byers et al [377]. Briefly, vaginal epithelial cell smears were collected daily in 5 ul of sterile Phosphate Buffer Saline (PBS), then spread on a glass slide under a 22x22 mm glass coverslip and visualized using light microscope Nikon CFW10XCM (Nikon Corporation, Tokyo, Japan). The determination of the estrous cycle stage was based on the presence or absence of nucleated epithelial cells, squamous or cornified epithelial cells, and leukocytes. Proestrous is characterised by presenting mostly nucleated, and some squamous epithelial cells; at the estrous stage mostly squamous epithelial cells are observed; metestrous is characterised by the presence of both squamous epithelial cells and leukocytes; while at diestrous leukocytes are the most abundant cell type.

4.2.4 Ovarian stimulation and tissue collection

To examine ovulation and collect ovarian cells at precise times in the ovarian cycle, mice underwent hormonally-induced ovarian hyperstimulation. To stimulate follicular growth, female mice received an intraperitoneal (IP) injection of Pregnant Mare Serum Gonadotropin (PMSG; National Hormone and Peptide Program, Torrence, USA) in sterile 0.9% saline at a dose of 5 IU/12 g of body weight. The mice then were humanely killed by cervical dislocation at 44 hours post-PMSG injection, the final body weight was recorded, and non-reproductive tissues (adipose tissue depots and liver) were individually collected by abdominal dissection and weighed. Reproductive tissues (ovaries, oviducts and uterus) were also collected at this time.

4.2.5 COC and granulosa-luteal cell collection and gene expression analysis by RT-qPCR

The reproductive tracts were dissected and placed in HEPES-buffered GIBCO minimal essential medium (aMEM, Invitrogen, Carlsbad, CA) at 37°C. Cumulus-oocyte complexes (COC) were collected by puncturing the follicles visible in the ovary using 30G needles to collect the COC and GC. COC and DO were separately transferred to clean HEPES-buffered α-MEM and counted. Only intact COC were collected and transferred in 5 ul volume of PBS with 1mg/ml polyvinylpyrrolidone (PVP, Sigma-Aldrich, Missouri, USA), and into an RNase-free tube (Axygen, Corning Life Sciences, USA). The remaining GC were then pipetted into an RNAse-free tube, centrifuged at 1200 rpm at 4° C for 3 min and the supernatant removed. All samples were then snap-frozen in liquid N2 and stored at -80°C until use. Gene expression in GC was analysed separately for each individual mouse (N_{GC} = 7-12 animals per dietary treatment); gene expression in COC was analysed by pooling samples from individual mice with similar body weights together in order to reach a minimum of 9-10 COC per group (N_{COC} = 5 groups per dietary treatment).

Total RNA was extracted from frozen cell pellets using Trizol (Thermo Fisher Scientific, Massachusetts, USA) following the manufacturer's instructions. RNA samples were treated with DNAFREE DNAse (Life Technologies, California, USA) to remove any residual DNA. After this, 1 ul was taken from each sample to quantify RNA and DNA content by measuring the ratio of absorbance between 260 and 280 nm using a spectrophotometer (Thermo Fisher Nanodrop spectrophotometer, Thermo Fisher Scientific). The manufacturer's instructions indicate that a ratio of ~1.8 is considered pure for DNA whereas a ratio of ~2.0 is considered pure for RNA. A given sample was considered free of DNA contamination when they had a

260/280 value of 1.98 or more. RNA concentration and purity were determined by Nanodrop (Thermo Fisher Scientific). 5 ng/mL of mRNA were used to make cDNA by RT-PCR in 10 uL reactions using Supertranscript III reverse transcriptase (Life Technologies, USA) in MicroAmp Fast Optical 96-Well Reaction Plate (Life Technologies). Quantitative real-time PCR was performed in triplicate with Quantstudio 12k Flex Real-time PCR system (Thermo Fisher Scientific), using Taqman Fast Universal Master Mix and hydrolysis probes (Taqman, Life Technologies). The efficiency and specificity of the Taqman probes used in this assay is batch tested by the manufacturer and shown to be of almost 100%. Gene products measured were HSF1, HSPA5, HSPA1A, HSPA1B, HSP90AA1, HSP90AB1, HSP90B1, HSPD1, ATF4, XBP1s, TNFa, IL-6, and IL-1b (see Appendix 4 for primer details). These genes are key markers for the activation of cellular stress pathways, namely the Heat Shock Response (HSR) and Endoplasmic reticulum stress (ER stress). HSR genes HSPA1A, HSPA1B and HSPA5; and ER stress genes ATF4 and XBP1S were examined to determine relative induction in response to the two diets as HFD is known to induce these genes in GC and COC [100, 304]. Similarly, gene expression levels for pro-inflammatory cytokines were measured in follicular cells to determine the relative induction in response to the two obesogenic diets. Real time PCR data was analyzed using the $2^{-(\Delta\Delta CT)}$ method. Expression of target genes was normalised against the expression of ribosomal protein L19 (rpl19), which was used as a validated internal control for every sample. The use of this reference gene has previously been validated for analysing mRNA levels in ovarian cells from mice [99, 100, 202]. Fold changes in gene expression were relative to a whole ovary (collected at 44h post-PMSG injection) cDNA sample, also included in each run. The calibrator sample in this case represents the amount of transcript that is expressed in the whole tissue, from which to obtain the relative number of mRNA copies of the target genes in the cell population of interest.

4.2.6 Statistical analysis

Statistical analyses were implemented in collaboration with Dr. Emma Knight, senior statistician at the Biostatistics Core Service at the Robinson Research Institute (University of Adelaide, Australia). First, a quadratic random coefficients model was implemented to analyse the changes in body weight over time for each individual mouse. The model was adjusted to account for the heteroscedasticity that resulted from the higher variability in the HFD mice weight trajectories. Therefore, to investigate the differences in the body weight trajectories overtime between the diets, a quadratic random coefficients linear mixed model was fitted with

heterogeneous variances for each of the diet groups. Results are shown as the estimated mean body weight (g) at each time point and associated 95% confident intervals (CI). Data were analysed using R programming language [378].

A Fixed Effects Mixed model was implemented to analyse the trajectories for circulating glucose levels over time during glucose and insulin tolerance tests. This method allowed comparison of not only the predicted means between dietary groups, but also how these change over time between 3 and 7 months of dietary treatment. Body weight was introduced as a variable to investigate its effect on the response to glucose or insulin challenge. Results are shown as the estimated mean value for blood glucose (mmol/mL) at each time point and the associated 95% CI. Data were analysed using the statistics software SAS system version for windows (SAS Institute, North Carolina, USA).

Variations in cyclicity were analysed using a cyclicity coefficient, defined as the number of different stages observed divided by 15 days of monitoring, which was used to obtain the estimated cycle progress during this time. A Poisson model of regression was used to model the cycle rate = count/exposure = (number of stages)/(number of days), including the exposure variable (number of days) as an offset. Body weight (BW) was included as a variable to explore its influence on estrous cycle regulation. Results are shown as the estimated mean number of stages per 14 days and associated 95% CI. Data were analysed using R programming language [378].

ANOVA (Type III tests) and Tukey's multiple comparison test were used to analyse the changes in gene expression levels between dietary treatments. Body weight at the final point was introduced as cofactor to investigate its effect in regulating follicular cell mRNA levels for the genes of interest. Results are shown as the mean ± the standard error of the mean (SEM). Data were analysed using R programming language [378].

For all other analyses, measures are reported as mean ± the standard error of the mean (SEM), unless indicated otherwise. Data were analysed using the statistics software GraphPad Prism 6 v008 for Windows (GraphPad software Inc., California, USA). Statistical significance was determined as indicated for each analysis. P values of <0.05 were considered statistically significant.

4.3 Results

4.3.1 Fructose combined with high-fat diet exacerbates obesity and alters systemic metabolism

Female mice were placed on two different obesogenic diets and their body weight was measured regularly for 40 weeks. Even though all the groups gained weight during their growth trajectories, the HSHFD were the heaviest. The variability between individual body weight gain trajectories necessitated the use of a quadratic random coefficients model. The significant interaction between $Time^2$ and Diet ($F_{2,\ 536}$=4.72, P=0.009) indicates that the quadratic relationship between body weight and time is significantly different between the diets (Figure 4.1.A).

Analysis of the confidence intervals at 95% allowed a direct comparison of the effects of each diet on body weight. By definition these that don't contain 0, indicate that the difference is significantly statistically different (Table 4-A). Confidence intervals at 95% for HSHFD-CD and HSHFD-HFD showed that HSHFD females gained significantly more weight than those in HFD (approximately 8 g more) and CD (approximately 5g more). Body weight gain was not significantly different between HFD and CD.

Analysis of body weight at the time of tissue collection validated these findings. The HSHFD-fed females were heaviest with body weight significantly higher than females fed CD (42.83 ± 3.8 g vs 35.94 ± 4.27 g; P=0.004 by ANOVA and Tukey's multiple comparison test) (Figure 4.1.B). Abdominal adipose tissue and liver were dissected from all mice to verify the basis of increased body weight. Abdominal fat pad weight in the HSHFD females was significantly increased compared to CD females (4.51 ± 0.88 g vs 2.7 ± 0.91 g; P=0.008). Mice fed HFD had mean abdominal fat pad weight intermediate to CD and HSHFD (3.75 ± 1.65 g) but that was not statistically different to either (Figure 4.1.C). Liver weights were similar across diets (Figure 4.1.D).

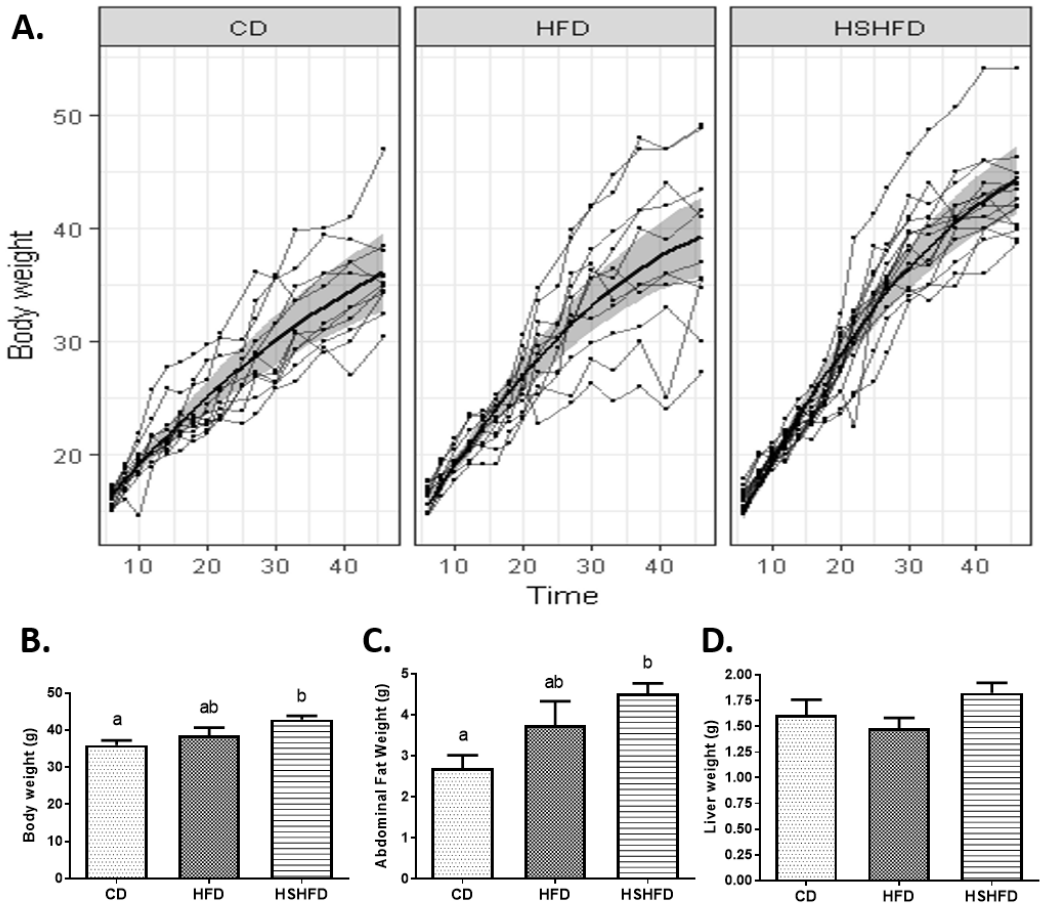

Figure 4.1 Effect of High-fat Diet versus High-Sugar plus High-Fat Diet on body weight and fat deposition.

Body weights (g) in female mice fed control diet (CD), high fat diet (HFD) or high-sugar plus high-fat diet (HSHFD). **A.** Graph plot shows individual mice (thin lines) the predicted body weight means (thick line) and confidence intervals (grey area) for the three dietary groups. HSHFD mice gained significantly more weight over time when compared to HFD and CD groups ($P_{Time2*Diet}$=0.009). **B.** Body weights at 47 weeks of age; (a vs. b P = 0.004). **C.** Abdominal fat pad weight; (a vs b P=0.008.). **D.** Liver weights. Results shown as mean ± SEM. N=11 (CD), N=11 (HFD), N=15 (HSHFD). Statistical analysis was a quadratic random coefficients linear mixed model (A) or One-Way ANOVA and Tukey's Multiple Comparison Test (B-D).

	Comparison difference	Lower limit (LL)	Upper limit (UL)
HFD vs CD	3.15 g	-1.64	7.94 *
HSHFD vs CD	8.19 g	3.74	12.64 *
HSHFD vs HFD	5.04 g	0.54	9.53 *

Table 4-A Body weight differences (g) after 40 weeks of dietary treatment.

Difference between the mean weights for each group comparison pair and confidence intervals at 95%. Statistical analysis was a quadratic random coefficients linear mixed model.

* indicates a significant effect of diet on body weight.

Then the effects of the different diets on glucose tolerance was investigated. Briefly, animals were fasted for 6 hours before measuring fasting blood glucose levels. Then, animals were given a glucose IP injection, and circulating glucose levels were measured at 0, 15, 30, 60 and 120 min after the glucose challenge.

First, fasting blood glucose levels were measured at 3 months into dietary treatment prior to a glucose challenge. There was a significant effect of the obesogenic diets on fasting blood glucose at 3 months ($F_{2,50}$=8.87; P=0.0005). Fasting blood glucose was 1.59 mmol/mL higher in the HFD (95% CI 0.48, 2.69; P=0.003), and 2.08 mmol/mL higher in the HSHFD group (95% CI 0.83, 3.33; P=0.0006) than in the CD group (Figure 4.2.A). The impact of the body weight on fasting glucose levels, and its interaction with the type of diet, was then explored. There was no evidence of an interaction between diet and weight ($F_{2,47}$=0.24, P=0.8). However, there was a weak relationship between fasting blood glucose and weight ($F_{1,49}$=2.88, P=0.096), where a 1g increase in body weight was associated with a 0.13 mmol/mL increase in fasting blood glucose (95% CI -0.02, 0.29).

After glucose challenge both HFD and HSHFD females showed similar glucose tolerance responses that were increased when compared to CD. Interestingly, while the CD only showed one single peak at 15 minutes both HFD and HSHFD females had two peaks in glucose levels, because some animals exhibited peak glucose levels at 15 minutes and some at 30 minutes, suggesting that the regulation of blood glucose levels was affected. However, all dietary groups had lowered blood glucose levels to those of baseline by 120 min (Figure 4.2.B).

At 7 months into dietary treatment regulation of glucose metabolism was re-assessed, and fasting blood glucose was measured. Again, the effect of the obesogenic diets on fasting blood glucose levels was significant at 7 months ($F_{2,50}$=18.807; P<0.0001). The HSHFD group had the highest glucose levels that were 1.28 mmol/mL higher than the HFD (95% CI 0.26, 2.30; P=0.01), and 3.09 mmol/mL higher than the CD group (95% CI 1.87, 4.31; P<0.0001), respectively. Moreover, the HFD group also had 1.80 mmol/mL higher glucose levels compared to CD (95% CI 0.73, 2.88; P=0.0005) (Figure 4.2.C). The influence of body weight on fasting blood glucose levels, and its interaction with diet, was again investigated at 7 months. There was no interaction between diet and body weight ($F_{1,50}$=2.62; P=0.1). Irrespective of diet, there was a significant relationship between fasting blood glucose and body weight. A 1g increase in body weight was associated with a 0.07 mmol/mL increase in fasting blood glucose (95% CI 0.04, 0.1).

Throughout the course of the glucose tolerance test at 7 months into the diet, both HFD and HSHFD females had increased blood glucose level trajectories compared to CD ones. Additionally, while both HFD and HSHFD had peaks in glucose levels at 30 minutes, the CD females peaked at 15 minutes. Moreover, both HFD and HSHFD groups were unable to lower their glucose levels to baseline by 120 min as seen in the CD group (Figure 4.2.D)

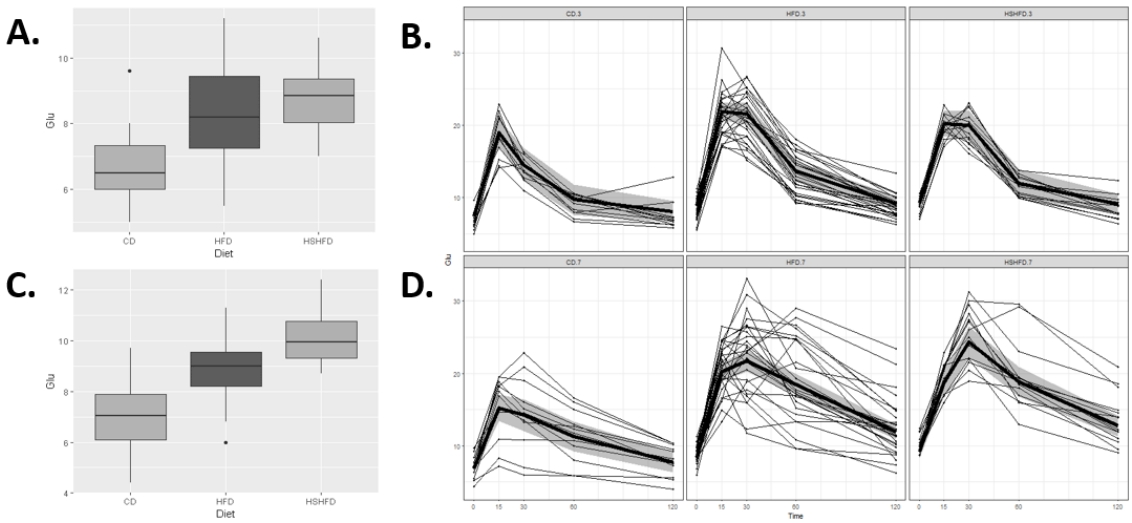

Figure 4.2 Glucose Tolerance in response to High-Fat and High-Sugar plus High-Fat Diets.

Glucose tolerance tests were conducted at either 3 months (A, B) or 7 months (C, D) of dietary treatment. **A.** Fasting blood glucose levels prior to glucose challenge at 3 months, CD vs HFD, CD vs HSHFD P=0.002. **B.** Glucose tolerance test (GTT) at 3 months. Graphs show individual mice (thin lines), predicted blood glucose means (thick line) and confidence intervals (grey area). **C.** Fasting blood glucose levels at 7 months, CD vs HFD and HFD vs HSHFD P<0.0001. **D.** GTT at 7 months showing individual mouse responses (thin lines), mean average blood glucose levels (thick line) and confidence intervals (grey area). Glucose trajectories were significantly different between the obesogenic diets (HFD and HSHFD) and the CD group (Diet*Time: $F_{8,137}$=8.12, P<0.0001) at both 3 and 7 months. Glucose trajectories at 3 months were significantly different from those at 7 months for both obesogenic diet groups (HFD and HSHFD), but not for CD (Diet*Month*Time: $F_{8,\ 137}$=2.13; P=0.04). Statistical analyses were One-Way ANOVA and Tukey's Multiple Comparison Test (A, C); and Mixed model of fixed effects (B, D). Results are shown as mean ± SEM. N=11 (CD), N=26 (HFD), N=15 (HSHFD).

Statistical models were used to determine the influence of diet, body weight and the time on diet on circulating glucose levels at 3 and 7 months. At 3 months (Table 4-B), the analysis of circulating blood glucose levels measured over 120 min after glucose challenge, showed a significant interaction between diet and time ($F_{8, 137}$=8.12; P<0.0001) indicating that the differences in blood glucose levels between the diets changed depending on the time point. The predicted mean trajectory for blood glucose levels was significantly higher at 0, 15, 30 and 60 min for the HFD group when compared to CD but had returned to normal levels by the 120 min time point. Similarly, blood glucose levels at 0 and 30 min were significantly higher for the HFHFD when compared to the CD group.

At 7 months (Table 4-C), analysis of blood glucose levels after the glucose challenge showed a significant interaction between diet and time ($F_{8, 137}$=8.12; P<0.0001) indicating that the differences in blood glucose levels between the diets changed depending on the time point. Both obesogenic groups had significantly higher circulating glucose levels at 0, 15, 30, 60 and 120 min when compared to CD females. Interestingly, when comparing the HFD and HSHFD groups, HSHFD females had significantly increased glucose levels at 0 and at the 30 minute peak.

Taken together, these data indicate that obesogenic diets reduce glucose tolerance in female mice, as shown by increased blood glucose levels at baseline. After 7 months into the diet, circulating glucose had not returned to normal levels by 120 minutes after glucose challenge, suggesting this reduction in glucose tolerance was exacerbated over time. Moreover, these results show a greater impact of the HSHFD on glucose metabolism compared to HFD, as indicated by the higher baseline and peak blood glucose levels.

	Time	Comparison difference (mmol/mL)	Lower limit (LL)	Upper limit (UL)	P value
HFD vs CD	0 min	1.53	1.08	1.98	0.001 *
	15 min	2.90	1.82	3.99	0.009 *
	30 min	7.04	5.71	8.38	<0.0001 *
	60 min	3.91	2.67	5.16	0.002 *
	120 min	1.13	0.26	1.99	0.2
HSHFD vs CD	0 min	1.94	1.42	2.45	0.0003 *
	15 min	1.26	0.03	2.49	0.3
	30 min	5.44	3.92	6.96	0.0005 *
	60 min	2.27	0.85	3.68	0.1
	120 min	1.03	0.05	2.01	0.3
HSHFD vs HFD	0 min	0.41	-0.02	0.84	0.3
	15 min	1.65	0.62	2.68	0.1
	30 min	1.60	0.33	2.87	0.2
	60 min	1.65	0.46	2.83	0.2
	120 min	0.09	-0.73	0.91	0.9

Table 4-B Comparison of circulating glucose concentration (mmol/mL) at 3 months into the dietary treatment.

Difference between the mean glucose readings at each time point during the GTT, for each group pair comparison. Statistical analysis was a mixed model of fixed effects. Data is shown as estimated differences of least square means, confidence intervals at 95% and adjusted P value.

* indicates a significant effect of diet on blood glucose levels.

	Time	Comparison difference (mmol/mL)	Lower limit (LL)	Upper limit (UL)	P value
HFD vs CD	0 min	1.48	1.01	1.94	0.002 *
	15 min	4.99	3.90	6.09	<0.0001 *
	30 min	7.52	6.18	8.86	<0.0001 *
	60 min	7.20	5.95	8.45	<0.0001 *
	120 min	4.25	3.38	5.12	<0.0001 *
HSHFD vs CD	0 min	2.38	1.80	2.96	<0.0001 *
	15 min	3.42	2.16	4.68	0.008 *
	30 min	10.11	8.57	11.65	<0.0001 *
	60 min	7.54	6.10	8.98	<0.0001 *
	120 min	5.00	3.99	6.02	<0.0001 *
HSHFD vs HFD	0 min	0.90	0.45	1.35	0.05 *
	15 min	1.57	0.53	2.61	0.1
	30 min	2.59	1.31	3.87	0.05 *
	60 min	0.34	-0.86	1.53	0.8
	120 min	0.08	-0.76	0.91	0.4

Table 4-C Comparison of circulating glucose concentration (mmol/mL) at 7 months into the dietary treatment.

Difference between the mean glucose readings at each time point during the GTT, for each group pair comparison. Statistical analysis was a mixed model of fixed effects. Data is shown as estimate differences of least square means, confidence intervals at 95% and adjusted P value.

* indicates a significant effect of diet on blood glucose levels.

To compare the evolution of glucose intolerance over time across dietary treatments, a statistical model was implemented to compare the results for the glucose tolerance tests at 3 and 7 months into the diet (Table 4-D). Circulating glucose levels in the CD group were similar at 3 and 7 months, except for a decrease in peak glucose levels at 15 minutes at 7 months. In contrast, it was found that, even though HFD and HSHFD females had similar blood glucose levels at the beginning of the glucose challenge at 3 and 7 months, blood glucose levels were significantly increased at 60 and 120 min for the HFD group at 7 months. Similarly, HSHFD females had significantly higher glucose levels at 30, 60 and 120 min at 7 months when compared to measures taken at 3 months. Thus, indicating that glucose regulation was affected over time in these obesogenic groups. Finally, it was explored if body weight at the time of the test affected the glucose tolerance response and found that it had no effect at 3 nor at 7 months. Taken together, these results show that both HFD and HSHFD reduce glucose tolerance in female mice, independently of body weight, and that this effect is accentuated over time in HSHFD females.

	Time	Comparison difference (mmol/mL)	Lower limit (LL)	Upper limit (UL)	P value
CD 3 mos vs 7 mos	0 min	0.48	-0.05	1.00	0.4
	15 min	3.74	2.46	5.01	0.004 *
	30 min	0.31	-1.26	1.88	0.8
	60 min	1.58	0.11	3.04	0.3
	120 min	1.13	0.26	1.99	0.2
HFD 3 mos vs 7 mos	0 min	0.53	0.03	1.03	0.3
	15 min	1.65	0.73	2.57	0.08
	30 min	0.16	-0.94	1.27	0.9
	60 min	4.86	3.82	5.90	<0.0001 *
	120 min	2.81	2.05	3.58	0.0004 *
HSHFD 3mos vs 7 mos	0 min	0.04	-0.62	0.69	0.9564
	15 min	1.57	0.31	2.83	0.2
	30 min	4.36	2.84	5.88	0.005 *
	60 min	6.85	5.42	8.28	<0.0001 *
	120 min	3.66	2.62	4.69	0.0006 *

Table 4-D Comparison of circulating glucose concentration (mmol/mL) between 3 and 7 months into the dietary treatment.

Difference between the mean glucose readings at each time point during the GTT, for each group pair comparison. Statistical analysis was a mixed model of fixed effects. Data is shown as estimate differences of least square means, confidence intervals at 95% and adjusted P value.

* indicates a significant effect of diet on blood glucose levels.

We next set out to investigate the effect of the obesogenic diets on insulin tolerance. Briefly, baseline blood glucose levels were measured in the absence of fasting. Then, animals were given an insulin IP injection, and circulating glucose levels were measured at 0, 15, 30, 60 and 120 min after the insulin challenge. Insulin tolerance tests (ITT) were also performed at both 3 months and 7 months following dietary treatment. Circulating glucose levels after insulin challenge were similar between the groups at 3 months into the diet (***Figure 4.3***.A.). However, minimum glucose levels were 0.75 mmol/mL lower for HSHFD than HFD females at 60 minutes (95% CI 0.43, 1.07; P=0.02). None of the dietary groups recovered similar blood glucose levels to the starting point and remained with lower levels after 120 minutes (Figure 4.3.A). This suggests there was not a great effect of obesogenic diets on the regulation of circulating insulin levels nor insulin tolerance after 3 months.

At 7 months into dietary treatment insulin tolerance was re-assessed (Figure 4.3.B). After the insulin challenge, HFD females had 1.91 mmol/mL higher blood glucose than those of CD at 0 min (95% CI 1.45, 2.38; P<0.0001); and then again 0.79 mmol/mL higher than control levels at 30 min (95% CI 0.45, 1.14; P=0.02). Similarly, HSHFD also had significantly higher levels of circulating glucose than the controls at 0 (2.10 mmol/mL difference; 95% CI 1.56, 2.65; P=0.0002), 15 (1.93 mmol/mL difference; 95% CI 1.27, 2.60; P=0.004) and 30 minutes post-insulin challenge (1.02 mmol/mL difference; 95% CI 0.61, 1.44; P=0.02). Meanwhile, the HFD and HSHFD fed-females had similar mean trajectories in circulating glucose over the course of the experiment. None of the groups recovered to the initial blood glucose levels after 120 minutes. Additionally, while the CD females reached their minimum glucose level at 30 minutes both the HFD and the HSHFD groups exhibited it at 60 minutes post-insulin challenge. All groups had similar levels of blood glucose at their minimum. Thus, at 7 months into their dietary treatments, females fed the obesogenic diets took twice as long as the controls to reduce circulating glucose levels after insulin challenge, even though they had higher normal blood glucose levels, suggesting a decreased insulin tolerance.

Next, a similar statistical model was implemented to study the influence of diet, body weight and the time that the test was taken on circulating glucose levels. There was no interaction between diet and time ($F_{8, 132}$=1.54; P=0.2), indicating that there was no significant effect of dietary treatment on circulating glucose trajectories measured at the different time points. When comparing the evolution of insulin tolerance between 3 and 7 months, there was a significant effect of the interaction Diet*Month*Time ($F_{8, 132}$=94.7; P=0.04), indicating that the glucose regulation responses were different over time for the different groups). The CD females also had 1.46 mmol/mL lower glucose at 30 minutes at 7 months than at 3 months (95% CI 1.04,

1.88; P=0.005), and this coincides with the minimum glucose levels shifting from 60 minutes post-insulin challenge at 3 months to 30 minutes at 7 months. HFD females had 0.68 mmol/mL lower circulating glucose minimum at the 60 minute time point at 7 months than at 3 months (95% CI 0.35, 1.02; P=0.04). Even though HSHFD females tended to have 1.31 mmol/mL lower blood glucose levels at 15 minutes at 7 months than at 3 months (95% CI 0.66, 1.97; P=0.05), their minimum glucose levels at 60 minutes did not vary significantly over time. Finally, analysis of whether body weight at the time of the test affected the insulin tolerance response found that it had no effect at 3 nor at 7 months. These results suggest that obesogenic diets affect insulin tolerance over time. Even though both CD and HFD females had lower minimum blood glucose levels at 7 months than at 3 months, the CD females reached this minimum at 30 minutes at 7 months, shifting from 60 minutes at 3 months. This was not observed in the obesogenic groups, suggesting they do not become more insulin sensitive with age. Interestingly, even though following 7 months of dietary treatment HSHFD females were the heaviest and had the highest blood glucose levels at baseline, they were not more affected in their ability to recover blood glucose levels following insulin challenge compared to the CD and HFD females.

These results overall show that the addition of sugar to HFD (HSHFD) causes a more pronounced obesity phenotype than HFD alone, and that this difference became more accentuated over time. After 3 months, the HSHFD females were significantly heavier than their HFD counterparts, yet at this time both groups showed similar metabolic profiles following glucose and insulin challenges. By seven months, circulating glucose and insulin regulation profiles were different between the dietary groups, with the HSHFD presenting the highest fasting blood glucose levels, and a decreased glucose tolerance. Both obesogenic groups had delayed regulation of circulating glucose levels, but only the HFD group had lower blood glucose minimum over time. Surprisingly though, body weight was not positively correlated to blood glucose levels in any of the obesogenic groups. Taken together, these results show that the composition of the diet influences the metabolic pathways affected by obesity and indicate that sugar exacerbates the severity of the phenotype.

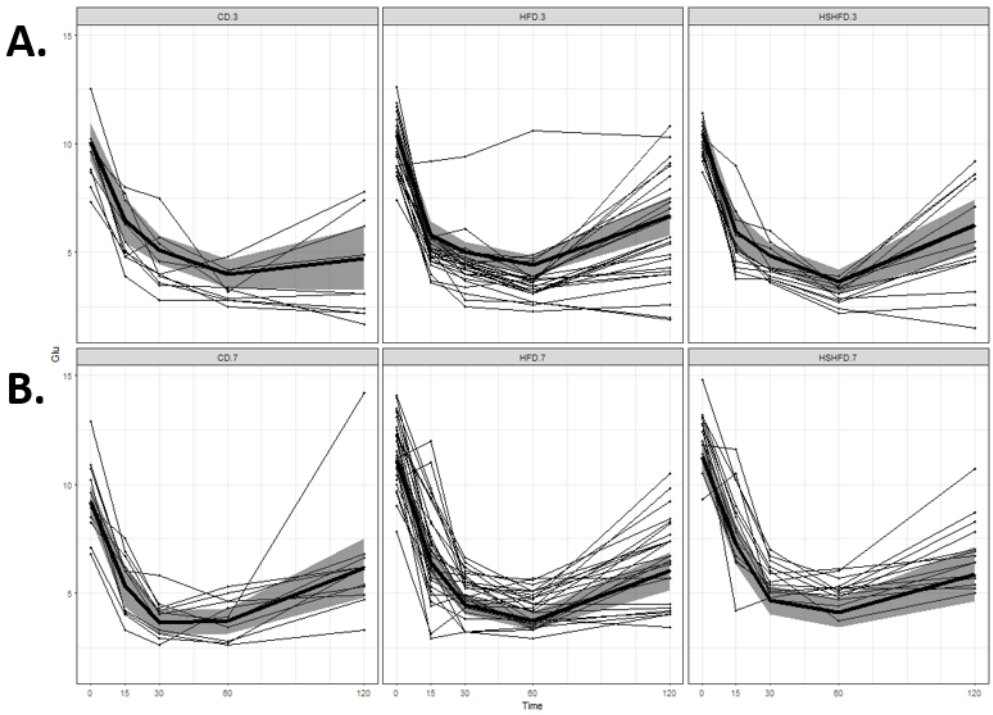

Figure 4.3 Insulin Tolerance in response to High-Fat versus High-Fat plus High-Sugar Diets.

Insulin tolerance tests (ITT) were conducted on mice at either 3 months (A) or 7 months (B) of dietary treatment. Graphs show individual mouse responses (thin lines), mean average blood glucose levels (thick line) and confidence intervals (grey areas). **A.** ITT at 3 months. **B.** ITT at 7 months. N=11 (CD), N=26 (HFD), N=15 (HSHFD). The interaction of Diet*Month*Time had a modified effect that was statistically significant (P=0.04). Results are shown as mean ± SEM. Statistical analysis was a Mixed model of fixed effects.

4.3.2 Effects of obesogenic diets on estrous cyclicity and growing ovarian follicles

Estrous cyclicity was monitored in a subset of mice via daily vaginal cytology, and microscopical analysis of epithelial cell morphology. We established a cyclicity coefficient, defined as the number of different stages observed divided by 15 days of monitoring, and used it to measure the estimated cycle progress over time. A Poisson regression model was implemented to explore the relationship between diets, body weight and cycle progress over time. Even though HSHFD females had a slightly lower cyclicity coefficient, therefore completing less cycles, this was not statistically different from the other two groups (χ^2=4.12; P=0.13;Figure 4.4.A). There was not a significant effect of body weight on estrous cycle (χ^2=0.04; P=0.85).

The number of cycles completed in 15 days was not affected by diet (Figure 4.4.B) and was an average of 1.5 cycles across all groups. Similarly, the length of the cycle was only slightly different; with the HSHFD group having the shortest average cycle duration (5.5 ± 1 days), followed by the HFD (6.08 ± 2.11 days), and then the CD diet group (7 ± 2.35 days) (Figure 4.4.C).

Next, all female mice were given PMSG to stimulate folliculogenesis, and 44h later ovaries were removed and the COCs were collected. A slightly lower number of preovulatory COCs were collected from the ovaries of HSHFD females at this time point (4.17 ± 3.64 COCs), followed by the HFD (6.13 ± 3.18 COCs), and then the CD (7.5 ± 3.51 COCs) (***Figure 4.4***.D.); however, these differences in means were not statistically different. Interestingly, there were on average 3.58 more denuded oocytes collected from the follicles of the HSHFD group compared to the CD (95% CI -6.48, -0.69; P=0.01). Follicles of the HFD group yielded an intermediate number of denuded oocytes which was not significantly different from the other groups (Figure 4.4.E).

These results suggest that obesogenic diets did not greatly impact cyclicity in female mice nor significantly impair the growth of preovulatory follicles in response to PMSG. However, the HSHFD likely affected the health of growing follicles, as shown by the higher number of denuded oocytes observed in this group.

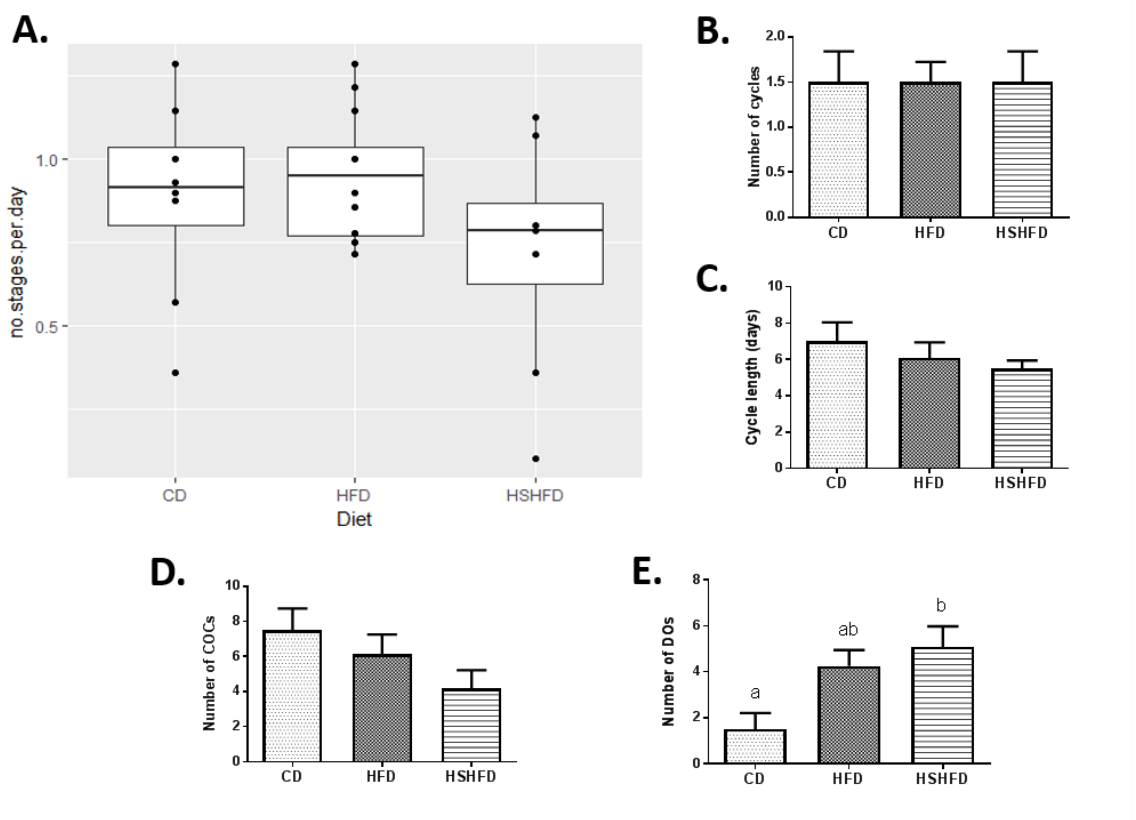

Figure 4.4 Effect of High-Fat Diet versus High-Fat plus High-Sugar Diet on cyclicity and COC number.

A. Box plot showing the relationship between the dietary treatments and their cyclicity coefficients (number of stages in 15 days). Each point represents a coefficient value for one female. Total number (**B**) and average length (**C**) of the cycles during the 15-day assessment period. Oocytes collected from pre-ovulatory follicles were classified as COC (**D**) or denuded oocytes (DO) (**E**), a vs b P=0.02. Results are mean ± SEM. N=8 (CD), N=8 (HFD), N=12 (HSHFD). Statistical analysis was Poisson regression model (A), or One-Way ANOVA and Tukey's Multiple Comparison Test (B-E).

4.3.3 Addition of fructose to high-fat diet causes differential cellular stress responses in ovarian follicular cells

Gene expression for three different stress pathways was analysed in the COC and GC collected from the animals at 44h post-PMSG treatment. These were 1) the HSR stress response which included transcriptional regulator Hsf1 and a cohort of its downstream HSP genes; 2) ER stress marker genes Atf4 and Xbp1s; and 3) inflammatory genes, specifically cytokines Tnfa, Il6 and Il1b.

Firstly, it was investigated if the obesogenic diets affected markers for the HSR in the ovarian cells. HFD-fed females had increased mRNA levels of the transcription factor Hsf1 in COCs, when compared to the HSHFD and CD groups ($F_{2, 12}$=6.28; P=0.01). Hsf1 levels in COCs were 40.8% higher than HSHFD (95% CI 0.28, 0.52; P=0.01), and 32.6% higher than CD (95% CI 0.2, 0.44; P=0.05), respectively. Hsf1 mRNA was slightly but not significantly increased in GC of HFD-fed mice. (Figure 4.5.A).

Analysis of HSR genes downstream of Hsf1 showed that expression of ER-specific chaperone Hspa5 and marker gene for the activation of the UPR response, was elevated in GCs and COCs from HFD females when compared to the other groups but this increase was not statistically different (Figure 4.5.B). Analysis of Hspa1a and Hspa1b, cytoplasmic markers of cellular stress, levels showed that, interestingly, they were both expressed at dramatically higher levels in granulosa cells compared to cumulus cells. Hspa1a expression in GCs from HFD ovaries was 30.6% higher compared to that of HSHFD (95% CI 1.26, 2.72; P=0.03), and 9.6% higher than in ovarian cells from CD (Figure 4.5.C). Similarly, Hspa1b mRNA levels in GCs from the HFD ovaries were 29.3% higher than in the HSHFD (95% CI 1.02, 2.34; P=0.05), while there was a trend of 27.5% lower expression in those from HSHFD compared to the controls (95% CI 0.89, 2.25; P=0.08). Expression for this gene was slightly higher COCs from females fed HFD and HSHFD than in the CD ones (Figure 4.5.D).

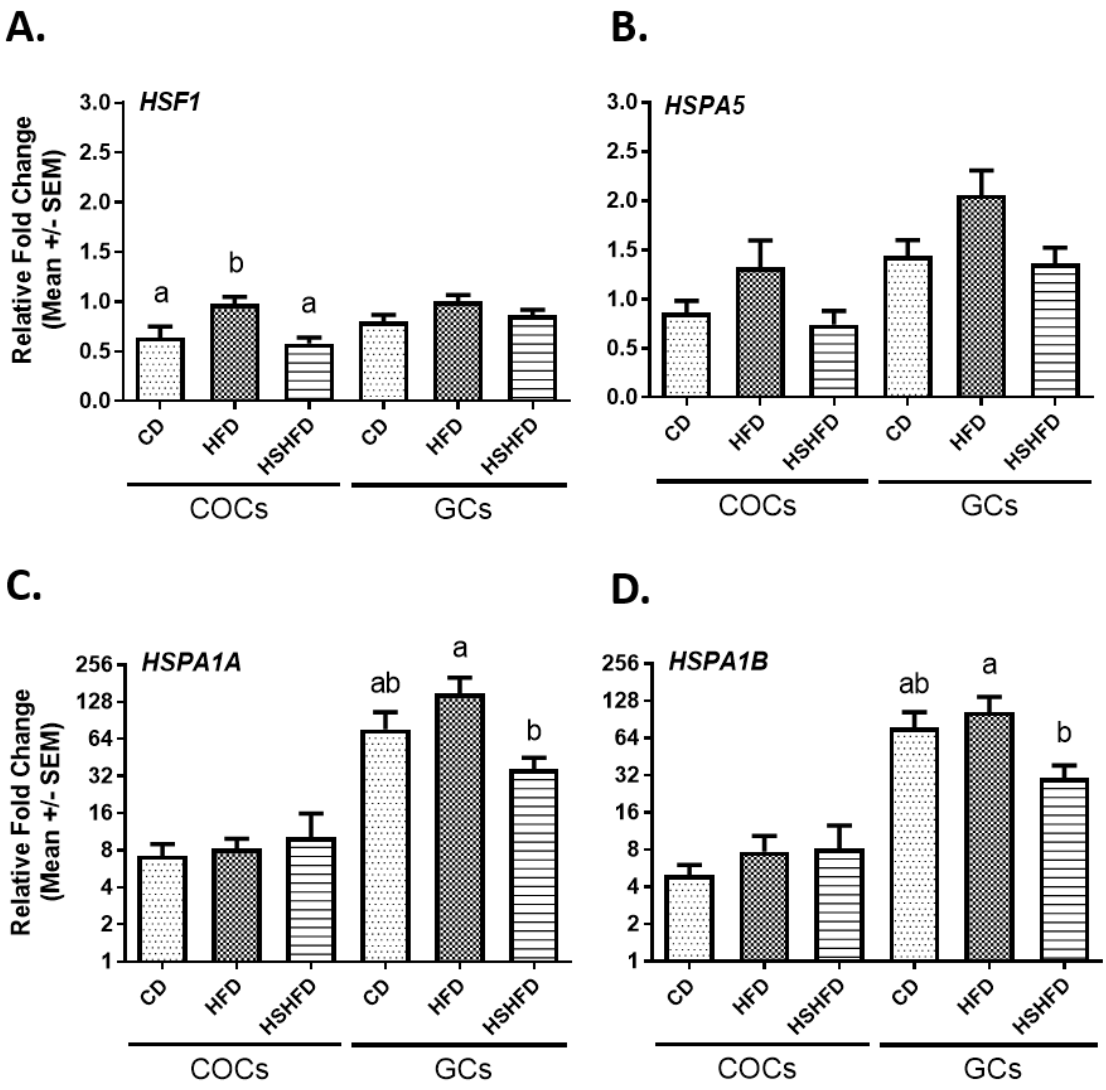

Figure 4.5 Effect of High-Fat Diet versus High-Fat plus High-Sugar Diet on the expression of Heat Shock Response genes.

A. Hsf1 gene expression was significantly different in COC between diets ($F_{2, 12}$=6.28; a vs b P=0.01). **B.** Hspa5 gene expression. **C.** Hspa1a gene expression was significantly different in GCs between the diets ($F_{2, 25}$=3.95; a vs b P=0.03). **D.** Hspa1b gene expression was significantly different in GC between the diets (F2, 25=4.08; a vs b P=0.03). N_{GC} = 8 (CD), 7 (HFD), 12 (HSHFD) animals per dietary treatment, and N_{COC} = 5 pools of ≥ 9 COCs per dietary treatment. Results are mean ± SEM. Gene expression is normalized to Rpl19 reference gene expression and relative to whole ovary cDNA calibrator. Note that the y-axis in C and D is log2 scale.

To further analyse chaperone gene expression, three genes from the HSP90 family and HSPD1 were also analysed. Hsp90aa1 is typically cytoplasmic and regulates oocyte meiosis. Hsp90aa1 expression was upregulated in GC from HFD-fed females when compared to HSHFD (95% CI 1.04, 2.16; P=0.02); while expression levels in COC were also 63.2% higher than in HSHFD (95% CI 0.04, 0.96; P=0.04) (Figure 4.6.A).

Hsp90ab1 is a homologue of Hsp90ab1, also mainly cytoplasmic, and it is more abundant in cumulus cells than in the oocyte [151, 193]. Its mRNA levels were slightly higher in GC from HFD when compared to HSHFD and CD, although this was not statistically significant. Gene expression levels were increased in COC from HFD when compared to the other two diets, but this difference was only marginally significant ($F_{2, 12}$=3.93; P=0.05), and disappeared when adjusted for multiple comparisons in post-hoc tests (Figure 4.6.B).

ER-specific Hsp90b1 expression was highest in GC from HFD ovaries but not significantly different to expression levels in the other groups. Expression levels were however 48.8% higher in COC from the HFD group when compared to those from the HSHFD (95% CI 0.27, 0.57; P=0.04) (Figure 4.6.C).

Finally, analysis of expression levels for mitochondria-specific Hspd1 showed dramatically higher expression in GC compared to COC in both the CD (P=0.03) and the HFD groups (P=0.02), but not in HSHFD females. However, the expression of Hspd1 was statistically similar in COCs and GC from all dietary groups (***Figure 4.6***.D).

Taken together, expression levels for HSR genes were generally increased in both GC and COC ovarian cells from HFD females when compared to the other dietary groups. This included significant increases in Hspa1a, Hspa1b, and hsp90aa1 in GC compared to at least one of the other dietary groups. Hsf1, Hsp90aa1, Hsp90ab1 and Hsp901 were significantly increased in COC of HFD-fed mice compared to at least one of the other dietary groups. In contrast and quite surprisingly, even though the HSHFD females presented exaggerated characteristics of an obesity phenotype, all of the HSR genes examined were expressed at similar levels to those of the CD.

.

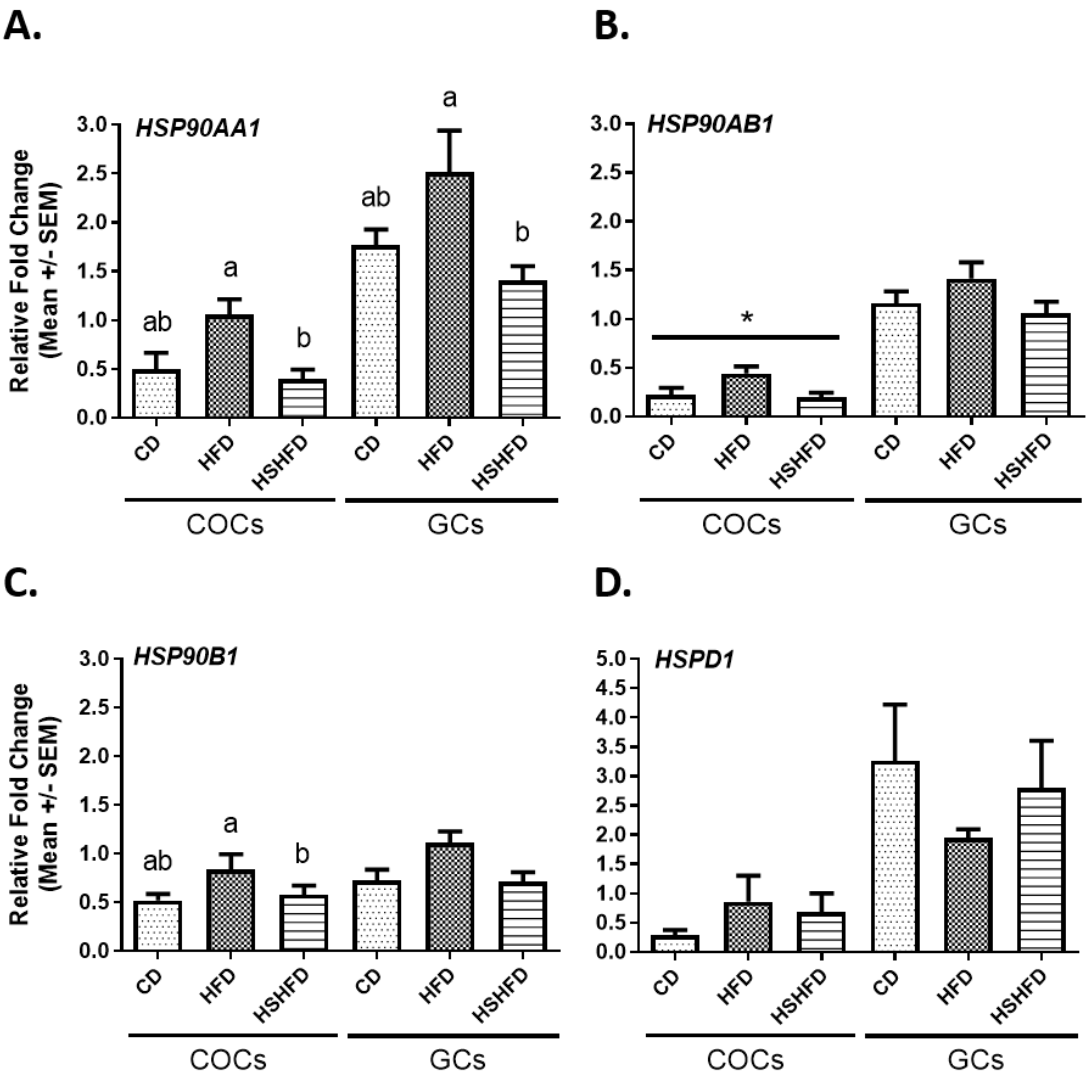

Figure 4.6 Effects of High-Fat Diet versus High-Fat plus High-Sugar Diet on the expression of Heat Shock Response genes.

A. Hsp90aa1 gene expression was significantly different in COC ($F_{2, 12}$=4.48; a vs b P=0.04) and GC ($F_{2, 25}$=4.53; a vs b P=0.02) between the diets. **B.** Hsp90ab1 gene expression was significantly different in COC between the diets ($F_{1, 12}$=3.93; a vs b P=0.05). **C.** Hsp90b1 gene expression was significantly different in COC between the diets ($F_{2, 11}$=4.42; a vs b P=0.04). **D.** Hspd1 gene expression. N_{GC} = 8 (CD), 7 (HFD), 12 (HSHFD) animals per dietary treatment, and N_{COC} = 5 pools of ≥ 9 COC per dietary treatment. Results are mean ± SEM. Gene expression is normalized to Rpl19 reference gene expression and relative to whole ovary cDNA calibrator.

Next, marker genes for ER-stress Atf4 and Xbp1s were examined. Atf4 gene expression levels in GC were similar across diets, but expression was slightly higher in COC from HFD females (Figure 4.7.A.). Xbp1s expression was higher in GC from HFD females when compared to the other two diets but this difference was just marginally significant ($F_{2, 24}$=3.42; P=0.05), and disappeared when adjusted for multiple comparisons in post-hoc tests. Xbp1s expression levels were also slightly higher in COC from HFD females compared to the other two groups (Figure 4.7.B).

Lastly, key pro-inflammatory genes Tnf-a, Il-6, and Il-1b, were chosen to study the relationship between the dietary treatments and obesity-associated inflammation. Gene expression for these inflammatory cytokines was generally more variable than expression of the HSR and ER stress genes. Thus, there were no significant differences in gene expression in GC or COC between the different dietary groups but some possible trends. Gene expression levels for Tnf-α were decreased in both the HFD and the HSHFD in both COC and GC, when compared to those from CD females (Figure 4.8.A). Meanwhile, expression for Il-6 was higher in COC from both HFD and HSHFD (***Figure 4.8***.B.). Expression levels for Il-1b were similar to that of IL-6, with expression levels increased in COC of females fed obesogenic diets (Figure 4.8.C).

In summary, obesogenic diets did not have a profound impact on the expression of either ER stress genes or pro-inflammatory genes in ovarian cells of female mice. This is in contrast to expression of HSR genes which were dysregulated in GC and COC from females fed obesogenic diets, in particular in response to HFD rather than HSHFD.

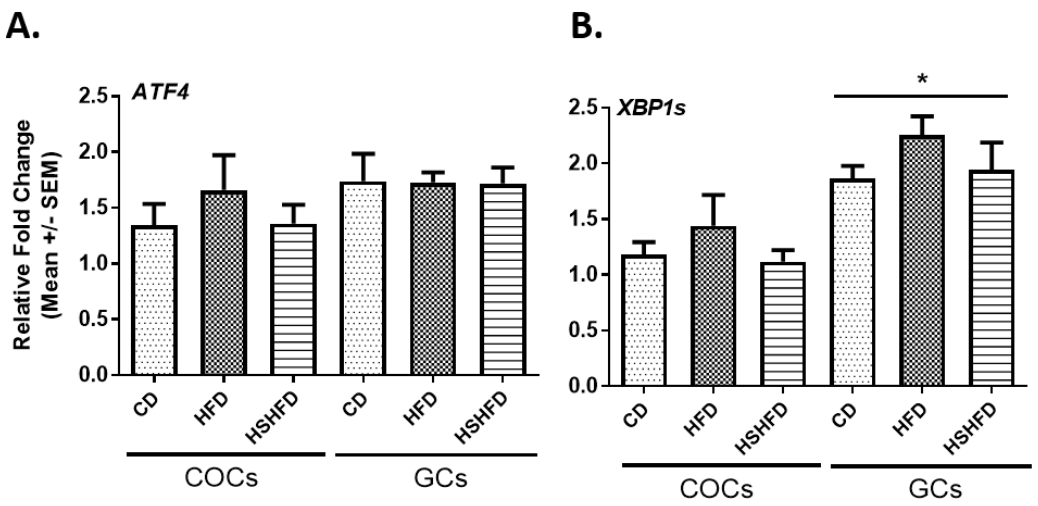

Figure 4.7 Effect of High-fat plus high sugar diet versus High-Fat diet on the expression of ER stress genes.

A. Atf4 gene expression. **B.** Xbp1s gene expression was marginally significantly different in GC between the diets ($F_{2, 24}$=3.42; * P=0.05). N_{GC} = 8 (CD), N=7 (HFD), N=12 (HSHFD) animals per dietary treatment, and N_{COC} = 5 pools of ≥ 9 COC per dietary treatment. Results are mean ± SEM. Gene expression is normalized to Rpl19 reference gene expression and relative to whole ovary cDNA calibrator.

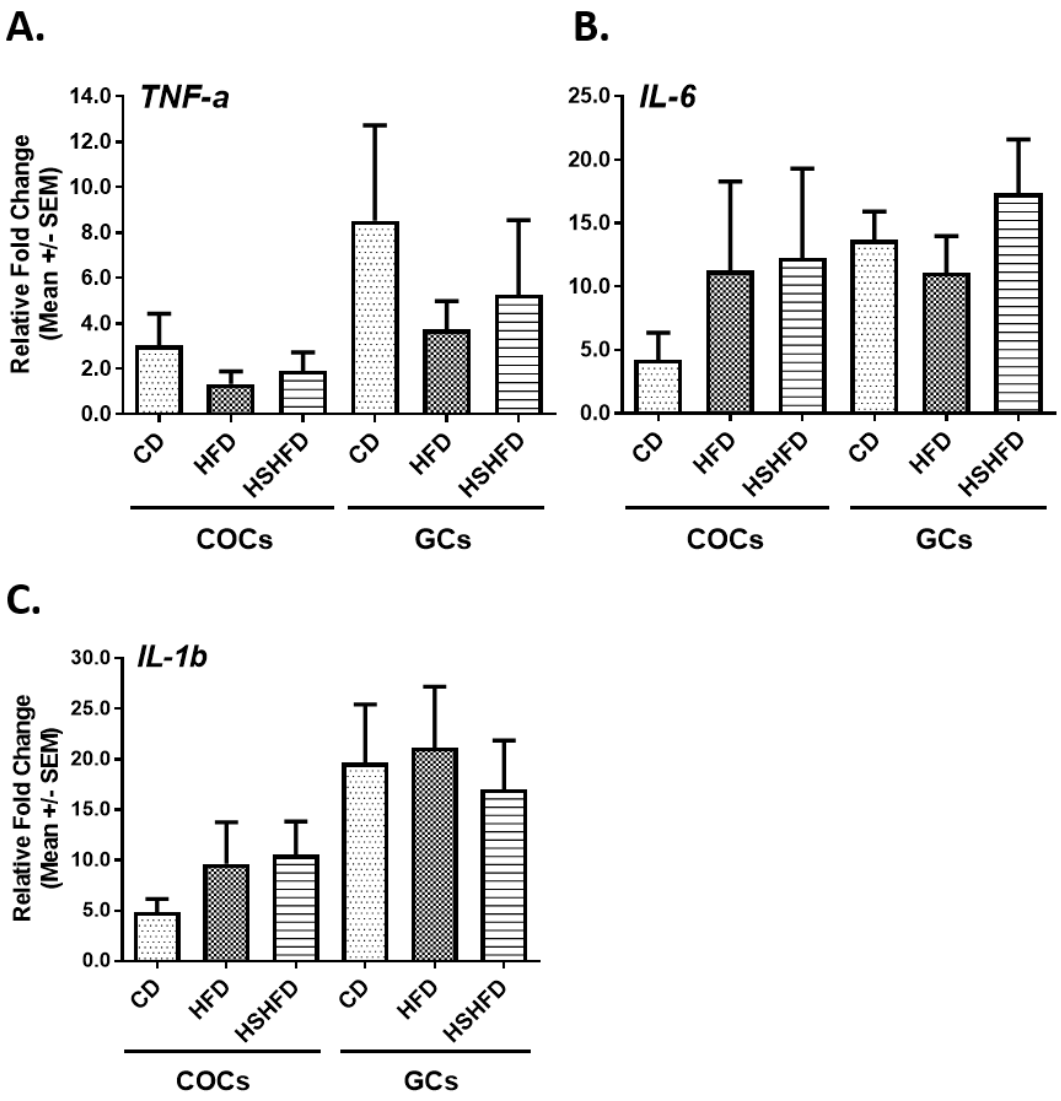

Figure 4.8 Effect of High-sugar plus high-fat diet versus High-Fat diet on the expression of pro-inflammatory genes.

A. Tnf-a gene expression. **B.** Il-6 gene expression. **C.** Il-1b gene expression. N_{GC} = 8 (CD), N=7 (HFD), N=12 (HSHFD) animals per dietary treatment, and N_{COC} = 5 pools of ≥ 9 COC per dietary treatment. Results are mean ± SEM. Relative gene expression is normalized to Rpl19 reference gene expression and relative to whole ovary cDNA calibrator.

Body weight at 40 weeks of diet was introduced into the statistical model to test its effect on gene expression in ovarian cells (Table 4-E**)**. There was not a significant impact of body weight in expression for most HSR genes. The exception was Hsp90b1 where there was a significant relationship between body weight and Hsp90b1 expression in COC ($F_{1, 11}$=6.03; P=0.03), with an estimated 0.026-fold increase in mRNA levels (95% CI 0.0028, 0.0505) with each 1g increase in body weight. Similarly, the expression of pro-inflammatory genes in GC and COC was not associated with increases in body weight.

Interestingly, even though there was not an effect of diet on the expression of ER stress markers (Figure 4.7), ER stress gene expression in COC was influenced by body weight (Table 4-E**)**. There was a significant relationship between body weight and expression of Atf4 in COC ($F_{1, 11}$=6.80; P=0.02), with an estimated 0.06-fold increase in mRNA levels (95% CI 0.0028, 0.0502) with each 1g increase in body weight. Similarly, there was a significant relationship between expression of Xbp1s in COC and body weight ($F_{2,}$ 24=5.30; P=0.04), with an estimated 0.042-fold increase in mRNA levels (95% CI 0.0019, 0.0825) with each 1g increase in body weight.

In summary, HFD was associated with significantly increased mRNA levels for Hspa1a, Hspa1b and Hsp90aa1 in GC. HSHFD was not associated with any significant changes in gene expression compared to CD and exhibited normalised gene expression of most genes compared to HFD. Similarly, in COC, HFD caused dysregulated gene expression of Hsf1 and the Hsp90 family (Hsp90aa1, Hsp90ab1, and Hsp90b1) compared to the other diets. HSHFD generally did not affect gene expression for stress marker genes in COC. Finally, increases in body weight were associated with increased expression of Hsp90b1, Atf4 and Xbp1s in COC, but it did not affect gene expression in granulosa cells.

Gene	Cell type	Sum Sq.	Df	F value	P value
Hsf1	**COCs**	0.07683	1, 11	2.4065	0.1
	GCs	0.00316	1, 24	0.0783	0.8
Hspa5	**COCs**	0.50999	1, 11	3.1911	0.1
	GCs	0.0167	1, 24	0.0456	0.8
Hspa1a	**COCs**	0.3548	1, 11	0.1933	0.7
	GCs	1.028	1, 24	0.3786	0.5
Hspa1b	**COCs**	0.1684	1, 11	0.0873	0.8
	GCs	1.076	1, 24	0.4856	0.5
Hsp90aa1	**COCs**	0.2740	1, 11	0.3293	0.6
	GCs	0.0016	1, 24	0.0047	0.9
Hsp90ab1	**COCs**	0.037386	1, 11	1.4551	0.3
	GCs	0.0332	1, 24	0.1825	0.7
Hsp90b1	**COCs**	0.25782	1, 11	6.0319	0.03 *
	GCs	0.0010	1, 24	0.0075	0.9
Hspd1	**COCs**	1.7875	1, 11	0.9235	0.3
	GCs	0.047	1, 24	0.0349	0.9
Atf4	**COCs**	1.31467	1, 11	6.7915	0.02 *
	GCs	0.0826	1, 24	0.3058	0.6
Xbp1s	**COCs**	0.65305	1, 11	5.3017	0.04 *
	GCs	5.206	1, 24	0.4283	0.5
Tnf-a	**COCs**	0.01258	2, 12	0.0152	0.9
	GCs	2.378	1, 21	1.4224	0.2
Il-6	**COCs**	157.55	1, 10	1.0386	0.3
	GCs	18.40	1, 21	0.1878	0.7
Il-1b	**COCs**	4.25	1, 11	0.0788	0.8
	GCs	405.6	1, 20	1.6894	0.2

Table 4-E Influence of body weight on gene expression in ovarian cells.

Changes in gene expression were analysed using ANOVA (Type III tests) and Tukey's multiple comparison test, with body weight as cofactor. Results are shown as Sum of the Squares (Sum Sq.), degrees of freedom (Df), and F and P values.

* indicates a significant effect of body weight on gene expression levels.

4.4 Discussion

These results show that long-term obesogenic diets increase body weight and abdominal fat mass and alter glucose tolerance and insulin sensitivity in female mice. These obesogenic diets also impact folliculogenesis and follicle health as shown by the increased number of denuded oocytes collected from preovulatory follicles. Gene expression analysis of follicular cells showed that either body weight or HFD tended to increase ER stress genes while HSHFD did not. Further, expression of pro-inflammatory genes appeared dysregulated by both the HFD and the HSHFD groups, although the increased variability in this response between individuals prevented definitive conclusions. Further, analysis of the panel of HSR marker genes showed that the two dietary treatments affected expression of individual genes in GCs and COCs in distinct patterns.

Both the HFD and the HSHFD group had a higher body weight and abdominal fat mass when compared to the CD group at the end of the 40 weeks, with the HSHFD group being the heaviest in both measures of obesity. Even though the HFD was heavier than the controls, it also had a higher inter-individual variability. This variability has been observed in HFD rat models [379], as well as our own previous studies, although reports from other HFD studies are inconsistent as to how variable the degree of weight gain caused by HFD diet is. Interestingly, mice on the HSHFD exhibited less variability, likely because the addition of sugar to the drinking water is highly palatable and therefore can increase calorie consumption, this resulting in a more uniform obesity phenotype.

To investigate if the different obesogenic diets could induce other characteristics of the obesity phenotype in female mice, and how these changed over time, we sought to measure their responses to gold-standard metabolic challenges at two different time points during the dietary treatment, at 3 and 7 months. We showed that both obesogenic diets resulted in altered metabolic phenotypes compared to CD females. The detrimental effects of obesogenic diets on the glucose and insulin tolerance responses in mice have been widely studied and confirmed in male mice [380, 381], although the findings are inconsistent for females [382-385], which are considered more resistant to obesity-induced metabolic disruptions. In the current study, both the HFD and the HSHFD groups showed altered glucose tolerance and increased fasting blood glucose levels, and this was exacerbated in the HSHFD females who also had dysregulated insulin tolerance. Moreover, the heterogeneity in the time of blood glucose peaks in both HFD group at 3 months and then the delayed peaks at 7 months suggest there are at least two impacts of the obesogenic diets in the regulation of blood glucose levels; increased baseline glucose

levels and a delayed response in the secretion of insulin, as shown by higher, longer spikes in circulating glucose levels. This is consistent with other high sugar diet models of obesity [380, 386]. To our knowledge, this is the first study to show that the addition of high sugar to high fat diet has the capacity to exacerbate obesity and metabolic phenotypes in female mice and delineates the timeframe over which these develop. We speculate that this exacerbated obesity is influenced specifically by the high percentage of fructose in the diet; whereas previous studies will have differed in the type of sugar and dietary formula composition, providing the explanation for discrepant results in the literature about the effect of diet on weight gain and metabolic dysfunction.

Even though the effects of obesity on female fertility are widely studied, the contribution of the different macronutrients in obesogenic diets is unclear. We sought to compare secondary markers of fertility between the groups, by studying the characteristics of the oestrus cycle and the morphology of immature developing cumulus-oocyte complexes. Cycle length followed the same trend as body weight/abdominal fat mass, where the heavier HSHFD group progressed through less cycle stages during the observed time. This is likely due to the effects of high sugar in the diet, as other studies have made observations that compliment this result in similar models. In one study, adult female rats fed high fructose corn syrup (HFCS) ad libitum for 28 days had dysregulated estrous cycles with extended estrous and diestrous stages, as well as altered ovarian morphology with increased ovarian weight and number of corpora lutea [368]. In another study, young female rats given 13% w/v HFCS to drink for 8 weeks did not present increased ovarian weight but also had longer cycles due to prolonged time in the estrous phase, suggesting delayed ovulation [376]. However, it was observed that the CD females had an average cycle length of approximately 7 days, which is abnormally long since the average cycle length is 4-5 days for unmated, unstimulated female mice [387], and thus an effect of obesogenic diets on estrous cycle cannot be concluded from this study.

Interestingly, the denuded oocyte phenotype also showed a reversed trend, with the most denuded oocytes collected from the heavier HSHFD group. Conversely, the number of COC collected followed the opposite direction, with the fewest total COCs collected from the HSHFD group. This indicates that obesity has an impact on the maturing follicle, very likely affecting the integrity of cellular communication between the oocytes and their surrounding cumulus cells. Thus overall, HSHFD had a worse effect on female fertility than HFD alone, suggested by the poorest oocyte quality as assessed by the highest numbers of denuded oocytes.

Characteristics of inflammation are well documented to occur in metabolic tissues such as adipose, liver and muscle during the progression of obesity [106]. More recent studies are now also finding that similar responses are occurring in the ovary and female reproductive tract and contributing to female infertility and the developmental programming of obesity phenotypes in offspring [96, 97]. Independent studies have shown dysregulation of inflammatory pathways in the ovaries and uteri of obese animal models, specifically induction of TNF-a and NFκB expression, as well as increased macrophage infiltration in the ovary in response to high fat diet, independent of increased body weight [370]. Therefore, we measured expression levels for pro-inflammatory genes in preovulatory ovarian follicles to determine the relative effects of two distinct obesogenic diets. We found that both obesogenic diet groups presented similar dysregulation for some key cytokines in COC, suggesting the presence of a low-inflammatory state or at least the activation of inflammatory pathways in these cells. In particular, IL-6 and IL-1b mRNA tended to be higher in COC from the mice fed either of the obesogenic diets. The elevated production of cytokines by ovarian cells may be the basis for the elevated levels of cytokines and inflammatory mediators that are observed in follicular fluid of obese women ([388] and our own unpublished data), in conjunction with high levels of follicular fluid lipids [389]. The variability of body weights of the females from which the follicles were collected could explain the high intra-group variation and lack of statistical significance.

ER stress and the subsequent UPR, together with the heat shock response are just a few of the mechanisms by which cells respond to stress. They are thought to be caused by the accumulation of denatured proteins, although some research has shown that the heat shock response can also stimulate pro-inflammatory cytokine production by immune cells (reviewed in [390]), and vice versa. Interestingly, in a previous study of human granulosa cells, HSP70 proteins expression was induced by exposure to cytokines in vitro, namely interferon gamma (IFN-ɣ) and TNF-a [391]. Our group has previously shown that obesity upregulates stress responses in ovarian cells, by activating cytoprotective mechanisms like the HSR, and organelle-specific pathways like the ER stress response or UPR [97, 100]. We had anticipated that the worse metabolic phenotype (HSHFD group) would correlate with greater alterations in these stress genes, but unexpectedly found that while several HSR genes were dysregulated in the HFD model consistent with our previous reports, the HSHFD ovarian cells had gene expression levels similar to those in the CD group, despite the very different metabolic phenotypes. This is consistent with the variability of HSR activation seen in other tissues in response to metabolic dysfunction. For instance, some studies in diabetic mouse models have shown that the altered glucose/insulin metabolism induces the activation of stress pathways in

target tissues [214, 392], while others have found that insulin resistance due to aging [372] and type 2 diabetes [393] is associated with reduced or depleted HSR in target tissues. It has been proposed that the underlying mechanism could be the inflammatory inhibition of HSF1 by stress kinases, capable of repressing HSF1 activation in insulin-resistant tissue by phosphorylation of key serine residues [111]. Alternatively, it is likely that the ovarian cells of females fed HSHFD had progressed beyond the ER stress activation phase and towards cell death. This is supported by the fact that many of the oocytes in follicles of HSHFD females were devoid of CC.

In conclusion, HSHFD diet increases the damage to both metabolic and reproductive tissues compared to high fat diet alone, by causing more severe insulin resistance and worse oocyte quality compared to HFD. Interestingly however, these defects were not associated with overt changes in gene expression for the HSR genes; which likely exhibit dynamic ranges of expression in response to medium versus extreme levels of weight gain.

4.5 References

96. Ma X, Hayes E, Prizant H, Srivastava RK, Hammes SR, Sen A. Leptin-Induced CART (Cocaine- and Amphetamine-Regulated Transcript) Is a Novel Intraovarian Mediator of Obesity-Related Infertility in Females. Endocrinology 2016; 157:1248-1257.
97. Wu LL, Dunning KR, Yang X, Russell DL, Lane M, Norman RJ, Robker RL. High-fat diet causes lipotoxicity responses in cumulus-oocyte complexes and decreased fertilization rates. Endocrinology 2010; 151:5438-5445.
99. Minge CE, Bennett BD, Norman RJ, Robker RL. Peroxisome proliferator-activated receptor-gamma agonist rosiglitazone reverses the adverse effects of diet-induced obesity on oocyte quality. Endocrinology 2008; 149:2646-2656.
100. Wu LL, Russell DL, Wong SL, Chen M, Tsai TS, St John JC, Norman RJ, Febbraio MA, Carroll J, Robker RL. Mitochondrial dysfunction in oocytes of obese mothers: transmission to offspring and reversal by pharmacological endoplasmic reticulum stress inhibitors. Development 2015; 142:681-691.
106. Weisberg SP, McCann D, Desai M, Rosenbaum M, Leibel RL, Ferrante AW, Jr. Obesity is associated with macrophage accumulation in adipose tissue. J Clin Invest 2003; 112:1796-1808.
107. Yudkin JS, Kumari M, Humphries SE, Mohamed-Ali V. Inflammation, obesity, stress and coronary heart disease: is interleukin-6 the link? Atherosclerosis 2000; 148:209-214.
108. Souza SC, Palmer HJ, Kang YH, Yamamoto MT, Muliro KV, Paulson KE, Greenberg AS. TNF-alpha induction of lipolysis is mediated through activation of the extracellular signal related kinase pathway in 3T3-L1 adipocytes. J Cell Biochem 2003; 89:1077-1086.
109. Berg AH, Scherer PE. Adipose tissue, inflammation, and cardiovascular disease. Circ Res 2005; 96:939-949.
111. Geiger PC, Gupte AA. Heat shock proteins are important mediators of skeletal muscle insulin sensitivity. Exerc Sport Sci Rev 2011; 39:34-42.
151. Metchat A, Akerfelt M, Bierkamp C, Delsinne V, Sistonen L, Alexandre H, Christians ES. Mammalian heat shock factor 1 is essential for oocyte meiosis and directly regulates Hsp90alpha expression. J Biol Chem 2009; 284:9521-9528.
193. Voss AK, Thomas T, Gruss P. Mice lacking HSP90beta fail to develop a placental labyrinth. Development 2000; 127:1-11.
202. Wu LL, Russell DL, Norman RJ, Robker RL. Endoplasmic reticulum (ER) stress in cumulus-oocyte complexes impairs pentraxin-3 secretion, mitochondrial membrane potential (DeltaPsi m), and embryo development. Mol Endocrinol 2012; 26:562-573.
214. Chung J, Nguyen AK, Henstridge DC, Holmes AG, Chan MH, Mesa JL, Lancaster GI, Southgate RJ, Bruce CR, Duffy SJ, Horvath I, Mestril R, et al. HSP72 protects against obesity-induced insulin resistance. Proc Natl Acad Sci U S A 2008; 105:1739-1744.
304. Yang X, Wu LL, Chura LR, Liang X, Lane M, Norman RJ, Robker RL. Exposure to lipid-rich follicular fluid is associated with endoplasmic reticulum stress and impaired oocyte maturation in cumulus-oocyte complexes. Fertil Steril 2012; 97:1438-1443.
307. Chen M, Wu L, Wu F, Wittert GA, Norman RJ, Robker RL, Heilbronn LK. Impaired Glucose Metabolism in Response to High Fat Diet in Female Mice Conceived by In Vitro Fertilization (IVF) or Ovarian Stimulation Alone. PLOS ONE 2014; 9:e113155.
360. AIHW. Australian Burden of Disease Study: impact and causes of illness and death in Australia 2011. Australian Burden of Disease Study series no. 3. Cat. no. BOD 4. Canberra: AIHW. In: Australian Institute of Health and Welfare; 2016.

361. AIHW. Impact of overweight and obesity as a risk factor for chronic conditions. Australian Burden of Disease Study series no. 11. Cat. no. BOD 12. Canberra: AIHW. In: Australian Institute of Health and Welfare; 2017.
362. AIHW. Evidence for chronic disease risk factors. Web report. Canberra: AIHW. In; 2017.
363. Malik VS, Popkin BM, Bray GA, Despres JP, Willett WC, Hu FB. Sugar-sweetened beverages and risk of metabolic syndrome and type 2 diabetes: a meta-analysis. Diabetes Care 2010; 33:2477-2483.
364. Malik VS, Pan A, Willett WC, Hu FB. Sugar-sweetened beverages and weight gain in children and adults: a systematic review and meta-analysis. Am J Clin Nutr 2013; 98:1084-1102.
365. Trumbo PR, Rivers CR. Systematic review of the evidence for an association between sugar-sweetened beverage consumption and risk of obesity. Nutr Rev 2014; 72:566-574.
366. Saben JL, Asghar Z, Rhee JS, Drury A, Scheaffer S, Moley KH. Excess Maternal Fructose Consumption Increases Fetal Loss and Impairs Endometrial Decidualization in Mice. Endocrinology 2015; 157:956-968.
367. Asghar ZA, Thompson A, Chi M, Cusumano A, Scheaffer S, Al-Hammadi N, Saben JL, Moley KH. Maternal fructose drives placental uric acid production leading to adverse fetal outcomes. Sci Rep 2016; 6:25091.
368. Ko E-A, Kim H-R, Kim Y-B, Kim H-S, Lee S-H. Effect of High Fructose Corn Syrup (HFCS) Intake on the Female Reproductive Organs and Lipid Accumulation in Adult Rats. Development & Reproduction 2017; 21:151-156.
369. Ouchi N, Parker JL, Lugus JJ, Walsh K. Adipokines in inflammation and metabolic disease. Nature Reviews Immunology 2011; 11:85.
370. Skaznik-Wikiel ME, Swindle DC, Allshouse AA, Polotsky AJ, McManaman JL. High-Fat Diet Causes Subfertility and Compromised Ovarian Function Independent of Obesity in Mice. Biol Reprod 2016; 94:108.
371. Henstridge DC, Whitham M, Febbraio MA. Chaperoning to the metabolic party: The emerging therapeutic role of heat-shock proteins in obesity and type 2 diabetes. Molecular Metabolism 2014; 3:781-793.
372. Gupte AA, Bomhoff GL, Geiger PC. Age-related differences in skeletal muscle insulin signaling: the role of stress kinases and heat shock proteins. J Appl Physiol (1985) 2008; 105:839-848.
373. Tiss A, Khadir A, Abubaker J, Abu-Farha M, Al-Khairi I, Cherian P, John J, Kavalakatt S, Warsame S, Al-Ghimlas F, Elkum N, Behbehani K, et al. Immunohistochemical profiling of the heat shock response in obese non-diabetic subjects revealed impaired expression of heat shock proteins in the adipose tissue. Lipids Health Dis 2014; 13:106.
374. Abubaker J, Tiss A, Abu-Farha M, Al-Ghimlas F, Al-Khairi I, Baturcam E, Cherian P, Elkum N, Hammad M, John J, Kavalakatt S, Khadir A, et al. DNAJB3/HSP-40 cochaperone is downregulated in obese humans and is restored by physical exercise. PLoS One 2013; 8:e69217.
375. Kleinridders A, Lauritzen HP, Ussar S, Christensen JH, Mori MA, Bross P, Kahn CR. Leptin regulation of Hsp60 impacts hypothalamic insulin signaling. J Clin Invest 2013; 123:4667-4680.
376. Light HR, Tsanzi E, Gigliotti J, Morgan K, Tou JC. The Type of Caloric Sweetener Added to Water Influences Weight Gain, Fat Mass, and Reproduction in Growing Sprague-Dawley Female Rats. Experimental Biology and Medicine 2009; 234:651-661.

377. Byers SL, Wiles MV, Dunn SL, Taft RA. Mouse Estrous Cycle Identification Tool and Images. PLoS One 2012; 7:e35538.
378. R: A Language and Environment for Statistical Computing. In: Computing RFfS (ed.); R core team, 2014.
379. Levin BE, Hogan S, Sullivan AC. Initiation and perpetuation of obesity and obesity resistance in rats. Am J Physiol 1989; 256:R766-771.
380. Surwit RS, Feinglos MN, Rodin J, Sutherland A, Petro AE, Opara EC, Kuhn CM, Rebuffe-Scrive M. Differential effects of fat and sucrose on the development of obesity and diabetes in C57BL/6J and A/J mice. Metabolism 1995; 44:645-651.
381. Surwit RS, Kuhn CM, Cochrane C, McCubbin JA, Feinglos MN. Diet-induced type II diabetes in C57BL/6J mice. Diabetes 1988; 37:1163-1167.
382. Chu DT, Malinowska E, Jura M, Kozak LP. C57BL/6J mice as a polygenic developmental model of diet-induced obesity. Physiol Rep 2017; 5.
383. Allan MF, Eisen EJ, Pomp D. The M16 mouse: an outbred animal model of early onset polygenic obesity and diabesity. Obes Res 2004; 12:1397-1407.
384. Medrikova D, Jilkova ZM, Bardova K, Janovska P, Rossmeisl M, Kopecky J. Sex differences during the course of diet-induced obesity in mice: adipose tissue expandability and glycemic control. International Journal Of Obesity 2011; 36:262.
385. Winzell MS, Ahrén B. The High-Fat Diet–Fed Mouse. A Model for Studying Mechanisms and Treatment of Impaired Glucose Tolerance and Type 2 Diabetes 2004; 53:S215-S219.
386. Sato Mito N, Suzui M, Yoshino H, Kaburagi T, Sato K. Long term effects of high fat and sucrose diets on obesity and lymphocyte proliferation in mice. J Nutr Health Aging 2009; 13:602-606.
387. Caligioni C. Assessing Reproductive Status/Stages in Mice. Current protocols in neuroscience / editorial board, Jacqueline N. Crawley ... [et al.] 2009; APPENDIX:Appendix-4I.
388. Robker RL, Akison LK, Bennett BD, Thrupp PN, Chura LR, Russell DL, Lane M, Norman RJ. Obese women exhibit differences in ovarian metabolites, hormones, and gene expression compared with moderate-weight women. J Clin Endocrinol Metab 2009; 94:1533-1540.
389. Pantasri T, Wu LL, Hull ML, Sullivan TR, Barry M, Norman RJ, Robker RL. Distinct localisation of lipids in the ovarian follicular environment. Reproduction, Fertility and Development 2015; 27:593-601.
390. Tsan MF, Gao B. Cytokine function of heat shock proteins. Am J Physiol Cell Physiol 2004; 286:C739-744.
391. Kim AH, Khanna A, Aten RF, Olive DL, Behrman HR. Cytokine induction of heat shock protein in human granulosa-luteal cells. Mol Hum Reprod 1996; 2:549-554.
392. Kokura S, Adachi S, Manabe E, Mizushima K, Hattori T, Okuda T, Nakabe N, Handa O, Takagi T, Naito Y, Yoshida N, Yoshikawa T. Whole body hyperthermia improves obesity-induced insulin resistance in diabetic mice. Int J Hyperthermia 2007; 23:259-265.
393. Kurucz I, Morva A, Vaag A, Eriksson KF, Huang X, Groop L, Koranyi L. Decreased expression of heat shock protein 72 in skeletal muscle of patients with type 2 diabetes correlates with insulin resistance. Diabetes 2002; 51:1102-1109.

Chapter 5: Effects of curcumin supplementation on a mouse model of diet-induced female obesity.

5.1 Introduction

Obesity affects approximately half the women in Australia, many of whom are in their reproductive years. Being overweight or obese is associated with reproductive dysfunction in women, with some of the reproductive problems experienced including dysregulated menstrual cycles, longer time to conception, increased risk of miscarriage, and increased risk of gestational diabetes [91]. The fact that obese women undergoing autologous IVF cycles have a reduced chance of both clinical pregnancy and live birth [91, 394-397] indicates that obesity is at least in part affecting the ovary and its capacity to produce a high quality, developmental competent oocyte. Reports by several groups that show delayed development and defects in pre-implantation embryos from obese women undergoing IVF [398, 399], also suggest obesity has a direct effect on oocyte quality and therefore diminishes its developmental potential.

Several studies in both humans and animal models have found that obesity alters not only follicle morphology [357], but it can also impact intracellular organelles and their function. Our group have shown that oocytes from obese mothers have altered mitochondrial function and exhibit endoplasmic reticulum (ER) stress [97, 100, 202]. Obese mice fed a commercial 60% Kcal HF diet presented structural abnormalities in the mitochondria of both oocytes and cumulus cells, specifically, increased biogenesis, altered distribution, and dysregulated respiration and oxidative stress markers [98, 101, 102, 400].

There are not many treatment options for obese women suffering from infertility and subfertility. While the evidence indicates that even a 5-10% weight loss can improve pregnancy outcomes for these women, dietary interventions and lifestyle modifications have proven to be ineffective [401, 402] and are not suitable for women who want to conceive soon [403, 404]. The insulin-sensitizer drug Metformin has been shown to reduce testosterone levels and waist circumference in women with polycystic ovary syndrome (PCOS) but it had no effect on weight loss or menstrual frequency [405]. There is an interest in “natural” products that can help improve fertility [406, 407]. Certain medicinal plants and spices may help treat the effects of obesity and other metabolic disorders when incorporated into the diet. Yet none have been conclusively demonstrated to be effective.

In other tissues, obesity is associated with increased levels of ER stress such as in adipose and liver cells, compounds that act as chemical chaperones and relieve ER stress can also ameliorate insulin resistance and hyperglycemia in mouse models of obesity [105]. One of these compounds is the polyphenol curcumin, extracted from turmeric (*Curcuma longa*), a spice that is widely used worldwide. Curcumin has attracted a great deal of research attention due to its

anti-inflammatory properties (reviewed in Shehzad et al. 2003 [408]). Several studies have shown that consumption of curcumin as a supplement decreased inflammation markers in multiple models of disease, including obesity (reviewed in [228]). Administration of curcumin has been shown to reduce hepatic ER stress in a rat model of stress-associated hepatic dyslipidemia. Adult male rats were injected over 4 weeks with Carbon tetrachloride (CCl_4), a hepatotoxic that dysregulates mitochondrial respiratory function and increases the levels of hepatic triglycerides. Rats that were orally treated with curcumin at 200 mg/kg during the CCl_4 treatment, had lower levels of ROS accumulation and reduced gene expression for ER stress markers (Hspa5, Chop, p-eIF2α, p-Perk, p-Ire-1α, and spliced Xbp1). These changes were associated with improved liver function demonstrating that curcumin treatment promoted recovery from CCl_4-induced hepatic stress [409].

In addition to reducing ER stress, curcumin has been shown to induce the expression of HSP, such as HSPA1A (HSP70), in vitro [410] and in vivo [411], which we have shown are abundant in the ovarian somatic cells and oocyte. Curcumin induced HSPA1A protein levels were induced in cultured HeLa cells exposed in a dose-dependent and time-dependent manner, by inhibiting the activation of nuclear factor-kappaB (NFK-B) and stimulating HSF1 activation and translocation into the nucleus [410]. Similarly, curcumin treatment increased HSPA1A levels in a dose dependent manner in cortical neurons in a rat model of neuronal cell dysfunction and apoptosis [411].

These properties combined with the higher oral bioavailability of curcumin when administered in a lipidic environment and its relatively low toxicity makes this spice a desirable compound to use in high fat diet-based dietary interventions such as for the treatment of obesity and insulin resistance. I hypothesized that curcumin could be used for the treatment of reproductive dysfunctions found in obesity. Thus, the aim of this study was to analyze the impact of obesity on ovarian function and oocyte quality and developmental competence, and to test if diet supplementation with Curcumin C3 Complex can reverse these effects on female fertility.

5.2 Materials and Methods

5.2.1 Animals and dietary treatment with Curcumin 3 Complex.

C57BL6J female mice were purchased at 6 weeks of age from the Laboratory Animal Services at the University of Adelaide (SA, Australia). Mice were randomly assigned to one of two dietary treatments upon arrival: control diet (CD; N=17), or high fat diet (HFD; N=44) for 9

weeks. The diets were made in-house. Briefly, the CD contained 10% Kcal from fat (Appendix 6), while the HFD had 60% Kcal derived from saturated fat (Appendix 7). The mice were weighed fortnightly to monitor changes in body weight.

After 9 weeks, the HFD group was split into two treatment groups to investigate the ability of oral treatment with curcuminoids to influence ovarian function in obese females. Approximately half the mice continued receiving the HFD only (HFD; N=24); and the other half received a HFD that contained 3% w/w Curcumin C3 Complex (HFD+C3C; N=20; Appendix 8) for 3 weeks. The Curcumin C3 Complex was a standardized *Curcuma longa* extract containing 95% curcuminoids as the active ingredient (Sabinsa Australia Pty Ltd, NSW, Australia). Animals were weighed weekly to monitor changes in body weight (BW). Body weight gain was calculated using the formula: $BW\ gain = BW_{final} - BW_{initial}$. Additionally, food consumption in both HFD treatment groups was monitored by providing mice with a known quantity of food 3 time a week and weighing the amount that was left over.

Virgin C57BL6 male mice were purchased at 6 weeks of age from the Laboratory Animal Services at the University of Adelaide. Males were fed 10% fat rodent chow (i.e. breeder chow; Specialty Feeds, WA, Australia), then mated 4-7 days prior to experimental mating to test virility. Mice of proven fertility were then mated with the experimental females for in vivo production of embryos.

All mice were housed at The University of Adelaide Medical School Laboratory Animal Services and maintained on a 12h light: 12h dark cycle with their assigned rodent diet and water provided at libitum. All procedures were approved by the University of Adelaide Animal Ethics Committee (approval M-2013-086) and followed the Australian Code for the Care and Use of Animals for Scientific Purposes.

5.2.2 Ovarian stimulation and tissue collection.

To collect ovarian cells at precise times in the ovarian cycle, mice underwent hormonally-induced ovarian hyperstimulation. To stimulate follicular growth, female mice received an intraperitoneal (IP) injection of Pregnant Mare Serum Gonadotropin (PMSG; National Hormone and Peptide Program, Torrance, USA) in sterile 0.9% saline at a dose of 5 IU/12 g of body weight. At 48 hours post-PMSG, the mice received a second IP injection of human chorionic Gonadotropin (hCG; Pregnyl, Merck Sharp & Dohme Pty Ltd, Australia) in sterile 0.9% saline at a dose of 5 IU/12 g of body weight; to onset ovulation.

The mice then were humanely killed by cervical dislocation at either 16h or 46h post-hCG injection, the final body weight was recorded, and tissues (adipose tissue depots and liver) were collected by abdominal dissection, and individually weighed.

5.2.3 Quantification of ovulation; and analysis of oocyte quality and developmental competence

To study ovulatory function and oocyte quality, hormonally stimulated female mice were humanely killed at 16 hours post-hCG injection. The reproductive tracts were dissected and placed in HEPES-buffered GIBCO minimal essential medium (aMEM; Life Technologies, California, USA) at 37°C. Ovulated cumulus-oocyte complexes (COCs) were collected by tearing open the oviduct and transferred to clean HEPES-buffered α-MEM and counted. Oocytes were then isolated from the COCs using hyaluronidase (1000 I.U./mL; Life Technologies) in HEPES aMEM media with 1mg/ml polyvinylpyrrolidone (PVP; Sigma-Aldrich, Missouri, USA) at 37°C, to observe their morphology. Oocytes presenting a spherical shape, and uniformity and integrity of the cytoplasm were considered as morphologically normal and healthy. Presence of the first polar body was also recorded as a definitive assessment of metaphase II (MII), and as a marker of the normal state of maturation of the ovulated oocyte. In contrast, oocytes presenting an unshapely, damaged or fragmented cytoplasm were considered morphologically unhealthy. The oocytes were then further examined in subsequent biochemical assays.

To investigate oocyte developmental potential, in vivo-produced 2-cell embryos were collected and grown to the blastocyst stage in vitro. For this, female mice were caged with strain-compatible C57BL6 males after hCG-injection, then checked for the presence of vaginal plug (indicative of coitus) at 15-16h post-hCG injection. Those females that were positively identified as mated were then humanely killed at 46h post-hCG injection. The reproductive tracts were dissected and placed in HEPES aMEM at 37°C, and the upper section of the uterine horns, together with the ovaries and oviducts, was cut off. Embryos were flushed out of the oviduct using a 20G needle to inject 1mL of HEPES aMEM through the cervix and into the uterine horns. Embryos were then collected and assessed for first cleave (2-cell stage). Those at the 2-cell stage or greater, were cultured in vitro for a further 68 hours (to developmental day 5) in Research Vitro Cleave medium (10 zygotes/20 uL drop; COOK Medical, QLD, Australia) at 37°C in 6% CO_2, 21% O_2. On developmental day 5, embryos were photographed using Nikon SMZ1500 stereomicroscope (Nikon instruments Inc., Melville, NY). On-time development of the embryos was analysed by assessing their developmental stage every 24

hours. Blastocysts were then examined in subsequent biochemical assays. Embryos from each individual female were kept separate during the analyses.

5.2.4 Mitochondrial assays and imaging

Mitochondrial activity profile and function in oocytes was measured by staining the cells with 2 complementary mitochondrial dyes. First, oocytes were stained using Mitotracker Orange (MTO) CM-H2TMRos mitochondrial activity dye (Life Technologies) at 500 nM in HEPES aMEM medium for 15 min in the dark. At this point, Mitotracker Green (MTG) FM mitochondrial mass dye (Life Technologies) was added to the solution at a final concentration of 200 nM. Oocytes were then left to incubate for another 15 min, followed by washing in HEPES aMEM medium with 1mg/ml PVP. Oocytes were kept in HEPES aMEM at 37°C throughout the staining process and subsequent imaging.

A subset of oocytes was incubated in a control HEPES aMEM that did not contain any Mitotracker dyes to test that the detected fluorescence was not caused by autofluorescence of intracellular structures in the oocytes. Oocytes tested were negative for autofluorescence. Secondly, the Mitotracker dyes were replaced with vehicle (DMSO; Sigma-Aldrich) at the same concentration as in the stain diluent to test for cell-toxicity. Oocyte viability was not affected indicating the vehicle is negative for cell toxicity. Imaging was done by Leica TCS SP5 spectral scanning confocal microscope system (Leica Microsystems, Heerbrugg, Switzerland) at identical settings throughout.

Fluorescence intensity was determined using ImageJ Fiji software (National Institutes of Health, Maryland, USA), then quantified by corrected total cell fluorescence (CTCF), which determines the levels of fluorescence in a given region of a confocal section, using the formula: CTCF = Integrated Density – (Area of selected cell) x (Mean fluorescence of background readings). This quantification is based on the published method from Burgess et al [308, 412]. MTO:MTG ratio was analysed to find out the relative mitochondrial activity per mitochondrial mass.

To study embryonic mitochondrial activity, expanded blastocysts (where the blastocoel occupied approximately 90% of the embryo volume) were stained using Mitotracker Orange CM-H2TMRos mitochondrial activity dye (Life Technologies) at 500 nM in HEPES aMEM medium for 15 min in the dark. Blastocysts were then washed in HEPES aMEM medium with 1mg/ml PVP at 37°C for 5 min. Embryos were imaged using Leica TCS SP5 spectral scanning confocal microscope system. The relative fluorescence levels in blastocyst embryos were quantified by corrected total embryo fluorescence (CTEF) that measures fluorescence intensity

levels in a confocal section of blastomeres from late, expanded blastocysts, using the formula: CTEF = Integrated Density – (Area of embryonic section) x (Mean fluorescence of background readings); based on the CTCF method used for single cells.

5.2.5 Statistical analysis

All measures are reported as mean ± the standard error of the mean (SEM), unless indicated otherwise. Data were analysed using the statistics software GraphPad Prism 6 v008 for Windows (GraphPad software Inc., California, USA). Statistical significance was determined using appropriate statistical tests as indicated. P values of <0.05 were considered statistically significant.

5.3 Results

5.3.1 Curcumin C3 Complex supplementation prevents weight gain in High-Fat Diet females

Female mice were fed a HFD for 9 weeks, weighed fortnightly, then split into two treatment groups to receive HFD+C3C or HFD only for another 3 weeks. During this time their weight gain was monitored weekly. HFD-fed females were heavier when compared to the CD group by 9 weeks after the start of the diet but by week 12 their weights were more similar. Compared to the HFD group, the HFD+C3C females had a significantly lower growth trajectory between week 9 and week 12 (Figure 5.1.A). During this time, both the HFD and HFD+C3C groups had similar levels of food intake, indicating that the addition of the curcumin extract did not alter the palatability and consumption of the HFD chow (Figure 5.1.B). While there were no differences in the rates of body weight gain between the groups before the start of the C3C treatment (Figure 5.1.D), during the course of the 3-week intervention the C3C-supplemented HFD group gained less weight (0.14 ± 1.39 g) when compared to the other groups (HFD = 1.15 ± 0.94 g; CD = 1.45 ± 0.97 g; $P<0.0001$) (Figure 5.1.E). Thus, by the end of the experiment the C3C-supplemented HFD group had significantly lighter total body weights (22.15 ± 2.27 g) than both the HFD (23.21 ± 2.14 g) and the CD mice (23.33 ± 1.38 g; $P=0.004$) (Figure 5.1.C).

The HFD females had heavier abdominal fat pads (0.94 ± 0.51 g) on average than the CD females (0.44 ± 0.34 g; $P=0.006$). The C3C-supplemented HFD females had slightly reduced abdominal fat weight that was no longer different to that from CD females (0.78 ± 0.53 g) (Figure 5.1.F). Liver weights on average were not altered by HFD (0.95 ± 0.19 g) and these

were not different to the CD ones (1.08 ± 0.22 g). Surprisingly, livers from HFD+C3C females were lighter (0.87 ± 0.23 g; P=0.01) than those from CD females (Figure 5.1.G).

These results show that treatment with C3C for 3 weeks prevented the increase in body weight observed in HFD-fed females, and this is consistent with the lighter abdominal fat pad size and liver weight. Taken together, these results suggest C3C in the diet may have altered metabolism because it did not alter food consumption.

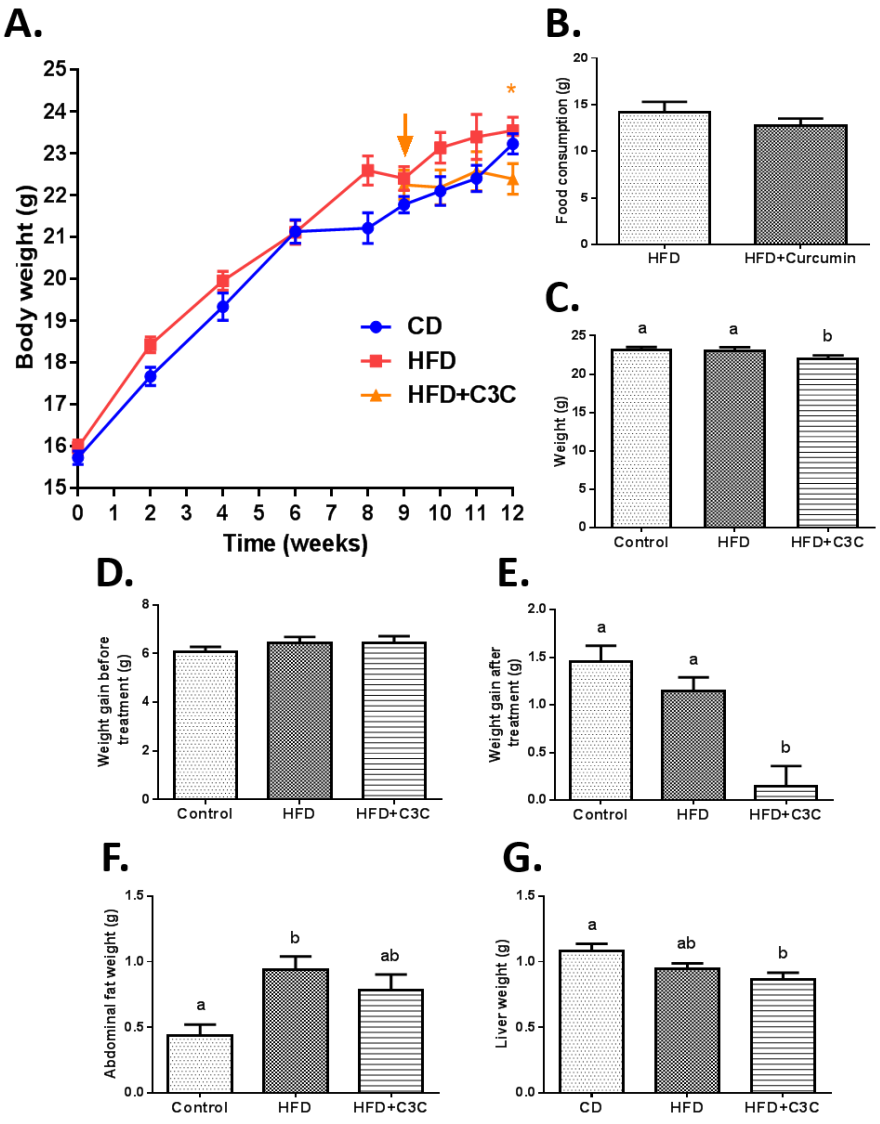

Figure 5.1 Effect of Curcumin C3 Complex-supplemented HFD diet on female body weight.

A. Body weight trajectory of female mice fed either Control (CD), High-fat (HFD), or C3C-supplemented High-fat diet (HFD+C3C). C3C-supplementation started on week 9 (arrow). The HFD+C3C group had a significantly different growth trajectory from HFD and CD * P=0.0003. **B.** Food consumption from week 9-12, after the start of C3C treatment. N=6 female mice per group. **C.** Total body weight at 16h post-hCG; a vs b P=0.004. **D.** Weight gain prior to C3C supplementation (weeks 0-9). **E.** Weight gain after C3C supplementation (weeks 9-12); a vs b P<0.0001. **F.** Abdominal Fat weight; a vs b P=0.006. **G.** Liver weight; a vs b P=0.01. Results are shown as mean ± SEM. N=17 (CD), 24 (HFD), 20 (HFD+C3C). Statistical analysis was Two-Way repeated measures ANOVA (A), Student's T-test (B) or One-Way ANOVA (C-G), and Tukey's Multiple Comparison Test.

5.3.2 Curcumin C3 Complex treatment alters the mitochondrial profile in both oocytes and embryos

After 12 weeks of dietary treatment, a subset of female mice underwent ovarian hyperstimulation using gonadotrophins, and their ovulated COC were collected and analysed. HFD females had slightly fewer oocytes collected from the oviduct at 16h post-hCG than the CD females. Surprisingly, the HFD+C3C females had the lowest number of ovulated oocytes (Figure 5.2.A).

Morphological assessment of the oocytes collected showed that all the dietary groups had similar numbers of morphologically normal oocytes, although HFD+C3C females had the lowest number of healthy-appearing oocytes. (Figure 5.2.B). Meanwhile, assessment of meiotic status of the oocytes showed that both HFD and HFD+C3C had slightly fewer oocytes that had reached MII stage. (Figure 5.2.C).

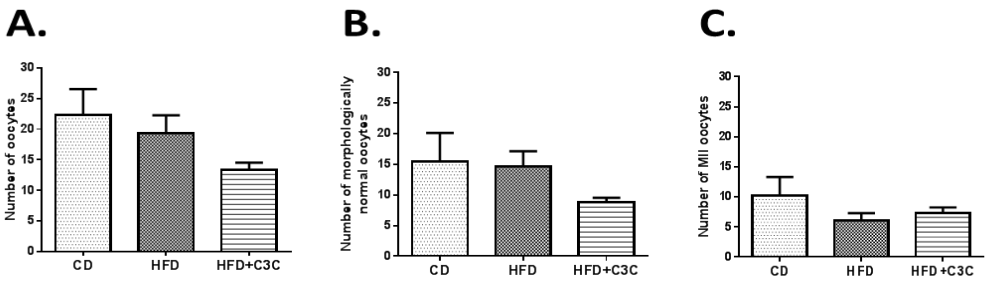

Figure 5.2 Effect of Curcumin C3 Complex supplemented HFD diet on oocyte number and morphology.

A. Number of ovulated oocytes collected from the oviducts. **B.** Number of morphologically healthy ovulated oocytes. **C.** Number of oocytes at MII. Results are mean ± SEM. N=6 (CD), N=12 (HFD), N=12 (HFD+C3C). Statistical analysis was One-Way ANOVA, and Tukey's Multiple Comparison Test.

Ovulated oocytes were isolated from their surrounding cumulus cells and double-stained using two mitochondria-specific dyes to analyse their mitochondrial profile. Mitotracker Orange (MTO) stain in oocytes showed high levels of fluorescence intensity concentrated in the area around the spindle as expected, as shown in the representative images (Figure 5.3.A). Corrected Total Cell Fluorescence (CTCF) analysis of confocal images showed that those from HFD (551.1 ± 294.8 AU) and HFD+C3C (628.8 ± 167 AU) females had higher MTO fluorescence intensity, with HFD+C3C oocytes presenting 1.5 times significantly increased intensity when compared to the controls (386.3 ± 156.2 AU; P=0.01) (Figure 5.3.B).

Mitotracker Green (MTG) stain in oocytes also showed higher fluorescence intensity in the spindle area, but had widespread fluorescence across the cytoplasm as well, as shown in the representative images (Figure 5.3.C). CTCF analysis of MTG fluorescence showed that those from the HFD (349.5 ± 365.9 AU) and HFD+C3C (591.9 ± 412.2 AU) females had higher fluorescence intensity than those of CD females, with the HFD+C3C oocytes presenting approximately 3 times significantly increased intensity when compared to CD oocytes (203.8 ± 241.5 AU; P=0.006) (Figure 5.3.D).

Analysis of the ratio of Mitotracker Orange to Green (MTO:MTG) in double-stained oocytes indicated the HFD and HFD+C3C groups had a different MTO:MTG ratio from the CD oocytes, as shown in the representative merged images. The merged channel images also suggested that the HFD+C3C oocytes had more “clumped” mitochondria than the other groups (Figure 5.3.E). Oocytes from the HFD+C3C had the lowest ratio (1.4 ± 1.1 AU) which was significantly reduced when compared to the CD group (3.5 ± 2.3 AU; P=0.0006), but not the HFD group (2.02 ± 1.3 AU) (Figure 5.3.F).

In summary, these results show that even in response to gonadotropin stimulation the HFD+C3C females tended to ovulate slightly less oocytes than the other dietary groups, suggesting the C3C treatment had an effect on ovarian function. Curcumin treatment did not improve the numbers of MII oocytes in HFD females. Isolated MII oocytes from HFD+C3C females presented higher fluorescence intensity for both mitochondrial activity and mass, while also showing a more “clumped” appearance. Thus, although oocyte maturation was not overtly affected, both HFD and HFD+C3C appear to cause subtle changes to oocyte mitochondria.

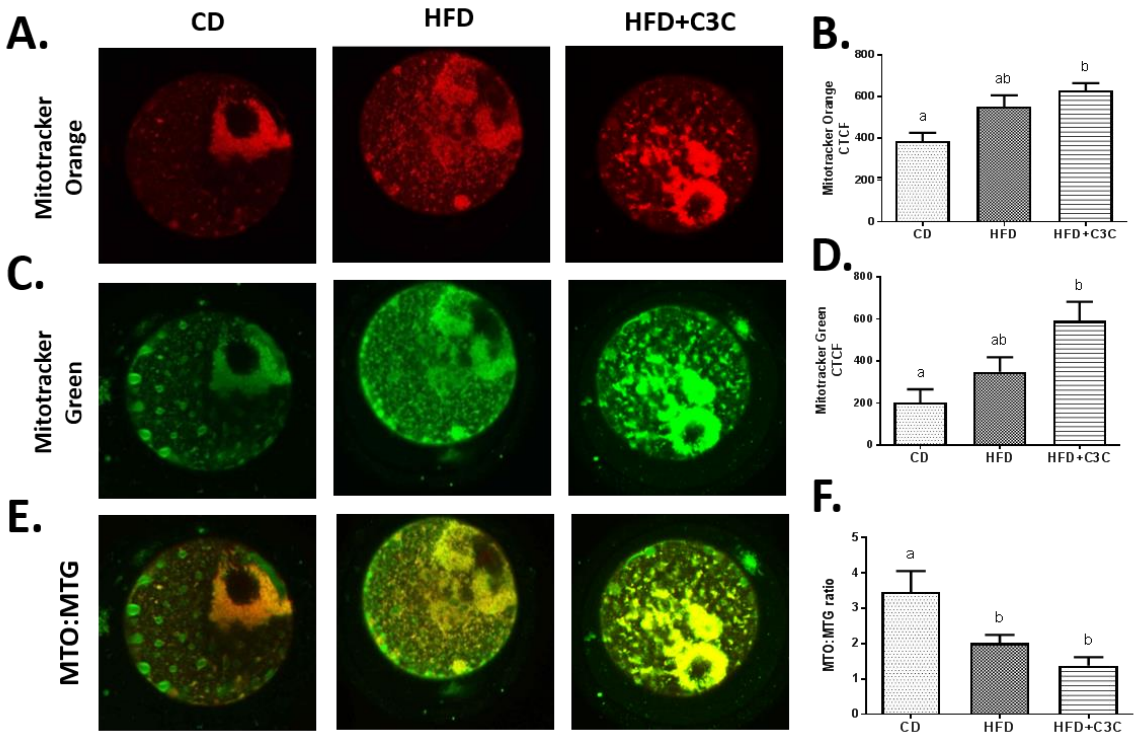

Figure 5.3 . Curcumin C3 Complex treatment alters mitochondrial activity profile of ovulated oocytes.

Representative images of ovulated oocytes stained with **(A)** MTO mitochondrial activity dye, **(C)** MTG mitochondrial mass dye, and **(E)** merged images (MTO:MTG). **B.** Corrected Total Cell Fluorescence (CTCF) analysis of MTO-stained oocytes; a vs b P=0.01. **D.** CTCF analysis of MTG-stained oocytes; a vs b P=0.006. **F.** MTO:MTG CTCF ratio; a vs b P=0.0006. Results are mean ± SEM. N=15 (CD), N=28 (HFD), N=21 (HFD+C3C) oocytes from at least 3 female mice. Statistical analysis was One-Way ANOVA, and Tukey's Multiple Comparison Test (B, D, F).

Following mating and collection of oviducts 24h later, HFD+C3C females yielded a similar number of embryos at the 2-cell stage and over (i.e. 3-cell and/or 4-cell) to that of the other groups (Figure 5.4.A). Similarly, the percentage of 2-cells from total embryos collected showed that there were no differences between the groups (Figure 5.4.C).

Embryos were then cultured in vitro for another 2.5 days, to the equivalent of dpc 5, to assess embryonic development to blastocyst stage. There were similar numbers of surviving blastocysts in each of the three dietary groups (Figure 5.4.B) and no differences in the percentage of blastocysts derived from 2-cells (Figure 5.4.D). Interestingly, blastocysts from the HFD+C3C and HFD groups had significantly reduced hatching rates of 26.1% and 20.3% respectively, while blastocysts derived from CD females had a hatching rate of 80.5% (P=0.0002) (Figure 5.4.E).

Representative images of MTO stained blastocysts indicated the embryos derived from HFD+C3C females had lower fluorescence when compared to the other groups (Figure 5.5.A). Similarly, CTCF analysis showed the HFD+C3C blastocysts had fluorescence intensity decreased by half (171 ± 111 AU) when compared to the CD embryos (330.4 ± 281.7 AU; P=0.02) (Figure 5.5.B).

These observations show that while HFD did not affect cleavage nor blastocysts rates of in vivo fertilised oocytes, it reduced the percentage of these blastocysts that hatched from the zona pellucida on time by day 5 dpc. Dietary treatment with Curcumin C3 Complex did not restore the hatching rates to control levels. Interestingly, blastocysts derived from HFD+C3C females presented decrease fluorescence intensity for MTO stain, indicating the embryos had lower levels of mitochondrial activity.

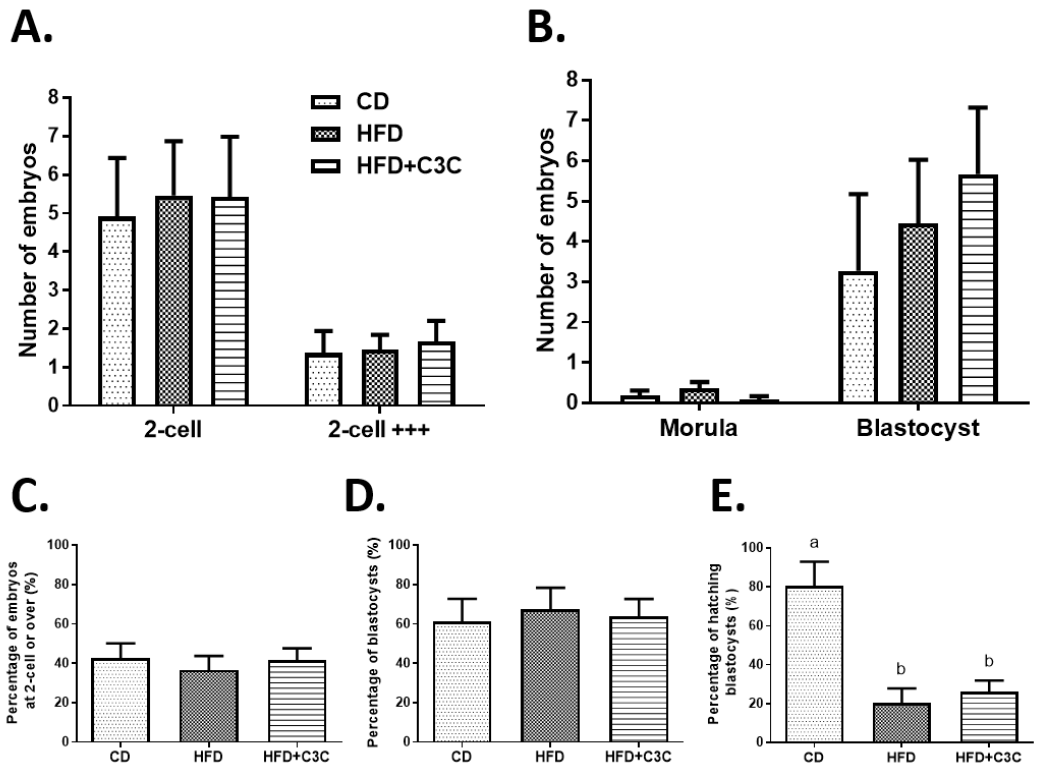

Figure 5.4. Effect of C3C supplementation of high fat diet on oocyte developmental competence.

A. Number of embryos at different developmental stages collected from the oviduct on day post-coital 2 (dpc 2). **B.** Number of embryos at different developmental stages assessed following 2.5 days of in-vitro culture (equivalent of dpc 5). **C.** Percentage of 2-cell embryos from total embryos collected on dpc 2. **D.** Percentage of blastocysts developed from 2-cells on day 2.5 of in-vitro culture (equivalent of dpc 5). **E.** Percentage of blastocysts hatching from the zona pellucida; a vs b P=0.0002. Results are mean ± SEM. N= 17 (CD), N=16 (HFD), N=16 (HFD+C3C) female mice per group. Statistical analysis was either Two-Way (A) or One-Way ANOVA (B-D), and Tukey's Multiple Comparison Test.

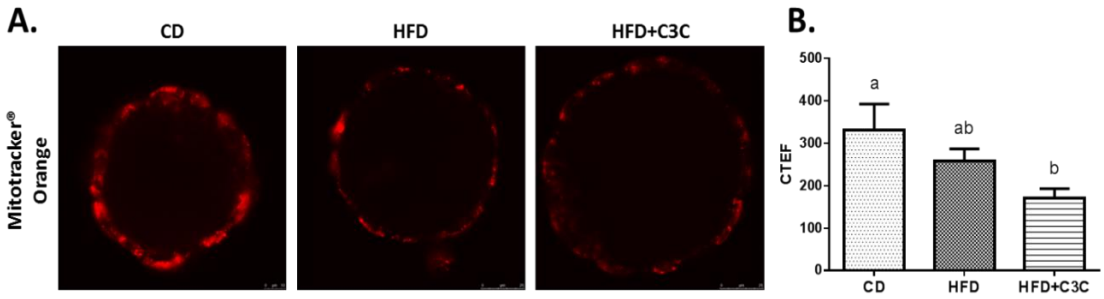

Figure 5.5 C3C supplementation reduces mitochondrial activity of blastocysts.

A. Representative images of blastocysts derived from 2 cell embryos of female mice fed CD, HFD or HFD+C3C stained with MTO mitochondrial activity dye. **B.** Corrected Total Embryo Fluorescence (CTEF) analysis of MTO stained blastocysts; a vs b P=0.02. Results are mean ± SEM. N=21 (CD), N=22 (HFD), N=26 (HFD+C3C) blastocysts from at least 3 female mice per group. Statistical analysis was One-Way ANOVA, and Tukey's Multiple Comparison Test (B).

5.4 Discussion

These results show that a three-week dietary intervention with Curcumin C3 Complex treatment reduces diet-induced obesity in female mice, preventing body weight and adipose tissue weight gain independent of food intake. Animals fed a high fat diet did not show overt signs of abnormal ovarian function in this study, while supplementation with curcuminoids slightly reduced ovulation and the number of morphologically healthy oocytes. At the same time, normal MII oocytes from the curcumin-treated group presented more abundant mitochondria that was also more active, as shown by the higher fluorescence intensity for both mitochondrial mass and mitochondrial activity dyes, and the ratio of mitochondrial activity to mitochondrial mass being closer to one. Similarly, high fat diet females presented normal rates of preimplantation embryo development indicating that oocyte developmental competence was not affected, although more of these blastocysts failed to hatch on time. Curcumin treatment did not affect embryo hatching rates, but it was associated with reduced blastocyst mitochondrial activity.

Female mice fed a diet rich in saturated fats for 9 weeks presented increased body weight when compared to those fed normal chow. Supplementation of the obesogenic diet with 3% Curcumin C3 Complex extract for three weeks prevented body weight gain in the high fat diet group, resulting in a small but significant decrease in body weight. While some studies have reported similar findings [105, 222, 225, 413], others have found no effect of curcumin on weight loss [414]. However, in this later study [414] considerably lower dosages of curcumin were added to the diet (0.5% or 1%) compared to the others. In this study, the curcumin-treated HFD females did not gain weight despite maintaining similar levels of food intake to the untreated HFD group, suggesting that the curcumin treatment, rather than hypophagia, protected against diet-induced obesity.

Similar to the findings presented here, a previous study by Weisberg et al [105] found that curcumin intervention given to obese mice was associated with decreased body weight and fat content in both genetic (ob/ob) and high fat diet-induced mouse models of obesity, the latter similar to the one used for this study. Moreover, they showed that curcumin treatment ameliorated the obesity phenotype. Specifically, curcumin-treated obese mice had improved glycemic status, increased circulating adiponectin levels, and reduced hepatic NF-kB expression and macrophage infiltration in perigonadal fat, indicating the beneficial effect of curcumin is due to its anti-inflammatory properties.

Although oral administration of curcuminoids has been shown to have beneficial effects and mitigate or even reverse obesity phenotypes, its effect on ovarian function and early embryonic development has not been studied. Even though neither of the diets had a significant impact on ovulation and oocyte morphology, the curcumin treated group had the lowest numbers for both ovulated COC and morphologically healthy oocytes (respectively 40.29% and 43.35% decrease, when compared to controls), therefore the possibility that the effects of curcumin treatment could have secondary effects on reproduction should be explored further. The majority of the studies using curcumin to treat obesity in rodents have only used males, and it was not determined whether the curcuminoid treatment had any effect on their reproductive function. In this study, fewer oocytes had reached meiotic maturation in both the untreated HFD and the C3C-treated HFD groups than in the control females (40.12% and 27.83% fewer ovulated MII oocytes, respectively). However, in this particular cohort of mice, for unknown reasons, ovulation and oocyte maturation were not as significantly affected as in previous cohorts. Thus, it is not possible to conclude whether curcumin treatment can restore oocyte maturation to control levels.

The mitochondrial activity profile was altered in oocytes from females fed a high fat diet, and more so in the curcumin-treated group. Mitochondrial activity and mass were respectively 1.6 and 2.9 higher in HFD+C3C oocytes than in those from control females, with the HFD group presenting intermediate levels, suggesting that curcumin increased the effect of HFD. However, both HFD and HFD+C3C oocytes presented MTO:MTG ratios closer to 1, indicating that they had less active mitochondria per mitochondrial mass unit than those from the CD group. It has been previously reported that obesity impacts mitochondrial profile in mature oocytes [100], and these results suggest that curcumin treatment exacerbates this dysfunction.

Dietary treatment did not seem to impact oocyte developmental competence, as suggested by the similar outcomes on embryo development between the groups. However, both obesogenic diet groups had less blastocysts hatching out of the zona pellucida. Moreover, the blastocysts from the HFD+C3C group also had significantly lower levels of mitochondrial activity in their outer cell layer, with the HFD embryos presenting an intermediate level. The outer cells of the embryo that form the trophectoderm (TE) have more mitochondria, and consume more oxygen and nutrients, unlike the inner cell mass (ICM), therefore it is expected that they show increased mitochondrial activity [415]. The reduced mitochondrial activity in embryos from curcumin-treated females suggests that curcumin may increase the negative impact of HFD on embryonic metabolism.

In conclusion, this preliminary study could not definitively determine if curcumin treatment improved oocyte quality and developmental potential in female mice fed a saturated fat-rich diet. However, the results indicate that the dietary intervention prevented further development of obesity in response to an obesogenic diet. The subtle changes that were observed in oocyte mitochondrial activity suggest that exposure to the curcumin extract influences oocyte developmental competence and deserves further, and more detailed investigation in larger cohorts of animals.

5.5 References

91. Jungheim ES, Moley KH. Current knowledge of obesity's effects in the pre- and periconceptional periods and avenues for future research. Am J Obstet Gynecol 2010; 203:525-530.
97. Wu LL, Dunning KR, Yang X, Russell DL, Lane M, Norman RJ, Robker RL. High-fat diet causes lipotoxicity responses in cumulus-oocyte complexes and decreased fertilization rates. Endocrinology 2010; 151:5438-5445.
98. Luzzo KM, Wang Q, Purcell SH, Chi M, Jimenez PT, Grindler N, Schedl T, Moley KH. High Fat Diet Induced Developmental Defects in the Mouse: Oocyte Meiotic Aneuploidy and Fetal Growth Retardation/Brain Defects. PLoS One 2012; 7:e49217.
100. Wu LL, Russell DL, Wong SL, Chen M, Tsai TS, St John JC, Norman RJ, Febbraio MA, Carroll J, Robker RL. Mitochondrial dysfunction in oocytes of obese mothers: transmission to offspring and reversal by pharmacological endoplasmic reticulum stress inhibitors. Development 2015; 142:681-691.
101. Boots CE, Boudoures A, Zhang W, Drury A, Moley KH. Obesity-induced oocyte mitochondrial defects are partially prevented and rescued by supplementation with co-enzyme Q10 in a mouse model. Hum Reprod 2016; 31:2090-2097.
102. Boudoures AL, Chi M, Thompson A, Zhang W, Moley KH. The Effects of Voluntary Exercise on Oocyte Quality in a Diet-Induced Obese Murine Model. Reproduction 2016; 151:261-270.
105. Weisberg SP, Leibel R, Tortoriello DV. Dietary curcumin significantly improves obesity-associated inflammation and diabetes in mouse models of diabesity. Endocrinology 2008; 149:3549-3558.
202. Wu LL, Russell DL, Norman RJ, Robker RL. Endoplasmic reticulum (ER) stress in cumulus-oocyte complexes impairs pentraxin-3 secretion, mitochondrial membrane potential (DeltaPsi m), and embryo development. Mol Endocrinol 2012; 26:562-573.
222. Ejaz A, Wu D, Kwan P, Meydani M. Curcumin inhibits adipogenesis in 3T3-L1 adipocytes and angiogenesis and obesity in C57/BL mice. J Nutr 2009; 139:919-925.
225. Jang EM, Choi MS, Jung UJ, Kim MJ, Kim HJ, Jeon SM, Shin SK, Seong CN, Lee MK. Beneficial effects of curcumin on hyperlipidemia and insulin resistance in high-fat-fed hamsters. Metabolism 2008; 57:1576-1583.
228. Alappat L, Awad AB. Curcumin and obesity: evidence and mechanisms. Nutr Rev 2010; 68:729-738.
308. Burgess A, Vigneron S, Brioudes E, Labbe JC, Lorca T, Castro A. Loss of human Greatwall results in G2 arrest and multiple mitotic defects due to deregulation of the cyclin B-Cdc2/PP2A balance. Proc Natl Acad Sci U S A 2010; 107:12564-12569.

357. Jungheim ES, Macones GA, Odem RR, Patterson BW, Lanzendorf SE, Ratts VS, Moley KH. Associations between free fatty acids, cumulus oocyte complex morphology and ovarian function during in vitro fertilization. Fertility and sterility 2011; 95:1970-1974.
394. Kawwass JF, Kulkarni AD, Hipp HS, Crawford S, Kissin DM, Jamieson DJ. Extremities of body mass index and their association with pregnancy outcomes in women undergoing in vitro fertilization in the United States. Fertil Steril 2016; 106:1742-1750.
395. Gesink Law DC, Maclehose RF, Longnecker MP. Obesity and time to pregnancy. Hum Reprod 2007; 22:414-420.
396. van der Steeg JW, Steures P, Eijkemans MJ, Habbema JD, Hompes PG, Burggraaff JM, Oosterhuis GJ, Bossuyt PM, van der Veen F, Mol BW. Obesity affects spontaneous pregnancy chances in subfertile, ovulatory women. Hum Reprod 2008; 23:324-328.
397. Luke B, Brown MB, Stern JE, Missmer SA, Fujimoto VY, Leach R. Female obesity adversely affects assisted reproductive technology (ART) pregnancy and live birth rates. Hum Reprod 2011; 26:245-252.
398. Pandey S, Pandey S, Maheshwari A, Bhattacharya S. The impact of female obesity on the outcome of fertility treatment. J Hum Reprod Sci 2010; 3:62-67.
399. DeUgarte DA, DeUgarte CM, Sahakian V. Surrogate obesity negatively impacts pregnancy rates in third-party reproduction. Fertil Steril 2010; 93:1008-1010.
400. Igosheva N, Abramov AY, Poston L, Eckert JJ, Fleming TP, Duchen MR, McConnell J. Maternal Diet-Induced Obesity Alters Mitochondrial Activity and Redox Status in Mouse Oocytes and Zygotes. PLoS One 2010; 5:e10074.
401. Wadden TA. Treatment of obesity by moderate and severe caloric restriction. Results of clinical research trials. Ann Intern Med 1993; 119:688-693.
402. Moran LJ, Noakes M, Clifton PM, Tomlinson L, Galletly C, Norman RJ. Dietary composition in restoring reproductive and metabolic physiology in overweight women with polycystic ovary syndrome. J Clin Endocrinol Metab 2003; 88:812-819.
403. Palomba S, Giallauria F, Falbo A, Russo T, Oppedisano R, Tolino A, Colao A, Vigorito C, Zullo F, Orio F. Structured exercise training programme versus hypocaloric hyperproteic diet in obese polycystic ovary syndrome patients with anovulatory infertility: a 24-week pilot study. Hum Reprod 2008; 23:642-650.
404. Tsagareli V, Noakes M, Norman RJ. Effect of a very-low-calorie diet on in vitro fertilization outcomes. Fertil Steril 2006; 86:227-229.
405. Tang T, Glanville J, Hayden CJ, White D, Barth JH, Balen AH. Combined lifestyle modification and metformin in obese patients with polycystic ovary syndrome. A randomized, placebo-controlled, double-blind multicentre study. Hum Reprod 2006; 21:80-89.
406. Kiani K, Sadati Lamardi SN, Laschke MW, Malekafzali Ardakani H, Movahedin M, Ostad SN, Aflatoonian R, Moini A. Medicinal plants and natural compounds in the treatment of experimental endometriosis: A systematic review protocol. Evidence-based Preclinical Medicine 2016; 3:1-6.
407. Tsobou R, Mapongmetsem PM, Van Damme P. Medicinal Plants Used for Treating Reproductive Health Care Problems in Cameroon, Central Africa(1). Economic Botany 2016; 70:145-159.
408. Shehzad A, Rehman G, Lee YS. Curcumin in inflammatory diseases. Biofactors 2013; 39:69-77.
409. Lee HY, Kim SW, Lee GH, Choi MK, Chung HW, Lee YC, Kim HR, Kwon HJ, Chae HJ. Curcumin and Curcuma longa L. extract ameliorate lipid accumulation through

the regulation of the endoplasmic reticulum redox and ER stress. Sci Rep 2017; 7:6513.
410. Dunsmore KE, Chen PG, Wong HR. Curcumin, a medicinal herbal compound capable of inducing the heat shock response. Crit Care Med 2001; 29:2199-2204.
411. Xia C, Cai Y, Li S, Yang J, Xiao G. Curcumin Increases HSP70 Expression in Primary Rat Cortical Neuronal Apoptosis Induced by gp120 V3 Loop Peptide. Neurochem Res 2015; 40:1996-2005.
412. McCloy RA, Rogers S, Caldon CE, Lorca T, Castro A, Burgess A. Partial inhibition of Cdk1 in G2 phase overrides the SAC and decouples mitotic events. Cell Cycle 2014; 13:1400-1412.
413. Soetikno V, Sari FR, Veeraveedu PT, Thandavarayan RA, Harima M, Sukumaran V, Lakshmanan AP, Suzuki K, Kawachi H, Watanabe K. Curcumin ameliorates macrophage infiltration by inhibiting NF-kappaB activation and proinflammatory cytokines in streptozotocin induced-diabetic nephropathy. Nutr Metab (Lond) 2011; 8:35.
414. Martinez-Morua A, Soto-Urquieta MG, Franco-Robles E, Zuniga-Trujillo I, Campos-Cervantes A, Perez-Vazquez V, Ramirez-Emiliano J. Curcumin decreases oxidative stress in mitochondria isolated from liver and kidneys of high-fat diet-induced obese mice. J Asian Nat Prod Res 2013; 15:905-915.
415. Hewitson LC, Leese HJ. Energy metabolism of the trophectoderm and inner cell mass of the mouse blastocyst. J Exp Zool 1993; 267:337-343.

Chapter 6: Effects of Tex-OE supplementation on female fertility in a mouse model of diet-induced obesity

6.1 Introduction

Approximately half of the women in Australia today are overweight or obese, with many young women in their reproductive years being affected. Obesity is associated with dysregulated menstrual cycles, longer time to conception, increased risk of miscarriage, and increased risk of gestational diabetes amongst other complications [91]. Moreover, embryos from obese women undergoing autologous IVF cycles had delayed and impaired pre-implantation development, as well as lower pregnancy and live birth rates [91, 394, 395, 397]. These reports suggest obesity has a direct effect on oocyte quality, diminishing its developmental potential.

Several studies in both humans and animal models have found that obesity alters ovarian follicles and markers of oocyte health; such as reduced cumulus cell expansion and oocyte maturation rates [357], increased Endoplasmic Reticulum (ER) stress in cumulus oocyte complexes (COC) [97] and oocyte mitochondrial dysfunction [98, 100-102, 400].

There is a relationship between obesity and the over-activation of stress pathways at the cellular level. Obesity has been shown to increase the expression of HSPA1A in skeletal muscle (Reviewed in Henstridge et al. 2014 [371]). Other HSP are also dysregulated by metabolic syndrome. Insulin-resistance reduced the expression of HSPB1 (HSP25) in aged rats [372]. Obese non-diabetic patients have increased levels of HSPA5 (GRP94), HSPD1 (HSP60), HSP90AA1 (HSP90) in adipose tissue [373] while DNAJB3 (HSP40) is decreased [374]. Downregulation of HSPD1 in the hypothalamus of mice in diabetes model caused hypothalamic insulin resistance and mitochondrial dysfunction [375]. Obesity also induces increased levels of ER stress in adipose and liver cells. More critically, obesity has also been shown to induce the HSR in the mouse ovary, increasing the expression of Hspa1a/b and Hspa5 in granulosa-luteal cells and ovulated COC [97, 100]. The hydroximic acid derivative BGP-15 is a known HSP inducer [416] and it has been shown to induce HSP expression in ovarian cells and to restore ovulation and oocyte quality in obese mice [100]. Thus, modulation of HSP may be a potential therapeutic for restoring fertility in the context of obesogenic cellular stress in the ovary.

In recent years, there is a growing interest in "natural" products that can help improve fertility [406, 407]. Studies have suggested that certain medicinal plants and spices may help treat the effects of obesity and other metabolic disorders when incorporated into the diet. Yet none have been identified that are effective. We have previously discussed how compounds that act as chemical chaperones and relieve ER stress, such as curcumin, can also ameliorate insulin resistance and hyperglycemia in mouse models of obesity [105]. We tested curcumin as

potential therapeutic to improve obesity-induced ovarian dysfunction and saw that some but not all measures were affected.

Prickly pear fruit (*Opuntia spp*.) is a member of the *Cactaceae* family, which are widely used in traditional medicine remedies [417, 418], and have more recently been shown to have high anti-oxidant activity and anti-inflammatory properties [419]. Tex-OE is an extract derived from the prickly pear cactus *Opuntia ficus indica*, which has been shown to be a chaperone-stimulating compound and to decrease oxidative injury [240, 420, 421]. It is registered as a traditional food stuff in the European Union and is widely used in human and animal food supplementation [422].

Opuntia extracts are potential therapeutic agents for the treatment of oxidative stress and inflammation-related conditions, such as obesity. The aim of this study was to test if oral treatment with the *Opuntia* extract Tex-OE can improve oocyte quality and developmental potential in a mouse model of diet-induced obesity.

6.2 Materials and Methods

6.2.1 Animals

To induce the effects of obesogenic diets on ovarian function, C57BL6J female mice (6 weeks old) were randomly assigned either control (CD, 10% Kcal from fat), or high fat (HFD, 60% Kcal from fat) dietary treatment upon arrival. The diets were made in house, and the complete list of ingredients can be seen in Appendix 6 (CD), and 7 (HFD). After a short term (8 weeks) or long term (38 weeks) HFD, half the mice in the obesogenic diet group received oral treatment with Tex-OE for a further 2 weeks, then we collected ovarian cells and embryos at different stages of development for further analysis of oocyte quality and developmental competence, as described below. This Tex-OE treatment experiment was conducted in parallel with additional long term cohorts of experimental mice, therefore results for CD and HFD groups are same as described in Chapter 4.

Tex-OE is a patented extract from the epicarp of the prickly pear fruit *Opuntia ficus indica* (ICP-Texinfine Laboratories, Malta). The product was obtained from Dr. Charles Saliba (ICP-Ltd, Malta) in a 100% ethanol solution, and kept at room temperature until use. To investigate the ability of oral treatment with the nutraceutical Tex-OE to influence ovarian function in obese females, approximately half the HFD mice received treatment with 2 ul/mL Tex-OE in the drinking water (HFD+Tex-OE) for two weeks. A cellulose-free HFD (60% Kcal derived

from fat) was implemented to use during the dietary intervention with Tex-OE, following the manufacturer's instructions (Appendix 9).

Virgin C57BL6J male mice (6 weeks) were purchased for the in vivo production of embryos. Males were fed the control diet (10% fat rodent chow (i.e. breeder chow; Specialty Feeds, WA, Australia)) and were time-mated 4-7 days prior to the mating experiment to ensure virility.

All mice were purchased from the Animal Resources Centre (Canning Vale, Australia); and housed at the Laboratory Animal Services (University of Adelaide, Australia). Animals were maintained on a 12h light: 12h dark cycle with their assigned rodent diet and water provided at libitum. All procedures were approved by the University of Adelaide Animal Ethics Committee (approval M-2013-086) and followed the Australian Code for the Care and Use of Animals for Scientific Purposes.

6.2.2 Ovarian stimulation and tissue collection

To obtain ovarian cells at precise times in the ovarian cycle, mice underwent hormonally-induced ovarian hyperstimulation. To stimulate follicular growth, female mice received an intraperitoneal (IP) injection of Pregnant Mare Serum Gonadotropin (PMSG; National Hormone and Peptide Program, Torrence, USA) in sterile 0.9% saline at a dose of 5 IU/12 g of body weight. To induce ovulation, some of the mice received a second IP injection of human chorionic Gonadotropin at 48 hours post-PMSG (hCG; Pregnyl, Merck Sharp & Dohme Pty Ltd, Australia) in sterile 0.9% saline at a dose of 5 IU/12 g of body weight.

The mice then were humanely killed by cervical dislocation at the appropriate times. Additionally, the final body weight was recorded, and tissues (adipose tissue depots and liver) were individually collected by abdominal dissection and weighed.

6.2.3 COC and granulosa cell collection and gene expression analysis by RT-qPCR

To examine the effect of obesity and its treatment with Tex-OE Opuntia extract on stress responses during folliculogenesis, mice were humanely killed at 44h post-PMSG injection. The reproductive tracts were dissected and placed in HEPES-buffered GIBCO minimal essential medium (aMEM, Invitrogen, Carlsbad, CA) at 37°C. Granulosa cells (GC) and unovulated cumulus-oocyte complexes (COC) were collected by puncturing unovulated Graafian follicles visible in the ovary using 30G needles. COC were separately transferred to clean HEPES-

buffered α-MEM and counted. Only intact COC were collected and transferred in 5 ul volume of sterile PBS with 1mg/ml polyvinylpyrrolidone (PVP, Sigma-Aldrich, Missouri, USA), and into an RNase-free tube (Axygen, Corning Life Sciences, USA). The remaining GC were then pipetted into an RNAse-free tube, centrifuged at 1200 rpm at 4°C for 3 min and the supernatant removed. All samples were then snap-frozen in liquid nitrogen and stored at -80°C until use. Gene expression in GC was analysed separately for each individual mouse (N_{GC} = 7-12 animals per dietary treatment). Gene expression in COC was analysed by pooling samples from individual mice with similar body weights together in order to reach a minimum of 9-10 COC per group (N_{COC} = 5 groups per dietary treatment).

Total RNA was extracted from frozen cell pellets using Trizol (Thermo Fisher Scientific, Massachusetts, USA) following the manufacturer's instructions. RNA samples were treated with DNAFREE DNAse (Life Technologies, California, USA) to remove any residual DNA. After this, 1 ul was taken from each sample to quantify RNA and DNA content by measuring the ratio of absorbance between 260 and 280 nm using a spectrophotometer (Thermo Fisher Nanodrop spectrophotometer, Thermo Fisher Scientific). The manufacturer's instructions indicate that a ratio of ~1.8 is considered pure for DNA whereas a ratio of ~2.0 is considered pure for RNA. A given sample was considered free of DNA contamination when they had a 260/280 value of 1.98 or more. RNA concentration and purity were determined by Nanodrop (Thermo Fisher Scientific). 5 ng/mL of mRNA were used to make cDNA by RT-PCR in 10 uL reactions using Supertranscript III reverse transcriptase (Life Technologies, USA) in MicroAmp Fast Optical 96-Well Reaction Plates (Life Technologies). Quantitative real-time PCR was performed in triplicate with Quantstudio 12k Flex Real-time PCR system (Thermo Fisher Scientific), using Taqman Fast Universal Master Mix and hydrolysis probes (Taqman, Life Technologies). The efficiency and specificity of the Taqman probes used in this assay is batch tested by the manufacturer and shown to be of almost 100%. Gene products measured were Hsf1, Hspa5, Hspa1a, Hspa1b, Hsp90aa1, Hsp90ab1, Hsp90b1, Hspd1, Atf4, and Xbp1s (see Table A.1. for primer details). These genes are markers for the activation of cellular stress pathways, namely the Heat Shock Response (HSR) and Endoplasmic Reticulum Stress (ER stress). Real time PCR data was analyzed using the $2^{-(\Delta\Delta CT)}$ method. Expression of target genes was normalised against the expression of ribosomal protein L19 (rpl19), which was used as an internal control for every sample. The use of this reference gene has previously been validated for analysing mRNA levels in ovarian cells from mice [99, 100, 202]. Fold changes in gene expression were relative to a whole ovary (collected at 44h post-PMSG injection) cDNA sample, also included in each run. The calibrator sample in this case represents the amount of

transcript that is expressed in the whole tissue, from which to obtain the relative number of mRNA copies of the target genes in the cell population of interest.

6.2.4 Quantification of ovulation; and analysis of oocyte quality and developmental competence

To study ovulatory function and oocyte quality, hormonally stimulated female mice were humanely killed at 16 hours post-hCG injection. The reproductive tracts were dissected and placed in HEPES-buffered GIBCO minimal essential medium (aMEM; Life Technologies, California, USA) at 37°C. Expanded, ovulated COC were collected by tearing open the oviduct, transferred to clean HEPES-buffered α-MEM and counted. Oocytes were then isolated from the COC using hyaluronidase (1000 IU/mL; Life Technologies) in HEPES aMEM media with 1mg/ml polyvinylpyrrolidone (PVP; Sigma-Aldrich, Missouri, USA) at 37°C, to observe their morphology. Oocytes presenting a spherical shape, and uniformity and integrity of the cytoplasm were considered as morphologically normal and healthy. Presence or not of the first polar body is a marker of the state of maturation of the oocyte, as it indicates the oocyte is in metaphase II (MII). In contrast, oocytes presenting an unshapely, damaged or fragmented cytoplasm were considered morphologically unhealthy. Healthy oocytes were then used in downstream assays.

To investigate oocyte developmental potential, either 2-cell or blastocyst embryos were collected after mating. Briefly, some female mice were mated to strain-compatible C57BL6J males after hCG-injection, then checked for the presence of vaginal plug (indicative of coitus) at 15-16h post-hCG injection. Those females that were positively identified as mated were then humanely killed at 46h post-hCG injection for day 2 embryo collection, or at 98h post-hCG injection for day 5 embryo collection. The reproductive tracts were dissected and placed in HEPES aMEM at 37°C. Day 2 embryos were flushed out of the oviduct, then assessed for first cleave (2-cell stage). Embryos at the 2-cell stage or over, were cultured in vitro for a further 68 hours (developmental day 5) in Research Vitro Cleave medium (10 zygotes/20 uL drop; COOK Medical, QLD, Australia) at 37°C in 6% CO_2, 21% O_2. On-time development of the embryos was analysed by assessing their developmental stage at collection (46h post-hCG) and then at the end of in vitro culture. Females that yielded zero viable embryos on day 2 of collection were not included in the on-time development analysis of in vitro cultured day 5 embryos. In vivo produced day 5 embryos were flushed out of the uterus as previously described [307]. Briefly, the uterine horns were separated from the oviducts, then flushed by injecting 1mL of HEPES aMEM at 37°C using a 30G needle. Blastocyst embryos collected were used in downstream

assays. To document their stage of development, all embryos were photographed using Nikon SMZ1500 stereomicroscope (Nikon instruments Inc., Melville, NY), and assessed by blind user. Embryos were kept separate for each individual female during the course of all assays.

6.2.5 Live cell assays and imaging

Mitochondrial profile and function in oocytes was measured by staining the cells with Mitotracker Orange CM-H2TMRos (MTO) mitochondrial activity dye (Life Technologies) at 500 nM in HEPES aMEM medium for 15 min in the dark. At this point, Mitotracker Green FM (MTG) mitochondrial mass dye (Life Technologies) was added to the solution at a final concentration of 200 nM. Oocytes were then left to incubate for another 15 min, followed by washing in HEPES aMEM medium with 1mg/ml PVP. Cell toxicity, background fluorescence and autofluorescence were controlled for using by replacing the respective dyes with vehicle (DMSO; Sigma-Aldrich) and Hoechst 33342 DNA stain (Thermo Fisher Scientific, Massachusetts, USA) only as control.

To study embryonic mitochondrial activity, late expanded blastocysts (where the blastocoel occupied approximately 90% of the embryo volume) were stained using MTO CM-H2TMRos mitochondrial activity dye (Life Technologies) at 500 nM in HEPES aMEM medium for 15 min in the dark. Blastocysts were then washed in HEPES aMEM medium with 1mg/ml PVP at 37 °C for 5 min.

Imaging was done by Leica TCS SP5 spectral scanning confocal microscope system (Leica Microsystems, Heerbrugg, Switzerland).Fluorescence intensity was determined using ImageJ Fiji software (National Institutes of Health, Maryland, USA), then quantified by corrected total cell fluorescence (CTCF), which determines the levels of fluorescence in a given region of a confocal section, using the formula: CTCF = Integrated Density – (Area of selected cell) x (Mean fluorescence of background readings). This quantification is based on the published method from Burgess et al [308, 412]. MTO:MTG ratio was analysed to find out the relative mitochondrial activity per mitochondrial mass and was the ratio of MTO CTCF and MTG CTCF.

6.2.6 Statistical analysis

All measures are reported as mean ± the standard error of the mean (SEM), unless indicated otherwise. Data were analysed using the statistics software GraphPad Prism 6 v008 for

Windows (GraphPad software Inc., California, USA). Statistical significance was determined by One or Two-way ANOVA as indicated, and Tukey's Multiple Comparison Test. P values of <0.05 were considered statistically significant.

6.3 Results

6.3.1 Effect of Tex-OE treatment on body weight after 40 weeks of diet

To investigate the potential Tex-OE on counteracting the effects of obesity on folliculogenesis and different ovarian stress pathways, a cohort of female mice was fed HFD followed by Tex-OE treatment in parallel with the dietary cohorts described in Chapter 6. Thus, female mice were fed either a control (CD) or high fat diet (HFD) for 38 weeks; and then, approximately half of the HFD females received oral Tex-OE treatment in the drinking water for two weeks. All mice were maintained during this time on a cellulose-free HFD, since Tex-OE becomes inactive if consumed together with cellulose. First, growth trajectories were analysed to measure any influence of Tex-OE treatment on body weight and composition. Both groups of HFD-fed females (TexOE-treated and non-treated) had overall similar body weight trajectories and were consistently heavier than the controls during the course of the diet (Figure 6.1.A). However, at the end of the experiment the final body weights were not statistically different between the groups (Figure 6.1.B).

Both HFD and HFD+Tex-OE groups had slightly heavier abdominal fat pads (28% and 22.8% increase, respectively) than the controls (Figure 6.1.C). Meanwhile Tex-OE-treated HFD females had the lowest liver weight (1.38 ± 0.2 g) when compared to the untreated HFD (1.482 ± 0.28 g) and CD (1.614 ± 0.41 g) groups (Figure 6.1.D) but this was not a significant reduction.

In summary, Tex-OE treatment did not cause any overt metabolic changes in mice exposed to a long-term HFD, as shown by the similar body weight trajectories within the obesogenic diet groups.

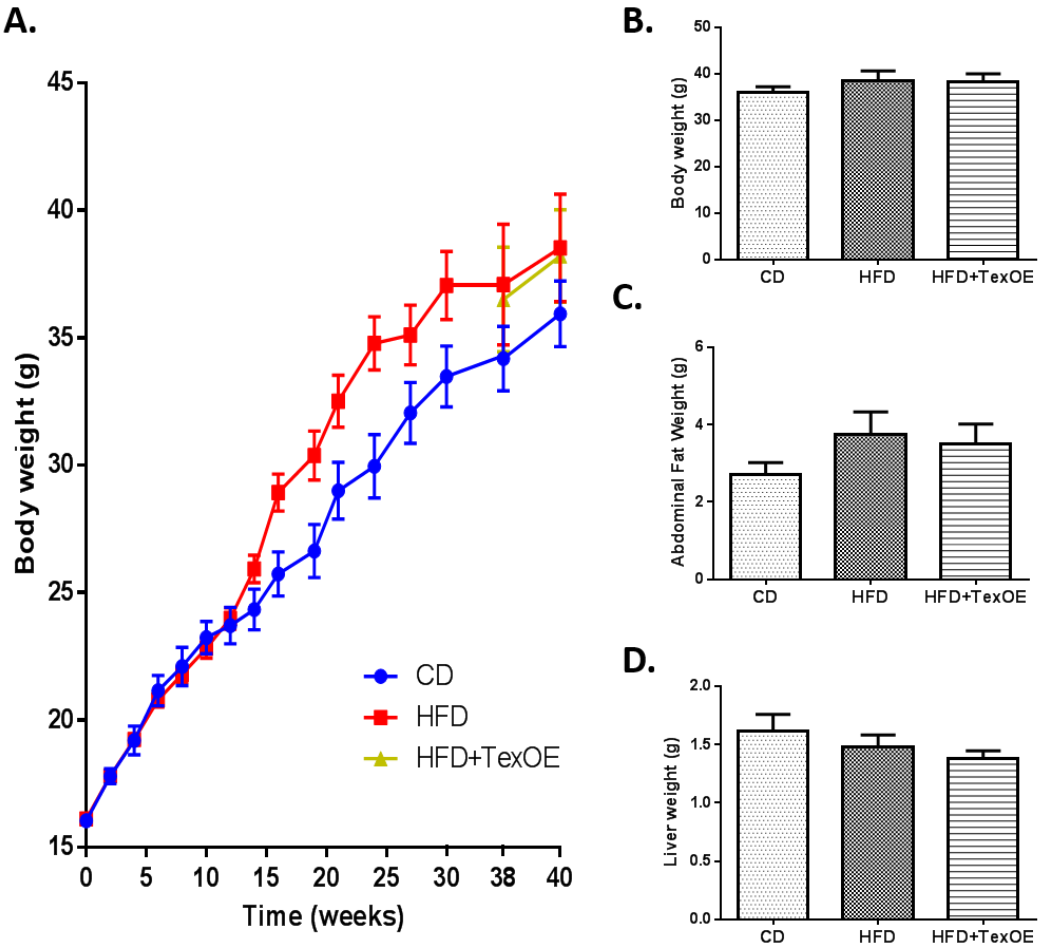

Figure 6.1 Effect of Tex-OE supplementation of High-Fat diet versus treatment on body and tissue weights.

A. Body weights in female mice fed a control diet (CD), high-fat diet (HFD) or Tex-OE-supplemented high-fat diet (HFD+Tex-OE) across 40 weeks. **B.** Body weight at 40 weeks of diet. **C.** Abdominal fat pad weight. **D.** Liver weight. Results are mean ± SEM. N=11 (CD), N=11 (HFD), N=12 (HFD+Tex-OE) female mice per dietary treatment. Statistical analysis was repeated measures Two-Way ANOVA (A) or One-Way ANOVA and Tukey's Multiple Comparison Test (B-D).

6.3.2 Effect of Tex-OE treatment on COC number and COC integrity

Next, we set out to analyse the effect of Tex-OE supplementation on folliculogenesis and COC integrity in obese females. Untreated HFD females had similar number of COC (6.1 ± 1.1) as Tex-OE-treated ones (5 ± 1.1) collected from the ovary at 44h after PMSG injection, however both had lower yields than the CD (7.5 ± 1.2) females (Figure 6.2.A). Denuded oocytes (DO) collected from the follicles were also counted. Tex-OE-treated HFD females had similar numbers of denuded oocytes (4.67 ± 1.4) as the HFD females at collection, and both groups had more than the CD (1.5 ± 0.7) (Figure 6.2.B). These findings suggested that exposure to HFD likely affected ovarian function and oocyte quality through follicle growth, as suggested by the lower number of oocyte-complexes collected, and impaired COC integrity; and that Tex-OE treatment did not influence this outcome in obese females.

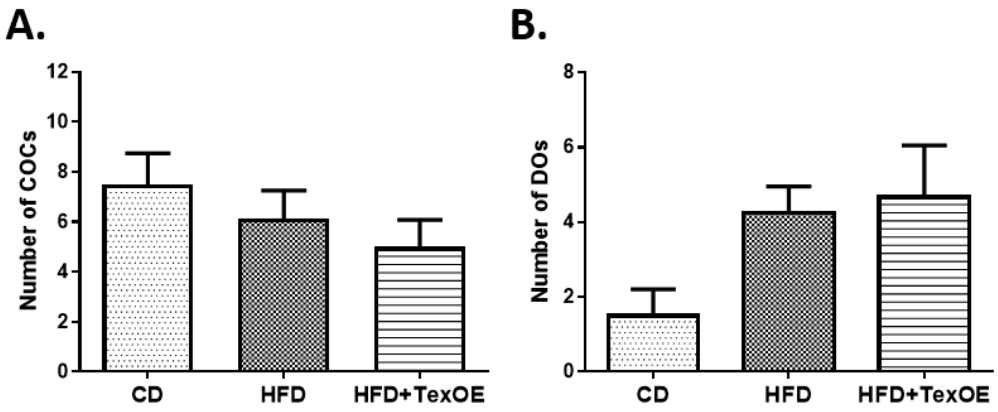

Figure 6.2 Effect of Tex-OE supplementation of High Fat Diet on the number of preovulatory cumulus oocyte complexes.

All pre-ovulatory follicles were punctured at 44 hours post-PMSG and were classified by the integrity of the cumulus cell layer as COCs (**A.**) or denuded oocytes (DOs) (**B.**). Results are mean ± SEM. N=8 (CD), N=8 (HFD), N=9 (HFD+Tex-OE) female mice per dietary treatment. Statistical analysis was One-Way ANOVA and Tukey's Multiple Comparison Test.

6.3.3 Tex-OE treatment normalises cellular stress responses in ovarian follicular cells

GC and COCs collected from the ovaries of female mice after 40 weeks of diet were analysed for a panel of heat shock response genes. The results for CD and HFD groups are the same as those presented in Chapter 4.3.3, and the gene expression in cells from HFD females treated with Tex-OE is now compared. First, we looked at the expression of HSR transcription factor Hsf1 and three genes from the HSP70 family, namely: Hspa1a and b, and Hspa5. These are markers for cellular and ER stress, respectively (Figure 6.3). Also analysed was expression of three genes representative of the HSP90 family, namely Hsp90aa1, Hsp90ab1 and Hsp90b1 and expression of Hspd1 (Hsp60), which is mainly localised to the mitochondria (Figure 6.4). HSR genes Hspa1a/b and Hspa5, and ER stress markers Atf4 and Xbp1s were examined to determine relative induction in response to the treatment as HFD is known to induce these genes in GC and COC [100, 304].

Overall, as described in detail in Chapter 4.3.3, gene expression levels of every HSR gene were higher in ovarian cells, both COC and GC, from HFD females, suggesting increased activity of the HSR pathway. The exception was Hspd1 which was lower in GC of HFD females (Figure 6.4). Interestingly, gene expression levels of every HSR gene in the ovarian cells of HFD+TexOE females was lower than expression in the HFD females. Again, the exception was Hspd1 where Tex-OE treatment was associated with higher levels in GC of obese females. None of the changes in gene expression levels were statistically significant but the pattern of these results suggested that Tex-OE treatment normalised the effects of HFD in ovarian cells to levels similar to the control group.

Lastly, to determine the effects of Tex-OE on ER stress we examined gene expression for Atf4 and Xbp1s, the two well-characterised markers for this distinct type of cellular stress and which we have previously shown to be increased in ovarian cells from obese mice [202]. Briefly, exposure to HFD alone did not have great impact the expression of markers for ER stress in ovarian cells, either COC or GC. Similarly, Tex-OE treatment did not have any significant effect on gene expression levels in either GC or COC. However, there was a subtle trend indicating reduced expression of Atf4 and Xbp1s in COC of HFD-TexOE fed females compared to those fed HFD (Figure 6.5).

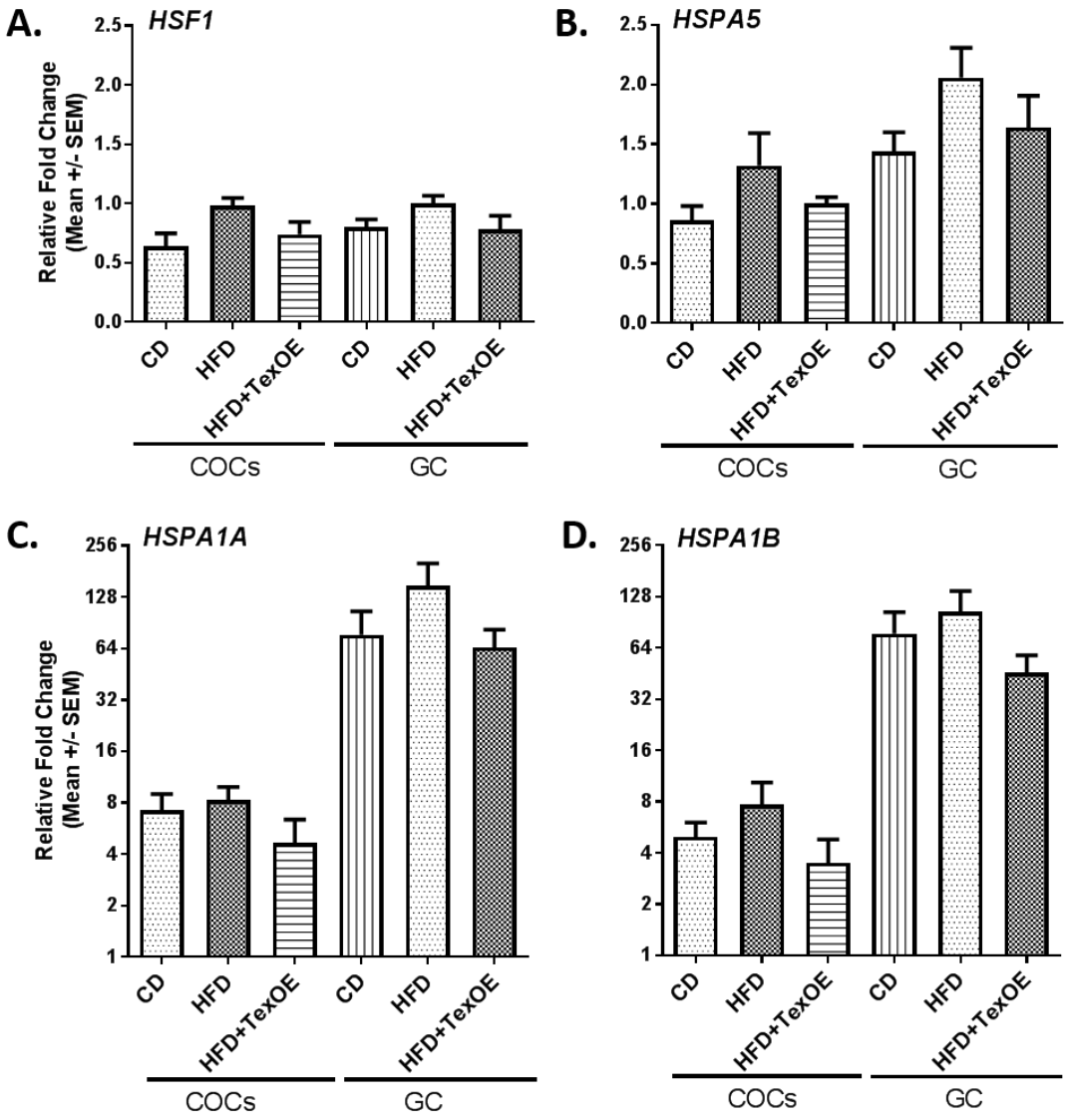

Figure 6.3 Effect of Tex-OE supplementation of High-Fat Diet on the expression of Heat Shock Response (HSR) genes.

GC and COC were collected at 44h post-PMSG injection for HSR gene expression analysis by real-time PCR. **A.** Hsf1 mRNA expression levels **B.** Hspa5 mRNA expression levels. **C.** Hspa1a mRNA expression levels. **D.** Hspa1b mRNA expression. Results are mean ± SEM. N_{GC}=7 (CD), N=7 (HFD), N=9 (HFD+Tex-OE); and N_{COC} = 5 pools of ≥ 9 COC per dietary treatment. Statistical analysis was One-Way ANOVA and Tukey's Multiple Comparison Test.

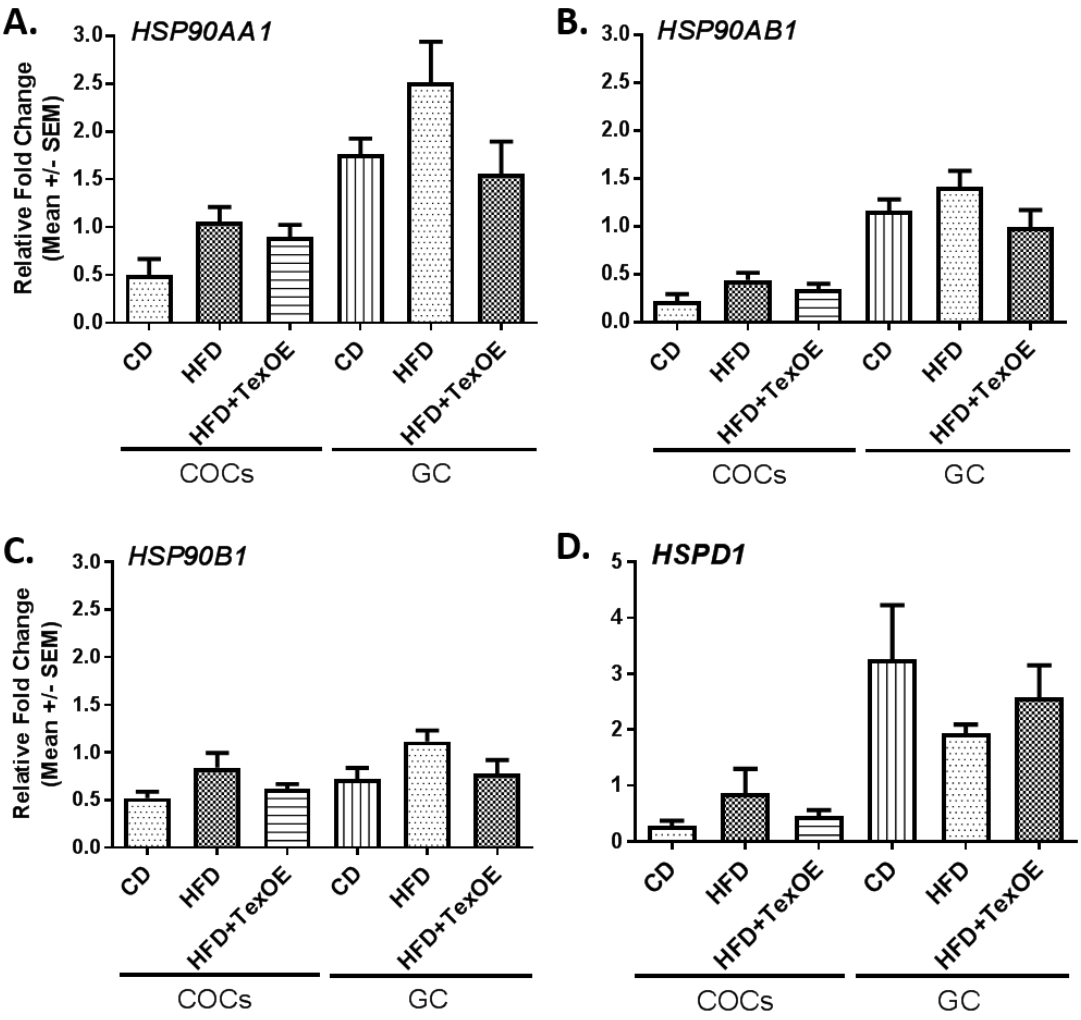

Figure 6.4 Effect of Tex-OE supplementation of High-Fat Diet on the expression of Heat Shock Response (HSR) genes.

GC and COCs were collected for HSR gene expression analysis by real-time PCR. **A.** Hsp90aa1 mRNA expression levels **B.** Hsp90ab1 mRNA expression levels. **C.** Hsp90b1 mRNA expression **D.** Hspd1 mRNA expression levels. Results shown as mean ± SEM. N_{GC} = 7 (CD), N=7 (HFD), N=9 (HFD+Tex-OE); and N_{COC} = 5 pools of ≥ 9 COC per dietary treatment. Statistical analysis was One-Way ANOVA and Tukey's Multiple Comparison Test.

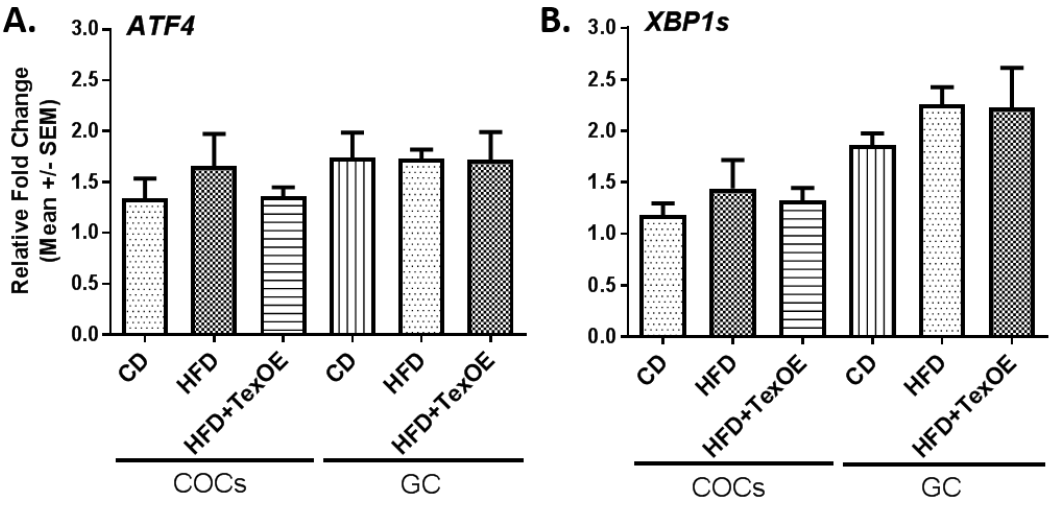

Figure 6.5 Effect of Tex-OE supplementation of High-Fat Diet on the expression of ER stress genes.

GC and COC were collected for ER stress gene expression analysis by real-time PCR.**A.** Atf4 mRNA expression. **B.** Xbp1s mRNA expression. Results shown as mean ± SEM. N_{GC}=7 (CD), N=7 (HFD), N=9 (HFD+Tex-OE); and N_{COC} = 5 pools of ≥ 9 COC per dietary treatment. Statistical analysis was One-Way ANOVA and Tukey's Multiple Comparison Test.

6.3.4 Effect of Tex-OE treatment on body weight after 10 weeks of HFD diet

To examine the acute effects of Tex-OE prior to the onset of profound obesity, female mice were fed either a CD or HFD for 8 weeks, then about half of the HFD females received oral Tex-OE treatment in the drinking water, for two weeks while on a cellulose-free HFD. Body weight trajectories were identical between the three groups after 8 weeks, and then again body weights were identical 2 weeks later at 10 weeks after 2 weeks of Tex-OE treatment (Figure 6.6.A). Similarly, body weight gain measured at 8 and 10 weeks, were not different between the groups (Figure 6.6.B and .C, respectively). Taken together, these results indicate that HFD had no effect on body weight in this timeframe, and that Tex-OE treatment did not have a major metabolic impact on female mice exposed to a short term HFD.

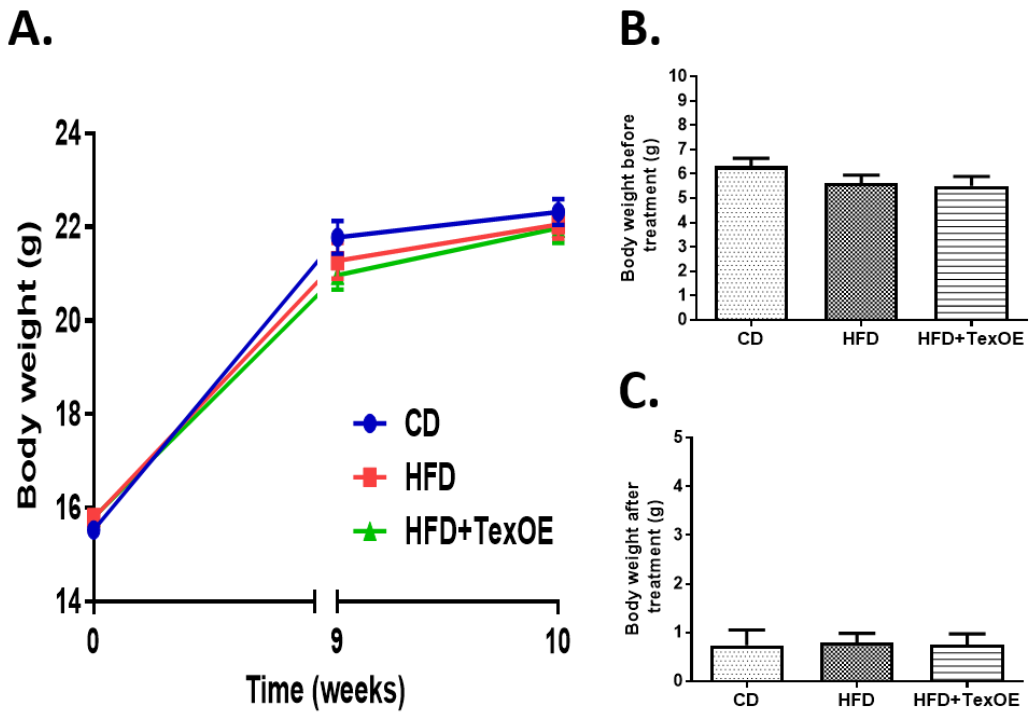

Figure 6.6 . Effect of Tex-OE treatment on body weight after 8 weeks of High Fat Diet.

Body weights of female mice fed either a control diet (CD), High-fat diet (HFD) or Tex-OE-supplemented High-fat diet (HFD+Tex-OE). **A.** Body weights trajectory during 10 weeks of diet. **B.** Weight gain before Tex-OE treatment. **C.** Weight gain at 10 weeks of diet after 2 weeks of Tex-OE treatment. Results are shown as mean ± SEM. N=15 female mice per group. Statistical analysis was One-Way ANOVA (B, C), and Tukey's Multiple Comparison Test.

6.3.5 Tex-OE supplementation of HFD restores mitochondrial profile and improves developmental competence in oocytes from obese females

We then analysed whether treatment of obese females with Tex-OE would affect ovulation and oocyte morphology at 16 hours post-hCG injection. Untreated HFD females yielded the lowest number of oocytes (22.67 ± 2.01), while those treated with Tex-OE had slightly increased numbers (25 ± 3.07) that were similar to those of the CD group (24.83 ± 3.33) (Figure 6.7.A). However, both the untreated and the Tex-OE-treated HFD females had fewer morphologically healthy oocytes (18 ± 1.76 and 19.08 ± 2.38, respectively) than the control group (21.73 ± 2.2) (Figure 6.7.B). Additionally, both groups of HFD females had fewer oocytes that had reached MII (8.25 ± 1.18 and 9.75 ± 2.05, respectively) at the time of collection compared to the controls (12.27 ± 1.17) (Figure 6.7.C). Overall however, even though oral supplementation using Tex-OE slightly increased ovulation and was similar to that of CD females, there was not a significant effect of the HFD or the Tex-OE supplementation on the number and morphology of ovulated oocytes.

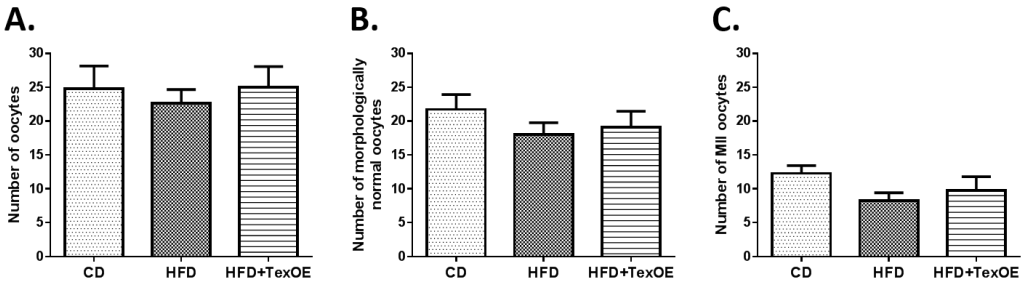

Figure 6.7 Effect of Tex-OE supplementation of High Fat Diet on ovulation and oocyte quality.

A. Total number of oocytes collected from the oviduct after ovarian hyperstimulation with hCG for 16h. **B.** Total number of morphologically normal oocytes at collection. **C.** Total number of morphologically normal oocytes that were at metaphase II (MII). Results are shown as mean ± SEM. N=15 female mice per group. Statistical analysis was One-Way ANOVA, and Tukey's Multiple Comparison Test.

Next, we analysed the mitochondrial profile of MII oocytes from the different dietary groups after 8 weeks HFD and 2 weeks Tex-OE treatment. When stained using MTO CM-H2TMRos mitochondrial activity dye MII oocytes collected from HFD-fed females showed similar fluorescence intensity to that of those from the control group. Oocytes from Tex-OE-treated females exhibited reduced staining compared to both other groups (Figure 6.8.A). This observation was confirmed by the significantly lower CTCF value in oocytes from the Tex-OE-treated group (90.24 ± 9.41 AU), when compared to the untreated HFD and control (153.4 ± 7.02 AU and 138.5 ± 12.77 AU, respectively) groups (N=6-11; P<0.0001; Figure 6.8.B).

Interestingly, MTG mitochondrial mass dye staining showed oocytes from HFD females presented higher fluorescence intensity than CD oocytes, and also had a clumped appearance (Figure 6.8.C). CTCF analysis also showed that the HDF group had the highest levels of MTG fluorescence (122.9 ± 32.4 AU), and that Tex-OE treatment reduced the CTCF value to be similar to that of the CD group (64.53 ± 5.97 AU and 85.99 ± 10.54 AU, respectively) (Figure 6.8.D).

Merged images of oocytes double stained with mitochondrial dyes showed that those from the HFD mice had the highest fluorescence intensity, while those from HFD+Tex-OE group were similar to the controls (Figure 6.8**Error! Reference source not found.**.E). MTO:MTG ratio analysis of the CTCF values confirmed these observations and showed a trend towards Tex-OE treatment reducing HFD ratio values closer to 1 (N=6-11; HFD vs HFD+Tex-OE P=0.09; Figure 6.8.F).

Briefly, these results indicate that medium exposure to HFD increased mitochondrial mass while also significantly increasing mitochondrial activity, and that oral supplementation with Tex-OE for two weeks normalised mitochondrial mass to control levels as well as reduced mitochondrial activity in MII oocytes.

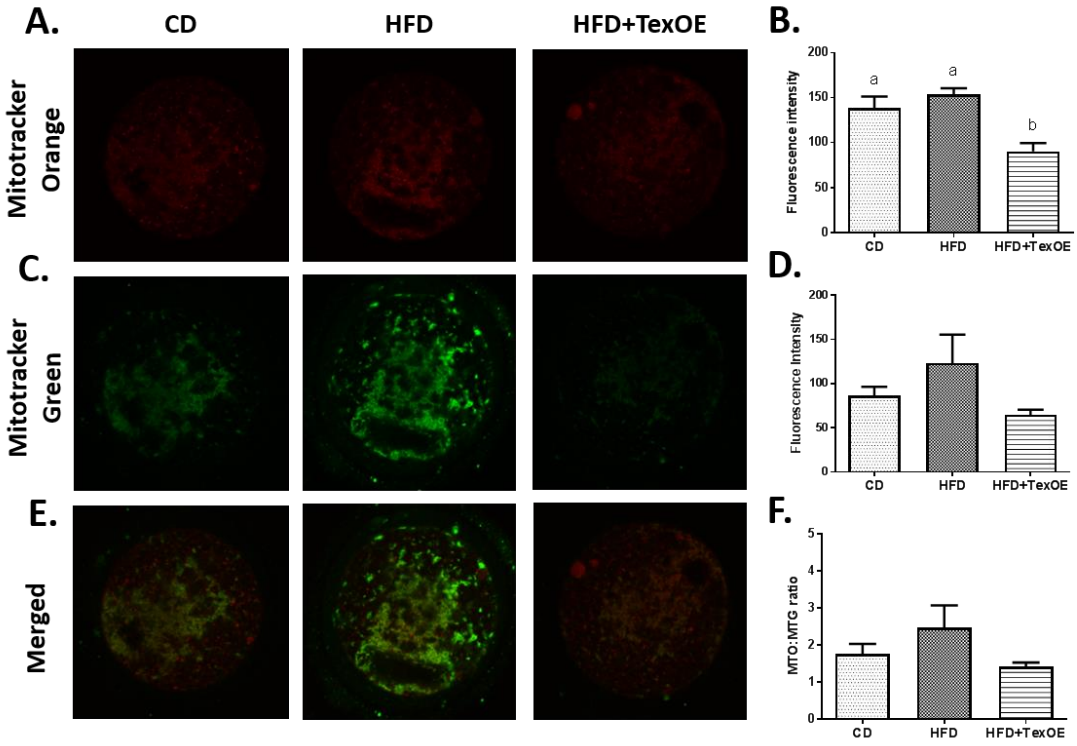

Figure 6.8 Tex-OE reduces mitochondrial activity in ovulated oocytes.

Ovulated oocytes double stained with MTO CM-H2TMRos and MTG. **A.** Representative images of oocytes stained with MTO CM-H2TMRos mitochondrial activity dye. **B.** Corrected Total Cell Fluorescence (CTCF) analysis for MTO CM-H2TMRos stained oocytes; a vs b $P<0.0001$. **C.** Representative images of oocytes stained with MTG mitochondrial mass dye. **D.** CTCF for MTG stained oocytes. **E.** Merged images. **F.** Orange:Green (MTO:MTG) CTCF ratio. Results shown as mean ± SEM. N = 6 (CD), N=11 (HFD), N=11 (HFD+Tex-OE) oocytes from at least 3 different females per group. Statistical analysis was One-Way ANOVA, and Tukey's Multiple Comparison Test.

Lastly, the effect of HFD on oocyte developmental competence, and the influence of Tex-OE treatment on the outcome was studied in females after 10 weeks of dietary treatment. Female mice underwent ovarian hyperstimulation, followed by mating with a male to produce embryos in vivo. Embryos were collected on either dpc 2 (Figure 6.9.A) or dpc 5 (Figure 6.9.B). The HFD and CD females yielded a similar number of 2-cell embryos (3.92 ± 1.45 embryos and 3.45 ± 0.63 embryos, respectively) on dpc 2; and this was significantly higher in the HFD+Tex-OE (7.42 ± 1.62 embryos) group (N=9-12; P=0.04). Additionally, the HFD group had fewer embryos that were developed past the cleavage stage (2-cell +++), then both the Tex-OE-treated HFD and the CD groups (0.84 ±0.39, 2.25 ± 0.75, and 1.89 ± 0.61 embryos respectively) (Figure 6.9.A).

The Tex-OE-treated HFD group had 57% of total putative zygotes cleave to the 2-cell (or greater) stage at the time of collection, which was significantly higher to that of the non-treated HFD (29.09%) group, and similar to control (47.34%) cleave levels (P=0.04; Figure 6.9.C). The collected dpc 2 embryos were cultured in vitro and their development observed until the end of the pre-implantation phase on approximately day 5 after mating. Culture of the 2-cell (or greater) embryos from Tex-OE-treated females in vitro resulted in 90.27% of embryos developing to blastocysts, and this was significantly higher than the 54.46% blastocyst rate from HFD females (P=0.02; Figure 6.9.D). These were not different from the CD (67.2%). Meanwhile, the HFD only and the Tex-OE supplemented HFD groups also had the highest percentage of hatching blastocysts (42.95% and 47.51%, respectively) when compared to the CD (29.76%) group (Figure 6.9.E).

As an additional analysis of the effects of Tex-OE on embryo development in obese females, blastocysts were flushed from additional cohorts of animals on dpc 5. Interestingly, on dpc 5 (Figure 6.9.B) the HFD+Tex-OE females also yielded significantly more blastocysts (9.58 ± 1.99 embryos) than the HFD (3.11 ± 1.58 embryos) or the CD groups (4.11 ± 1.01 embryos; P=0.02). The number of embryos still at morula stage on dpc 5 was similar for all three groups (Figure 6.9.B).

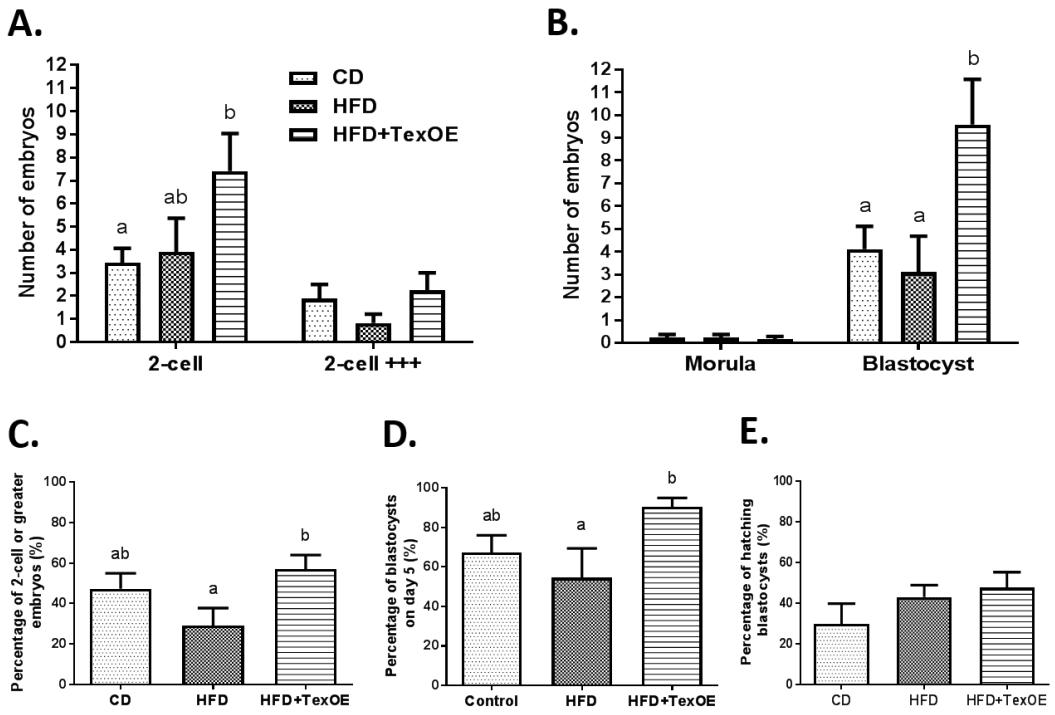

Figure 6.9 Treatment with Tex-OE improves oocyte developmental competence.

A. Number of embryos collected that had achieved 2-cell stage or beyond by day 2 after mating; a vs b P=0.04; N=9 (CD), N=12 (HFD), N=12 (HFD+Tex-OE). **B.** Number of embryos collected that had achieved morula or blastocyst stage by day 5 after mating; a vs b P=0.02; N=9 (CD), N=9 (HFD), N=12 (HFD+Tex-OE). **C.** Percentage of 2-cell or greater from total of embryos collected from the oviduct on day 2 after mating; a vs b P=0.04; N=9 (CD), N=12 (HFD), N=12 (HFD+Tex-OE). **D.** Percentage of blastocysts on day 5 derived from the in vitro culture of day 2 embryos; a vs b P=0.02; N=9 (CD), N=5 (HFD), N=11 (HFD+Tex-OE). **E.** Percentage of blastocysts hatching out of the zona pellucida on day 5 from in vitro cultured day 2 embryos. Results are shown as mean ± SEM. Statistical analysis was either Two-Way (A, B) or One-Way ANOVA (C-E), and Tukey's Multiple Comparison Test.

Mitochondrial activity was measured in blastocysts collected on dpc 5 after ovarian hyperstimulation and mating of female mice after 10 weeks of diet. Confocal microscopy imaging of blastocysts stained with MTO CM-H2TMRos suggested that those derived from HFD females had the highest fluorescence intensity (Figure 6.10.A). Similarly, CTEF analysis showed that these HFD blastocysts had increased fluorescence levels (51.2 ± 5.24 AU) compared to those from the CD group (30.68 ± 5.38 AU). Moreover, blastocysts from Tex-OE-treated females (32.27 ± 4.35 AU) had significantly lower CTEF values, which were in turn more similar to the control (P=0.02; Figure 6.10.B). Fluorescence intensity was particularly bright in the trophectoderm cells in all embryos.

Taken together, these findings indicate that short-term exposure to HFD had a negative effect on pre-implantation embryo development in vivo, and that this persists even after in vitro culture of day 2 embryos. Moreover, HFD increased embryonic mitochondrial activity. However, supplementation of HFD with Tex-OE for two weeks improves embryonic development and restored mitochondrial activity levels.

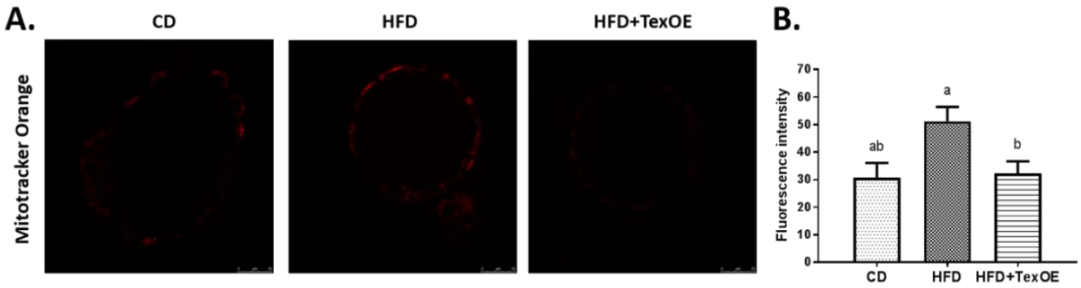

Figure 6.10 Effect of Tex-OE on mitochondrial activity of blastocysts.

A. Representative images of in vitro cultured blastocysts stained with Mitotracker Orange mitochondrial activity dye. **B.** Corrected Total Embryo Fluorescence (CTEF) analysis for Mitotracker Orange stained blastocysts; a vs b P=0.02. Results shown as mean ± SEM. N=6 (CD), N=11 (HFD), N=18 (HFD+Tex-OE) blastocysts from at least 3 different females per group. Statistical analysis was One-Way ANOVA and Tukey's Multiple Comparison Test (B).

6.4 Discussion

There is great interest in natural fertility diets and thus we conducted this preliminary study to determine whether an approved *O. indica* dietary supplement that is thought to act via induction of cytoprotective HSP could improve female fertility in the context of obesity.

The results presented in this chapter showed that a long term exposure to High Fat Diet for 40 weeks affected the number of normal COC in preovulatory follicles and dysregulated the stress pathways in ovarian follicular cells. Moreover, after only 10 weeks of obesogenic diet, female mice had slightly reduced ovulation and decreased number of morphologically healthy oocytes, even in the absence of strong metabolic characteristics of obesity. These ovulated oocytes presented an altered mitochondrial profile and reduced developmental competence, as indicated by the decreased number of pre-implantation embryos collected after hyperstimulation and mating. A 2 week oral dietary supplementation with Tex-OE tended to normalised gene expression for key markers of cellular stress pathways in the ovaries of obese female. This dietary supplement to obese females also normalised mitochondrial profile in ovulated oocytes, while improving embryo development.

During the course of this study, both cohorts of mice in the obesogenic diet groups had similar body weights to the controls at the time of tissue collection. Further, treatment with Tex-OE did not affect body or tissue weights in these female mice. Similarly, oral administration of phenolic compounds derived from *Opuntia spp*. was previously shown to not have any effect on food consumption, body weight gain or relative organ weight in hypercholesterolemic male mice compared to the untreated group. However, these compounds normalized serum lipid profile to that of the normocholesterolemic group [235]. In this study we did not examine circulating metabolites and thus we cannot determine whether Tex-OE might have normalized these markers in mice fed HFD.

Our group has shown that increased body weight increases the expression of chaperones and ER stress markers in ovarian cells [100, 202]. We have also shown that a diet high in saturated fats activates the expression of genes for the HSR in ovarian follicles in Chapter 4.3.3. In this study, although there were not significant differences in HSP gene expression between the diets, mRNA levels in the HFD+Tex-OE group were always more similar to those of the CD than HFD. It was also observed that the HFD females had decreased cumulus cell integrity in cumulus-oocyte complexes, but not the Tex-OE treated HFD mice. In a similar study using a hyperphagia-induced obesity mouse model the induction of Hspa1a and Hspa1b in GC and

COC in the post-ovulatory ovary was associated to altered extracellular matrix secretion in the cumulus cells and spindle abnormalities in the oocytes [100].

Other phenolic compounds extracted from *Opuntia spp*. have previously been shown to stimulate chaperone expression as protection against oxidative damage caused by cytotoxic agents. Balb/c mice orally given the mycotoxin Zearalenone, an immunotoxin produced by some *Fusarium* species that produces tissue atrophy [423], showed increased levels of Hspa1a in liver and kidney, but preventive treatment a day before with increasing concentrations of an extract from whole *Opuntia* cladodes reduced expression in a dose-dependent manner [236]. In a similar study, pre-treatment of male mice with whole cladode extract before intra-peritoneal administration of the hepatotoxin and carcinogenic Aflatoxin B1, also reduced liver Hspa1a expression compared to the untreated Aflatoxin B1 group [241]. Furthermore, they showed that *Opuntia* extract supplementation reduced oxidative damage, prevented chromosomal aberrations and DNA fragmentation, and restricted the cytotoxic effects of the mycotoxin treatment by differential modulation of the expression of pro-apoptotic genes; and we speculate that this antioxidant activity could be a potential mechanism of action for Tex-OE extract in ovarian cells.

Obesity damages oocyte quality through the mitochondria. Mature, ovulated oocytes presented an altered mitochondrial profile, consisting of higher mitochondrial mass and activity, which we have previously shown in obese HFD-fed mice [100]. Alterations to the oocyte mitochondria have been associated with reduced in vitro fertilisation and blastocyst development rates [202]. Healthy mitochondria are thought to be at the basis of successful embryo development, since it has been shown that their impairment in mouse oocytes and zygotes alters posterior fetal and placental development [400]. Interestingly, not only did Tex-OE treatment reverse the altered mitochondrial profile in the oocytes, but it also increased oocyte developmental competence, as shown by the significantly improved pre-implantation embryonic development. We speculate that the therapeutic target for this compound must be found within the oocyte and before the 2-cell stage, as suggested by the fact that Tex-OE not only increased the percentage of blastocysts embryos produced in vivo, but also of those derived from dpc 2 cleaved embryos cultured in vitro. Moreover, while the HFD embryos presented higher mitochondrial activity in their outer cell layer, the blastocysts from the HFD+Tex-OE group had significantly lower levels that were similar to those of the CD group. The outer cells of the embryo that form the trophectoderm (TE) have more mitochondria, and consume more oxygen and nutrients, unlike the inner cell mass (ICM), therefore it is expected that they show increased mitochondrial activity [415]. However, abnormal activity levels are associated with impaired growth later on

in development [424, 425]. The normalised mitochondrial activity in embryos from Tex-OE-treated females suggests that this extract may decrease the negative impact of HFD on the developmental competence of the oocyte. Additionally, this reduced embryo metabolic activity also indicates improved oocyte quality as a result of Tex-OE treatment, since all of the embryonic mitochondria are derived from the oocyte.

These preliminary results indicate that the phytocompound Tex-OE is a potential therapeutic for the treatment of female infertility due to obesity, and thus warrants further exploration. More detailed investigation of its effects on oocyte mitochondria and embryo mitochondria should be carried out, as well as further characterisation of its induction of cellular HSP using in situ localisation or Western blot to detect protein levels. Additionally, future investigations should explore the effect of Tex-OE treatment in different models of female infertility, such as advanced maternal age.

In conclusion, we found that the exposure to high fat diet, even in the absence of body weight gain, likely affects ovarian function and oocyte quality and developmental competence but the latter is improved by therapeutic treatment with the *Opuntia* extract Tex-OE.

6.5 References

91. Jungheim ES, Moley KH. Current knowledge of obesity's effects in the pre- and periconceptional periods and avenues for future research. Am J Obstet Gynecol 2010; 203:525-530.
97. Wu LL, Dunning KR, Yang X, Russell DL, Lane M, Norman RJ, Robker RL. High-fat diet causes lipotoxicity responses in cumulus-oocyte complexes and decreased fertilization rates. Endocrinology 2010; 151:5438-5445.
98. Luzzo KM, Wang Q, Purcell SH, Chi M, Jimenez PT, Grindler N, Schedl T, Moley KH. High Fat Diet Induced Developmental Defects in the Mouse: Oocyte Meiotic Aneuploidy and Fetal Growth Retardation/Brain Defects. PLoS One 2012; 7:e49217.
99. Minge CE, Bennett BD, Norman RJ, Robker RL. Peroxisome proliferator-activated receptor-gamma agonist rosiglitazone reverses the adverse effects of diet-induced obesity on oocyte quality. Endocrinology 2008; 149:2646-2656.
100. Wu LL, Russell DL, Wong SL, Chen M, Tsai TS, St John JC, Norman RJ, Febbraio MA, Carroll J, Robker RL. Mitochondrial dysfunction in oocytes of obese mothers: transmission to offspring and reversal by pharmacological endoplasmic reticulum stress inhibitors. Development 2015; 142:681-691.
101. Boots CE, Boudoures A, Zhang W, Drury A, Moley KH. Obesity-induced oocyte mitochondrial defects are partially prevented and rescued by supplementation with co-enzyme Q10 in a mouse model. Hum Reprod 2016; 31:2090-2097.
102. Boudoures AL, Chi M, Thompson A, Zhang W, Moley KH. The Effects of Voluntary Exercise on Oocyte Quality in a Diet-Induced Obese Murine Model. Reproduction 2016; 151:261-270.

105. Weisberg SP, Leibel R, Tortoriello DV. Dietary curcumin significantly improves obesity-associated inflammation and diabetes in mouse models of diabesity. Endocrinology 2008; 149:3549-3558.
202. Wu LL, Russell DL, Norman RJ, Robker RL. Endoplasmic reticulum (ER) stress in cumulus-oocyte complexes impairs pentraxin-3 secretion, mitochondrial membrane potential (DeltaPsi m), and embryo development. Mol Endocrinol 2012; 26:562-573.
235. Osorio-Esquivel O, Ortiz-Moreno A, Garduno-Siciliano L, Alvarez VB, Hernandez-Navarro MD. Antihyperlipidemic effect of methanolic extract from Opuntia joconostle seeds in mice fed a hypercholesterolemic diet. Plant Foods Hum Nutr 2012; 67:365-370.
236. Zourgui L, Golli EE, Bouaziz C, Bacha H, Hassen W. Cactus (Opuntia ficus-indica) cladodes prevent oxidative damage induced by the mycotoxin zearalenone in Balb/C mice. Food Chem Toxicol 2008; 46:1817-1824.
240. Loro JF, del Rio I, Perez-Santana L. Preliminary studies of analgesic and anti-inflammatory properties of Opuntia dillenii aqueous extract. J Ethnopharmacol 1999; 67:213-218.
241. Brahmi D, Bouaziz C, Ayed Y, Ben Mansour H, Zourgui L, Bacha H. Chemopreventive effect of cactus Opuntia ficus indica on oxidative stress and genotoxicity of aflatoxin B1. Nutr Metab (Lond) 2011; 8:73.
304. Yang X, Wu LL, Chura LR, Liang X, Lane M, Norman RJ, Robker RL. Exposure to lipid-rich follicular fluid is associated with endoplasmic reticulum stress and impaired oocyte maturation in cumulus-oocyte complexes. Fertil Steril 2012; 97:1438-1443.
307. Chen M, Wu L, Wu F, Wittert GA, Norman RJ, Robker RL, Heilbronn LK. Impaired Glucose Metabolism in Response to High Fat Diet in Female Mice Conceived by In Vitro Fertilization (IVF) or Ovarian Stimulation Alone. PLOS ONE 2014; 9:e113155.
308. Burgess A, Vigneron S, Brioudes E, Labbe JC, Lorca T, Castro A. Loss of human Greatwall results in G2 arrest and multiple mitotic defects due to deregulation of the cyclin B-Cdc2/PP2A balance. Proc Natl Acad Sci U S A 2010; 107:12564-12569.
357. Jungheim ES, Macones GA, Odem RR, Patterson BW, Lanzendorf SE, Ratts VS, Moley KH. Associations between free fatty acids, cumulus oocyte complex morphology and ovarian function during in vitro fertilization. Fertility and sterility 2011; 95:1970-1974.
371. Henstridge DC, Whitham M, Febbraio MA. Chaperoning to the metabolic party: The emerging therapeutic role of heat-shock proteins in obesity and type 2 diabetes. Molecular Metabolism 2014; 3:781-793.
372. Gupte AA, Bomhoff GL, Geiger PC. Age-related differences in skeletal muscle insulin signaling: the role of stress kinases and heat shock proteins. J Appl Physiol (1985) 2008; 105:839-848.
373. Tiss A, Khadir A, Abubaker J, Abu-Farha M, Al-Khairi I, Cherian P, John J, Kavalakatt S, Warsame S, Al-Ghimlas F, Elkum N, Behbehani K, et al. Immunohistochemical profiling of the heat shock response in obese non-diabetic subjects revealed impaired expression of heat shock proteins in the adipose tissue. Lipids Health Dis 2014; 13:106.
374. Abubaker J, Tiss A, Abu-Farha M, Al-Ghimlas F, Al-Khairi I, Baturcam E, Cherian P, Elkum N, Hammad M, John J, Kavalakatt S, Khadir A, et al. DNAJB3/HSP-40 cochaperone is downregulated in obese humans and is restored by physical exercise. PLoS One 2013; 8:e69217.
375. Kleinridders A, Lauritzen HP, Ussar S, Christensen JH, Mori MA, Bross P, Kahn CR. Leptin regulation of Hsp60 impacts hypothalamic insulin signaling. J Clin Invest 2013; 123:4667-4680.
394. Kawwass JF, Kulkarni AD, Hipp HS, Crawford S, Kissin DM, Jamieson DJ. Extremities of body mass index and their association with pregnancy outcomes in

women undergoing in vitro fertilization in the United States. Fertil Steril 2016; 106:1742-1750.
395. Gesink Law DC, Maclehose RF, Longnecker MP. Obesity and time to pregnancy. Hum Reprod 2007; 22:414-420.
397. Luke B, Brown MB, Stern JE, Missmer SA, Fujimoto VY, Leach R. Female obesity adversely affects assisted reproductive technology (ART) pregnancy and live birth rates. Hum Reprod 2011; 26:245-252.
400. Igosheva N, Abramov AY, Poston L, Eckert JJ, Fleming TP, Duchen MR, McConnell J. Maternal Diet-Induced Obesity Alters Mitochondrial Activity and Redox Status in Mouse Oocytes and Zygotes. PLoS One 2010; 5:e10074.
406. Kiani K, Sadati Lamardi SN, Laschke MW, Malekafzali Ardakani H, Movahedin M, Ostad SN, Aflatoonian R, Moini A. Medicinal plants and natural compounds in the treatment of experimental endometriosis: A systematic review protocol. Evidence-based Preclinical Medicine 2016; 3:1-6.
407. Tsobou R, Mapongmetsem PM, Van Damme P. Medicinal Plants Used for Treating Reproductive Health Care Problems in Cameroon, Central Africa(1). Economic Botany 2016; 70:145-159.
412. McCloy RA, Rogers S, Caldon CE, Lorca T, Castro A, Burgess A. Partial inhibition of Cdk1 in G2 phase overrides the SAC and decouples mitotic events. Cell Cycle 2014; 13:1400-1412.
415. Hewitson LC, Leese HJ. Energy metabolism of the trophectoderm and inner cell mass of the mouse blastocyst. J Exp Zool 1993; 267:337-343.
416. Crul T, Toth N, Piotto S, Literati-Nagy P, Tory K, Haldimann P, Kalmar B, Greensmith L, Torok Z, Balogh G, Gombos I, Campana F, et al. Hydroximic acid derivatives: pleiotropic HSP co-inducers restoring homeostasis and robustness. Curr Pharm Des 2013; 19:309-346.
417. Tesoriere L, Fazzari M, Angileri F, Gentile C, Livrea MA. In vitro digestion of betalainic foods. Stability and bioaccessibility of betaxanthins and betacyanins and antioxidative potential of food digesta. J Agric Food Chem 2008; 56:10487-10492.
418. Bisson JF, Daubie S, Hidalgo S, Guillemet D, Linares E. Diuretic and antioxidant effects of Cacti-Nea, a dehydrated water extract from prickly pear fruit, in rats. Phytother Res 2010; 24:587-594.
419. Cho JY, Park SC, Kim TW, Kim KS, Song JC, Kim SK, Lee HM, Sung HJ, Park HJ, Song YB, Yoo ES, Lee CH, et al. Radical scavenging and anti-inflammatory activity of extracts from Opuntia humifusa Raf. J Pharm Pharmacol 2006; 58:113-119.
420. Powers SK, Lennon SL. Analysis of cellular responses to free radicals: focus on exercise and skeletal muscle. Proc Nutr Soc 1999; 58:1025-1033.
421. Budinsky A, Wolfram R, Oguogho A, Efthimiou Y, Stamatopoulos Y, Sinzinger H. Regular ingestion of opuntia robusta lowers oxidation injury. Prostaglandins Leukot Essent Fatty Acids 2001; 65:45-50.
422. Pharmacology ILIo. Opuntia Tex-OE products. In.
423. Hueza IM, Raspantini PCF, Raspantini LER, Latorre AO, Górniak SL. Zearalenone, an Estrogenic Mycotoxin, Is an Immunotoxic Compound. Toxins 2014; 6:1080-1095.
424. Lane M, Gardner DK. Understanding cellular disruptions during early embryo development that perturb viability and fetal development. Reprod Fertil Dev 2005; 17:371-378.
425. Wakefield SL, Lane M, Mitchell M. Impaired mitochondrial function in the preimplantation embryo perturbs fetal and placental development in the mouse. Biol Reprod 2011; 84:572-580.

Chapter 7: Conclusions and future directions

7.1 Heat Shock proteins have a dynamic expression in the mouse ovary during folliculogenesis and ovulation

Ovarian folliculogenesis and oocyte maturation are cyclical processes driven centrally by hypothalamic hormones, and intra-ovarian paracrine factors. Some members of the cytoprotective HSP family have been shown to be necessary for female fertility, as shown by the infertility and embryonic lethality phenotypes in the KO mouse models for HSF1, HSPA5, HSP90B1 and HSPD1. Lack of HSPA1A/B and HSP90AA1 have not been reported to induce infertility phenotypes under normal laboratory conditions. However, they are highly inducible under stress, constitute the core of the main cytoplasmic chaperone complexes and thus may play roles in stress responses, including in reproductive tissues, under conditions of stress such as metabolic stress. I characterised the expression and localisation of a large panel of HSR genes in ovarian cells during hormone-induced follicle growth and maturation.

I have shown that HSF1, HSPA1A/B, HSPA5, HSP90AA1, HSP90B1 and HSPD1 are all highly expressed in follicular cells during folliculogenesis. Interestingly, gene expression in GC was the lowest around the time of ovulation, increasing again at the beginning of the luteal phase. It is possible that the transcription of these proteins is regulated by changes in the type of steroid hormone receptor, as they differentiate from granulosa to luteal cells and commence progesterone production. HSPA1A/B and HSP90AA1 are part of multi-protein complexes that form the steroid receptors [272]. Moreover, HSPA1A and HSPA1B are necessary for luteal regression and inhibition of inhibition of hormone dependent steroidogenesis in the rat ovary [268], therefore the upregulation of these proteins could be associated with currently unknown functions in CL development.

I have also shown that expression for Hsf1 and Hsp90b1 increases in cumulus cells after ovulation, and HSP90B1 protein strongly localises to the cumulus cells of cumulus-oocyte complex collected from the oviduct, suggesting this HSP could have a novel function in these cells in preparation for or during fertilisation. The strong localisation of HSP90B1 to the membrane and outer oocyte cytoplasm that remains after ovulation support this as well. CC have a role in oocyte growth and maturation, as well as fertilization, but the full extent of their functions in the COC is continuing to be revealed. Focusing on the oocyte, this study showed that HSP proteins are present and localised to the cytoplasm in the transcriptionally silent oocyte during and after ovulation, likely stored there for later use by the embryo.

Even though the role of HSF1 and HSP have been extensively studied in the male tract and during spermatogenesis, their role in the ovary and particularly in GC and COC is largely

unknown. Overall, this thesis showed that HSP are expressed in all ovarian cells, and that their expression and localisation changes during hormonally-induced follicle growth and ovulation. The data presented here indicates that specific HSP have specialised functions in supporting ovarian cells and COC, which warrant further exploration.

7.2 Impact of obesity on female reproduction and challenges in understanding the factors behind reproductive phenotype variability

Obesity affects approximately half the women in western countries, yet it is still not understood how different factors can determine the reproductive phenotypes associated with obesity. The wide-ranging effects in animal models of obesity reflects the variability in humans, which has likely hampered progress understanding the separate impact of hormonal and dietary factors on female fertility. Considering the negative impact of obesity in women's fertility observed in clinical studies and the absence of effective strategies to treat the obesity epidemic, it is important to understand how the different factors influence the ovarian environment and oocyte quality, as it can give clues as to how prevent or diminish reproductive issues in obese women.

PCOS is associated with obesity and/or metabolic dysfunction, particularly insulin resistance. It is the most common endocrine disorder and affects an estimated 10% of women of reproductive age, which is why many attempts have been made to create a suitable rodent model that resembles the characteristics of PCOS in humans. However, issues arise in the use of different hormonal treatments used to induce polycystic ovary syndrome in rodent models, with accumulating evidence showing that rodent hyperandrogenic PCOS models share many of the key symptoms and metabolic variability that characterize this syndrome in women (reviewed in Walters et al. 2012 [318]). Postnatal androgen treatment produces varying degrees of hyperandrogenism, acyclicity, anovulation and polycystic ovaries in rodents but more importantly, is also accompanied by a metabolic phenotype [300, 322, 324, 326-334].

This study further characterised the phenotype of a DHT-induced obesity mouse model and showed that hyperandrogenism caused abnormal glucose metabolism, oligo-ovulation and impeded the progression of early embryo development. The negative effect of high circulating androgen levels on oocyte developmental competence should be examined further in future studies in order to better understand the effects of hyperandrogenemia on oocyte quality and the mechanisms by which it affects the development of pre-implantation embryos. However, there was no effect of DHT treatment observed in mRNA levels for marker genes for ovarian

stress pathways, in contrast to the dysregulated levels seen in other rodent obesity studies, suggesting that this mild degree of metabolic dysfunction does not induce the HSR nor ER stress pathways in ovarian cells.

This thesis also investigated the impact of diet-induced obesity on both systemic metabolism and ovarian function. The vast majority of studies on mouse models of diet-induced obesity utilise only male mice and further, the use of different diets amongst rodent studies is a significant confounder for the understanding of the underlying mechanisms driving obesity. However, even in the few studies investigating the effects of obesity on female fertility there is a high degree of variability in the diets. These diets differ in the percentage of calories from either fats or carbohydrates as well as their source. Further, the diet recipes vary depending on whether they are made in-house or purchased from any number of companies. It is not unexpected that different diets produce slightly different phenotypes [426, 427]. Another key difference between studies is the age at which mice begin consuming the obesogenic diet, and for how long.

In this thesis, I used two different diet-induced obesity models and showed that both affected body weight gain, regulation of glucose metabolism and ovarian function in females. Compared to high fat diet, the combination of high dietary sugar and fat increased the damage to both metabolic and reproductive tissues within 40 weeks, by causing more severe insulin resistance and worse oocyte quality. Additionally, the finding that female mice fed a high fat diet for 10 weeks had abnormal embryo development further supports this, by suggesting that even a short exposure to high fat diet and in the absence of body weight gain, likely affected ovarian function and oocyte quality and developmental competence.

While there was no effect of hyperandrogenism in the mitochondrial profile of ovulated oocytes, mitochondrial activity and mass were affected by exposure to an obesogenic diet. Given the importance of the mitochondria in oocyte and embryo quality and their prevalence as a key target in obesity, more research is needed to clarify how and when the disruption of the mitochondrial profile happens in female gametes. Evidence is accumulating showing that pre-pregnancy obesity changes the oocyte even before conception, meaning that it is important for women to have healthy body weight prior to pregnancy.

7.3 Obesity and diet produce differential expression of ovarian stress genes

Cytokines, chaperones and other proteins that are part of stress response mechanisms are not only important in the cell's response to cellular damage, but they also play an important role in normal ovarian physiology. This thesis showed that chaperones of the heat shock response cascade have a dynamic expression in ovarian follicles supporting cells throughout the ovulatory cycle, and therefore any dysregulation of their expression could lead to impaired follicular development. The analyses of ER stress and heat shock response stress markers in ovarian follicular cells showed that these mechanisms are not disrupted, at least not at the mRNA level, by hyperandrogenism in the DHT-induced model of PCOS, likely because of the less pronounced body weight gain, compared to the diet-induced models. In contrast, macronutrient composition of the diet very strongly influenced stress pathways in the ovary, specifically the HSR. Interestingly, I was also able to identify three ER proteins which gene expression in COC were regulated by body weight, namely HSP90B1, ATF4 and XBP1s. Expression of ER stress markers ATF4 and XBP1s have previously been shown to be dysregulated in the ovarian cells of obese mice [100, 202] but have not previously been linked with increments in body weight. The relationship between increased mRNA levels for HSP90B1 in COC and weight gain suggests a previously unknown regulatory mechanism of this ER chaperone by obesity. This combined with the characteristic pattern of expression of HSP90B1 in COC during folliculogenesis and oocyte maturation support the need to further study its function in the ovarian follicle and what are the downstream targets of the effect of obesity on its expression.

Overall, little is known about the function and regulation of these stress mechanisms in the ovary and more research is warranted to fully comprehend and elucidate the mechanism and regulation of these pathways in the ovary in response to the obesity. Moreover, this thesis has shown the influence of maternal obesity in the ovarian environment is negatively affecting gamete and embryo quality and development, therefore understanding how obesity-induced stress pathways may affect folliculogenesis and oocyte maturation needs further consideration.

7.4 Phytocompounds as therapeutic agents in the treatment of obesity-related subfertility

The findings in this thesis contribute to the body of evidence indicating that obesity during the peri-conception window impacts embryo development, and this is likely caused by impaired oocyte quality. Lifestyle and diet are important factors not only at the base of the obesity

epidemic but also in its treatment and prevention. The lack of reliable therapeutic treatments for the consequences of obesity in women needs further exploration. With respect to improving reproductive outcomes in obese women of reproductive age, the identification of natural compounds that can be incorporated into the diet and are safe for embryo development are sought after and warrants investigation. The phytocompound extracted from *Curcuma* and *Opuntia* are widely available and highly bio-available when administered orally. I focused on them in my research because they are inducers of chaperone proteins of the HSR. This makes them a potential therapeutic agent for the treatment of infertility-related obesity, since I have shown that HSP expression is dysregulated by fat-rich diets and obesity.

My preliminary study could not definitively determine if treatment with curcumin extract C3C improved oocyte developmental potential in female mice fed a saturated fat-rich diet, and therefore the effect on the HSR was not further explored. Even though the curcumin treatment stopped the further development of diet-induced obesity, the subtle changes that were observed in oocyte mitochondrial activity suggest these treatment influences oocyte developmental competence. These observations deserve further, and more detailed investigation in larger cohorts of animals.

Interestingly, treatment with the *Opuntia* extract Tex-OE was shown to improve embryo development, likely by improving mitochondrial function in the oocyte. This finding identified Tex-OE as a novel compound for improving oocyte quality, as well as pointing to the existence of a previously unknown mechanism by which chaperone therapy can reverse the negative effects of obesity on female fertility and necessitates further investigation.

Overall, this work is the first demonstration that phytocompounds can be used in the treatment of obesity-related infertility. Thus, the findings contribute significantly to our current understanding of potential therapeutic targets for female infertility.

In conclusion, this thesis demonstrated that chaperones of the HSR have distinct expression and localization in the mouse ovary across follicle growth and oocyte maturation and presented evidence that suggested these proteins may have currently unknown roles in ovarian cells. For this reason, the HSR pathway was identified as a likely target of the negative impact of obesity in the ovary. I firstly then showed that obesogenic hormones and diets distinctly disrupt female metabolism and impact ovarian function, and affects oocyte developmental competence, irrespectively of type of obesogenic insult. This occurs in association with ovarian cell dysregulation of stress pathways, especially the HSR in somatic cells. Moreover, I showed that the gene expression for stress markers can be differentially regulated by diet. Finally, I demonstrated that ovarian function and oocyte developmental potential can be restored by dietary intervention with chaperone-inducing compounds and identified a novel therapeutic property of *Opuntia* extract in the treatment of female infertility.

7.5 References

100. Wu LL, Russell DL, Wong SL, Chen M, Tsai TS, St John JC, Norman RJ, Febbraio MA, Carroll J, Robker RL. Mitochondrial dysfunction in oocytes of obese mothers: transmission to offspring and reversal by pharmacological endoplasmic reticulum stress inhibitors. Development 2015; 142:681-691.
202. Wu LL, Russell DL, Norman RJ, Robker RL. Endoplasmic reticulum (ER) stress in cumulus-oocyte complexes impairs pentraxin-3 secretion, mitochondrial membrane potential (DeltaPsi m), and embryo development. Mol Endocrinol 2012; 26:562-573.
268. Khanna A, Aten RF, Behrman HR. Heat shock protein-70 induction mediates luteal regression in the rat. Mol Endocrinol 1995; 9:1431-1440.
272. Pratt WB, Toft DO. Steroid receptor interactions with heat shock protein and immunophilin chaperones. Endocr Rev 1997; 18:306-360.
300. Caldwell AS, Middleton LJ, Jimenez M, Desai R, McMahon AC, Allan CM, Handelsman DJ, Walters KA. Characterization of reproductive, metabolic, and endocrine features of polycystic ovary syndrome in female hyperandrogenic mouse models. Endocrinology 2014; 155:3146-3159.
318. Walters KA, Allan CM, Handelsman DJ. Rodent models for human polycystic ovary syndrome. Biol Reprod 2012; 86:149, 141-112.
322. Huffman L, Hendricks SE. Prenatally injected testosterone propionate and sexual behavior of female rats. Physiol Behav 1981; 26:773-778.
324. Swanson HE, Werfftenbosch JJ. The "Early-Androgen" Syndrome; Differences in Response to Pre-Natal and Post-Natal Administration of Various Doses of Testosterone Propionate in Female and Male Rats. Acta Endocrinol (Copenh) 1964; 47:37-50.
326. Tyndall V, Broyde M, Sharpe R, Welsh M, Drake AJ, McNeilly AS. Effect of androgen treatment during foetal and/or neonatal life on ovarian function in prepubertal and adult rats. Reproduction 2012; 143:21-33.
327. Edwards DA. Neonatal administration of androstenedione, testosterone or testosterone propionate: effects on ovulation, sexual receptivity and aggressive behavior in female mice. Physiol Behav 1971; 6:223-228.
328. Beloosesky R, Gold R, Almog B, Sasson R, Dantes A, Land-Bracha A, Hirsh L, Itskovitz-Eldor J, Lessing JB, Homburg R, Amsterdam A. Induction of polycystic ovary by testosterone in immature female rats: Modulation of apoptosis and attenuation of glucose/insulin ratio. Int J Mol Med 2004; 14:207-215.
329. Weisz J, Lloyd CW. Estrogen and androgen production in vitro from 7-3-H-progesterone by normal and polycystic rat ovaries. Endocrinology 1965; 77:735-744.
330. Arai Y, Yamanouchi K, Mizukami S, Yanai R, Shibata K, Nagasawa H. Induction of anovulatory sterility by neonatal treatment with 5 beta-dihydrotestosterone in female rats. Acta Endocrinol (Copenh) 1981; 96:439-443.
331. Ota H, Fukushima M, Maki M. Endocrinological and histological aspects of the process of polycystic ovary formation in the rat treated with testosterone propionate. Tohoku J Exp Med 1983; 140:121-131.
332. Kamijo T, Mizunuma H, Yamada K, Ibuki Y. In vitro fertilization of androgen sterilized mice. Life Sci 1994; 55:527-531.
333. McDonald PG, Doughty C. Comparison of the effect of neonatal administration of testosterone and dihydrotestosterone in the female rat. J Reprod Fertil 1972; 30:55-62.
334. Pinilla L, Trimino E, Garnelo P, Bellido C, Aguilar R, Gaytan F, Aguilar E. Changes in pituitary secretion during the early postnatal period and anovulatory syndrome induced by neonatal oestrogen or androgen in rats. J Reprod Fertil 1993; 97:13-20.
426. Nilsson C, Raun K, Yan F-f, Larsen MO, Tang-Christensen M. Laboratory animals as surrogate models of human obesity. Acta Pharmacol Sin 2012; 33:173-181.

427. Rosini TC, Ramos da Silva AS, de Moraes C. Diet-induced obesity: rodent model for the study of obesity-related disorders. Revista da Associação Médica Brasileira (English Edition) 2012; 58:383-387.

APPENDIX

Appendix 1 **Detailed information on nomenclature, molecular size of the synthesized protein, as well as the gene ID and chromosome location in both mouse and human for the members of the HSP70 family**

Gene Name (Adapted from [127])	Other Names (Old Nomenclature)	Molecular Size (kDa)	Human (adapted from [189])		Murine (adapted from [189])	
			Gene ID	Chromosome Location	Gene ID	Chromosome Location
HSPA1A	Hsp72; Hsp 70.1; HSPA1; HSP70I; HSP70-1A	70.0	3303	6p21.3	193740	17 B1; 17 18.51 cM
HSPA1B	Hsp70-2; HSP70-1B	70.0	3304	6p21.3	15511	17 B1; 17 18.5 cM
HSPA1L	Hum70t; HSP70T; HSP70-1L; HSP70-HOM	70.4	3305	6p21.3	15482	17 B1; 17 18.51 cM
HSPA2	Hsp70.2; HSP70-3	70.0	3306	14q24.1	15512	12 C3; 12 33.73 cM
HSPA5	Grp78, Bip, MIF2	71.0	3309	9q33-q34.1	14828	2 B; 2 22.94 cM
HSPA6	Hsp70B	71.0	3310	1q23	No murine homologue	No murine homologue
HSPA7	Heat Shock Protein 7; HSP70B	71.0	3311	1q23.3	No murine homologue	No murine homologue
HSPA8	HSC70; LAP1; HSC54; HSC71; HSP71; HSP73; NIP71; HSPA10	70.9	3312	11q24.1	15481	9 A5.1; 9 21.55 cM
HSPA9	Grp75; MOT; mortalin; CSA; MOT2; PBP74; HSPA9B; MTHSP75	73.7	3313	5q31.1	15526	18 C; 18 18.8 cM
HSPA12A	FLJ13874	141.0	259217	10q26.12	73442	19 D2-D3; 19
HSPA12B	RP23-32L15.1; C20orf60; dJ1009E24.2	75.7	116835	20p13	72630	2; 2 F3
HSPA13	Stch	51.9	6782	21q11	110920	16 C3.2; 16 43.36 cM
HSPA14	HSP70-4, HSP70L1	54.8	51182	10p14	50497	2 A1; 2

Appendix 2 **Detailed information on nomenclature, molecular size of the synthesized protein, as well as the gene ID and chromosome location in both mouse and human for the members of the HSP90 and Chaperonin families.**

Gene Name (Adapted from [127])	Other Names (Old Nomenclature)	Molecular Size (kDa)	Human (adapted from [189])		Murine (adapted from [189])	
			Gene ID	Chromosome Location	Gene ID	Chromosome Location
HSP90AA1	Hsp90; HSPCA; HSP90α; EL52; HSPN; LAP2; HSP86; HSPC1; Hsp89; HSP89A; HSP90A; HSP90N; HSPCAL1;HSPCAL4	85	3320	14q32.33	15519	12 F1; 12 60.75 cM
HSP90AA2	HSPC2; HSP90α; HSPCA; HSPCAL3;HSP90ALPHA	83	3324	11p14.1	No murine homologue	No murine homologue
HSP90AB1	HSPC3, HSP90β; HSP84; HSPC2; HSPCB; D6S182; HSP90B	84	3326	6p12	15516	17 B3; 17 22.59 cM
HSP90B1	HPSC4; GRP94; endoplasmin; ECGP; GP96; TRA1	94	7184	12q24.2-q24.3	22027	10 C1; 10 43.05 cM
TRAP1	HSPC5; HSP75; HSP90L	80.1	10131	16p13.3	68015	16 A1; 16 2.38 cM

Appendix 3 **Antibodies used for IHC/IC analysis of protein expression.**

Protein name & source	MW (kDa)	Immunogen (Uniprot ID)	Host & Clonality	Manufacturer & Cat. #	Antibody Dilution used
HSF1 (human)	82		Rabbit (Polyclonal)	Cell Signaling #4356	1:1000
HSPA1A/B (human)	72		Goat	Santa Cruz Biotech	1:500
HSPA5	72	aa340 – aa617 (P11021)	Rabbit (Polyclonal)	Novus Biologicals #NBP2-16746	1:400
HSP90AA1					1:250
HSP90B1 (mouse)	94	aa787 – aa802	Rabbit (Polyclonal)	Novus Biologicals #NB200-426	1:500
HSP60 (human)	60	(P10809)	Rabbit (Monoclonal)	Cell Signaling #12165	1:400

Appendix 4 **Primers used for real-time PCR analysis of gene expression.**

GENE NAME	GENE SYMBOL	Thermo Fisher Scientific Cat. #	Amplicon Size	Ref. Seq.
Ribosomal Protein L19	**Rpl19**	Mm02601633_g1	69	NM_009078
Heat Shock Factor 1	**Hsf1**, AA960185, Hsf1alpha, Hsf1beta	Mm01201402_m1	70	NM_008296
Heat Shock Protein 1A	**Hspa1a**, Hsp70-3, Hsp70.3, Hsp72, hsp68, hsp70A1	Mm01159846_s1	113	NM_010479
Heat Shock Protein 1B	**Hspa1b**, Hsp70, Hsp70-1, Hsp70.1, hsp68	Mm03038954_s1	141	NM_010478
Heat Shock Protein 5	**Hspa5**, GRP78, AL022860, AU019543, Bip, D2Wsu141e, D2Wsu17e, Grp78, Hsce70, SEZ-7, Sez7, baffled, mBiP	Mm00517691_m1	75	NM_001163434
Heat shock protein 90, alpha (cytosolic), class A member 1	**Hsp90aa1**, 86kDa, 89kDa, AL024080, AL024147, Hsp86-1, Hsp89, Hsp90, Hspca, hsp4	Mm00658568	128	NM_010480
Heat shock protein 90, beta (cytosolic), class A member 2	**Hsp90ab1**, 84KDa, 90kDa; Hsp84; Hsp90; Hspcb; C81438; Hsp84-1; AL022974	Mm00833431_g1	167	NM_008302.3
Heat shock protein 90, beta (Grp94), member 1	**Hsp90b1**, GRP94, ERp99, GRP94, TA-3, Targ2, Tra-1, Tra1, endoplasmin, gp96	Mm00441926_m1	67	NM_011631
Heat shock protein D1 (chaperonin)	**Hspd1**, Hsp60, 60kDa	Mm00849835_g1	138	NM_010477

GENE NAME	GENE SYMBOL	Thermo Fisher Scientific Cat. #	Amplicon Size	Ref. Seq.
Activating Transcription Factor 4	**Atf4**, Atf-4, C/ATF, CREB2, TAXREB67	Mm00515325_g1	78	NM_001287180.1
X-box Binding Protein 1 – spliced	**Xbp1s**, D11Ertd39e, TREB-5, TREB5	Mm00457357_m1	56	NM_001271730.1
Tumor Necrosis Alpha	**TNFa**, TNF-alpha, TNFSF2, TNF alpha, Tnfsf1a, DIF	Mm01159846_s1	61	NM_01369.3
Interleukin 6	**Il-6**	Mm00446190_m1	78	NM_031168.1
Interleukin 1 beta	**Il-1b**, Il-1beta	Mm00434228_m1	90	NM_008361.3

Appendix 5 **In vitro fertilisation and culture of pre-implantation mouse embryos.**

In vitro fertilisation is a useful technique to model and observe oocyte fertilisation and pre-implantation embryonic development. It consists in the fertilisation of MII oocytes using capacitated sperm in a culture dish. Here, I will describe the protocol for in vitro fertilisation (IVF) of mouse oocytes and pre-implantation embryo culture.

A 6 week old C57BL6 male mice was mated to a super-ovulated C57BL6 female 4-7 days prior to IVF. The female mouse received an intraperitoneal (IP) injection of Pregnant Mare Serum Gonadotropin (PMSG; National Hormone and Peptide Program, Torrence, USA) in sterile 0.9% saline at a dose of 5 IU/12 g of body weight. At 48 hours post-PMSG, the mice received a second IP injection of human chronic Gonadotropin (hCG; Pregnyl, Merck Sharp & Dohme Pty Ltd, Australia) in sterile 0.9% saline at a dose of 5 IU/12 g of body weight; to onset ovulation. After hCG injection, the female was caged with strain-compatible C57BL6 male, then checked for the presence of vaginal plug (indicative of coitus) at 15-16h post-hCG injection.

Those males that were positively identified as mated were humanely killed by cervical dislocation on the day of IVF (day 1), and the vas deferens and epididymis were dissected, cleaned of any attached adipose tissue. The tissue was placed in 1mL of warm Research Vitro Fertilisation Medium (COOK Medical, QLD, Australia) under paraffin oil (Merck Millipore, Massachusetts, USA), previously left to equilibrate overnight at 37°C in 6% CO_2, 21% O_2. The neat semen was collected then by squeezing the epididymis and vas deferens using fine-tip forceps. The leftover tissue was then removed from the medium and the sperm was left to capacitate for 1 hour at 37°C in 6% CO_2, 21% O_2.

Female C57BL6 mice underwent ovarian hyperstimulation, then were humanely killed by cervical dislocation at 16 hours after injection with hCG (IVF day 1). The reproductive tracts were dissected and placed in HEPES-buffered GIBCO minimal essential medium (aMEM, Life Technologies Australia Pty Ltd) at 37°C. Ovulated cumulus-oocyte complexes (COCs) were collected by tearing open the oviduct using 30G needles. The COCs were then washed twice in warm Research Vitro Wash Medium (COOK Medical) at 37°C, then placed in 90 ul of Research Vitro Fertilisation Medium (10-20 COCs/90 ul drop; COOK Medical) under paraffin oil. Immediately, an aliquot of 10 ul (1:100 final concentration) of sperm solution is used to fertilise the mouse oocytes, and the culture dish is then placed at 37°C in 6% CO_2, 21% O_2 for 4 hours.

After 4 hours, the presumptive zygotes were collected from the fertilisation medium, then washed and cleaned out of excess sperm still attached to the zona pellucida in Research Vitro

Cleave medium (COOK Medical) under paraffin oil using a fine glass pipette tip. The embryos were then transferred to a clean drop of cleave medium (10 zygotes/20 uL drop) for in-vitro embryo culture to blastocyst stage at 37°C in 6% CO_2, 21% O_2. Developmental embryonic stage of the pre-implantation embryos was assessed and recorded daily for 5 days. On-time development of the embryos was analysed by assessing their developmental stage every 24 hours.

Appendix 6 **In-house control diet formulation and ingredients.**

FORMULA: **IN-HOUSE CONTROL DIET**	**Weight (%)**	**Energy (%)**
Protein	18.96	19.74
Carbohydrate	67.58	70.37
Fat	4.27	9.89
Total (%)		100
Kcal/g	3.84	

Ingredient	**Weight (g)**	**Energy (kcal)**
Lactic Acid Casein, pasteurised (Fonterra Australia TM)	200	800
Corn Starch, unbleached (Coles Supermarkets Australia Pty Ltd)	506.2	2024.8
Maltodextrin (D2550, Syn-tec Nutriceuticals)	125	500
Sucrose (S9378, Sigma-Aldrich)	68.8	275.2
α-Cellulose (C8002, Sigma-Aldrich)	50	0
Potassium Citrate, 1 H_2O (Sanders Fodder SA)	16.5	0
DiCalcium Phosphate (Sanders Fodder SA)	13	0
Mineral Mix S10026 (960401, MP Biomedicals, LLC)	10	0
Vitamin Mix AIN-93-VX (960402, MP Biomedicals, LLC)	10	40
Calcium Carbonate (Sanders Fodder SA)	5.5	0
L-Cysteine (C8755, Sigma Aldrich)	3	12
Choline Bitartrate (C1629, Sigma Aldrich)	2	0
Soybean Oil (King's choice TM, Chia Khim Lee food ind Pte Ltd)	25	221
Lard (Premium Frytol, Peerless Holdings Pty Ltd) *	20	180
TOTAL	1055	4053

Appendix 7 **In-house high-fat diet formulation and ingredients.**

FORMULA: **IN-HOUSE HIGH-FAT DIET**	**Weight (%)**	**Energy (%)**
Protein	25.85	16.80
Carbohydrate	33.18	17.37
Fat	34.89	65.83
Total		100
Kcal/gm	4.76	

Ingredient	**Weight (g)**	**Energy (kcal)**
Lactic Acid Casein, pasteurised (Fonterra Australia TM)	258.44	800
Maltodextrin (D2550, Syn-tec Nutriceuticals)	161.50	500
Sucrose (S9378, Sigma-Aldrich)	88.88	275.2
α-Cellulose (C8002, Sigma-Aldrich)	64.60	0
Potassium Citrate, 1 H_2O (Sanders Fodder SA)	21.32	0
DiCalcium Phosphate (Sanders Fodder SA)	16.80	0
Mineral Mix S10026 (960401, MP Biomedicals, LLC)	12.92	0
Vitamin Mix AIN-93-VX (960402, MP Biomedicals, LLC)	12.92	40
Calcium Carbonate (Sanders Fodder SA)	7.11	0
L-Cysteine (C8755, Sigma Aldrich)	3.88	12
Choline Bitartrate (C1629, Sigma Aldrich)	2.59	0
Soybean Oil (King's choice TM, Chia Khim Lee food ind Pte Ltd)	32.3	285.5
Lard (Premium Frytol, Peerless Holdings Pty Ltd) *	316.54	2848.9
TOTAL	999.8	4761.6

Appendix 8 **In-house 3% curcumin high-fat diet formulation and ingredients.**

FORMULA: **IN-HOUSE HIGH-FAT DIET with 3% C3C**	**Weight (%)**	**Energy (%)**
Protein	25.10	16.80
Carbohydrate	32.22	17.37
Fat	33.87	65.83
Total (%)		100
Kcal/g	4.62	

Ingredient	**Weight (g)**	**Energy (kcal)**
Lactic Acid Casein, pasteurised (Fonterra Australia TM)	258.44	800
Maltodextrin (D2550, Syn-tec Nutriceuticals)	161.50	500
Sucrose (S9378, Sigma-Aldrich)	88.88	275.2
α-Cellulose (C8002, Sigma-Aldrich)	64.60	0
Potassium Citrate, 1 H_2O (Sanders Fodder SA)	21.32	0
DiCalcium Phosphate (Sanders Fodder SA)	16.80	0
Mineral Mix S10026 (960401, MP Biomedicals, LLC)	12.92	0
Vitamin Mix AIN-93-VX (960402, MP Biomedicals, LLC)	12.92	40
Calcium Carbonate (Sanders Fodder SA)	7.11	0
L-Cysteine (C8755, Sigma Aldrich)	3.88	12
Choline Bitartrate (C1629, Sigma Aldrich)	2.59	0
Soybean Oil (King's choice TM, Chia Khim Lee food ind Pte Ltd)	32.3	285.5
Lard (Premium Frytol, Peerless Holdings Pty Ltd) *	316.54	2848.9
Curcumin C3 Complex (Sabinsa Australia Pty Ltd)	30	0
TOTAL	1029.85	4761.6

Appendix 9 **In-house cellulose-free high-fat diet formulation and ingredients.**

FORMULA: **IN-HOUSE CELLULOSE-FREE HIGH-FAT DIET**	**Weight (%)**	**Energy (%)**
Protein	27.63	16.80
Carbohydrate	30.85	17.37
Fat	37.30	65.83
Total (%)		100
Kcal/g	5.09	

Ingredient	**Weight (g)**	**Energy (kcal)**
Lactic Acid Casein, pasteurised (Fonterra Australia TM)	258.44	800
Maltodextrin (D2550, Syn-tec Nutriceuticals)	161.50	500
Sucrose (S9378, Sigma-Aldrich)	88.88	275.2
Potassium Citrate, 1 H_2O (Sanders Fodder SA)	21.32	0
DiCalcium Phosphate (Sanders Fodder SA)	16.80	0
Mineral Mix S10026 (960401, MP Biomedicals, LLC)	12.92	0
Vitamin Mix AIN-93-VX (960402, MP Biomedicals, LLC)	12.92	40
Calcium Carbonate (Sanders Fodder SA)	7.11	0
L-Cysteine (C8755, Sigma Aldrich)	3.88	12
Choline Bitartrate (C1629, Sigma Aldrich)	2.59	0
Soybean Oil (King's choice TM, Chia Khim Lee food ind Pte Ltd)	32.3	285.5
Lard (Premium Frytol, Peerless Holdings Pty Ltd) *	316.54	2848.9
TOTAL	935.2	4761.6

127. Kampinga HH, Hageman J, Vos MJ, Kubota H, Tanguay RM, Bruford EA, Cheetham ME, Chen B, Hightower LE. Guidelines for the nomenclature of the human heat shock proteins. Cell Stress Chaperones 2009; 14:105-111.
189. Christians ES, Zhou Q, Renard J, Benjamin IJ. Heat shock proteins in mammalian development. Semin Cell Dev Biol 2003; 14:283-290.